La collana della Scuola di Alta Formazione Dottorale accoglie le migliori tesi di dottorato dell'Università degli Studi di Bergamo, insignite della dignità di stampa e sottoposte a procedura di *blind peer review*.

The present research deals with the dynamic response of one-dimensional structural elements, of both finite and infinite extension, lying on a continuous elastic foundation, under a high-velocity moving load. Pertaining finite systems, the transient response of a simply-supported Euler-Bernoulli beam resting on spatially uniform Winkler nonlinear elastic foundations under a concentrated harmonic moving load is studied by an autonomous FEM implementation. In addition, two analytical solutions for the static deflection of the same beam on a spatially varying Winkler elastic support are derived. Regarding infinite systems, the steady-state responses of a taut string and a Euler-Bernoulli beam, resting on a Winkler and a Pasternak support, respectively, under a concentrated moving load are analysed by an effective Discontinuous Least-Squares Finite Element Method (DLSFEM) coupled with an original Perfectly-Matched Layer (PML).

Diego Froio received his Ph.D. degree in Engineering and Applied Sciences (30th cycle) from the University of Bergamo, Italy, in 2018. Presently, he works on topics of earthquake engineering and structural dynamics. His research interests include structural vibrations under high-velocity moving loads, fluid-soil-structure interaction, seismic assessment and design of concrete dams.

ISBN: 978-88-940721-6-7
DOI: 10.6092/978-88-940721-6-7

Diego Froio STRUCTURAL DYNAMICS MODELIZATION

12

Collana della Scuola di Alta Formazione Dottorale
- 12 -

Diego Froio

STRUCTURAL DYNAMICS MODELIZATION OF ONE-DIMENSIONAL ELEMENTS ON ELASTIC FOUNDATIONS UNDER FAST MOVING LOAD

UNIVERSITÀ DEGLI STUDI DI BERGAMO

2020

Collana della Scuola di Alta Formazione Dottorale

Diretta da Paolo Cesaretti

Ogni volume è sottoposto a *blind peer review*.

ISSN: 2611-9927

Sito web: https://aisberg.unibg.it/handle/10446/130100

Diego Froio

STRUCTURAL DYNAMICS MODELIZATION OF ONE-DIMENSIONAL ELEMENTS ON ELASTIC FOUNDATIONS UNDER FAST MOVING LOAD

Università degli Studi di Bergamo

Structural Dynamics Modelization of One-Dimensional Elements on Elastic Foundations under Fast Moving Load / Diego Froio. – Bergamo : Università degli Studi di Bergamo, 2020.
(Collana della Scuola di Alta Formazione Dottorale; 12)

ISBN: 978-88-940721-6-7
DOI: 10.6092/978-88-940721-6-7

Progetto grafico: Servizi Editoriali – Università degli Studi di Bergamo
© 2018 Università degli Studi di Bergamo
via Salvecchio, 19
24129 Bergamo
Cod. Fiscale 80004350163
P. IVA 01612800167

https://aisberg.unibg.it/handle/10446/157473

Mà ricordiamoci, che siamo trà gl'infiniti, e gl'indivisibili, quelli incomprensibili dal nostro intelletto finito [. . .]; con tuttociò veggiamo, che l'humano discorso non vuol rimanersi dall'aggirarsegli attorno.

Galileo Galilei
Discorsi e Dimostrazioni Matematiche intorno á due nuove Scienze Attenenti alla Mecanica & i Movimenti Locali

Acknowledgements

The support and guidance provided by Professor Egidio Rizzi is gratefully acknowledged, also for the suggested significant improvements in drafting this manuscript.

I would like to express my gratitude to Professor Fernando M.F. Simões at the Instituto Superior Técnico de Lisboa for providing me with useful material, very good advice and enlightening ideas for the present research. He is also especially thanked for offering kind hosting from November 2015 to February 2016, making me feeling like at home.

I would also like to extend my thanks to Professor Giuseppe Cocchetti from Politecnico di Milano for fruitful mathematical discussions and confrontations.

The members of the Board of Examiners, Professor António Pinto da Costa at the Instituto Superior Técnico de Lisboa and Professor Karel van Dalen at the Delft University of Technology, are much thanked as well, together with the PhD School Coordinator, Professor Valerio Re.

A ministerial doctoral grant and funds at the ISA Doctoral School, University of Bergamo, Department of Engineering and Applied Sciences (Dalmine), are gratefully acknowledged.

I would like to thank all friends, colleagues and students I have encountered during this unforgettable research experience.

A special heartfelt thank is addressed to my partner Ilenia, for her love and patience. I'm truly in debt to her, for all the time I have not devoted to.

Finally, I wish to thank my family, and in particular my parents Antonio and Cesarina, for their understanding and encouragement, and for having always believed in me, even in the hard times. I will always be grateful to them.

Contents

Chapter 1

Engineering context and motivation

1.1 Structural problems addressed in the thesis

Dynamic problems involving moving objects are very common in various engineering fields. Railways, roads and concrete pavements, bridges, cableways, guideways, overhead cranes, rocket testing facilities, wood-saws, computer discs, machine tools and ice plates (on this specific case see e.g. Schulkes and Sneyd, 1988 [233] and Squire et al., 1996 [244]) constitute characteristic application contexts. In transportation engineering, the need of predicting the dynamic response of continuous systems under moving vehicles becomes crucial for guaranteeing vehicle stability, monitoring maintenance costs and avoiding possible passenger discomfort (see e.g. Hadi and Bodhinayake, 2003 [118]), specifically as a result of the continuous development of fast transportation systems throughout Europe, far East and North America, nowadays at increasingly high vehicle velocities.

Thereby, it appears fundamental to investigate how the interaction between the support structures and the moving mechanical system influences the amplitude of the track displacements and in which manner they may depend on the velocity of the moving vehicle and on the nature of the acting forces. In the last few decades, numerous research works have been presented, with the majority of them considering a "moving load" problem, i.e. that particular mechanical problem occurring when the point of application of concentrated or distributed loads acting on a certain structural element, usually supported by an elastic foundation (see Kerr, 1972 [157]), changes in time, at a constant or variable velocity. Hence, in contrast to other dynamic loading conditions, moving loads change their position in time. This makes the moving load problem a special topic of structural dynamics.

As it had been demonstrated theoretically, first by Timoshenko (1927) [252]

and then by the extended number of other research works concerning moving load problems, which will be discussed more in detail in the following chapters of this doctoral thesis, excessive dynamic amplification of structural vibrations of elastically supported elements induced by moving loads may become rather high, when the load velocity attains a certain characteristic value, named *critical velocity*. Such a velocity corresponds to the minimum phase velocity of the waves propagating within the structural system. Unfortunately, little data from the observations, analyses and validated predictions have so far been reported in the literature, despite for the severity of the problem.

In the context of railways, the field where most research efforts have been devoted to, the moving vehicle velocity record exceeds 500 km/h (TGV French train). Demands on high train velocities and short travel times calls for straight lines which make the crossing of soft soil zones unavoidable, where problems with high-speed lines, and even with traditional tracks, reaching the critical velocity may therefore be expected, to an increasing amount. Results from instrumented test runs with a high-speed train on a soft soil site in Sweden where presented by Madshus and Kaynia (2003) [185]. Extensive measurements of the dynamic response of the rail, embankment and soil made at a selected site during the Autumn of 1997 showed that dynamic amplifications of displacements increased drastically as the train velocity approached a critical value. Analysis of recorded train-induced displacements revealed also that dynamic strains in the ground and embankment for high-velocity train passages were so high that the materials actually behave nonlinearly.

Hence, demands for safe lines, rapid construction and cost-effective design solutions are becoming apparent. Part of the success of these scopes strongly depends on the availability of robust and efficient analytical and computational tools designed for the accurate and reliable numerical simulation of the dynamic response of structural elements under the action of moving loads. By the analysis of the outcomes of the numerical simulations, potential practical implications in contemporary transportation engineering shall be revealed, especially in terms of lowering down the admissible high-speed vehicle velocities, and the effectiveness of possible remediation measures for the mitigation of system vibrations may be explored. Thus, as a main background practical context of the analytical-numerical investigations exposed in the present doctoral dissertation, the appropriate description of track vibrations induced by high-velocity vehicles, e.g. trains, looks crucial in contemporary transportation engineering.

The idea of modeling the moving vehicle as a moving load may be assumed to be valid if the vehicle mass involved in the motion is not that relevant, compared to that of the supporting systems; “moving mass” problems may be further considered, when the inertial effects due to the mass of the moving object cannot be neglected. The moving mass problem has also been

studied by several authors; among those, noteworthy to be mentioned are the works of Cifuentes (1989) [59], Duffy (1990) [78], Metrikine and Dieterman (1997) [194], Mofid and Shadnam (2000) [198], Yavari et al. (2002) [279], Mofid et al. (2010) [199], Dyniewicz (2012) [79], Dimitrovová (2017) [71].

Finally, if the vertical constraint between the moving system and the support structure is relaxed, i.e. it is no longer assumed as infinitely rigid, "moving oscillator" models (moving spring-mass-damper system) may be taken into account, by introducing the stiffness and damping couplings between the moving mass and the support (see e.g. Wolfert et al., 1998 [272], Metrikine and Verichev, 2001 [195], Mazilu, 2013 [192]). In this context, the recent attempt by Rodrigues et al. (2016) [229], with references quoted therein, shall be considered, where a full FEM approach has been developed for obtaining the numerical response of nonlinear beam-foundation systems under a moving-oscillator.

However, the simplified moving load model is still widely used in both scientific and technical fields since it is often sufficient to answer to issues arising from problems of a practical interest. The determination of the dynamic response induced by a high-velocity moving load constitutes a rather challenging problem, since it involves quite sophisticated modelization and intensive computation. Comprehensive literature reviews about the moving load problem for beams and plates may be found in Frýba (1972) [105], Kerr (1981) [159], Beskou and Theodorakopoulos (1981) [29] and Ouyang (2011) [212]. Frýba's monograph (1971) [105] presents many simple moving-load problems concerning continuous elastic media that are amenable to an analytical treatment, such as strings, rods, beams, plates and shells.

Although the group of problems regarding beams carrying moving loads displays a rather long history in the literature of civil and mechanical engineering, some discrepancies exist among existing papers, and some of the results does not appear conclusive. Hence, the present thesis is focused on moving load problems.

In the literature, elastic beams and various types of foundation models have been adopted to represent tracks, i.e. flexible structures that are mainly one-dimensional in geometry. The main scope of the elastic foundation is that of providing a simplified description of the contact between the beam and the supporting system. The problem of modeling the mechanical behavior of the structural elements and the underlying support, as well as the modeling of the interaction between them, is very often encountered in civil engineering, for instance in the analysis of the foundations of buildings and general geotechnical structures, where the support usually represents the soil, but also in mechanical and aerospace engineering.

The Winkler model, analyzed in following Chapter 2, for which the inertial effects due to the mass of the supporting medium are not considered, thus

accounting for wave propagation just within the supported structure, has been widely used to model the support. Further, recent most accurate models could even consider wave propagation phenomena in both beam and underlying substratum, described as a continuum, leading to an even more comprehensive description in terms of characteristic features, have appeared in the literature and are still now arising as potential alternatives (Dieterman and Metrikine, 1997 [67], Kaynia et al., 2000 [153], Van Dalen and Metrikine, 2008 [263], Van Dalen et al., 2015 [265], Van Dalen and Steenbergen, 2016 [264], Dimitrovová, 2016, 2017 [69, 70]).

1.2 Aims and structure of the thesis

The main subject of the present doctoral dissertation is the structural dynamics analysis of one-dimensional elements (strings, beams) on continuous elastic support. In particular, the research focuses on the determination of the mechanical response of linear and nonlinear structural element-foundation systems under the action of a transverse concentrated moving load, traveling at a high constant velocity along the structural element. The aim of the thesis is to reveal the physical response of such interacting beam-foundation structural systems and to identify its characteristic features through the formulation and implementation of analytical and/or numerical methodologies, specifically conceived to handle the mathematical issues inherent to the modelization of the mechanical problems under consideration.

The thesis is organized in two main parts: determination of the structural response of *finite* beam-foundation systems, in both static and dynamic contexts (fixed reference frame); analysis of the structural dynamic response of *infinite* systems through a moving reference frame. These topics are addressed within four chapters. Chapters 2 and 3 refer to the fist part, while Chapters 4 and 5 to the second one. Such conceptual subdivision stems from the profound differences existing between finite and infinite structural systems, both from the mechanical and the modelization points of view.

Within each chapter, a brief introduction on the analyzed problem is provided, which briefly describes the state of the art, by discussing the main references of the literature on the subject under consideration. At the end of each chapter, conclusive observations about the main results obtained within the chapter are also reported. In the following, the main contents of the various chapters are concisely exposed.

Chapter 2 first reviews the state of the art on the existing constitutive models of the foundation and focuses on the well-known model with independent elastic springs, originally attributed to Emil Winkler (1835–1888), characterized by a constant stiffness coefficient (see also Appendix). Then, the analytically

little-explored case of a space-dependent stiffness coefficient is newly considered, by determining, in closed-form, the static bending response of a finite uniform Euler-Bernoulli elastic beam resting on a Winkler elastic foundation with a spatially inhomogeneous stiffness coefficient. Two trends of variation in space of the stiffness coefficient of the foundation are considered, allowing for consistent analytical solutions: a linear variation and a nonlinear minus four power variation. Different external actions and boundary conditions have been assumed for the two distinct mechanical problems. In both cases, the analytical solution of the governing Ordinary Differential Equation (ODE) is derived and represented in explicit closed form. Through the derived solution, parametric analyses are carried out, by interpreting the parametric variation of the mechanical response of the beam-foundation system due to changes in its mechanical properties.

The modelization and the determination of the transient dynamic response of a finite Euler-Bernoulli beam resting on a spatially homogeneous elastic foundation under the action of a transverse concentrated load, moving at a high constant velocity along the beam and displaying a harmonic-varying magnitude in time, constitute the subject of *Chapter 3*. Two types of models have been considered for describing the mechanical behavior of the elastic foundation: (a) a bilinear Winkler model and (b) a cubic superlinear Winkler model. A standard Galerkin Finite Element Method (FEM) approach coupled with a direct integration algorithm has been developed for efficiently tracing the nonlinear dynamic response of a simply supported beam, with focus on determining several characteristic response features, such as the so-called critical velocities of the moving load, leading to high transverse beam deflections. For all the considered foundation models, extensive analyses are performed, with the following two main goals: (1) to demonstrate the reliability, consistency and accuracy of the various implementations, specifically by the comparison of the obtained numerical critical velocities with previously-published analytical and numerical results; (2) to investigate how the frequency of the harmonic moving load as well as its velocity do influence the response of the whole beam-foundation system, with or without the presence of viscous damping.

Pertaining to the bilinear foundation model, characterized by two different stiffness coefficients in compression and in tension, extensive numerical analyses have been performed to investigate how the frequency of the zero-mean harmonic moving load amplitude and the ratio between the foundation's moduli in compression and in tension affect the critical velocities. Analytical interpolating expressions have been proposed as well and fitted for the achieved two-branch critical velocity trends.

The characterization of the effects of a harmonic moving load with non-zero mean amplitude on the dynamic response of the beam-foundation system and on the critical velocities has constituted the main scope of the vast numerical

investigation performed for cubic superlinear Winkler model (b). As for bilinear foundation model (a), the relationship between the amplitude frequency of the moving load and the critical velocity of the beam-foundation system is explicitly depicted in appropriate three-branch curves, for both types of elastic foundations.

Chapter 4 deals with the numerical solution of the steady-state response of a uniform infinite taut string on a Winkler elastic support, subjected to a concentrated transverse moving load. By describing the response in a moving reference frame attached to the position of the load, the stationary solution is obtained similarly to solving a static problem. By recasting the second-order differential equation as a first-order system in a convected coordinate system, a local Discontinuous Least-Squares Finite Element Method (DLSFEM) formulation is developed within a complex-valued function space, to overcome the numerical instabilities for high-velocity loads and to properly handle far-field conditions through a Perfectly Matched Layer (PML) technique. The discontinuous formulation takes care of the jump conditions arising at the interface where the moving load is acting.

Coercivity and uniform error estimates are established for the finite element approximation for both L_2- and H^1-norms. Numerical examples are presented to illustrate the feasibility of the method and its accuracy in reproducing the trends expected for the a priori error estimates. In fact, before attacking more complicated problems, it looks essential to validate the new techniques developed here by applying them to a simple class of problems that would still highlight all the basic numerical phenomena involved, and would provide a good evaluation of the method performance.

In *Chapter 5*, the steady-state response of a uniform infinite Euler-Bernoulli elastic beam resting on a Pasternak elastic foundation and subjected to a concentrated load moving at a constant velocity along the beam is investigated, both analytically and numerically. In the first part of the chapter a universal closed-form analytical solution is derived through a Fourier transform, apt to represent the response for all possible beam-foundation parameters. A rigorous mathematical procedure is formulated, for classifying the parametric behavior of the solution, including for viscous damping. Depending on such a classification, different types of bending wave shapes are shown to propagate within the beam, ahead and behind the moving load position, and crucial physical characteristics, such as critical velocity and critical damping, are reinterpreted into a wholly exact and complete mathematical framework. Mechanical features of the solution are revealed for the steady-state response in terms of normalized deflection, cross-section rotation, bending moment and shear force.

Then, the second part of *Chapter 5* concerns a computational implementation for solving the same moving load physical problem, by a numerical approach with discretization over a finite domain, thus implying possible spu-

rious reflections of non-evanescent waves. The whole is efficiently solved by: (a) analytically formulating a wholly new, true, Perfectly Matched Layer (PML) approach for the underlying fourth-order differential problem with far-field boundary conditions, without any additional special boundary conditions; (b) outlining a local Discontinuous Least-Squares FEM (DLSFEM) formulation, apt to provide a general and robust numerical approach for the present non self-adjoint problem and to conveniently handle the jump condition in the shear force at the moving load position. Consistent numerical outcomes are illustrated and compared to an available analytical representation, showing a perfect match, with complete removal of spurious boundary effects and proof of theoretical a priori error estimates. Further, it is shown that the present DLSFEM-PML formulation is effectively apt to numerically solve a steady-state moving load problem on an infinite beam, setting up a new convenient computational tool of a rather general validity in such a challenging mechanical vibration context.

Finally, main conclusions, pertaining to the global achievements of the present doctoral dissertation, the interrelation between the results derived in each chapter and the outline of possible future developments of the present work are reported in closing *Chapter 6*.

By virtue of the effectiveness of all the derived analytical-numerical solutions and of the resulting extensive parametric analyses attached to the various features revealed from the physical response, the thesis sheds light on the study of the considered moving load problems, thus allowing to truly describe and interpret the characteristic features of the considered interacting beam-foundation structural systems, pointing out to outcomes that are amenable to practical context of engineering application and design.

1.3 Adopted notation

This concise summary briefly exposes the notation adopted in the thesis, for denoting the basic mathematical symbols, the operations and the conventions employed in the discussion.

The sets of real and complex numbers are denoted by $\mathbb{R}$ and $\mathbb{C}$, respectively. $\mathbb{R}^n$ ($\mathbb{C}^n$) is the n-dimensional vector space of the n-uples of real (complex) numbers. Given a complex number z, $z^R{=}\Re\, z$ and $z^I{=}\Im\, z$ will denote its real and imaginary parts, respectively. The imaginary unit will be denoted by i, while italic letter i will be sometimes used as a subindex.

Vector quantities will be denoted by bold-face lowercase or uppercase symbols, while matrices will be marked by bold uppercase roman letters. Partial of total derivatives of an arbitrary function f with respect to variable ξ, will be expressed as $f_{\xi}^{(k)}$, where index k represents the order of the derivative.

Regarding standard notations and definitions of functional analysis, $(\cdot,\cdot)_{m,\Omega}$ and $\|\cdot\|_{m,\Omega}$ will connote the inner product and norm on classical Sobolev space $H^m(\Omega)$, defined on open domain Ω, of all square integrable real- (or complex-) valued functions with square integrable distributional derivatives up to order m. If $m{=}0$, usual Hilbert space $L_2(\Omega){=}H^0(\Omega)$ of square integrable functions is indicated.

In order to ease the understanding of the reader among the large number of physical quantities involved in the definition of the analyzed problems, units will be specified within the text, each time a physical quantity is introduced for the first time. Units will be labeled according to the International System of Units and will be pointed out among square brackets, e.g. F [N] means that variable F displays the dimensions of a force and that it may be measured in Newton.

Chapter 2

Modelization of the elastic support

2.1 Elastic foundation models

From the second half of the nineteenth century to present, several research studies have dealt with the structural analysis of beams lying on elastic foundations, within various fields of engineering applications, involving for the design and assessment of ballasted railway tracks, beam trusses, pipelines, piles subjected to horizontal loads, shallow foundations, buried structures, floating structures, etc. (see e.g. Hetényi, 1966 [127]). In such applications, it is well known that the interaction of the structure with the foundation, named also support or substratum, still represents a non-trivial problem and plays a key role in the determination of the structural response to given operating loads (Kerr, 1964 [156]), both in the static and in the dynamic response ranges. Therefore, it is of main interest to accurately analyze the response of structures lying on elastic supports, especially under spatial variations and/or a nonlinear character of the elastic support behavior.

In the literature, as far as the underlying support is assumed to be homogeneous, isotropic and to display an elastic behavior, the interaction with the structure is tackled by considering two major categories of foundation models (see Hetényi, 1946 [125]): (a) continuous medium models and (b) so-called "mechanical" models. The former are constituted by full-scale approaches that consider the support as a semi-infinite elastic continuum; the latter take off the substratum from the analysis and reduce the problem to adjust the differential equation of the beam by including the contribution from the foundation reaction; this latter case is especially adopted when the response of the beam is of a main interest, with respect to the assessment of the stresses, strains and displacements in the substratum. It is worth noting that, while the continuous approach usually becomes unsuitable since the analysis turns-out excessively cumbersome, the second approach may be characterized by oversimplified assumptions, which sometimes may not be fully representative of

real cases. Nevertheless, there appears a large class of practical cases where the structure-substratum interaction may be described by the latter approach. Thus, the problem reduces to finding a relatively simple mathematical expression which should describe the response of the foundation at the contact area with a reasonable degree of accuracy (Kerr, 1964 [156]).

2.1.1 Linear elastic foundation models

In the attempt to develop a theoretical, physically-reliable and, at the same time, mathematically-simple representation of the elastic support, various types of foundation models and computational tools for structures supported along their longitudinal axis have been proposed in the literature, such as those of Winkler (1867) [271], Filonenko-Borodich (1940) [93], Hetényi (1950) [126], Pasternak (1954) [213], Reissner (1958) [227], Kerr (1965) [157], Vlasov and Leontiev (1966) [267]. Among these, the well-known Winkler model has been usually selected by engineers and researchers, by virtue of its widespread diffusion in several practical applications due to its simplicity and its mathematical clarity, particularly in the design practice of continuous foundations (see e.g. Bowles, 1974 [42] and Selvadurai, 1979 [235]). Even though, according to Timoshenko (1953) [253], Winkler main contribution to Strength of Materials was his theory of bending of curved bars, such as hooks, rings, chains and links, nowadays the name of Winkler is inextricably linked to the bending analysis of structural elements resting on a continuous support.

A few years after the practical bending theory of Navier (1785–1836) was presented (1826) and the expansion of the trussed framework theory of Culmann (1821–1881) into graphical statics (1864–1866) (see Kurrer, 2008 [169]), Winkler[1] [1835–1888] first implemented Hooke's law for the occurring need of predicting the bending of railroad rails with longitudinal sleepers (a system which afterward was soon abandoned) in his book entitled *Die Lehre von der Elastizität und Festigkeit* (1867) [271] (Theory of Elasticity and Strength). In fact, just as the railway networks started to spread, thus placing higher demands on the building of large bridges, the economic policy to raise the intended construction with a minimum of material led designers to carry out all stability investigations and all determinations on the forces acting on the individual constructions (see Kurrer, 2008 [169]).

In more detail, Winkler assumed the railway track as an infinite beam lying on an elastic support consisting of a continuous array of vertical, closely-spaced, mutually-independent, linear elastic springs, with symmetric behavior for both tension and compression (bilateral support). According to such a purely mechanical model, the relation between continuously distributed transverse reaction force $r(x)$ [N/m] acting on the beam, provided by the elastic

[1] A short historical sketch of the life of Emil Winkler is reported in Appendix on behalf of the interested reader.

support, and deflection of the beam $w(x)$ [m], as a function of longitudinal spatial coordinate x [m] is the following:

$$r(x) = -k(x)\, w(x), \qquad k(x) > 0; \tag{2.1}$$

where $k(x)$ [N/m^2] is the support elastic stiffness coefficient or modulus of subgrade reaction or Winkler foundation modulus, i.e. the elastic stiffness per unit length of the distributed foundation springs; such coefficient was originally assumed as constant, i.e. $k(x)$=k (one may think about the foundation as being equivalent to an ideal fluid, viewing $k(x)$ as its specific weight, as underlined by Kerr, 1964 [156]). The problem of the estimation of this coefficient, usually taken as constant, particularly in the context of Soil-Structure Interaction (SSI), has been widely treated in the dedicated technical and practical literature (see for instance Terzaghi, 1955 [249], Selvadurai, 1979 [235], Jones 1997 [147], Kerr, 2000 [160]).

Despite its simplifying assumptions, Winkler model appeared in all subsequent writings and, progressively, spread over its application to a wide set of engineering problems. The studies which appear to constitute the most important research investigations pursuing the analysis of beams on an elastic Winkler foundation with *constant elastic modulus* are listed below.

Schwedler (1882) [234] solved the problem of a beam of infinite length on elastic supports with concentrated loading, by means of Eq. (2.1), apparently without mentioning Winkler's name (such solution was already known to Winkler, see Kurrer, 2008 [169]) and used such derivation to calculate the railway track for loads of any magnitude acting at any relative spacing. Schwedler presented his solution and its experimental safeguards at the Institution of Civil Engineers in London in the same year, and helped to validate and establish the Winkler model, in particular owing to the agreement between theory and measurements. Two years later, Hertz (1884) [124] adopted Winkler assumptions by solving a floating infinite elastic plate subjected to a concentrated load.

A few years later Zimmermann (1888) [286] in his notable book asserted that the application of Eq. (2.1) was certainly admissible for small deformations and made further progress towards the subject by preparing tables for simplifying Winkler analysis, as reported also by Timoshenko (1953) [253]. Zimmermann further applied the theory in calculating the deflection of ties and developed a method for calculating the infinite bar with point loads at any position. According to Hetényi (1966) [127] and Kurrer (2008) [169], Zimmermann's work eliminated misconceptions and contradictions that had existed up to that time, leading to a coherent and relatively simple railway theory and spread over Winkler's ideas in the 20th century.

The subsequent development of foundation engineering theory in the 1920s brought with it the first signs of a specific theory of elastic supports for beam and slab structures, a development that was completed in the wake of the estab-

lishment of reinforced concrete foundations. For instance, it was in 1921 that Japanese structural engineer Hayashi published a monograph on the use of the theory of the beam on elastic supports for problems in foundation engineering (Hayashi, 1921 [122]).

Thereafter, the study of beams resting on elastic Winkler foundations had received considerable attention for over a century, most of all limited to prismatic beams on homogeneous foundations. Timoshenko (1927) [252] developed analytical calculations for the lateral deflection and twisting of rails under the action of a static load using Winkler model; he also showed that Eq. (2.1) can be used for transverse as well as for longitudinal sleepers. Comparisons between the results obtained by considering the elastic continuous approach on one hand and the Winkler model on the other hand have been reported by Biot (1937) [34]. A classical treatise about Winkler model is provided by the book of Hetényi (1946) [125], which illustrates a comprehensive analysis of beams of infinite and finite length lying on a continuous elastic foundation.

Efforts have also been produced for solving the problem through approximate evaluation methods. Levinton's investigations (1949) [176] were concerned with the method of redundant reactions, in which the problem is reduced to the solution of a set of simultaneous equations by means of an approximate pressure distribution. Popov (1951) [220] obtained solutions through a procedure based on successive graphical approximations; Gazis (1958) [108] and Penzien (1960) [215] used iterative methods for the solution of this problem, similar to the well-known Cross method for the analysis of continuous beams and frames. Malter (1958) [187] employed the Newmark method and Finite Differences (FD), based on the moment-area method. Lee et al. (1961) [173] analyzed continuous beam-columns deriving the slope-deflection equations. Barden (1962) [16] computed the contact pressure distribution based on the displacement compatibility between beam and soil, assuming a stepped variation of the contact pressure. Pipes (1946) [216] and later Iwinski (1967) [134] demonstrated the application of integral transform techniques to the finite beam problem.

Miranda and Nair (1966) [196] have applied the method of initial parameters for the treatment of the finite beam problem, reducing the boundary value problem to the solution of a simple two by two linear system of equations. Szuladzinski (1975) [248] solved the problem constructing a discrete model, in which the beam was substituted by a chain of rigid links interlocked with pins and the flexural stiffness was lumped into rotational springs, placed in correspondence of each pin.

Beaufait (1977) [23] gained a complete numerical solution and an approximate value of the critical axial load by using the midpoint difference method. Later, Ting (1982) [254] improved an integral approach for studying finite uniform beams on a Winkler foundation with elastic restraints on deflection

and slope, placed at the ends. Hosur and Bhavikatti (1996) [131] developed a FD scheme assuming a parabolic variation of the contact pressure distribution, obtaining the influence lines of the bending moments. Borák and Marcián (2014) [41] applied modified Betti's theorem for developing an alternative analytical solution of beams on an elastic foundation.

Influence lines for the deflection, bending moment and shear force of a finite beam were deduced analytically by Hetényi (1946) [125] and numerically by Ray (1958) [224], who presented a set of ready-made tables for design purposes, by using a FD approach. The employment of non-dimensional influence functions was shown by Dodge (1964) [76].

Also matrix methods have been heavily applied. Fraser (1968) [96] obtained a matrix formulation by means of a FD technique and the conjugate beam analogy. In Bowles's textbook, both FD and FEM solutions have been employed (see Bowles, 1974 [42]), and, in particular, a stiffness matrix using a conventional beam element supported on discrete soil springs at the ends of the element was formulated. Miyahara and Ergatoudis (1976) [197] and later Eisenberger and Yankelevsky (1985) [84] formulated exact stiffness matrices for both a beam and a beam-column element on a Winkler foundation, suitable for a finite element implementation of the problem. Aydogan (1995) [11] considered also shear effects in the beam differential-equation and consequently derived a formulation of the finite element stiffness matrix accounting also for shear effects.

A fundamental limitation of the elastic Winkler foundation model is that of neglecting the interactions between adjacent foundation springs, thus overlooking for the cohesive and frictional bonds between medium particles. This may lead to unrealistic results (Limkatanyu et al., 2015 [178]). To narrow down the gap between the real behavior of continuous media and elastic Winkler foundation models, several researchers have enriched the Winkler model by introducing a coupling effect between continuous Winkler springs and different embedded structural elements, thus accounting for the effect of the adjacent supporting medium.

Among these models, the Pasternak (1954) [213] one accounts for the existence of a shear interaction between the spring elements, by connecting the top end of each spring to an incompressible layer, which deforms under transverse shear only and whose shear elastic modulus dictates the amount of shear coupling between neighboring springs (Selvadurai, 1979 [235]), as follows:

$$r(x) = -k(x)\, w(x) + \left(G_P(x)\, w_x^{(1)}(x)\right)_x^{(1)}, \qquad k(x) > 0; \tag{2.2}$$

where stiffness coefficient $k(x)$ is the first stiffness parameter of the Pasternak elastic foundation (as in the Winkler model) and $G_P(x)$ [N] is the Pasternak shear modulus of the interconnecting shear layer, namely the second stiffness parameter of the Pasternak elastic foundation (in Eq. (2.2) recall that $w_x^{(1)}(x)$

marks the first-order derivative of deflection $w(x)$ with respect to x, see notation Section 1.3). For this reason, this model is often classified as a "two-parameter" foundation model, where the first parameter represents the vertical stiffness of the foundation springs, like in a classical Winkler model, while the second parameter accounts for their shear coupling. The Pasternak shear modulus is usually assumed as constant as well, $G_P(x)$=G_P.

The simplified continuum analysis by Vlasov and Leontiev (1966) [267] showed that the mechanical behavior of an elastic continuum can be simulated by using springs with such a shear-type interaction. Because of the lack of appropriate laboratory tests or in situ measurement methodologies (Selvadurai, 1979 [235]), the problem of specifying realistic values of the soil parameters involved in two-parameter foundation models has been analytically addressed by Vlasov and Leontiev (1966) [267] and by Vallabhan and Das (1988, 1991a,b) [260–262], which is founded on a quite different formulation of the equations of the two-parameter Vlasov model (modified Vlasov model).

Zhaohua and Cook (1983) [283] developed two kinds of finite elements for an Euler-Benoulli elastic beam on a two-parameter elastic foundations, one based on the displacement functions of the exact analytical solution of the problem and the other based on usual cubic displacement functions. Eisenberger and Clastornik (1987) [83] derived the element stiffness, geometric and mass matrix by considering a variable two-parameter foundation model by assuming that all variable quantities in the problem can be represented as a polynomial series. Razaqpur and Shah (1991) [225] derived the stiffness matrix and nodal load vector of the beam element on two-parameter elastic foundation using polynomial displacement shape functions.

On behalf of the interested reader, "three-parameter" foundation models have also been formulated in the literature, such as those of Hetényi (1950) [126], Reissner (1958) [227] and Kerr (1965) [157]. The basic features of three-parameter models is the flexibility and convenience that they offer in the determination of the level of "continuity" of the vertical displacements at the boundaries between the loaded and the unloaded surfaces of the soil (Hetényi, 1950 [126]). In fact, three-parameter models allow to take into account the following factors: (a) consideration of the influence of soil on either side of the frames; (b) consideration of the shear stresses developing in the soil and (c) consideration of the local deformations under the loaded surface of the soil.

Among all three-parameter models, the Kerr model is of a particular interest, due to a series of solutions and applications which are available in the literature. This model consists of two linear elastic spring layers of constants $k_1(x)>0$ and $k_2(x)>0$ [N/m^2], respectively, interconnected by a unit thickness shear layer of uniform $G(x)$ [N]. Therefore, the support reaction-displacement relation for a Kerr foundation model, derived from the general constitutive relations of the various support layers of the Kerr model, may be

expressed as:

$$\left(1+\frac{k_2(x)}{k_1(x)}+\frac{\Big(k_1(x)G(x)k_{1\,x}^{(1)}(x)\Big)_x^{(1)}-3G(x)k_{1\,x}^{(1)}(x)^2}{k_1^3(x)}\right)r(x)-\frac{G(x)}{k_2(x)}r_x^{(2)}(x)$$
$$-k_2(x)\left(\frac{G(x)}{k_1^2(x)}\right)_x^{(1)}r_x^{(1)}(x)=-k_2(x)w(x)+\Big(G(x)w_x^{(1)}(x)\Big)_x^{(1)}; \tag{2.3}$$

which, for constant support elastic coefficients, reduces to the formula reported by Kerr (1965) [157]:

$$\left(1+\frac{k_2}{k_1}\right)r(x)-\frac{G}{k_1}\,r_x^{(2)}(x)=-k\,w(x)+G\,w_x^{(2)}(x). \tag{2.4}$$

It may be noted that the derivatives of support reaction $r(x)$ also appears in the constitutive law in Eqs. (2.3)-(2.4), as opposed to Eqs. (2.1)-(2.2).

Avramidis and Morfidis (2006) [10] formulated and solved the static problem of a Timoshenko beam resting on Kerr-type elastic foundation within the context of first-order theory, while Morfidis (2010) [203] studied the dynamics of this model within the context of second-order theory. Although these two studies showed the superiority of the Kerr-type foundation model, compared to one or two-parameter models, to approximate a FEM-based reference solution of the corresponding two-dimensional continuum model, the application of this model appears to be rather cumbersome, since it requires the solution of a system of two sixth-order linear differential equations. For this reason, hereinafter only one (Winkler) or two (Pasternak)-parameter models will be employed for studying the mechanical response of beams on elastic foundation.

2.1.2 Nonlinear elastic foundation models

According to the Winkler model introduced in the previous section, a linear elastic constitutive law between foundation reaction and beam displacement is assumed, as shown in Fig. 2.1a. As seen in the previous section, many authors successfully addressed Soil-Structure Interaction (SSI) problems concerning static loads by employing linear elastic foundation models. However, in practice, very often the support structure shows a highly nonlinear behavior, which, if ignored by assuming a linear behavior, may lead to considerable errors in the ensuing analysis (see e.g. the case of soil, Selvadurai, 1979 [235]).

It results very challenging to develop static and dynamic analyses and solutions of systems that include nonlinear underlying supports and are able to predict their behavior over a wide range of loading conditions. Studies pertaining to the static response of nonlinear beam-foundation systems are shortly

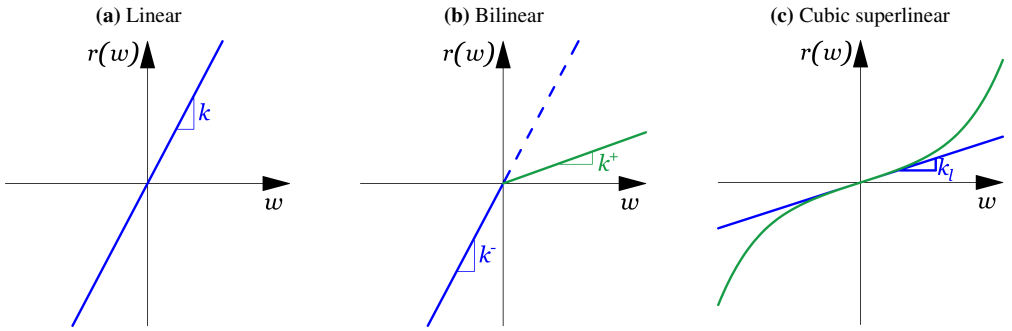

Figure 2.1: Considered behaviors of the elastic Winkler foundation: linear law (a), bilinear law (b), cubic superlinear law (c).

reviewed below, while dynamic investigations will be discussed in the following chapters.

Beaufait and Hoadley (1980) [24] iteratively applied the midpoint difference method for solving the problem of an elastic beam supported by a tensionless nonlinear elastic foundation under arbitrary loads. The nonlinear behavior of the support was approximated by a piecewise linear curve, as in Yankelevsky et al. (1988) [277]. Soldatos and Selvadurai (1985) [242] presented the applications of a perturbation technique for the solution of the nonlinear equation governing the static bending of an Euler-Bernoulli beam resting on a Winkler foundation of the hyperbolic type and subjected to an arbitrary external loading; by using this technique, the initially nonlinear problem was reduced to the solution of a set of linearized equations. It must be pointed out that, the hyperbolic law describing the foundation behavior may not be so realistic, particularly within dynamic contexts, since an unbounded reaction force may be predicted within the admissible range of beam displacements.

Ayoub (2001, 2003) [12, 13] developed a finite element mixed formulation capable of capturing the nonlinear elastic behavior of both the beam and the foundation elements, without sacrificing the computational efficiency.

Up to this point, research studies were pertaining to beams lying on foundations with symmetric mechanical behavior, i.e. displaying the same compression and tension stiffnesses. The extensive use of such supposition was more motivated by the need of the simplifying assumptions toward the mathematical model than by the consistency with physical reality. On the contrary, more realistic models must sometimes be characterized by a foundation producing a reaction which depends not only on the amount of beam displacement, but also on its sign, i.e. if it is upward or downward, even under small deformations.

In the literature, the word “bimodulus” is often used for referring to a material whose stress-strain law is piecewise linear, namely when the material is

characterized by different material parameters in compression and in tension (see e.g. Curnier et al. (1995) [63], in the realm of mechanics of solids). In the context of structural mechanics this type of foundation is defined as bilinear. Thus, by assuming an asymmetric but linear behavior of the foundation, reaction force $r(w)$ supplied by a bilinear elastic support may be defined as follows:

$$r(w) = r\,(w) = k^{+}\,H(w)\,w + k^{-}\,H(-w)\,w, \qquad 0 \leq k^{+} \leq k^{-}; \tag{2.5}$$

where $H(\cdot)$ is the Heaviside function, k^{+} [N/m^2] is the tension stiffness and k^{-} [N/m^2] is the compression stiffness of the bilinear Winkler foundation, as shown in Fig. 2.1b.

The discrepancy in the beam analysis incurred from ignoring the effect of a bilinear behavior of the foundation may be relevant, because the reduced overall stiffness of the system may cause a consistent increase of the beam displacements (Castro et al., 2015 [49]). However, this aspect comes to complicate the analysis and makes it highly non-linear, since the location and extent of the regions of compression and tension is not known in advance. As a result, only a limited number of studies dealing with a bilinear foundation appear to have been explored in the literature, mostly based on numerical methods.

In the earliest work reported in the literature on this class of problems, the static behaviour of infinite beams resting on tensionless elastic foundations (reacting in compression only, k^{+}=0), subjected to a concentrated load and to a uniform distributed weight, was studied by Weitsman (1970) [270]. The employed approach was not very rigorous since the response of the beam placed below the load was directly described by means of the analytical solution of the linear foundation case, thus neglecting the interaction existing along the entire beam length between the segments of the system in compression and in tension.

Pavlović and Tsikkos (1982) [214] developed a simple analytical method for obtaining the static deflection of a beam on a bilinear Winkler foundation based on an a priori guess of the beam deflection shape. As stated by the authors, their method becomes unsuitable when the number of different regions into which the beam deflection changes sign is not small, e.g. long beams subjected to complex loading conditions. To overcome such limitation, Adin et al. (1985) [3], devised an iterative technique to determine the beam tension/compression transition points by using the exact stiffness matrix of finite beams on a linear elastic foundation. Ma et al. (2009) [182] generalized such an approach for obtaining the static response of an infinite beam supported on a tensionless elastic foundation and subjected to arbitrary complex loading, including self-weight.

Zhang and Murphy (2004) [282] developed a simple analytical solution for the static response of a finite beam resting on a tensionless elastic foundation

subjected to a lateral point load of arbitrary position, by assuming that only one contact region may exist along the beam length. Silveira et al. (2008) [238] developed a nonlinear modal solution procedure, based on the Ritz method, capable of solving equilibrium and stability problems of uni-dimensional structural elements (beams, columns and arches) with tensionless Winkler foundation. The limitation of these two studies was an imposed restriction on the type or number of loads or on the number of contact regions, thus adapting a case-by-case resolution according to the most likely deflection shape, which is clearly possible only for simple structural configurations.

Using a FEM approach together with a Newton-Raphson method Kaschiev and Mikhajlov (1995) [152] developed a general method for the calculation of the deflection of a straight beam resting on a tensionless Winkler foundation for different loading conditions. Mullapudi and Ayoub (2010) [205] adopted the mixed formulation of Ayoub (2001,2003) [12, 13] for developing a new element for the nonlinear analysis of inelastic beams resting on two-parameter tensionless foundations. The latter issue was also tackled by Limkatanyu et al. (2015) [179], differing in that a displacement-based formulation was mantained and the displacement shape functions were analytically derived based on the homogeneous solution of the linear beam-foundation system, resulting in an accurate beam-foundation model.

The nonlinear elastic Winkler foundation model with linear plus cubic constitutive law has also been widely recognized as one of the most reliable, particularly in the context of dynamic analyses of railway tracks (Castro et al., 2015 [50]). According to such a model, the reaction-displacement relation of the foundation may be described by the following polynomial cubic law:

$$r(w) = k_l\, w(x) + k_{nl}\, w(x)^3; \tag{2.6}$$

where k_l [N/m^2] is a classical linear Winkler coefficient and k_{nl} [N/m^4] describes an additional nonlinear stiffness coefficient attached to the cubic term. A graphical representation of this model is shown in Fig. 2.1c.

The cubic superlinear model above was employed by Jang and his coworkers (2011, 2012, 2014) [138–140] for validating the method they developed for analyzing the general nonlinear static deflection of an infinite beam resting on a non-linear elastic foundation. By recasting the differential equation into an integral equation using the Green's function of the linear beam-foundation system, the solution was obtained by an iterative technique, based on the Banach contraction mapping theorem. Bhattiprolu et al. (2013) [32] studied the static (and also dynamic) response of a simply-supported beam on both cubic superlinear and tensionless elastic foundation subjected to axial load and arbitrary transverse loads, by the mode superposition method, where each modal amplitude equations were solved by using a Newton-Raphson technique and lift-off points were obtained from the mode shape predicted

at each stage of the iteration. Further studies pertaining to the context of moving load dynamic problem are discussed in Chapter 3.

2.1.3 Spatial variation of stiffness foundation coefficient $k(x)$

Although in the literature numerous investigations pertaining to the complete solution (deflection, pressure, slope, bending moment and shear force) of a beam resting on a Winkler foundation have been reported, to the best of the author's knowledge, very few of them have treated the case of a *variable foundation coefficient*, $k{=}k(x)$, specifically within a *full analytic context*, as briefly discussed below. There might arise circumstances in which the spatial variation of the elastic stiffness coefficient could play a considerable role and thus may not be neglected.

Hayashi (1921) [122] firstly considered a uniform beam on elastic support whose stiffness coefficient varies linearly along the beam's axis and solved the problem by means of a Taylor series expansion; a similar solution technique was also considered by Hetényi (1946) [125]. Hendry's method (1958) [123] constitutes a valuable contribution to the general case of a non-prismatic beam on a non-homogeneous foundation, based on a weighted average of the variable flexural stiffness of the beam and of foundation coefficient $k(x)$ with respect to some appropriate "basic functions". Iyengar and Anantharamu (1963) [135] suggested solutions in the form of series of characteristic functions representing the normal modes of transverse vibration of a beam on a Winkler foundation with uniform stiffness coefficient; at a later stage, they also proved the method to be suitable for the construction of tables for the influence lines (see Iyengar and Anantharamu (1965) [136]). The same year Klepikov (1965) [165] proposed a numerical method to determine the static response for a general space variation of $k(x)$. Snitko (1968) [241] determined the static response of a beam embedded in a Winkler support under axial and transverse loading, with a subgrade coefficient having a parabolic variation $k(x){=}k\,x^2$.

Another solution approach, based on the generalized Laplace transform and on an asymptotic analysis (see e.g. Bleistein and Handelsman, 1986 [35]), was later proposed by Franklin and Scott (1979) [95]. The authors presented an integral-form solution for a uniform beam on an elastic foundation, whose coefficient varies linearly with axis coordinate x, by using contour integrals. In addition, they developed a numerical method applied to semi-infinite beams for a foundation coefficient going as a general power law, i.e. $k(x){=}k\,x^p$. Also, Lentini (1979) [174] numerically solved the same problem by applying a FD scheme. Further, Clastornik et al. (1986) [60] proposed a power series approximation of the solution and a method to assemble the structural stiffness matrix for finite beams with support coefficient represented by a general polynomial of x. By developing a Green's function formulation, Guo and Weits-

man (2002) [117] derived the beam static response for a non-uniform elastic support.

Boundary integral equation methods may be found in the work of Horibe (1996) [130]. Chen (1998) [52] developed a numerical approach, the Differential Quadrature Element Method (DQEM), for solving the static response of a beam resting on an elastic foundation. Guo and Weitsman (2002) [117] evaluated the static response of beams on a non-uniform elastic foundation by employing a Green's function formulation, which resulted in a system of non-singular integral equations, solved numerically by a Gauss–Legendre quadrature scheme. Frydrýšek (2012) [106] derived an approximate solution in the form of polynomial functions and used it for a probabilistic analysis (SBRA: Simulation-Based Reliability Assessment method)

Liang et al. (2014) [177] developed a simplified approximate analytical solution for laterally loaded long piles, embedded in a soil with a stiffness linearly increasing with depth, based on a Fourier-Laplace integral approach, together with a power series solution for small depths and a Wentzel-Kramers-Brillouin (WKB) asymptotic expansion for large depths. On the other hand, it appears that there are no works in the literature pertaining to the closed-form analytical solution for the static deformed configuration of a beam lying on a Winkler foundation with a linear variation of the elastic support coefficient.

Fully numerical techniques, such as Finite Differences schemes (FD) and the Finite Element Method (FEM), have also become very popular and have been successfully applied for solving problems based on Winkler-like or even more complicated nonlinear models of the support, such as uniform beams on nonlinear elastic foundation (Yankelevsky et al., 1989 [278], Filipich and Rosales, 2002 [92], Ebrahimi and Barati, 2016 [81]) or non-uniform beams on nonlinear elastic foundation (Tsiatas, 2010 [256], Jang, 2014 [138]).

Although such widespread diffusion of numerical techniques, analytical and semi-analytical methods are still needed and constitute an essential part of the theoretical background. This not only in view of a parametric interpretation of the static and dynamic response of the structural system, but also because analytical solutions appear to be more suitable than FEM-based or numerical modelizations, towards final design and identification purposes (see e.g. Prasad, 1981 [221] and Froio et al., 2017 [102], for moving load problems; Joodaky and Joodaky, 2015 [148], for plate-foundation interaction; Jang, 2013 [137], in the framework of large deflection analysis of infinite beams; Khajeansari et al., 2012 [161], in the context of nanostructures).

However, it appears that there are no works available in the literature pertaining to the analytical solution for the static deformed configuration when the elastic support coefficient varies analytically along the beam axis, with trends other than linear (treated in Franklin and Scott, 1979 [95]). For the just-mentioned reasons, in the following, the exact closed-form analytical so-

lutions of a finite beam embedded within an elastic Winkler foundation whose coefficient varies in space according to two different specific trends are derived.

According to Ince (1978) [133], apart from equations with constant coefficients, and such equations which, by a change of variables, can be brought back to the latter case, there is no known general method for the full and explicit integration in terms of *"elementary functions"* of Ordinary Differential Equations of a general order n, even if linear. Sometimes, equations which arise out of problems of applied mathematics and which are not reducible to equations with constant coefficients, generate as their solutions new *"transcendental functions"*. Both these two occurrences are treated in this chapter, as outlined next.

In Section 2.2, the analytical static bending response of a uniform free-free Euler-Bernoulli elastic beam resting on an elastic Winkler foundation with linearly varying foundation coefficient is derived by employing generalized hypergeometric functions. On the other hand, by a change of variable, the analytical solution of the static deflection of a simply-supported Euler-Bernoulli elastic beam lying on an elastic Winkler foundation endowed with a nonlinear, minus four power spatial variation of the stiffness coefficient $k(x)$ is sought in terms of elementary functions in Section 2.3. Then, by the achieved analytical solutions, parametric studies are carried out to accurately investigate the influence of the beam-foundation mechanical parameters on the resulting elastic bending structural response. A discussion on the two solutions has been reported by Froio and Rizzi (2017) [99] for the linear case and by Froio and Rizzi (2016) [98] for the nonlinear case.

2.2 Analytical bending solution for linear $k(x)=k_0+k_1x$

2.2.1 Problem formulation

Consider now a uniform free-free elastic beam lying on a Winkler foundation, whose schematic representation is depicted in Fig. 2.2a, under the action of a horizontal force F [N] and a moment W [Nm] applied at its top-end. A right-handed Cartesian coordinate system (x,y,z) is assumed, with the origin at the centroid of the top-end beam cross-section (point A); the x-axis is taken downward, while the y- and z-axes are taken along the principal axes of the beam cross-section (positive y direction is taken horizontally leftward). Positive cross-section rotations are taken according to a right-handed screw rule. Positive bending moment M [Nm] marks tensile stresses in the left beam edge and positive shear S [N] corresponds to the top beam side moving rightward.

Within this reference, the well-known Ordinary Differential Equation (ODE) governing the transverse static deflection of a slender uniform Euler-Bernoulli elastic beam resting on an elastic Winkler foundation in the infinitesimal strain

framework is the following (e.g. Hetényi, 1946 [125]):

$$\big(E(x)J(x)w_x^{(2)}(x)\big)_x^{(2)}+k(x)\,w(x)=p(x);\quad 0\le x\le L,\quad k(x)>0; \tag{2.7}$$

where $E(x)$ [N/m^2] is the elastic modulus of the material, $J(x)$ [m^4] is the moment of inertia of the beam cross-section around the z-axis and L is the beam length; beam deflection has been labeled by $w(x)$ [m] (positive along the y direction), as represented in Fig. 2.12, meanwhile $p(x)$ [N/m] and $k(x)$ denote the externally-applied distributed vertical forces acting on the beam and the stiffness coefficient of the elastic support, respectively, the latter with the meaning exposed in Section 2.1. It is straightforward to note that differential operator

$$\mathcal{L}(\,\cdot\,)=\big(E(x)J(x)(\,\cdot\,)_x^{(2)}\big)_x^{(2)}+k(x)(\,\cdot\,); \tag{2.8}$$

acting on $w(x)$ is linear, since it is made of a linear combination of derivatives, which are themselves linear operators. Then, since unknown function $w(x)$ is derived four times in spatial variable x, Eq. (2.7) is a non-homogeneous linear fourth–order ODE in unknown function $w(x)$.

Further, consider the case where elastic stiffness coefficient $k(x)$ may be expressed as a linear function of spatial position $x{=}\xi L$, as follows:

$$\begin{aligned} &k(x)=k_0+\frac{k_L-k_0}{L}\,x=k_0+k_1x=k_0(1+\beta\,\xi);\\ &k_1=\frac{k_L-k_0}{L};\qquad \beta=\frac{k_1L}{k_0}=\frac{k_L}{k_0}-1; \end{aligned} \tag{2.9}$$

where k_0 and k_L [N/m^2] are the point-wise values of the spring stiffness at the top and bottom ends of the beam, respectively, k_1 [N/m^3] is the slope of $k(x)$, while β is a non-dimensional parameter describing the relative difference between k_L and k_0; both the latter parameters represent the steepness of $k(x)$.

In such a frame, the transverse static deflection of a geometrically-linear uniform Euler-Bernoulli elastic beam lying on an elastic Winkler support is governed by Eq. (2.7). By neglecting now the presence of external distributed horizontal forces ($p(x){=}0$), the mechanical problem in Fig. 2.2a is described through the following two-point BVP:

$$EJw_x^{(4)}(x)+(k_0+k_1x)\,w(x)=0,\qquad 0<x<L; \tag{2.10a}$$

$$w_x^{(2)}(0)=-W/EJ; \tag{2.10b}$$

$$w_x^{(3)}(0)=-F/EJ; \tag{2.10c}$$

$$w_x^{(2)}(L)=0; \tag{2.10d}$$

$$w_x^{(3)}(L)=0; \tag{2.10e}$$

where Eqs. (2.10b)-(2.10e) represent the boundary conditions.

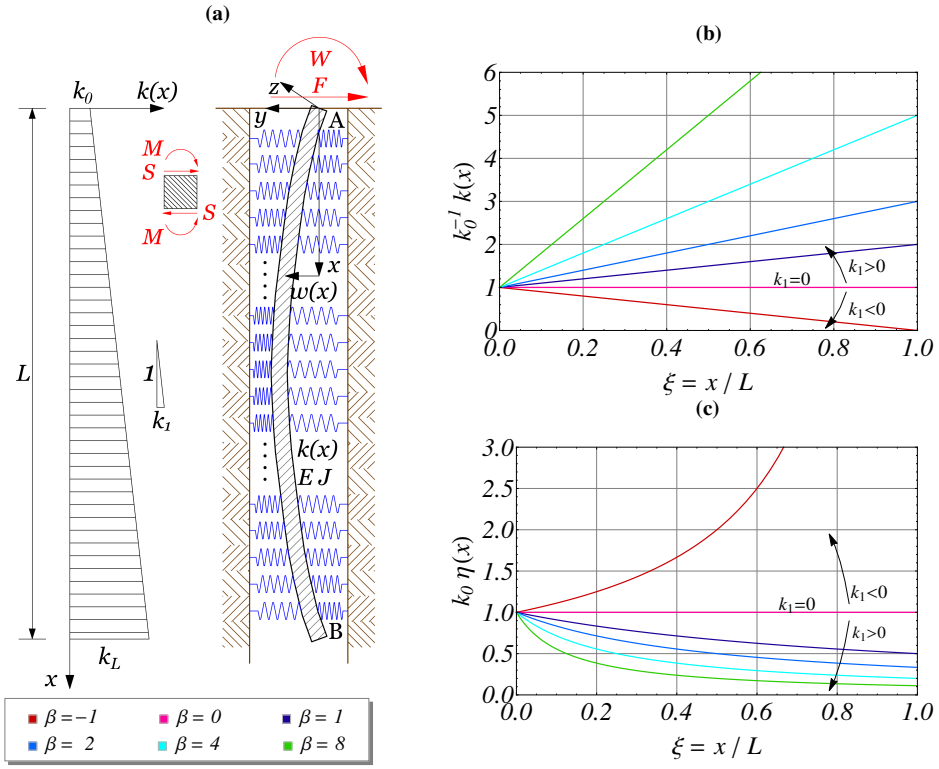

Figure 2.2: Finite free-free Euler-Bernoulli elastic beam on elastic Winkler support with linearly-varying stiffness coefficient $k(x)$ **(a)**, trends of stiffness coefficient $k(x)$ **(b)** and of its reciprocal compliance coefficient $\eta(x)$ **(c)** vs. non-dimensional space coordinate $\xi{=}x/L$, for various values of $\beta{=}k_1/(k_0/L){=}k_L/k_0 - 1$.

This type of problem may resemble practical situations encountered in foundation engineering, for instance when dealing with piles embedded in cohesionless soils (Madhav et al., 1971 [183]), subjected to horizontal loads, and with shallow foundations, where the stiffness of the foundation medium may be modeled as a linear function of depth (Randolph, 1981 [222]).

In order to fulfill physical condition $k(x){\leq}0$ in the interval $[0,\ L]$, parameters k_0, k_L and k_1 must satisfy the following restrictions:

$$k_0 > 0, \qquad k_L > 0 \qquad \text{and} \qquad k_1 \geq -\frac{k_0}{L}; \tag{2.11}$$

or, equivalently, parameter $\beta{\geq}{-}1$, due to the third condition in Eq. (2.11). A representation of the trends of stiffness $k(x)$ ensuing from Eq. (2.9) is given in Fig. 2.2b, for various values of parameter $\beta{\geq}{-}1$. In Fig. 2.2c, its reciprocal compliance $\eta(x)$ [L]^2/[F] is represented as well.

The solution of Eq. (2.10a) may be derived by employing generalized hypergeometric functions (see Erdélyi, 1953 [87]), as outlined in the next section.

2.2.2 Solution of the homogeneous equation

For solving BVP (2.10) with a linear $k(x)$ as given in Eq. (2.9), it is convenient to change independent variable x to a new nondimensional variable s, defined as

$$s = \frac{k(x)}{\gamma}; \qquad \gamma = \sqrt[5]{EJk_1^4} > 0 \quad \frac{[\mathrm{F}]}{[\mathrm{L}]^2}; \qquad \frac{k_0}{\gamma} < s < \frac{k_L}{\gamma}; \tag{2.12}$$

and, consequently, the derivative of s with respect to x is

$$s_x^{(1)} = \frac{k_L - k_0}{\gamma L} = \frac{k_1}{\gamma}. \tag{2.13}$$

Such a change of variable leads to the following new BVP problem:

$$w_s^{(4)}(s) + s\, w(s) = 0; \qquad k_0/\gamma < s < k_L/\gamma; \tag{2.14a}$$

$$w_s^{(2)}(k_0/\gamma) = w_s^{(2)}\left(\alpha^{\frac{1}{5}}\,\beta^{-\frac{4}{5}}\right) = -(\alpha\,\beta)^{-\frac{2}{5}}\, WL^2/EJ; \tag{2.14b}$$

$$w_s^{(3)}(k_0/\gamma) = w_s^{(3)}\left(\alpha^{\frac{1}{5}}\,\beta^{-\frac{4}{5}}\right) = -(\alpha\,\beta)^{-\frac{3}{5}}\, FL^3/EJ; \tag{2.14c}$$

$$w_s^{(2)}(k_L/\gamma) = w_s^{(2)}\left(\alpha^{\frac{1}{5}}\,\beta^{-\frac{4}{5}}(1+\beta)\right) = 0; \tag{2.14d}$$

$$w_s^{(3)}(k_L/\gamma) = w_s^{(3)}\left(\alpha^{\frac{1}{5}}\,\beta^{-\frac{4}{5}}(1+\beta)\right) = 0; \tag{2.14e}$$

where non-dimensional parameter α is defined as follows:

$$\alpha = 4(\lambda_0 L)^4 > 0; \qquad \lambda_0 = \sqrt[4]{\frac{k_0}{4EJ}}; \tag{2.15}$$

and λ_0 1/[L] is the so-called wave number of the static solution in case of a classical elastic Winkler foundation with constant coefficient $k(x)$=k_0, namely 2π times the inverse of the wavelength of the resulting static displacement function (Hetényi, 1946 [125]).

Notice that such reformulation of BVP (2.10) is possible by a limitation on the admissible values of k_1, due to existence condition $\gamma \neq 0$ ensuing from the definition of s in Eq. (2.12). Condition k_1=0 (γ=0, β=0), corresponding to a constant elastic stiffness coefficient $k(x)$=k_0 (classical Winkler model), represents a singular case in the following derivation, meaning that the solution of such a case cannot be directly obtained from the solution that is going to be determined in the next section. The solution for $k(x)$=k_0, whose general integral is available from many classical sources (e.g. Hetényi, 1946 [125]), is also derived later (Section 2.2.4), for the specific boundary conditions considered in Eqs. (2.10).

Both real, non-dimensional parameters $\alpha > 0$ and $\beta \geq -1$, as defined in Eqs. (2.15) and (2.9), respectively, represent the influence of the characteristic features of both the beam and the substratum on the global behavior of

the beam-foundation system. In particular, α is a parameter describing the relative flexibility of the beam-foundation system evaluated at the top end of the beam (x=0), while β is a ratio representing the steepness of the elastic stiffness coefficient variation along the beam axis with respect to its starting value k_0.

Since Eq. (2.14a) is a homogeneous linear ODE, it is well-known that its general integral $w_H(s)$, also called complementary function, if it exists, is given by a linear combination of four linearly independent functions $w_{H_i}(s)$ with complex coefficients C_i (Ince, 1978 [133]), each satisfying Eq. (2.14a):

$$w(s) = \sum_{i=1}^{4} C_i w_{H_i}(s); \tag{2.16}$$

where four constants C_i have to be determined by imposing boundary conditions (2.14b)-(2.14e) on the obtained expression of $w(s)$.

It may be noticed that, as a results of the substitution provided by Eq. (2.12), characteristic parameters α and β appear only in the boundary conditions of BVP (2.14), i.e. none of them appears in differential Eq. (2.14a). Therefore, the fundamental set of solutions $w_{H_i}(s)$ is invariant with respect to parameters α and β, which influence only four constants C_i.

For the purpose of the forthcoming analytical developments, at this stage it is worthwhile to introduce the *generalized hypergeometric function*, which, as reported by Erdélyi (1953) [87], is a high-transcendental function endowed with the following form:

$${}_pF_q\left(\mathbf{a};\mathbf{b};t\right) = {}_pF_q\left(a_1,\ldots,a_p;b_1,\ldots,b_q;t\right) = 1 + \sum_{n=1}^{\infty} \frac{\prod_{j=1}^{p}(a_j)_n}{\prod_{j=1}^{q}(b_j)_n} \frac{t^n}{n!}; \tag{2.17}$$

where p numbers a_j are called numerator-parameters, q numbers b_j are referred to as denominator-parameters and $(c)_n$ is the Pochhammer symbol, defined as follows:

$$(c)_n = c(c+1)\ldots(c+n-1) = \frac{\Gamma(c+n)}{\Gamma(c)}; \tag{2.18}$$

and $\Gamma(\cdot)$ is the *Gamma function* (see e.g. Bleistein and Handelsman,1986 [35]). In case of null indexes p, q the corresponding finite products are assumed to be equal to one. The derivation of the fundamental set of solutions $w_{H_i}(s)$ (i=1,...,4) of Eq. (2.14a) and the complete determination of the analytical solution of BVP (2.14) are carried out in the following section.

In order to determine a fundamental set of solutions $w_{H_i}(s)$, the differential equation may be multiplied by s^4 yielding:

$$s^4\, w_s^{(4)}(s) + s^5\, w(s) = 0; \qquad k_0/\gamma < s < k_L/\gamma; \tag{2.19}$$

and by further introducing a new independent, always negative, non-dimensional variable t for $w(t)$, defined as follows:

$$\begin{aligned} t &= -\frac{s^5}{5^4}, \qquad\qquad w_s^{(1)} = -5^{\frac{1}{5}} t^{\frac{4}{5}} w_t^{(1)}, \\ w_s^{(4)} &= 5^{\frac{4}{5}} t^{\frac{16}{5}} w^{(4)} + \frac{24}{5^{\frac{1}{5}}}\, t^{\frac{11}{5}} w_t^{(3)} + \frac{96}{5^{\frac{6}{5}}}\, t^{\frac{6}{5}} w_t^{(2)} + \frac{24}{5^{\frac{11}{5}}}\, t^{\frac{1}{5}} w_t^{(1)}; \end{aligned} \tag{2.20}$$

Eq. (2.19) becomes

$$\begin{aligned} & t^4 w_t^{(4)} + \frac{24}{5} t^3 w_t^{(3)} + \frac{96}{25} t^2 w_t^{(2)} + \frac{24}{125} t w_t^{(1)} - t w = 0; \\ & -\frac{k_0^5}{5^4 \gamma^5} < t < -\frac{k_L^5}{5^4 \gamma^5}. \end{aligned} \tag{2.21}$$

Upon denoting δ differential operator $t(\ \cdot\ )_t^{(1)}$, which gives the general relation

$$t^i (\ \cdot\ )_t^{(i)} = \delta(\delta - 1)(\delta - 2) \cdots (\delta - i + 1); \tag{2.22}$$

Eq. (2.21) may be finally written in the form

$$\delta \left(\delta - \frac{1}{5}\right) \left(\delta - \frac{2}{5}\right) \left(\delta - \frac{3}{5}\right) w - t w = 0. \tag{2.23}$$

The general integral of Eq. (2.23) may be expressed as a linear combination of independent generalized hypergeometric functions (see Erdélyi, 1953 [87]), as follows:

$$\begin{aligned} w(t) = & \sum_{i=1}^{4} C_i w_{H_i}(t) = \\ = & C_1\ {}_0F_3\left(\text{-}; \frac{2}{5}, \frac{3}{5}, \frac{4}{5}; t\right) + C_2\ t^{\frac{1}{5}}\ {}_0F_3\left(\text{-}; \frac{3}{5}, \frac{4}{5}, \frac{6}{5}; t\right) + \\ & C_3\ t^{\frac{2}{5}}\ {}_0F_3\left(\text{-}; \frac{4}{5}, \frac{6}{5}, \frac{7}{5}; t\right) + C_4\ t^{\frac{3}{5}}\ {}_0F_3\left(\text{-}; \frac{6}{5}, \frac{7}{5}, \frac{8}{5}; t\right); \end{aligned} \tag{2.24}$$

where, for instance, the first solution in the linear combination above takes the form

$$\begin{aligned} {}_0F_3\left(\text{-}; \frac{2}{5}, \frac{3}{5}, \frac{4}{5}; t\right) = & 1 + \sum_{n=1}^{\infty} \frac{1}{\left(\frac{2}{5}\right)_n \left(\frac{3}{5}\right)_n \left(\frac{4}{5}\right)_n} \frac{t^n}{n!} = \\ = & 1 + \sum_{n=1}^{\infty} \frac{\Gamma\left(\frac{2}{5}\right) \Gamma\left(\frac{3}{5}\right) \Gamma\left(\frac{4}{5}\right)}{\Gamma\left(\frac{2}{5} + n\right) \Gamma\left(\frac{3}{5} + n\right) \Gamma\left(\frac{4}{5} + n\right)} \frac{t^n}{n!}; \end{aligned} \tag{2.25}$$

obtained by setting p=0 and q=3 in the definition provided in Eq. (2.17). As a consequence, according to Erdélyi (1953) [87], ${}_pF_q\left(\mathbf{a}; \mathbf{b}; t\right)$ converges for

all finite t when $p \leq q$, the point at infinity being the only singularity of the differential equation, as displayed in Fig. 2.3.

Hence, the general integral of Eq. (2.19) is obtained by substituting the definition of t provided in Eq. (2.20) into Eq. (2.26), as follows:

$$\begin{aligned} w(s) = C_1\, {}_0F_3\left(\text{-}\,;\frac{2}{5},\frac{3}{5},\frac{4}{5};-\frac{s^5}{5^4}\right) + C_2\, {}_0F_3\left(\text{-}\,;\frac{3}{5},\frac{4}{5},\frac{6}{5};-\frac{s^5}{5^4}\right)s + \\ C_3\, {}_0F_3\left(\text{-}\,;\frac{4}{5},\frac{6}{5},\frac{7}{5};-\frac{s^5}{5^4}\right)s^2 + C_4\, {}_0F_3\left(\text{-}\,;\frac{6}{5},\frac{7}{5},\frac{8}{5};-\frac{s^5}{5^4}\right)s^3; \end{aligned} \tag{2.26}$$

with C_i already introduced in Eq. (2.16). A necessary and sufficient condition for functions $w_{H_i}(s)$ in Eq. (2.31) being linearly independent, i.e. to form a fundamental set of solutions of Eq. (2.21) is that (see Ince, 1978 [133]):

$$\mathcal{W}(w_{H_1}, \ldots, w_{H_4})(s) \neq 0; \tag{2.27}$$

where, by defining fundamental matrix $\mathbf{\Phi}_H(s)$ as follows:

$$\mathbf{\Phi}_H(s) = \begin{pmatrix} w_{H_1}(s) & w_{H_2}(s) & w_{H_3}(s) & w_{H_4}(s) \\ w_{H_1}^{(1)}(s) & w_{H_2}^{(1)}(s) & w_{H_3}^{(1)}(s) & w_{H_4}^{(1)}(s) \\ w_{H_1}^{(2)}(s) & w_{H_2}^{(2)}(s) & w_{H_3}^{(2)}(s) & w_{H_4}^{(2)}(s) \\ w_{H_1}^{(3)}(s) & w_{H_2}^{(3)}(s) & w_{H_3}^{(3)}(s) & w_{H_4}^{(3)}(s) \end{pmatrix}; \tag{2.28}$$

Wronskian $\mathcal{W}(w_{H_1}, \ldots, w_{H_4})(s) = \det\, \mathbf{\Phi}_H(s)$ is its determinant.

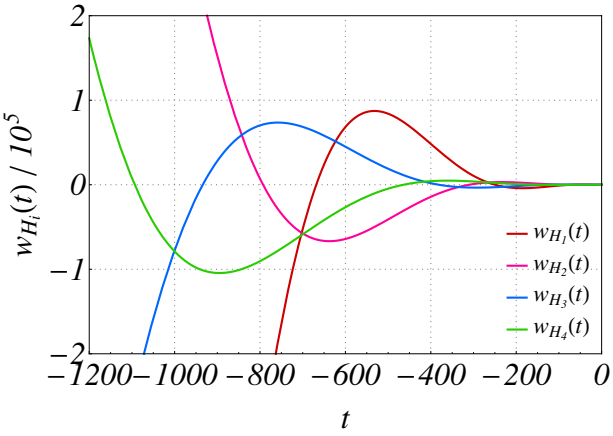

Figure 2.3: Fundamental set of solutions of differential Eq. (2.21).

By virtue of Abel identity (Ince, 1978 [133]), it suffices to verify non-zero property $\mathcal{W}(s_0) \neq 0$ for an arbitrary point s_0, to demonstrate condition $\mathcal{W}(s) \neq 0$

for all s. Then, by fixing s_0=0 one gets

$$\mathcal{W}(w_{H_1},\ldots,w_{H_4})(0)=\det\,\mathbf{\Phi}_H(0)=\begin{vmatrix}1&0&0&0\\0&1&0&0\\0&0&2&0\\0&0&0&6\end{vmatrix}=12; \tag{2.29}$$

where the following identity has been applied for derivatives

$${}_0F_3\Big(\text{-};b_1,\ldots,b_q;g(t)\Big)_t^{(1)}=\frac{g_t^{(1)}(t)}{\prod_{j=1}^{q}b_j}\;{}_0F_3\Big(\text{-};b_1+1,\ldots,b_q+1;g(t)\Big). \tag{2.30}$$

Hence, $w_{H_i}(s)$ in Eq. (2.24) indeed form a fundamental set of solutions of Eq. (2.21).

2.2.3 Solution of the boundary value problem

The imposition of boundary conditions (2.14b)-(2.14e) to the general integral in Eq. (2.31) leads to the following linear system:

$$\underbrace{\begin{pmatrix} w_{H_1}^{(2)}\!\left(\frac{k_0}{\gamma}\right) & w_{H_2}^{(2)}\!\left(\frac{k_0}{\gamma}\right) & w_{H_3}^{(2)}\!\left(\frac{k_0}{\gamma}\right) & w_{H_4}^{(2)}\!\left(\frac{k_0}{\gamma}\right)\\ w_{H_1}^{(3)}\!\left(\frac{k_0}{\gamma}\right) & w_{H_2}^{(3)}\!\left(\frac{k_0}{\gamma}\right) & w_{H_3}^{(3)}\!\left(\frac{k_0}{\gamma}\right) & w_{H_4}^{(3)}\!\left(\frac{k_0}{\gamma}\right)\\ w_{H_1}^{(2)}\!\left(\frac{k_L}{\gamma}\right) & w_{H_2}^{(2)}\!\left(\frac{k_L}{\gamma}\right) & w_{H_3}^{(2)}\!\left(\frac{k_L}{\gamma}\right) & w_{H_4}^{(2)}\!\left(\frac{k_L}{\gamma}\right)\\ w_{H_1}^{(3)}\!\left(\frac{k_L}{\gamma}\right) & w_{H_2}^{(3)}\!\left(\frac{k_L}{\gamma}\right) & w_{H_3}^{(3)}\!\left(\frac{k_L}{\gamma}\right) & w_{H_4}^{(3)}\!\left(\frac{k_L}{\gamma}\right) \end{pmatrix}}_{\mathbf{B}}\underbrace{\begin{pmatrix}C_1\\C_2\\C_3\\C_4\end{pmatrix}}_{\mathbf{C}}=\underbrace{\begin{pmatrix}0\\\hat{F}\\0\\0\end{pmatrix}}_{\mathbf{f}_F}+\underbrace{\begin{pmatrix}\hat{M}\\0\\0\\0\end{pmatrix}}_{\mathbf{f}_W} \tag{2.31}$$

where

$$\hat{F}=-\frac{FL^3}{(\alpha\,\beta)^{\frac{3}{5}}\,EJ},\qquad \hat{M}=-\frac{WL^2}{(\alpha\,\beta)^{\frac{2}{5}}\,EJ}; \tag{2.32}$$

which in compact form may be written as

$$\mathbf{B}\,\mathbf{C}=\mathbf{f}_F+\mathbf{f}_W,\qquad \sum_{j=1}^{4}B_{ij}C_j=f_{F_i}+f_{W_i},\qquad i=1,2,3,4; \tag{2.33}$$

with corresponding meaning of symbols.

In order to provide a complete understanding of the behavior of the beam-foundation system, by taking advantage of the linearity of Eq. (2.10a), the

superposition principle may be applied to decompose the response into two contributions, each one relative only to the action either of force F or of moment W, respectively, as follows:

$$w(\xi) = w_F(\xi) + w_W(\xi). \tag{2.34}$$

Therefore, it is possible to split the linear system in Eq. (2.31) into two subsystems, the first with $F{\neq}0$, $W{=}0$ and the second with $F{=}0$, $W{\neq}0$:

$$\mathbf{B}\,\mathbf{C}_F = \mathbf{f}_F; \tag{2.35a}$$

$$\mathbf{B}\,\mathbf{C}_W = \mathbf{f}_W. \tag{2.35b}$$

Then, the expressions of coefficients C_i of Eq. (2.26) such that $w(s)$ is the solution of boundary value problem (2.14) may be written as

$$C_i = C_{F_i} + C_{W_i} = \left(c_{F_i}\,FL + c_{W_i}\,W\,(\alpha\,\beta)^{\frac{1}{5}}\right)\frac{(\alpha\,\beta)^{-\frac{3}{5}}\,L^2}{D(\alpha,\beta)\,EJ}; \tag{2.36}$$

provided that denominator term $D(\alpha,\beta)$, which is the determinant of matrix $\mathbf{B}$ in Eqs. (2.31)-(2.33), is different from zero. The expression of determinant $D(\alpha,\beta)$ is rather lengthy; then, it is not reported here. Coefficients c_{F_i} and c_{W_i} represent the unknown non-dimensional counterparts of C_{F_i} and C_{W_i}, respectively, as defined in Eq. (2.36). Since the $w_{H_i}(s)$ form a fundamental set of solutions, it is possible to check that $D(\alpha,\beta){=}\det(\mathbf{B})$ is a non-zero quantity provided that $k_0{\neq}k_L$, that is except for the limit cases when $k_1{=}0$ ($\beta{=}0$) (see the following section). Hence, coefficients C_i are always well-defined for every value of parameters $\alpha{>}0$ and $\beta \in [-1,0)\cup(0,\infty)$.

Coefficients c_{W_i} and c_{F_i} are listed in Table 2.1 and Table 2.2. All calculations have been developed within Mathematica [274]. Once the existence of a solution of BVP (2.10) has been proven, its uniqueness is straightforward, by virtue of the linearity of Eq. (2.10a).

From the expressions of coefficients C_i in Eq. (2.36), the solution is proportional to both external actions F and W, as it was expected from the linearity of the differential equation. The representation and interpretation of the achieved analytical solution is presented and discussed in following Section 2.2.5, but, first, the particular case of a constant foundation coefficient ($\beta{=}0$, classical Winkler foundation) is commented below. The achieved analytical representation is finally resumed in synoptic form in the sketch provided in Fig. 2.4.

2.2.4 Singular case

In the previous section it has been noticed that functions $w_{H_i}(s)$ are improper to represent the solution of Eq. (2.10a) when $\beta{=}\gamma{=}k_1{=}0$. In fact, for $\beta{=}0$ the linear system in Eq. (2.31) is not invertible, hence, not leading to a definition of

SYNOPSIS OF THE ANALYTICAL SOLUTION

Governing differential equation and boundary conditions

- $EJw^{(4)}(x) + k(x)\,w(x) = 0; \qquad 0 < x < L, \qquad k(x) = k_0 + k_1 x \geq 0;$
- $w^{(2)}(0) = -W/EJ; \quad w^{(3)}(0) = -F/EJ; \quad w^{(2)}(L) = 0; \quad w^{(3)}(L) = 0;$

Definitions

- $\xi = \dfrac{x}{L}; \qquad \lambda_0 = \sqrt[4]{\dfrac{k_0}{4EJ}}; \qquad \alpha = 4(\lambda_0 L)^4; \qquad \beta = \dfrac{k_1\,L}{k_0}.$

General solution

- $w(\xi) = \displaystyle\sum_{i=1}^{4} C_i w_{H_i}(\xi); \qquad 0 < \xi < 1;$
- $w_{H_i}(\xi) = {}_0F_3\left(\text{-}; \left\{\dfrac{\iota_{ij}}{5}\right\}; -\dfrac{s^5(\xi)}{5^4}\right) s^{i-1}(\xi); \quad i=1,2,3,4; \quad j=1,2,3; \quad \boldsymbol{\iota} = \begin{pmatrix} 2 & 3 & 4 \\ 3 & 4 & 6 \\ 4 & 6 & 7 \\ 6 & 7 & 8 \end{pmatrix};$
- ${}_0F_3\left(\text{-}; \{\iota_{ij}\}; t\right) = 1 + \displaystyle\sum_{n=1}^{\infty} \frac{\Gamma(\iota_{i1})\,\Gamma(\iota_{i2})\,\Gamma(\iota_{i3})}{\Gamma(\iota_{i1}+n)\,\Gamma(\iota_{i2}+n)\,\Gamma(\iota_{i3}+n)}\,\frac{t^n}{n!};$
- $s(\xi) = \alpha^{\frac{1}{5}}\,\beta^{-\frac{4}{5}}(1+\beta\,\xi);$
- $C_i = \left(c_{F_i}\,FL + c_{W_i}\,W\,(\alpha\,\beta)^{\frac{1}{5}}\right) \dfrac{(\alpha\,\beta)^{-\frac{3}{5}}\,L^2}{D(\alpha,\beta)\,EJ};$
- $D(\alpha,\beta) = \det\Big(\mathbf{B}(\alpha,\beta)\Big); \quad B_{ij}(\alpha,\beta) = w_{H_j}^{\left(\frac{5+(-1)^i}{2}\right)}\left(\dfrac{k_\kappa}{\gamma}\right); \quad \kappa = \begin{cases} 0 & i = 1,2 \\ L & i = 3,4 \end{cases};$
- $c_{F_i} \rightarrow Table\ 2.1; \qquad c_{W_i} \rightarrow Table\ 2.2.$

Figure 2.4: Summary of the main steps of the analytical solution.

c_{F_1}:	$B_{12}\,(B_{33}B_{44} - B_{34}B_{43}) + B_{13}\,(B_{34}B_{42} - B_{32}B_{44}) + B_{14}\,(B_{32}B_{43} - B_{33}B_{42})$
c_{F_2}:	$B_{11}\,(B_{34}B_{43} - B_{33}B_{44}) + B_{13}\,(B_{31}B_{44} - B_{34}B_{41}) + B_{14}\,(B_{33}B_{41} - B_{31}B_{43})$
c_{F_3}:	$B_{11}\,(B_{32}B_{44} - B_{34}B_{42}) + B_{12}\,(B_{34}B_{41} - B_{31}B_{44}) + B_{14}\,(B_{31}B_{42} - B_{32}B_{41})$
c_{F_4}:	$B_{11}\,(B_{33}B_{42} - B_{32}B_{43}) + B_{12}\,(B_{31}B_{43} - B_{33}B_{41}) + B_{13}\,(B_{32}B_{41} - B_{31}B_{42})$

Table 2.1: Expressions of coefficients c_{F_i} of C_{F_i}.

c_{W_1}:	$B_{22}\,(B_{34}B_{43} - B_{33}B_{44}) + B_{23}\,(B_{32}B_{44} - B_{34}B_{42}) + B_{24}\,(B_{33}B_{42} - B_{32}B_{43})$
c_{W_2}:	$B_{21}\,(B_{33}B_{44} - B_{34}B_{43}) + B_{23}\,(B_{34}B_{41} - B_{31}B_{44}) + B_{24}\,(B_{31}B_{43} - B_{33}B_{41})$
c_{W_3}:	$B_{21}\,(B_{34}B_{42} - B_{32}B_{44}) + B_{22}\,(B_{31}B_{44} - B_{34}B_{41}) + B_{24}\,(B_{32}B_{41} - B_{31}B_{42})$
c_{W_4}:	$B_{21}\,(B_{32}B_{43} - B_{33}B_{42}) + B_{22}\,(B_{33}B_{41} - B_{31}B_{43}) + B_{23}\,(B_{31}B_{42} - B_{32}B_{41})$

Table 2.2: Expressions of coefficients c_{W_i} of C_{W_i}.

four constants C_i. For these specific value of β, the solution has to be derived independently from Eq. (2.26).

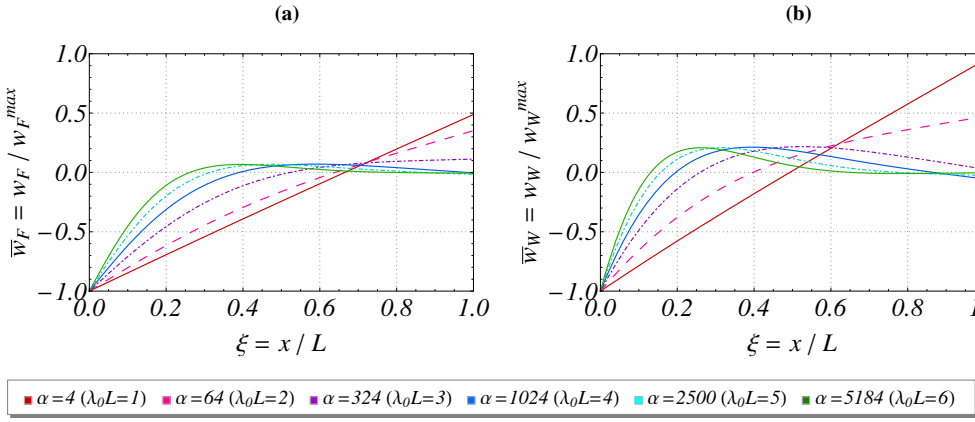

Figure 2.5: Normalized shape of elastic deflection $\overline{w}_F(\xi)$ for various values of $\lambda_0 L$ when the elastic stiffness coefficient of the foundation is constant, $k(x)=k$ ($F\neq 0$, $W=0$ (a); $F=0$, $W\neq 0$ (b)).

If $\beta=0$, that is $k_1=0$, the problem is brought back to that of a free-free beam lying on an elastic Winkler foundation with constant modulus ($k(x)=k_0$). The solution, derived according to the theory of linear ODE with constant coefficients, is the following:

$$w(\xi)_{\beta=0} = \big(w_F(\xi) + w_W(\xi)\big)_{\beta=0} = \frac{4\,F}{\lambda_0\,E J\,d}\,h_F(\xi) + \frac{W}{E J\,d}\,h_W(\xi); \quad (2.37a)$$

$$d = 4\lambda_0^2\Big(\cos(2\lambda_0 L) + \cosh(2\lambda_0 L) - 2\Big); \quad (2.37b)$$

$$h_F(\xi) = \sin(\lambda_0 L)\cosh(\lambda_0 L\xi)\cos\Big(\lambda_0 L\,(1-\xi)\Big) + \\ - \sinh(\lambda_0 L)\cos(\lambda_0 L\xi)\cosh\Big(\lambda_0 L\,(1-\xi)\Big); \quad (2.37c)$$

$$h_W(\xi) = -2\Big(\cos(\lambda_0 L\xi)\cosh\big(\lambda_0 L(\xi-2)\big) + \\ -\cos\big(\lambda_0 L(\xi-2)\big)\cosh(\lambda_0 L\xi) + \sin\big(\lambda_0 L(\xi-2)\big)\sinh(\lambda_0 L\xi) + \\ + \sin(\lambda_0 L\xi)\Big(\sinh\big(\lambda_0 L(\xi-2)\big) - 2\sinh\big(\lambda_0 L\xi\big)\Big)\Big); \quad (2.37d)$$

where $\lambda_0 = \sqrt[4]{k_0/(4EJ)}$, already introduced in Eq. (2.15), is the characteristic parameter of the system (Heténi, 1946 [125]).

A representation of the normalized solution provided by Eqs. (2.37) is depicted in Figs. 2.5a–2.5b for various values of $\lambda_0 L$, between 1 and 6, a realistic range given in Selvadurai (1979) [235]. In these figures, the normalized deflections are defined as

$$\overline{w}_F(\xi) = \frac{w_F(\xi)}{w_F^{max}}; \qquad \overline{w}_W(\xi) = \frac{w_W(\xi)}{w_W^{max}}; \quad (2.38)$$

where w_F^{max} and w_W^{max} are the maximum beam transverse deflections induced by force F or moment W, respectively, which always appear at their point of application (top end), as expected and as it may be observed in Figs. 2.5a–2.5b.

Even though the solution of this particular case cannot be obtained directly from Eq. (2.26), it can be approached by a limit process taking values of β tending to 0, as it could be inspected by the representations presented next.

2.2.5 Results and discussion

From the general integral in Eq. (2.26) it is revealed that the beam elastic bending response non-proportionally depends on two real characteristic non-dimensional parameters α and β, as introduced in Section 2.2.1. In this section, a parametric investigation is carried out to inspect the effect of α and β on the analytical solution. As noticed in Section 2.2.1, α is a positive parameter and here it has been taken in terms of a realistic range of $\lambda_0 L$, the same considered for the case of the constant foundation coefficient in the previous section.

About parameter β, it must be greater than or equal to -1, due to the third condition in Eq. (2.11); nevertheless, it is expected that too high values of β, for instance beyond 8, would entail a very stiff foundation almost everywhere in $[0,\, L]$. Then, the assumed ranges of values of two non-dimensional parameters α and β have been taken as follows:

$$\alpha = \left[4 \cdot 1^4,\, 4 \cdot 6^4\right] = [4,\, 5184]\,; \qquad \beta = [-1, 0) \cup (0, 8]\,; \tag{2.39}$$

In the following, the effect of both characteristic parameters α and β on the solution patterns, namely static deflection, bending moment and shear is firstly analyzed for the case of a free-free beam subjected to a force F on its top end; then, the same type of analysis is performed by replacing force F with moment W.

Effect of external force

The shape of elastic deflection $\overline{w}_F$, normalized as in Eq. (2.38), versus non-dimensional spatial coordinate ξ, for various values of parameter α is displayed in the sequence of Figs. 2.6a–2.6f, each one for a fixed value of β.

The influence of parameter α, which is representative of the ratio between the stiffness of the foundation, evaluated at the top end of the beam, and the beam bending stiffness, is clearly seen from each graph shown in Figs. 2.6a–2.6f. In particular, for relatively small values of α, a situation occurring in case of either a stiff beam or a soft foundation, the tendency of the beam deflection is that of approaching a linear shape. This reveals the fact that the solution consistently approaches the final configuration of a free-free rigid rod embedded within a linearly varying elastic Winkler foundation.

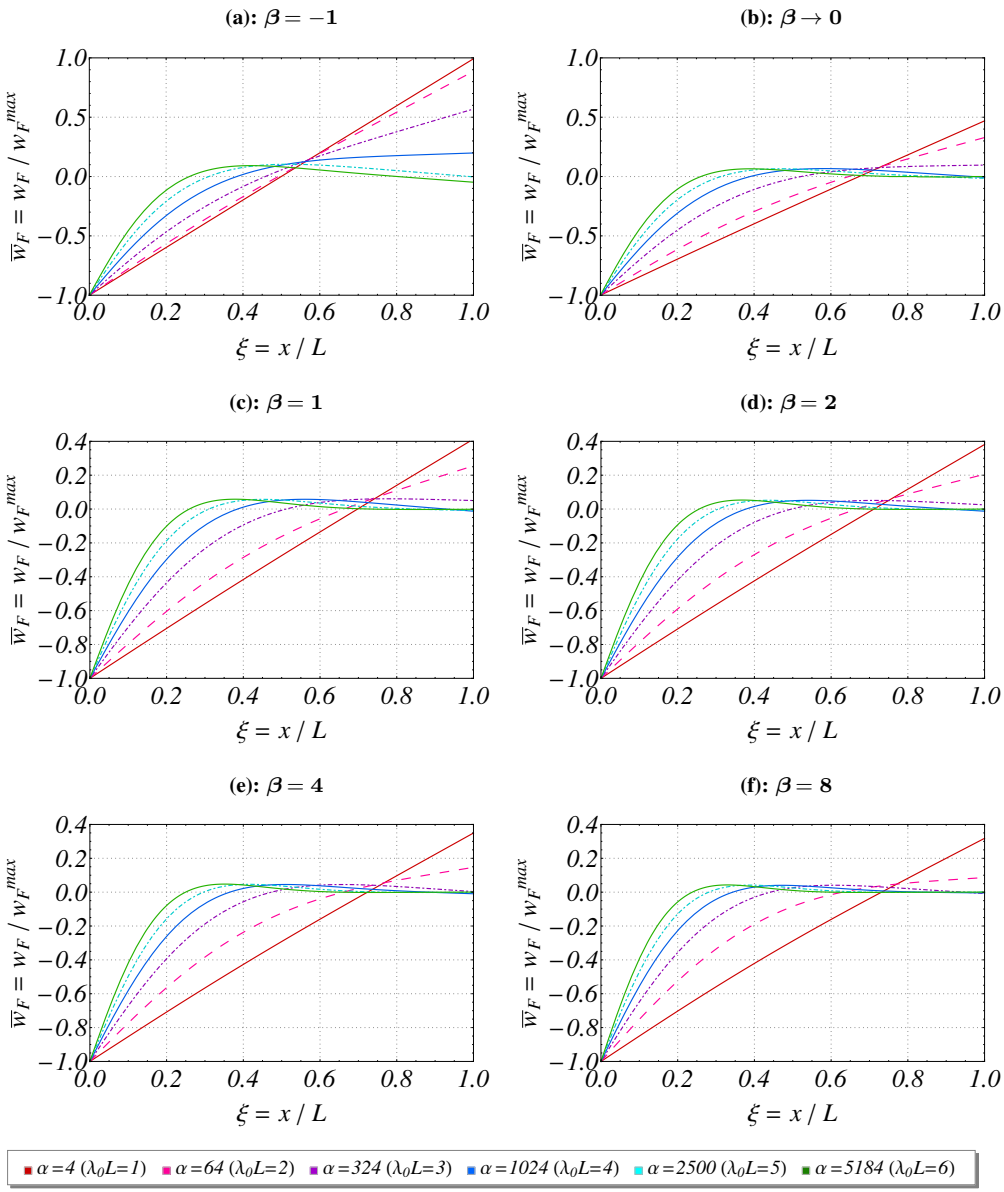

Figure 2.6: Normalized shape of elastic deflection $\overline{w}_F(\xi)$ for various values of α (β=−1 (a); β→0 (b); β=1 (c); β=2 (d); β=4 (e); β=8 (f)).

On the other hand, as α approaches relatively high values, the beam longitudinal axis starts deforming more, displaying an asymmetric evolution that decays very rapidly moving away from the point of application of the load (ξ=0). As expected, the maximum displacements are always in correspondence of the point of application of force F.

The effect of the variable elastic foundation, attached to β, i.e. the parame-

ter representing the steepness of the elastic stiffness coefficient variation along the beam axis, on the normalized shape of the deflection is less pronounced. It may be noticed that for negative values of β the displacements are large even in the lower part of the beam, due to a decreasing stiffness of the elastic springs (Fig. 2.6a); further, if α is also small, the displacements appear nearly symmetric with respect to the midspan of the beam. Positive values of β, corresponding to an increasing stiffness of the foundation along the beam axis, produce a reduction of the beam displacements towards zero, in the second half of the beam, even though this reduction is accompanied by a non-significant change of the deflection profile (Figs. 2.6c–2.6f).

From Fig. 2.6b it is evident that the results obtained for β approaching zero agree well with the analytical solution in Eqs. (2.37), displayed in Fig. 2.5a, and, hence, the singular case $\beta{=}0$ can be recovered in a limit process as $\beta{\to}0$.

Figs. 2.7a–2.7f show the normalized bending moment versus non-dimensional spatial coordinate ξ, and its shape variation with the same parameters considered for the deflection. Normalized bending moment $\overline{M}_F$ in Figs. 2.7a–2.7f is introduced as:

$$\overline{M}_F(\xi) = \frac{M_F(\xi)}{M_F^{max}}; \qquad M_F(\xi) = -\frac{EJ}{L^2} w_F^{(2)}(\xi); \tag{2.40}$$

where M_F^{max} is the maximum bending moment recorded along the beam.

All the normalized bending moments vanish at the edges of the beam, as imposed by the free-free boundary conditions, and always display a positive maximum peak value in the first half of the beam. Such peak moves towards the beam's top ends ($\xi{=}0$), for either increasing values of α or decreasing values of β, which is equivalent to increasing the stiffness of the foundation in the upper zone of the beam with respect to the lower zone.

Small negative values of the bending moment can also be observed in the second half of the beam, in particular for large values of α and β. The maximum negative bending moment remains in any case less than ten percent of the maximum positive value. Accordingly, the deflection profile may be characterized by a change in concavity sign, from its initial sign determined by the direction of applied force F.

As mentioned earlier, for a reduced-stiffness foundation (small values of α) the response curves, independently from β, tend to approach a quartic polynomial, e.g. the evolution of the bending moment of a rigid beam, while larger values of α yield more winding trends.

The plots further depicted in Figs. 2.8a–2.8b show the effect of α and β on the maximum displacement and bending moment, respectively. As previously exposed, the maximum shear is equal to applied force F, independently from parameters α and β. The amplitude of the maximum displacement, always located at the point of application of external force F, decreases of several

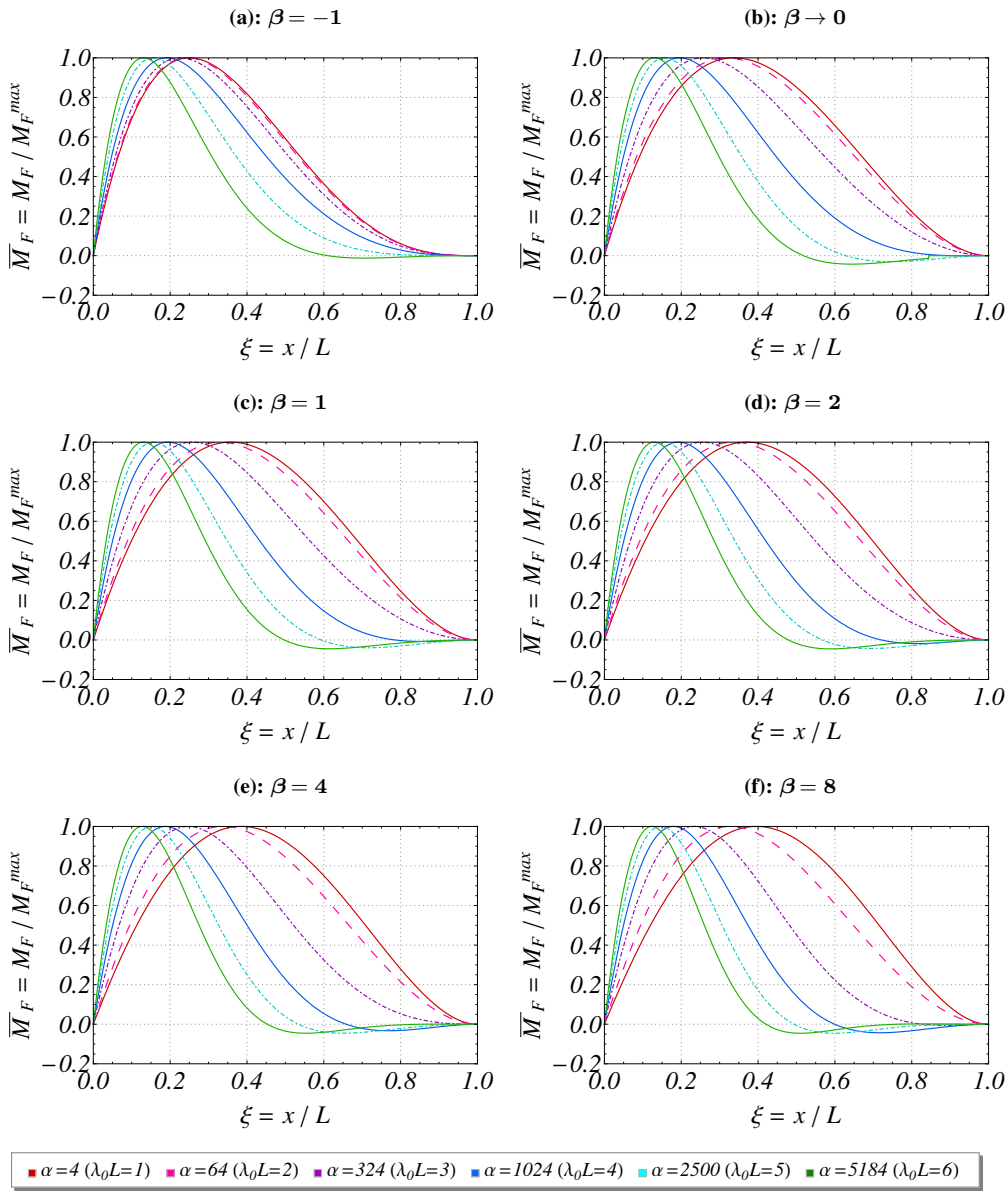

Figure 2.7: Normalized shape of bending moment $\overline{M}_F(\xi)$ for various values of α (β=−1 (a); β→0 (b); β=1 (c); β=2 (d); β=4 (e); β=8 (f)).

order of magnitudes by increasing α, bringing the need of a representation in logarithmic scale on the ordinate axis in Fig. 2.8a.

The effect of parameter β results effective on the displacement amplitudes, by contrast with its relatively small action on the shape of the deflection curves. As β increases, the curves of the maximum displacements always decrease for each α, exponentially decaying towards zero when α is large and even

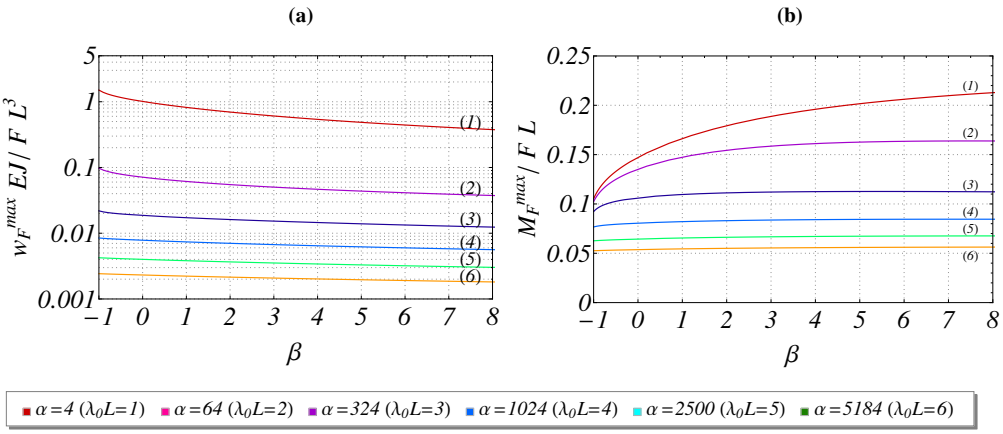

Figure 2.8: Variation of maximum displacement w_F^{max} in logplot (a) and maximum bending moment M_F^{max} (b) vs. β, for six values of α.

more than exponentially when α is small. However, it is noted that the case of an everywhere rigid substrate, corresponding to an everywhere zero displacement, cannot be completely achieved only by letting β going to infinity, because near ξ=0 the coefficient of subgrade reaction remains always finite. To achieve a good approximation of such a limit case, it suffices to increase parameter α, since its effect on reducing the displacements is made more drastic with respect to that of β, meaning that the initial value of the elastic foundation coefficient is more decisive than its relative increment along the beam on the static response of the beam-foundation system.

Regarding the maximum bending moment, it increases with β according to a sublinear fashion for small values of α, whereas it results quite insensitive with respect to parameter β for high values of α (flexible-beam/rigid-foundation system).

Effect of the external moment

In this section the effect of applied moment W on the beam-foundation response is discussed. Normalized shape of elastic deflection $\overline{w}_W$ in Eq. (2.38) versus non-dimensional spatial coordinate ξ for various values of parameter α is displayed in the succession of Figs. 2.9a–2.9f, each one for a fixed value of β, as before.

The influence of parameter α may be resumed as follows. For modest values of α the behavior of the beam is again that of approaching a linear deflection profile, consistently with the configurations displayed in the previous section. Besides, as α increases, the deformation of the beam becomes evident with a trend which decays moving away from the point of application of the moment (ξ=0). Such a decay is faster, with respect to the case of applied force,

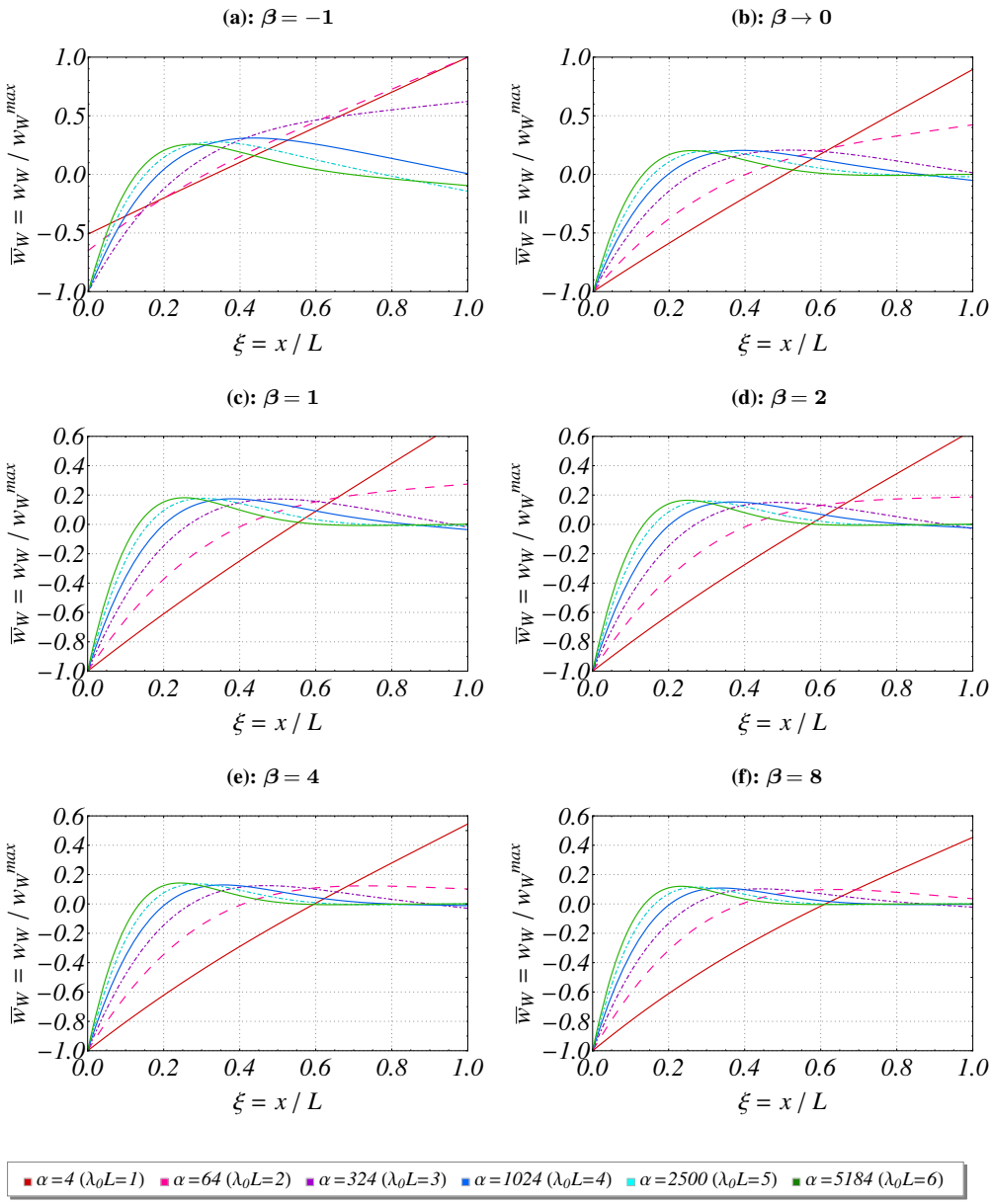

Figure 2.9: Normalized shape of elastic deflection $\overline{w}_W(\xi)$ for various values of α (β=−1 (a); β→0 (b); β=1 (c); β=2 (d); β=4 (e); β=8 (f)).

in the initial part of the beam (small values of ξ), while it appears slower in the reaming part of the beam. Curvatures, if compared with the case of applied force, are always more prominent and maintain almost the same sign.

The effect of β on the normalized shape of the deflection results quite negligible in the first quarter of the beam, while it appears more effective in the

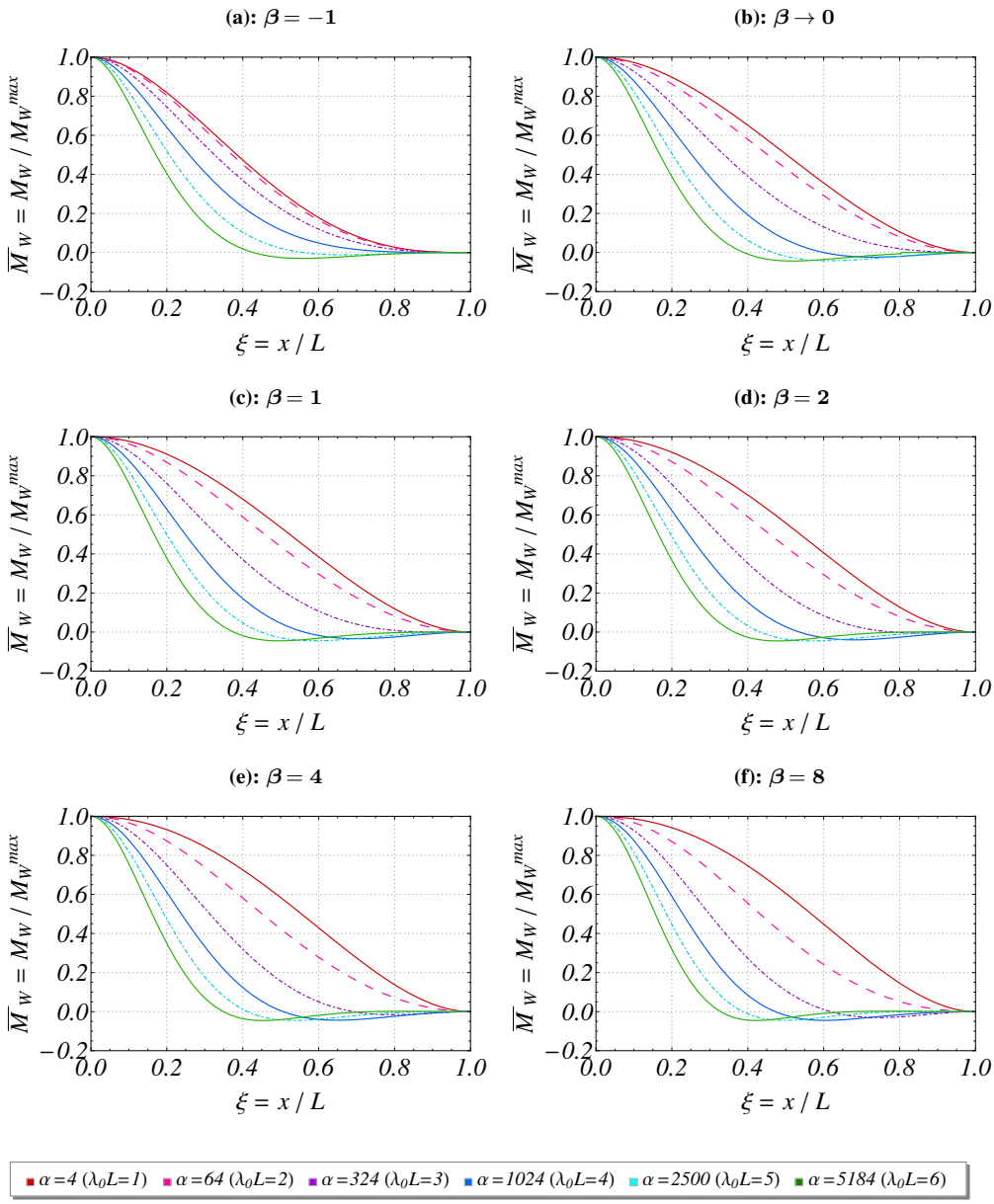

Figure 2.10: Normalized shape of bending moment $\overline{M}_W(\xi)$ for various values of α (β=−1 (a); β→0 (b); β=1 (c); β=2 (d); β=4 (e); β=8 (f)).

remaining part of it, where positive values of β produce a reduction of the beam displacements towards zero. Thus, the effect of β on the displacements seems analogous to what recorded for the case of the applied force. Except for small values of α and negative values of β, the maximum displacements are always in correspondence to the point of application of moment W (ξ=0).

From Fig. 2.9b it is evident that results obtained for β approaching zero agree well with the analytical solution in Eqs. (2.37) represented in Fig. 2.5b, and, again singular case β=0 can be reached by a limit process as $\beta \to 0$.

The parametric variation of the normalized bending moment (with respect to M_W^{max}) versus non-dimensional spatial coordinate ξ is shown in Figs. 2.10a–2.10f. All the normalized curves start from a unitary value and vanish at the other extremity of the beam (ξ=1), meaning that the applied moment always represents the maximum bending moment along the beam, i.e. $M_W^{max} = W$. Such curves exhibit a sigmoid shape characterized by a faster decay at increasing α. In this latter case, the number of inflection points become two instead of one (double change of concavity), thus displaying a very small peak in the fourth quarter of the beam.

For high values of α, small negative values of bending moments can also be detected in the second half of the beam, the maximum of which remains always less than ten percent of the applied moment. On the other side, an increase of parameter β causes the decrease of the bending moment for all the considered α, except for the case α=4 (red curves), i.e. a foundation with reduced stiffness, where the opposite effect is produced.

The plots finally presented in Figs. 2.11a–2.11b show the effect of parameters α and β on the maximum displacement and maximum shear, respectively. In this case the maximum bending moment remains the same and equal to applied moment W. The amplitudes of the maximum displacements are higher with respect to the case of the applied force, but displaying a qualitatively similar evolution with both parameters α and β. Further, by observing Figs. 2.11b, the maximum shear increases for an increasing slope of the foundation stiffness (β), and even more as the foundation initial stiffness increases (α).

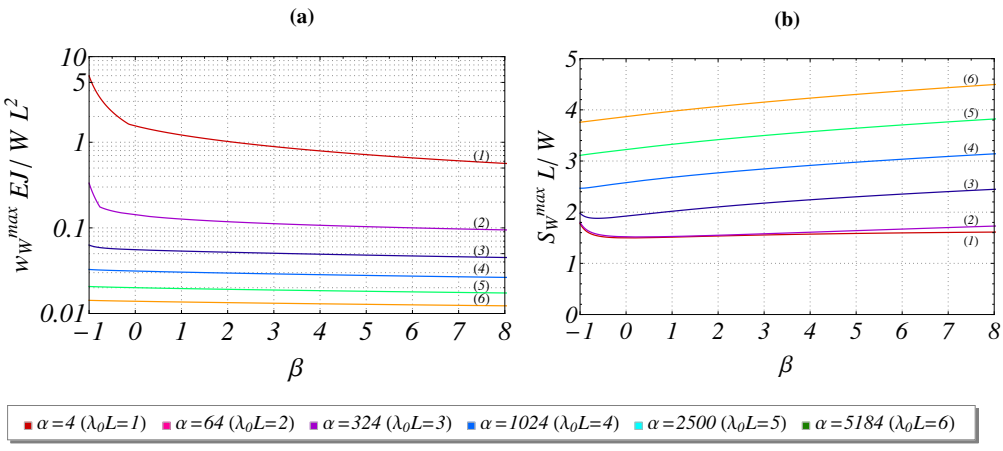

Figure 2.11: Variation of maximum displacement w_W^{max} in logplot (a) and maximum shear S_W^{max} (b) vs. β, for six values of α.

2.3 Analytical bending solution for nonlinear $k(x)=(c_0+c_1x)^{-4}$

2.3.1 Problem formulation

Consider a beam of a finite length L, briefly sketched in Fig. 2.12, endowed with a right-handed system of rectangular coordinates (x,y,z), with the origin at the centroid of the left-end cross-section of the beam; the x-axis is taken along the axis of the beam while the y- and z-axes are taken along the principal axes of the cross-section, the positive direction of the y-axis being vertically downward. The positive direction for measuring slopes is in conformity with universal usage, i.e. according to the right-handed screw rule. Positive bending moment indicates tensile stresses in the bottom of the beam and positive shear indicates that the left sides of the beam tends to rise.

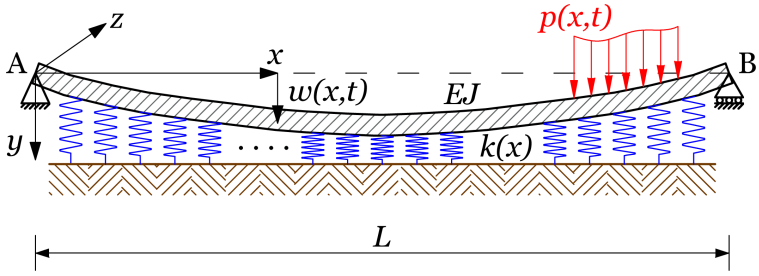

Figure 2.12: Simply-supported beam resting on a Winkler foundation with variable stiffness coefficient $k(x)$.

A uniform ($E(x)J(x)=EJ$) simply-supported elastic beam lying on a Winkler-type foundation is described through the subsequent two-point boundary value problem (BVP):

$$EJw_x^{(4)}(x)+k(x)\,w(x)=p(x); \qquad 0\le x\le L, \qquad k(x)>0; \tag{2.41a}$$

$$w(0)=0; \tag{2.41b}$$

$$w(L)=0; \tag{2.41c}$$

$$w_x^{(2)}(0)=0; \tag{2.41d}$$

$$w_x^{(2)}(L)=0; \tag{2.41e}$$

where both $k(x)$ and $p(x)$ are real-valued continuous functions in the interval of interest $[0,L]$. Eqs. (2.41b)-(2.41e) are called boundary or end point conditions of the problem.

A preliminary phase in the solution of two-point BVP (2.41) concerns the discussion about its well-posedness. The existence and uniqueness of the solution of differential problem (2.41) is guaranteed by the work of Usmani (1979)

[258]. In fact, he proved that a solution of boundary value problem (2.41) exists if $k(x)$ and $p(x)$ are continuous functions on $[0, L]$. Also, the solution is unique provided that

$$\inf_x k(x) \; > \; -\pi^4. \tag{2.42}$$

Since function $k(x)$, which represents point-wisely the stiffness of each infinitesimal spring, makes physical sense only if it is greater than zero, the validity of the above condition is straightforward. Hence, the mathematical feature which guarantees the existence and uniqueness of the solution of (2.41) is the positiveness of the foundation coefficient, $k(x) > 0$.

Consider the situation in which the variable support elastic stiffness coefficient may be described by the following nonlinear expression

$$k(x) = (c_0 + c_1 x)^{-4} = \frac{1}{(c_0 + c_1 x)^4}; \tag{2.43}$$

where c_0 and c_1 are constant parameters, with restrictions defined as discussed below.

In the expression of Eq. (2.43), the required positivity of $k(x)$ at any x is guaranteed by the exponent four in its definition, meanwhile its fractional form assures $k(x)$ to be never null in the interval $[0,\ L]$. In addition, the continuity of $k(x)$, required for satisfying the hypotheses of the existence theorem (Usmani, 1979 [258]), constrains quantity $c_0 + c_1 x$ to be non-zero in the interval $[0,\ L]$. So, it is assumed that c_0 and c_1 may be any real numbers provided that

$$c_0 > 0 \quad \text{and} \quad c_1 > -\frac{c_0}{L}. \tag{2.44}$$

Actually, it may be enough having $c_0 \neq 0$ for ensuring $k(x)$ not becoming unbounded when x is equal to zero, but, since the exponent four in Eq. (2.43) makes $k(x)$ independent from the sign of $c_0 + c_1 x$, c_0 will be considered just as a positive quantity ($c_0 > 0$). Further, the second condition guarantees the continuity of $k(x)$ for all x belonging to $(0,\ L]$. A representation of the trends of stiffness $k(x)$ ensuing from Eq. (2.43) is given in Fig. 2.13a. In Fig. 2.13b, its reciprocal, compliance $\eta(x) = 1/k(x)$ is also represented.

For the purposes of the analytical developments and of further discussion it is convenient to introduce the following non-dimensional variables and parameters:

$$\xi = \frac{x}{L}; \qquad \alpha = \sqrt[4]{EJ}\,\frac{c_0}{L}; \qquad \beta = \frac{c_1}{c_0/L} = \sqrt[4]{\frac{k(0)}{k(L)}} - 1; \tag{2.45}$$

where ξ is the non-dimensional spatial coordinate, α is a ratio representing the relative flexibility of the beam-soil system evaluated at the left extreme of the beam ($x = 0$) and β is a parameter describing how rapidly the elastic

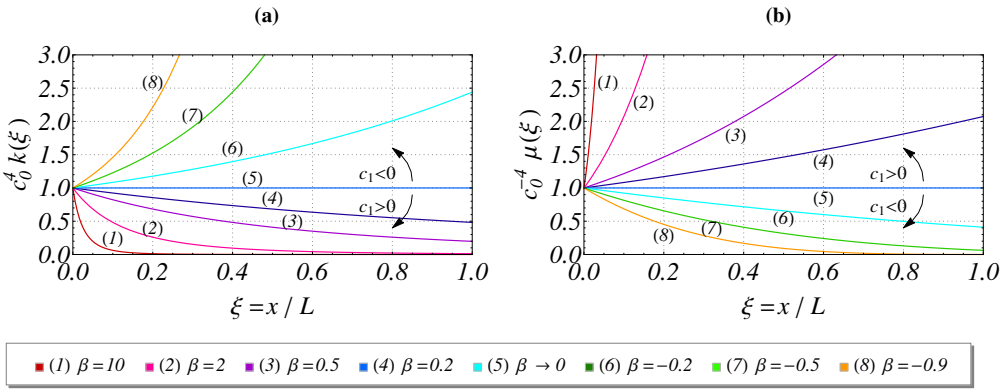

Figure 2.13: Trends of support elastic stiffness coefficient $k(x)$ (a), and of its reciprocal, support elastic compliance $\eta(x)$ (b) vs. non-dimensional space coordinate $\xi{=}x/L$, for different values of $\beta{=}c_1/(c_0/L)$.

stiffness coefficient changes along the beam axis with respect to its starting value $k(0){=}c_0^{-4}$.

It is well-known that the general integral of non-homogeneous linear differential equation (2.41a) is given by the sum of any of its particular solutions $w_P(x)$ and general solution $w_H(x)$ of the corresponding associated linear homogeneous equation

$$EJw_x^{(4)}(x) + k(x)\, w(x) = 0; \qquad 0 \le x \le L, \quad k(x) > 0; \tag{2.46}$$

obtained from Eq. (2.41a) by setting $p(x){=}0$. General integral $w_H(x)$ of Eq. (2.46), also called complementary function (Murphy, 1960 [206]), is given by a linear combination with complex coefficients of four linear independent functions $w_{H_i}(x)$, each satisfying Eq. (2.46).

A necessary and sufficient condition for $w_{H_i}(x)$ being linearly independent is that (see Coddington and Levinson, 1955 [61])

$$\mathcal{W}(w_{H_1}, \ldots, w_{H_4})(x) \neq 0; \qquad 0 \le x \le L; \tag{2.47}$$

where quantity $\mathcal{W}(w_{H_1}, \ldots, w_{H_4})(x){=}\det\, \mathbf{\Phi}_H(x)$, called Wronskian, is the determinant of fundamental matrix $\mathbf{\Phi}_H(x)$, defined as

$$\mathbf{\Phi}_H(x) = \begin{pmatrix} w_{H_1}(x) & w_{H_2}(x) & w_{H_3}(x) & w_{H_4}(x) \\ w_{H_1}{}^{(1)}(x) & w_{H_2}{}^{(1)}(x) & w_{H_3}{}^{(1)}(x) & w_{H_4}{}^{(1)}(x) \\ w_{H_1}{}^{(2)}(x) & w_{H_2}{}^{(2)}(x) & w_{H_3}{}^{(2)}(x) & w_{H_4}{}^{(2)}(x) \\ w_{H_1}{}^{(3)}(x) & w_{H_2}{}^{(3)}(x) & w_{H_3}{}^{(3)}(x) & w_{H_4}{}^{(3)}(x) \end{pmatrix}. \tag{2.48}$$

If condition (2.47) is satisfied, functions $w_{H_i}(x)$ are said to form a fundamental set of solutions of Eq. (2.46). If a fundamental set of solutions of Eq. (2.46) is

known, a particular integral $w_P(x)$ is always obtainable by using the *Variation of Parameters* formula (see e.g. Coddington and Levinson, 1955 [61]):

$$w_P(x) = \sum_{i=1}^{4} w_{H_i}(x) \int_0^x \frac{W_i(w_{H_1}, \ldots, w_{H_4})(s)}{W(w_{H_1}, \ldots, w_{H_4})(s)} p(s)\, ds; \tag{2.49}$$

where $W_i(w_{H_1}, \ldots, w_{H_4})(x)$ is the determinant of the fundamental matrix above with the $i\text{-}th$ column replaced by $(0,\ 0,\ 0,\ 1)^T$. Once $w_P(x)$ is determined, the general integral of the solution of Eq. (2.41a) may be written as

$$w(x) = \sum_{i=1}^{4} C_i w_{H_i}(x) + w_P(x); \tag{2.50}$$

where four constants C_i have to be determined from the boundary conditions, Eqs. (2.41b)-(2.41e). Therefore, the analytical solution of Eq. (2.41a) is obtainable if a fundamental set of solutions $w_{H_i}(x)$ of Eq. (2.46) is known. Unfortunately, this represents the hardest point of the solution, since closed-form expressions for the exact solutions of Eq. (2.46) have not been found yet in many cases of interest, except for the linear case already derived in Section 2.2. A solution is developed in the following for the minus four power variation of the stiffness coefficient $k(x)$ stated in Eq. (2.43).

2.3.2 Solution of the homogeneous equation

When $k(x)$ is described by Eq. (2.43), homogeneous equation (2.46) is known as the *Euler equation* (Coddington and Levinson,1955 [61]), which is straightforward to be solved in closed-form by using elementary functions. In fact, by virtue of substitution:

$$\eta(\xi) = \ln(\beta\, \xi + 1); \tag{2.51}$$

Eq. (2.46) may be transformed into the following linear equation with constant coefficients:

$$e^{-4\eta}\left(v_H^{(4)}(\eta) - 6v_H^{(3)}(\eta) + 11v_H^{(2)}(\eta) - 6v_H^{(1)}(\eta) + \frac{v_H(\eta)}{(\alpha\beta)^4}\right) = 0. \tag{2.52}$$

The solution of Eq. (2.52) is readily obtained by determining the four distinct roots of the characteristic equation (Coddington and Levinson, 1955 [61])

$$r(r-1)(r-2)(r-3) + \gamma^4 = 0, \qquad \gamma = \frac{1}{\alpha\beta} = \frac{1}{c_1\sqrt[4]{EJ}}; \tag{2.53}$$

which may be written as

$$r_1 = \frac{3-a_2}{2}; \quad r_2 = \frac{3+a_2}{2}; \quad r_3 = \frac{3-a_3}{2}; \quad r_4 = \frac{3+a_3}{2}; \tag{2.54}$$

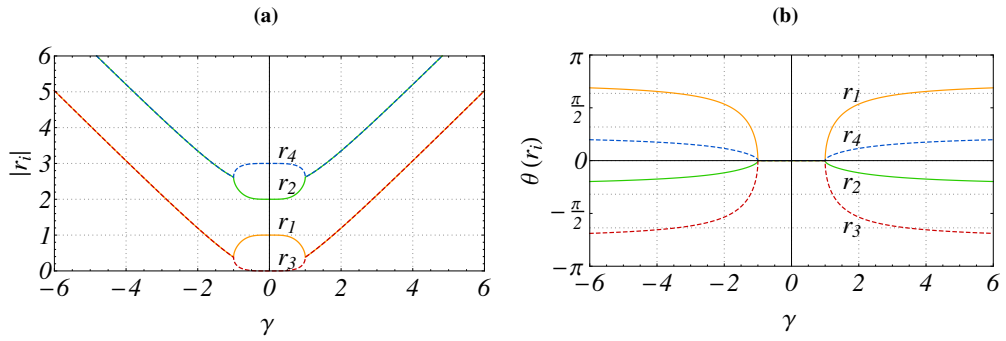

Figure 2.14: Absolute value (a) and argument (b) of the four roots r_i as a function of γ.

where $a_1{=}4\sqrt{1-\gamma^4}$, $a_2{=}\sqrt{5-a_1}$ and $a_3{=}\sqrt{5+a_1}$. Then, the general integral of Eq. (2.52) is

$$w_H(\eta) = C_1 e^{r_1\eta} + C_2 e^{r_2\eta} + C_3 e^{r_3\eta} + C_4 e^{r_4\eta}; \tag{2.55}$$

where the C_i are four constants, which shall be linked later to boundary conditions (2.41b)-(2.41e).

Each of four solutions $w_{H_i}(\eta){=}e^{r_i\eta}$ of Eq. (2.52) may be real or complex-valued, depending on the value of γ, as shown in Fig. 2.14. In particular, if the roots are real, that is for $|\gamma|{\leq}1$ ($|c_1|{\geq}1/\sqrt[4]{EJ}$), i.e. $-1{\leq}\gamma{\leq}1$, accordingly functions $w_{H_i}(\xi)$ are real-valued; on the contrary, if r_i are complex numbers, that is for $|\gamma|{>}1$ ($|c_1|{<}1/\sqrt[4]{EJ}$), then $w_{H_i}(\xi)$ are complex-valued. Substituting back the expressions in Eq. (2.51) into Eq. (2.55), the final form of the solution of homogeneous Eq. (2.46) becomes

$$v_H(\xi) = \sum_{i=1}^{4} C_i v_{H_i}(\xi) = \sum_{i=1}^{4} C_i \left(1+\beta\xi\right)^{r_i}. \tag{2.56}$$

2.3.3 Solution of the boundary value problem

A downward uniform distributed external load $p(x){=}p$ of constant magnitude p is considered now. The particular integral of Eq. (2.41a) may be obtained directly from formula (2.49), leading to the following general integral:

$$\begin{aligned} w(\xi) &= w_H(\xi) + w_P(x) = \\ &= \sum_{i=1}^{4} C_i \left(1+\beta\xi\right)^{r_i} + P \sum_{i=1}^{4} a_{i+3} \left(\left(1+\beta\xi\right)^4 - \left(1+\beta\xi\right)^{r_i} \right); \end{aligned} \tag{2.57}$$

where

$$P = \frac{p\,L^4}{\beta^4\,EJ}; \tag{2.58}$$

and

$$\begin{aligned} a_4 &= -\frac{8}{a_2(a_2+5)(a_2^2-a_3^2)}; \quad a_5 = -\frac{8}{a_2(a_2-5)(a_2^2-a_3^2)}; \\ a_6 &= -\frac{8}{a_3(a_3+5)(a_2^2-a_3^2)}; \quad a_7 = -\frac{8}{a_3(a_3-5)(a_2^2-a_3^2)}. \end{aligned} \tag{2.59}$$

It is worthwhile to mention that factors a_2, a_3, $a_2 \pm 5$, $a_3 \pm 5$ in the denominators are always different from zero, due to the positivity of γ, which occurs from its definition reported in Eq. (2.53). Also, the case $a_2^2{=}a_3^2$ corresponds to $\gamma{=}\pm 1$ and it will be treated in the following as a particular case.

Let

$$B = 1 + \beta = \sqrt[4]{\frac{k(0)}{k(L)}}; \tag{2.60}$$

the expressions of coefficients C_i of Eq. (2.57) such that $w(\xi)$ is the solution of the boundary value problem (2.41) may be written as

$$C_i = \frac{P}{D}\sum_{j=1}^{9} c_{i,j}B^{e_j} \quad i = 1,3,4; \qquad C_2 = \frac{P}{D}B^{-(a_2+a_3)/2}\sum_{j=1}^{9} c_{i,j}B^{e_j}; \tag{2.61}$$

where denominator term D takes the following form:

$$\begin{aligned} D = (B^{a_2}-1)(B^{a_3}-1)\Big(a_2^4 - 2a_2^2(a_3^2+8) + a_3^2(a_3^2-16) + \\ 32a_2a_3\left(B^{a_2+a_3} - 4B^{(a_2+a_3)/2} + B^{a_2} + B^{a_3} + 1\right)\Big). \end{aligned} \tag{2.62}$$

Coefficients $c_{i,j}$ and exponents e_i are listed from Table 2.3 to Table 2.7. All calculations have been developed within a Mathematica [274] environment.

Furthermore, when the non-homogeneous term coming from external distributed load $p(x)$ has derivatives whose form varies a little with respect to the parent function (e.g. exponential, polynomials, sine and cosine), to find a particular integral $w_P(x)$ it is often more suitable to apply the *Method of Undetermined Coefficients* (see Murphy, 1960 [206]), which, in general, leads to simpler expressions than those provided by Eq. (2.57). In fact, with the definitions in Eqs. (2.51), (2.52) and (2.53), Eq. (2.41a) becomes

$$w_H^{(4)}(\eta) - 6w_H^{(3)}(\eta) + 11w_H^{(2)}(\eta) - 6w_H^{(1)}(\eta) + \gamma^4 w_H(\eta) = Pe^{4\eta}. \tag{2.63}$$

Since the term on the right-hand side of Eq. (2.63) is an exponential, it is advantageous to apply the Method of Undetermined Coefficients. Assuming $w_P(x){=}\lambda P e^{4\eta}$, the substitution of $w_P(x)$ back into Eq. (2.63) gives

$$Pe^{4\eta}\beta^4 EJ\left((23+\gamma^4)\lambda - 1\right) = 0; \tag{2.64}$$

which allows for the determination of unknown coefficient λ. Then, another much compact form of the general integral of Eq. (2.41a) turns out to be

$$w(\xi) = w_H(\xi) + w_P(\xi) = \sum_{i=1}^{4} \widetilde{C}_i \left(1 + \beta\xi\right)^{r_i} + \frac{P(1+\beta\xi)^4}{23 + \gamma^4}. \tag{2.65}$$

The imposition of boundary conditions (2.41b)-(2.41e) allows to determine constants $\widetilde{C}_i$ in Eq. (2.65) by the solution of the resulting linear system. The expressions of coefficients $\widetilde{C}_i$ of Eq. (2.65) such that $w(\xi)$ is the solution of boundary value problem (2.41) may still be written as

$$\widetilde{C}_i = \frac{P}{\widetilde{D}} \sum_{j=1}^{9} \tilde{c}_{i,j} B^{e_j}; \tag{2.66}$$

where denominator term $\widetilde{D}$ takes now the following form:

$$\widetilde{D} = \left(\gamma^4 + 23\right) D; \tag{2.67}$$

and coefficients $\tilde{c}_{i,j}$ for this case are listed in Table 2.8.

It is possible to check that both D and $\widetilde{D}$ are non-zero quantities, except for the cases when $\gamma \to \infty$ ($\beta = 0$) or $\gamma = \pm 1$ (see the following section). Then, coefficients C_i and $\widetilde{C}_i$ are always well-defined for every value of parameters α and β, consistently with what was expected, thanks to the existence and uniqueness theorem provided by Usmani (1979) [258].

From the expressions of the coefficients in Eq. (2.66), the solution is proportional to P (thus to the load p), as it was expected from the linearity of the differential equation. The representation and interpretation of the achieved analytical solution is presented and discussed in Section 2.3.5, but, first, singular cases are commented below. The achieved analytical representation is finally resumed in synoptic form in the sketch provided in Fig. 2.15.

2.3.4 Singular cases

The expression of the Wronskian given by the fundamental set of solutions of Eq. (2.56), which is

$$W(\xi, \beta, \gamma) = \frac{4}{\alpha^6} \sqrt{16\gamma^4 + 9} \left(1 - \gamma^4\right) \gamma^{-\frac{3}{2}}; \tag{2.68}$$

shows that $w_H(\xi)$ is improper to represent the solution of Eq. (2.46) when $\gamma \to \infty$ or $\gamma = \pm 1$. In fact, for $\gamma \to \infty$ the four roots in Eq. (2.54) are undefined, while for $\gamma = \pm 1$ they result pairwise equal, hence, not leading to four independent solutions. For these specific values of γ, the solution has to be derived independently from Eq. (2.65).

$c_{1,1} =$	$8\,a_3\left(a_2^2+4a_2-45\right)\left(a_4+a_5+a_6+a_7\right)$
$c_{1,2} =$	$-\left(a_2^2+4a_2-a_3^2+4a_3\right)\left(a_3^2+4a_3-45\right)\left(a_4+a_5+a_6+a_7\right)$
$c_{1,3} =$	$\left(a_2^2+4a_2-a_3^2-4a_3\right)\left(\left(a_2^2-4a_2-45\right)a_4+\left(a_3^2-4a_3-45\right)\left(a_5+a_6+a_7\right)\right)$
$c_{1,4} =$	$8\,a_3\left(\left(a_2^2-12a_2-45\right)a_4+\left(a_2^2+4a_2-45\right)\left(a_5+a_6+a_7\right)\right)$
$c_{1,5} =$	$\left(a_3^2-4a_3-45\right)\left(a_2^2+4a_2-a_3^2-4a_3\right)\left(a_4+a_5+a_6+a_7\right)$
$c_{1,6} =$	0
$c_{1,7} =$	$-\left(a_2^2+4a_2-a_3^2+4a_3\right)\left(\left(a_2^2-4a_2-45\right)a_4+\left(a_3^2+4a_3-45\right)\left(a_5+a_6+a_7\right)\right)$
$c_{1,8} =$	$-a_4\left(a_2+a_3\right)^2\left(a_2^2-2a_2a_3+a_3^2-16\right)$
$c_{1,9} =$	$\left(a_2-a_3\right)^2\left(a_2^2+2a_2a_3+a_3^2-16\right)$

Table 2.3: Expressions of coefficients $c_{1,j}$ of C_1.

$c_{2,1} =$	0
$c_{2,2} =$	$\left(a_3^2+4a_3-45\right)\left(a_2^2-4a_2-a_3^2+4a_3\right)\left(a_4+a_5+a_6+a_7\right)$
$c_{2,3} =$	$a_5(a_2-a_3)^2\left(a_2^2+2a_2a_3+a_3^2-16\right)$
$c_{2,4} =$	$-8\,a_3\left(\left(a_2^2-4a_2-45\right)\left(a_4+a_6+a_7\right)+\left(a_2^2+12a_2-45\right)a_5\right)$
$c_{2,5} =$	$\left(a_3^2-4a_3-45\right)\left(-a_2^2+4a_2+a_3^2+4a_3\right)\left(a_4+a_5+a_6+a_7\right)$
$c_{2,6} =$	$-8\,a_3\left(a_2^2-4a_2-45\right)\left(a_4+a_5+a_6+a_7\right)$
$c_{2,7} =$	$-a_5(a_2+a_3)^2\left(a_2^2-2a_2a_3+a_3^2-16\right)$
$c_{2,8} =$	$-\left(a_2^2-4a_2-a_3^2-4a_3\right)\left(\left(a_2^2+4a_2-45\right)a_5+\left(a_3^2-4a_3-45\right)\left(a_4+a_6+a_7\right)\right)$
$c_{2,9} =$	$\left(a_2^2-4a_2-a_3^2+4a_3\right)\left(\left(a_2^2+4a_2-45\right)a_5+\left(a_3^2+4a_3-45\right)\left(a_4+a_6+a_7\right)\right)$

Table 2.4: Expressions of coefficients $c_{2,j}$ of C_2.

$c_{3,1} =$	$\left(a_2^2-4a_2-a_3^2-4a_3\right)\left(a_2^2+4a_2-45\right)\left(a_4+a_5+a_6+a_7\right)$
$c_{3,2} =$	$8\,a_2\left(a_3^2+4a_3-45\right)\left(a_4+a_5+a_6+a_7\right)$
$c_{3,3} =$	$-\left(a_2^2+4a_2-4a_3-a_3^2\right)\left(\left(a_2^2-4a_2-45\right)\left(a_4+a_5+a_7\right)+\left(a_3^2-4a_3-45\right)a_6\right)$
$c_{3,4} =$	$8\,a_2\left(\left(a_3^2+4a_3-45\right)\left(a_4+a_5+a_7\right)+\left(a_3^2-12a_3-45\right)a_6\right)$
$c_{3,5} =$	0
$c_{3,6} =$	$-\left(a_2^2-4a_2-45\right)\left(a_2^2+4a_2-a_3^2-4a_3\right)\left(a_4+a_5+a_6+a_7\right)$
$c_{3,7} =$	$-a_6(a_2+a_3)^2\left(a_2^2-2a_2a_3+a_3^2-16\right)$
$c_{3,8} =$	$\left(a_2^2-4a_2-a_3^2-4a_3\right)\left(\left(a_2^2+4a_2-45\right)\left(a_4+a_5+a_7\right)+\left(a_3^2-4a_3-45\right)a_6\right)$
$c_{3,9} =$	$a_6(a_2-a_3)^2\left(a_2^2+2a_2a_3+a_3^2-16\right)$

Table 2.5: Expressions of coefficients $c_{3,j}$ of C_3.

$c_{4,1} =$	$-\left(a_2^2-4a_2-a_3^2+4a_3\right)\left(a_2^2+4a_2-45\right)\left(a_4+a_5+a_6+a_7\right)$
$c_{4,2} =$	0
$c_{4,3} =$	$a_7(a_2-a_3)^2\left(a_2^2+2a_2a_3+a_3^2-16\right)$
$c_{4,4} =$	$-8a_2\left(\left(a_3^2-4a_3-45\right)\left(a_4+a_5+a_6\right)+\left(a_3^2+12a_3-45\right)a_7\right)$
$c_{4,5} =$	$-8a_2\left(a_3^2-4a_3-45\right)\left(a_4+a_5+a_6+a_7\right)$
$c_{4,6} =$	$\left(a_2^2+4a_2-a_3^2+4a_3\right)\left(a_2^2-4a_2-45\right)\left(a_4+a_5+a_6+a_7\right)$
$c_{4,7} =$	$\left(a_2^2+4a_2-a_3^2+4a_3\right)\left(\left(a_2^2-4a_2-45\right)\left(a_4+a_5+a_6\right)+\left(a_3^2+4a_3-45\right)a_7\right)$
$c_{4,8} =$	$-a_7(a_2+a_3)^2\left(a_2^2-2a_2a_3+a_3^2-16\right)$
$c_{4,9} =$	$-\left(a_2^2-4a_2-a_3^2+4a_3\right)\left(\left(a_2^2+4a_2-45\right)\left(a_4+a_5+a_6\right)+\left(a_3^2+4a_3-45\right)a_7\right)$

Table 2.6: Expressions of coefficients $c_{4,j}$ of C_4.

$e_1 =$	$(5+a_2)/2+a_3$	$e_4 =$	$(a_2+a_3)/2$	$e_7 =$	a_2
$e_2 =$	$(5+a_3)/2+a_2$	$e_5 =$	$(5+a_2)/2$	$e_8 =$	a_3
$e_3 =$	a_2+a_3	$e_6 =$	$(5+a_3)/2$	$e_9 =$	0

Table 2.7: Expressions of exponents e_i.

	$\tilde{c}_{i,1}$	$\tilde{c}_{i,2}$	$\tilde{c}_{i,3}$	$\tilde{c}_{i,4}$	$\tilde{c}_{i,5}$	$\tilde{c}_{i,6}$	$\tilde{c}_{i,7}$	$\tilde{c}_{i,8}$	$\tilde{c}_{i,9}$
$\widetilde{C}_1$:	b_1	b_2	b_3	b_2	b_3	0	b_1	0	0
$\widetilde{C}_2$:	b_4	0	0	b_5	b_6	b_5	0	b_6	b_4
$\widetilde{C}_3$:	b_7	b_8	b_9	b_7	0	b_9	0	b_8	0
$\widetilde{C}_4$:	0	b_{10}	0	b_{11}	b_{11}	b_{12}	b_{12}	0	b_{10}

$$
\begin{aligned}
b_1 &= -\left(a_3^2+4a_3-45\right)\left(a_2^2+4a_2-a_3(a_3-4)\right)\\
b_2 &= 8a_3\left(a_2^2+4a_2-45\right)\\
b_3 &= \left(a_3^2-4a_3-45\right)\left(a_2^2+4a_2-a_3(a_3+4)\right)\\
b_4 &= \left(a_3^2+4a_3-45\right)\left(a_2^2-4a_2-a_3(a_3-4)\right)\\
b_5 &= -8a_3\left(a_2^2-4a_2-45\right)\\
b_6 &= -\left(a_3^2-4a_3-45\right)\left(a_2^2-4a_2-a_3(a_3+4)\right)\\
b_7 &= 8a_2\left(a_3^2+4a_3-45\right)\\
b_8 &= \left(a_2^2+4a_2-45\right)\left(a_2^2-4a_2-a_3(a_3+4)\right)\\
b_9 &= -\left(a_2^2-4a_2-45\right)\left(a_2^2+4a_2-a_3(a_3+4)\right)\\
b_{10} &= -\left(a_2^2+4a_2-45\right)\left(a_2^2-4a_2-a_3(a_3-4)\right)\\
b_{11} &= -8a_2\left(a_3^2-4a_3-45\right)\\
b_{12} &= \left(a_2^2-4a_2-45\right)\left(a_2^2+4a_2-a_3(a_3-4)\right)
\end{aligned}
$$

Table 2.8: Expressions of coefficients $\tilde{c}_{i,j}$ of $\widetilde{C}_i$.

SYNOPSIS OF THE ANALYTICAL SOLUTION

Governing differential equation and boundary conditions

- $EJw^{(4)}(x)+k(x)\,w(x)=\,p(x); \qquad 0\le x\le L, \qquad k(x)>0;$
- $w(0)=\,0; \qquad w(L)=\,0; \qquad w^{(2)}(0)=\,0; \qquad w^{(2)}(L)=\,0;$

Definitions

- $\xi=\dfrac{x}{L}; \quad \alpha=\sqrt[4]{EJ}\,\dfrac{c_0}{L}; \quad \beta=\dfrac{c_1}{c_0/L}; \quad B=1+\beta; \quad P=\dfrac{p\,L^4}{EJ\,\beta^4}.$

Solution for $k(x)=(c_0+c_1x)^{-4}$, $p(x)=p$

- $w(\xi)=w_H(\xi)+w_P(\xi);$
- $w_H(\xi)=\displaystyle\sum_{i=1}^{4}\widetilde{C}_i\,(1+\beta\xi)^{r_i}\,; \qquad w_P(\xi)=\dfrac{P(1+\beta\xi)^4}{23+(\alpha\beta)^{-4}};$
- $r_1=(3-a_2)/2; \quad r_2=(3+a_2)/2; \quad r_3=(3-a_3)/2; \quad r_4=(3+a_3)/2;$
- $a_1=4\sqrt{1-(\alpha\beta)^{-4}}; \qquad a_2=\sqrt{5-a_1}; \qquad a_3=\sqrt{5+a_1};$
- $\widetilde{C}_i=\dfrac{P}{\widetilde{D}}\displaystyle\sum_{j=1}^{9}\tilde{c}_{i,j}B^{e_j}; \qquad \widetilde{D}=\left((\alpha\beta)^{-4}+23\right)D;$
- $D=(B^{a_2}-1)(B^{a_3}-1)\Big(a_2^4-2a_2^2(a_3^2+8)+a_3^2(a_3^2-16)+$
  $+32a_2a_3\left(B^{a_2+a_3}-4B^{(a_2+a_3)/2}+B^{a_2}+B^{a_3}+1\right)\Big);$
- $e_j \rightarrow$ Table 2.7; $\qquad \tilde{c}_{i,j} \rightarrow$ Table 2.8.

Figure 2.15: Summary of the main steps of the analytical solution.

If $\gamma \to \infty$, that is $c_1 = \beta = 0$, the problem is brought back to that of a simply-supported beam lying on an elastic foundation with constant modulus. The solution, reported e.g. in Hetényi (1946) [125], is the following:

$$w(\xi) = \frac{p}{k} - \frac{p}{k} \frac{\cosh(\lambda L \xi)\cos\big(\lambda L(1-\xi)\big) + \cosh\big(\lambda L(1-\xi)\big)\cos(\lambda L \xi)}{\cosh(\lambda L) + \cos(\lambda L)}; \quad (2.69)$$

where $k = c_0^{-4}$, consistently with Eq. (2.43) and $\lambda = \sqrt[4]{k/(4EJ)}$ is the so-called characteristic of the system (see Hetényi (1946) [125]).

If $\gamma = 1$, that is $c_1 = L/\sqrt[4]{EJ}$, the general integral of Eq. (2.41a) is

$$w(\xi) = s(\xi)^{\frac{3}{2} - \frac{\sqrt{5}}{2}} \Big(s(\xi)^{\sqrt{5}} \big(C_1 \eta(\xi) + C_2 \big) + \big(C_3 \eta(\xi) + C_4 \big) \Big) + \frac{P}{25} s(\xi)^4; \quad (2.70)$$

where $s(\xi) = \beta \xi + 1$.

On the other hand, if $\gamma = -1$, that is $c_1 = -L/\sqrt[4]{EJ}$, the general integral becomes

$$w(\xi) = s(\xi)^{\frac{3}{2}} \Big(C_1 s(\xi)^t + C_2 s(\xi)^{-t} + C_3 \sin\big(u\,\eta(\xi)\big) + C_4 \cos\big(u\,\eta(\xi)\big) \Big) + \frac{P}{23} s(\xi)^4; \quad (2.71)$$

where $t = \frac{1}{2}\sqrt{5 + 4\sqrt{2}}$ and $u = \frac{1}{2}\sqrt{4\sqrt{2} - 5}$.

Again, the imposition of the boundary conditions leads to very long expressions for coefficients C_i. Then, the complete solutions of the boundary value problem are not reported here. However, even though the three solutions of these special cases cannot be obtained directly from Eq. (2.65), they can be approached by a limit process taking values of c_1 tending to 0 or to $\pm L/\sqrt[4]{EJ}$, respectively, as it could be inspected by the representations presented next.

2.3.5 Results and discussion

The general integral of Eq. (2.65) reveals that the elastic flexural response of the beam non-proportionally depends upon both two characteristic parameters α and β defined in Section 2.3.1. To investigate their effect on the solution, a complete parametric study is carried out in this section. As observed in the previous section, α may take any value greater than zero; a comparison of its definition given in Eq. (2.45) with classical characteristic λ of solution (2.69) reveals that

$$\alpha = (\sqrt{2}\lambda L)^{-1}; \quad (2.72)$$

The value of α has been selected by the realistic range of λL given in Selvadurai (1979) [235]. Concerning parameter β, it must be greater than minus one;

nevertheless, values of β beyond 10 entail null values of $k(x)$ almost everywhere in the interval $[0,\ L]$ (simply-supported beam without foundation), as shown in Fig. 2.13a. Then, the ranges of values of these two non-dimensional parameters have been worked out by considering the previous observations and are given as follows:

$$\alpha = (0,\ 1]; \qquad \beta = (-1,\ 10]; \tag{2.73}$$

The normalized shape of the elastic line versus non-dimensional spatial coordinate ξ for various values of ratio β is displayed in the sequence of Figs. 2.16a–2.16f, each one with a fixed value of α. Normalized deflection $\overline{w}$ in these figures is introduced as

$$\overline{w} = \frac{w(\xi)}{w^{max}}; \tag{2.74}$$

where w^{max} is the maximum transverse deflection of the beam along its length.

The effect of the variable elastic foundation in transforming the shapes of the non-dimensional curves of the deflection is clearly seen from these plots, in particular for α less than 0.3. In fact, from the observation of the graphs in Figs. 2.16a–2.16d it is possible to see that for negative values of β, e.g. when the stiffness of the elastic springs is greater in the right part of the beam (*biased towards the right*), the beam deforms mainly on the left side, while for positive values of β, e.g. for greater stiffness of the foundation in the left part of the beam (*biased towards the left*), the higher displacements shift to the right side.

From Table 2.9 it is evident that results agree well with Hetenyi's classical solution, and that case β=0 can be reached from a limit process. It is also noted that the profile of the elastic line is characterized by changes in the sign of the second derivative when β is less than zero, while for positive β the concavity sign remains always the same, according to the direction of the load.

The reduction of the stiffness of the foundation, obtained by increasing α from 0.3 to 1 and beyond, is accompanied by a non-significant change of the deflection profile with β, with the curves overlapping towards a symmetric shape (Figs. 2.16e–2.16f). This reveals the fact that the solution consistently approaches the symmetric shape of the elastic line typical of a simply-supported beam without elastic foundation. The polynomial expression of this latter case can be deduced analytically by setting γ=0 into Eq. (2.53).

The graphs presented in Figs. 2.17a–2.17b show the effect of α and β on the maximum downward displacement and on the position of occurrence of such maximum, respectively. When β is near minus one and α is not approaching zero (case of a very stiff foundation), the maximum displacement accordingly becomes very small for each α. However, it is noted that the case of an everywhere rigid substrate cannot be completely achieved only by letting β going

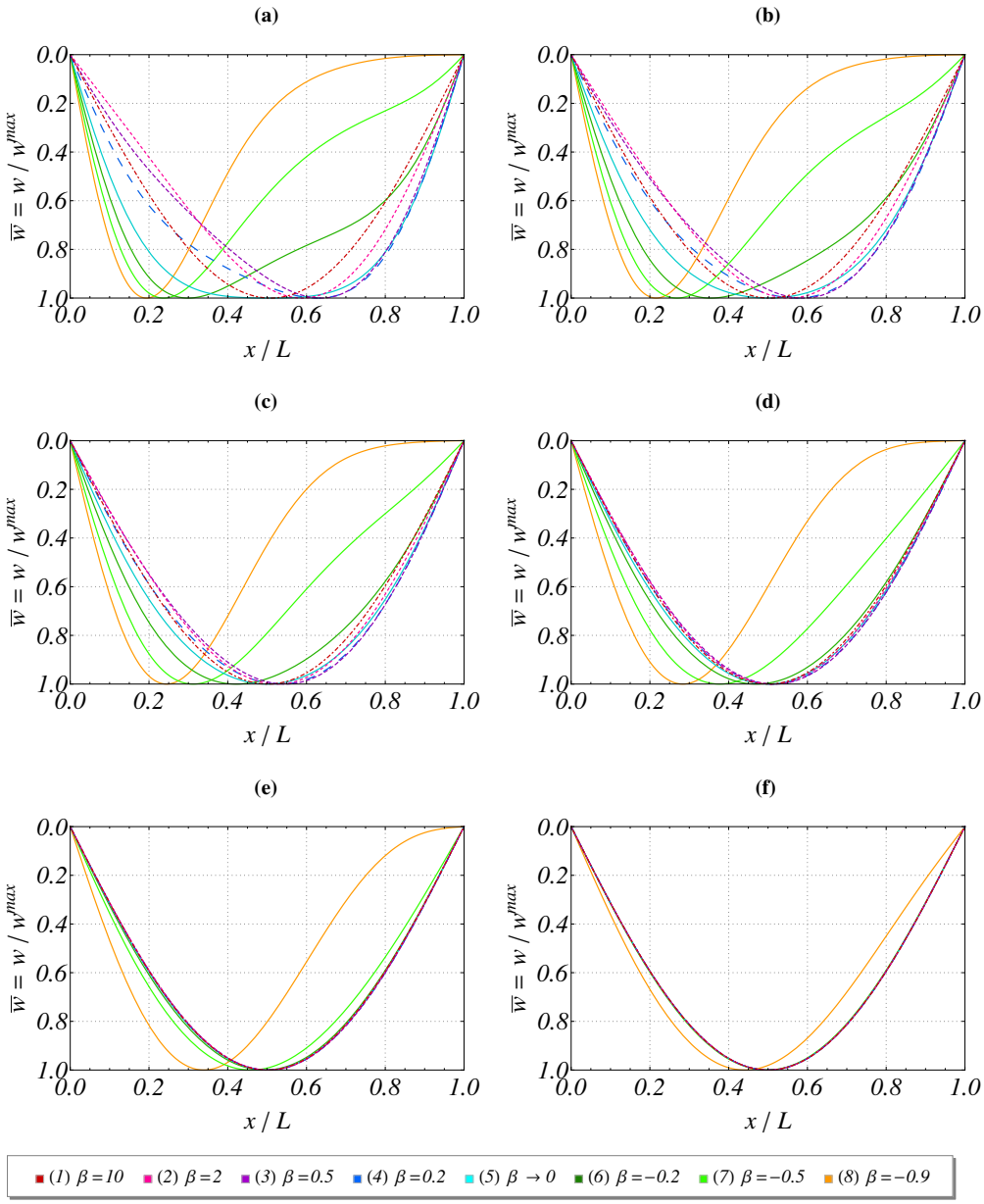

Figure 2.16: Normalized shape of elastic line $\overline{w}(\xi)$ for various values of β ($\alpha{=}\sqrt{2}/12{\simeq}0.118$, i.e. $\lambda L{=}6$ (a); $\alpha{=}\sqrt{2}/10{\simeq}0.141$, i.e. $\lambda L{=}5$ (b); $\alpha{=}\sqrt{2}/8{\simeq}0.177$, i.e. $\lambda L{=}4$ (c); $\alpha{=}\sqrt{2}/6{\simeq}0.236$, i.e. $\lambda L{=}3$ (d); $\alpha{=}\sqrt{2}/4{\simeq}0.354$, i.e. $\lambda L{=}2$ (e); $\alpha{=}\sqrt{2}/2{\simeq}0.707$, i.e. $\lambda L{=}1$ (f)).

to minus one, because near $\xi{=}0$ the coefficient of subgrade reaction remains always finite.

As β increases, the maximum displacement amplitudes get considerably

ξ	0.1	0.2	0.3	0.4	0.5
$\beta = 10^{-2}$	0.597009	1.09706	1.45876	1.67415	1.74672
$\beta = 10^{-3}$	0.590448	1.08402	1.43962	1.64992	1.71922
$\beta = 10^{-4}$	0.589796	1.08272	1.43771	1.64750	1.71648
Exact	0.589723	1.08257	1.43750	1.64723	1.71618

Table 2.9: Numerical experience of the limit process $\beta \to 0$. Comparison between the displacements given by Eq. (2.69) (exact solution when $\beta=0$) with those obtained with formula (2.63) by taking smaller and smaller values of β and $\alpha=0.2$ (deflection expressed in units of $10^{-3}\, EJ/\left(p\, L^4\right)$).

larger (Fig. 2.17a), with a growth rate which depends also from α; in fact, with increasing values of α, that is with an increase of foundation compliance, the sigmoidal curves of Fig. 2.17a slightly flatten out towards an horizontal line of ordinate $5/384$, also for small values of β; this latter case classically corresponds to the maximum deflection when there is no elastic foundation under the beam. Fig. 2.18 depicts the dependence of w^{max} on both α and β in a three-dimensional plot, for the range of parameters considered in this study.

Regardless of the value of α, for negative values of β, the position of the displacement peak is placed before the center of the beam (Fig. 2.17b), while for β greater than zero it is located beyond the center. The peak is always located at $\xi=0.5$ for every α when $\beta=0$ (case of constant modulus of subgrade reaction), and such position represents also the limit position as β becomes larger and larger (case of no elastic foundation). Parameter α affects the amplitude of the range of variation of the position of the peak: for α in the neighborhood of 0.1 the range is wide, going from $\xi^{max} \simeq 0.2$ to $\xi^{max} \simeq 0.65$, while for α near 1 the range is narrow, with the peak moving approximately in the

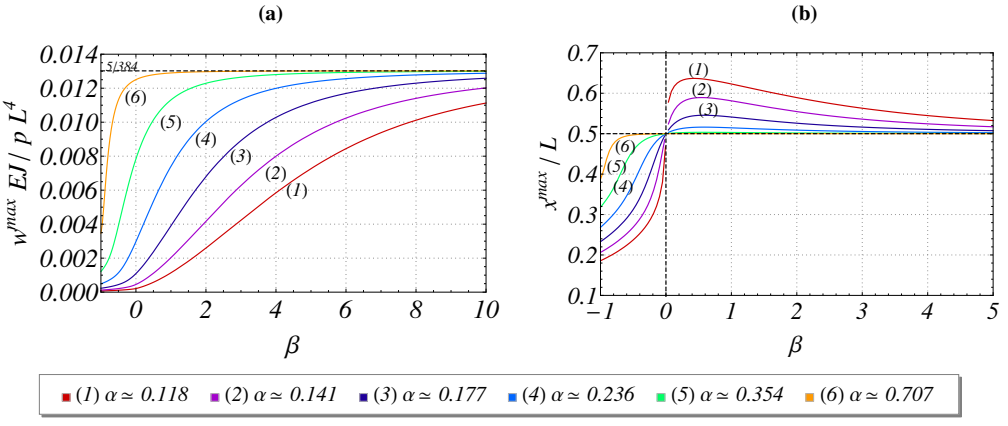

Figure 2.17: Variation of maximum downward displacement w^{max} (a) and position of maximum $\xi^{max}=x^{max}/L$ (b) vs. β, for the six values of α defined in the caption of Fig. 2.16.

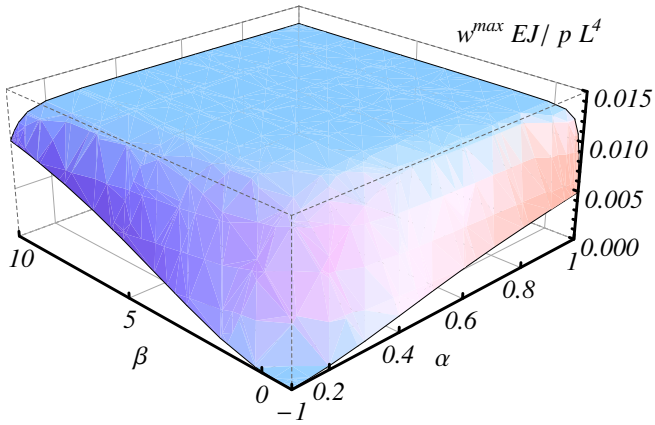

Figure 2.18: Variation of maximum downward displacement w^{max} vs. α and β.

interval $\xi^{max}\simeq 0.4$ to $\xi^{max}\simeq 0.5$.

Figs. 2.19a–2.19f show the variation of the shape of the normalized bending moment versus non-dimensional spatial coordinate ξ, depending on the same parameters considered for the deflection. Normalized bending moment $\overline{M}$ in Figs. 2.19a–2.19f is defined as:

$$\overline{M} = \frac{M(\xi)}{M^{max}}; \qquad M(\xi) = -\frac{EJ}{L^2} v^{(2)}(\xi); \tag{2.75}$$

where M^{max} is the maximum absolute bending moment of the beam along its length. It is noted that the bending moment is always zero at the edges of the beam, as well as the deflection, confirming the exactness of the solution for the simply-supported beam.

As mentioned before, for a foundation with reduced stiffness (Figs. 2.19e–2.19f) the bending moment curves produced by variations of β tend to collapse on the parabolic profile of the bending moment of a simply-supported beam without elastic foundation. On the other hand, small values of α yield to an enhanced irregularity of the curves. From Figs. 2.19a–2.19c one can see that

ξ	0.1	0.2	0.3	0.4	0.5
$\beta = 10^{-2}$	1.02212	1.41045	1.47158	1.42590	1.40262
$\beta = 10^{-3}$	1.02158	1.40681	1.46173	1.40773	1.37595
$\beta = 10^{-4}$	1.02153	1.40646	1.46075	1.40593	1.37330
Exact	1.02152	1.40642	1.46065	1.40573	1.37300

Table 2.10: Numerical experience of the limit process $\beta\to 0$. Comparison between the bending moment derived by Eq. (2.69) (exact solution when β=0) with those obtained with formula (2.63) by taking smaller and smaller values of β and α=0.2 (bending moment expressed in units of $10^{-2}\,(p\,L^2)^{-1}$).

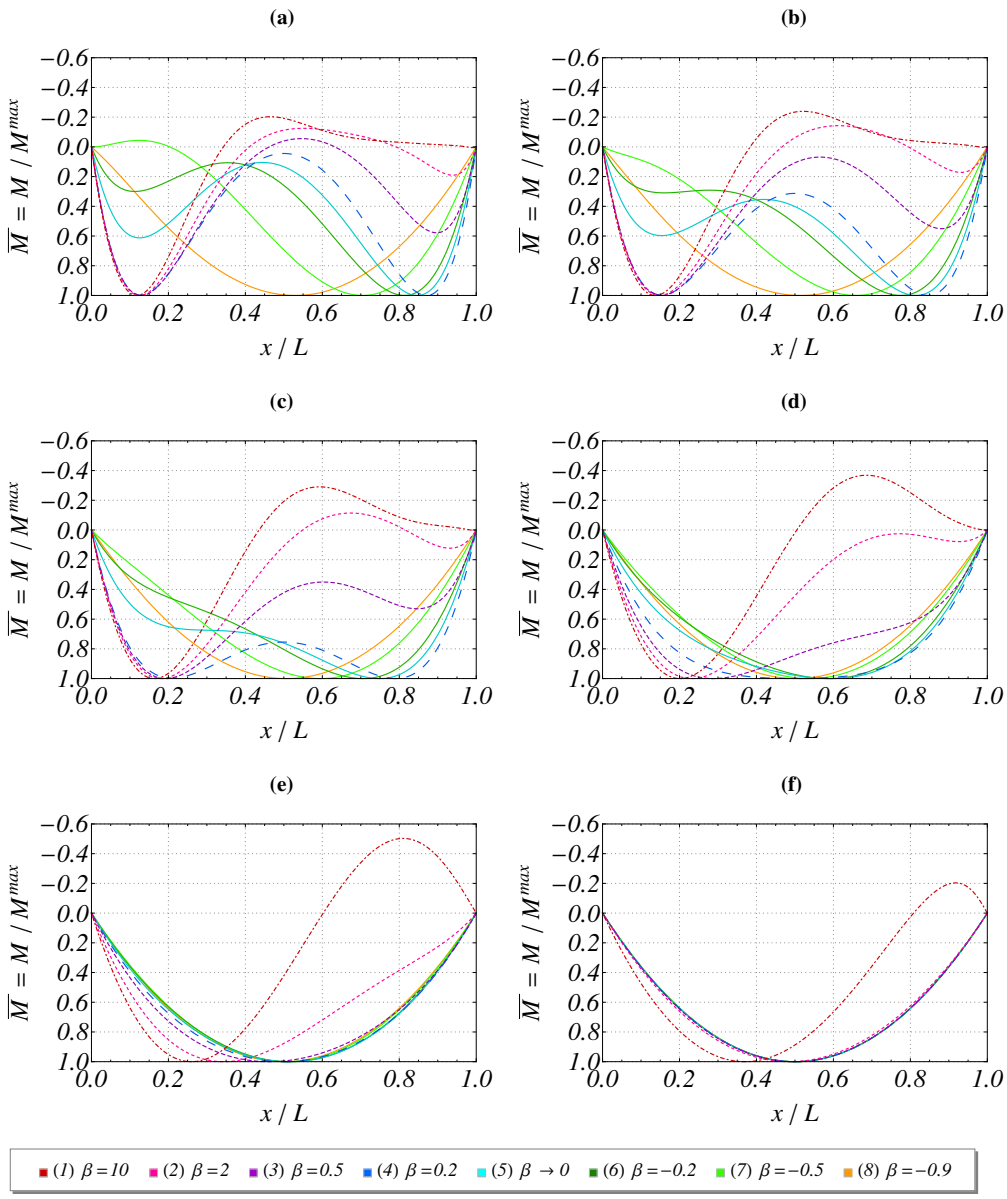

Figure 2.19: Normalized shape of bending moment curves $\overline{M}$ for various values of β and for the six values of α defined in the caption of Fig. 2.16.

bending moment curves depict three stationary points, with large values of α and β less than zero (rigid foundation); out of this range, decreasing α and increasing β, two or only one stationary points appear (Figs. 2.19d–2.19f).

The maximum peak value is always positive in each of these figures and located before the center of the beam for negative values of β, while it shifts beyond the center when β is positive. Also, negative values of the bending

moment can be observed, in particular when β is negative, with increasing intensity as α increases. The maximum negative bending moment remains in any case less than half of the maximum positive value. From Table 2.10 it is evident that results agree well with Hetenyi's classical solution (β=0).

Figs. 2.20a–2.20b illustrate the variation of the maximum (positive) bending moment and its spatial location, respectively. Regarding the values of the maximum bending moment (Fig. 2.20a) the trends are similar to those of the maximum displacements. As it was expected, from Fig. 2.20a it is possible to see that the decrease of the stiffness of the foundation, due to high values of α or β is accompanied by an increase of the bending moment. In fact, the curves are all asymptotic to an horizontal line of ordinate 1/8 for large values of β and gradually tends to that level for every β as α is greater than 0.8, which is in agreement with the results presented for the deflection in Fig. 2.17a.

As for the displacements, it can be clearly seen from Fig. 2.20b that for negative β the position of the peak of the displacements is placed before the center of the beam, while for positive β it is located beyond the center. In contrast to what happens for the deflection, in not all the cases the peak occurs at ξ=0.5 when β is zero, but, it depends also on the values of α. For small values of α and β=0 the existence of two equal peaks, placed symmetrically with respect to the mid-span of the beam, is indeed observed. So, as β crosses the zero point, the peak on the right becomes higher than that on the left, causing a sudden change in the peak's location: a jump discontinuity appears, with the two limits symmetrically located with respect to the center of the beam (Fig. 2.20b).

For higher values of α the tendency is similar to that of the displacement ones. Then, again the peak's position gradually decreases towards ξ=0.5 as β becomes larger and larger. The range of variation of the peak's position is wide for small values of α, while it reduces as α gets near to 1.

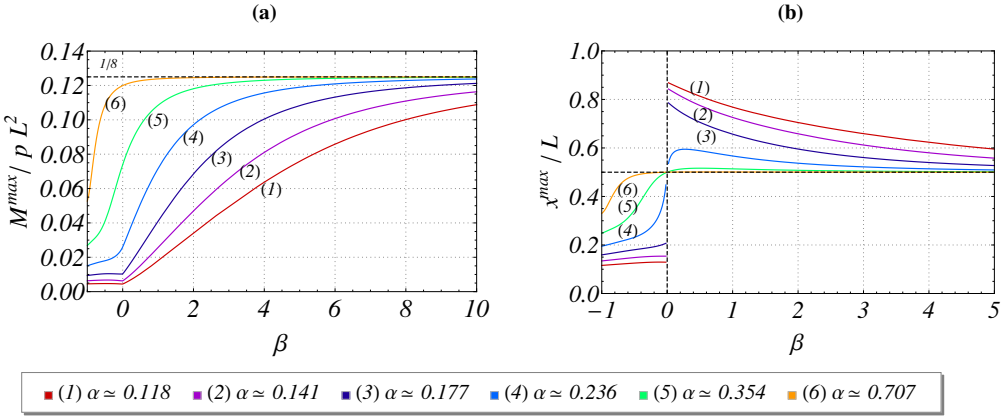

Figure 2.20: Variation of maximum bending moment M^{max} (a) and position of maximum $\xi^{max}=x^{max}/L$ (b) vs. β, for the six values of α defined in the caption of Fig. 2.16.

From the present results it can be seen that acting on the flexural rigidity EJ of the beam and on its length L induces a double effect. One is indeed the global proportionality of the displacements to these parameters; in fact, for converting the non-dimensional displacements shown in Fig. 2.17a into actual displacements w, they have to be multiplied by $p\,L^4/\,EJ$. The other effect is due to parameter α, which depends on EJ and L and considerably affects the displacement profiles. The same applies to the bending moment. These observations appear to constitute fundamental points for the design of beam-like structures lying on a variable Winkler foundation of this non-linear type and of similar ones.

2.3.6 Validation comparison of the analytical solution with independent numerical approaches

In this section an investigation is carried out through a validation comparison of the exact solution, in terms of vertical displacements and bending moments, with results achieved from an original independent implementation of three numerical methods previously proposed in the literature. In particular, the *finite power series* (PS) approximation examined by Clastornik et al. (1986) [60], the *sine series expansion* (SS) inspected by Iyengar and Anantharamu (1963) [135] and the *central-difference scheme* (FD) reported in Bowles (1974) [42] have been considered.

For this purpose, taking into account the definitions reported in Eqs. (2.43) and (2.45), it is more suitable to rewrite Eq. (2.41a) into the following form (for constant load $p(x)$=p):

$$(1+\beta\xi)^4 w_x^{(4)}(\xi) + \frac{w(\xi)}{\alpha^4} = \frac{pL^4}{EJ}(1+\beta\xi)^4. \tag{2.76}$$

Such rearrangement simplifies the implementation of the considered numerical methods, since all the expressions involving non-dimensional variable ξ appear at the numerator on both sides of differential equation (2.76).

As a first approach, the *finite power series* (PS) approximation examined by Clastornik et al. (1986) [60] has been considered, a method that conceives the following power series expansion of approximation $\tilde{w}(\xi)$ of unknown function $w(\xi)$:

$$w(\xi) \simeq \tilde{w}(\xi) = \sum_{n=0}^{N} a_n \xi^n; \tag{2.77}$$

where a_n are N unknown coefficients to be found to obtain the sought approximation of $w(\xi)$. Let

$$(1+\beta\xi)^4 = \sum_{n=0}^{N} q_n \xi^n; \tag{2.78}$$

be the power series approximation of the variable coefficient in Eq. (2.76); then, the substitution of the expressions of Eqs. (2.76)-(2.77) into Eq. (2.78) gives

$$\sum_{n=0}^{N}\left((n{+}4)(n{+}3)(n{+}2)(n{+}1)\sum_{m=0}^{n}q_m a_{n+4-m}+\frac{a_n EJ}{\alpha^4 pL^4}-q_n\right)\xi^n=0. \quad (2.79)$$

To satisfy the previous equation for every value of ξ, coefficients a_n must verify the following relations ($n{=}0,\ldots,N-4$)

$$(n+4)(n+3)(n+2)(n+1)\sum_{m=0}^{n}q_m a_{n+4-m}+\frac{a_n EJ}{\alpha^4 pL^4}-q_n=0; \quad (2.80)$$

which, together with boundary conditions (2.41b)-(2.41e), constitute a linear system of equations, whose solution are N unknown coefficients a_n.

The second numerical method which has been considered is the *sine series expansion* (SS) reported by Iyengar and Anantharamu (1963) [135]. In handling it, the finite sine series expansion

$$w(\xi)\simeq\tilde{w}(\xi)=\sum_{n=1}^{N}a_n\sin(n\pi\xi); \quad (2.81)$$

is considered for unknown function $w(\xi)$. Substituting this expression into Eq. (2.76), multiplying both sides by $\sin(m\pi\xi)$ and, lastly, integrating between $\xi{=}0$ and $\xi{=}1$, it results

$$\sum_{n=1}^{N}a_n\left((n\pi)^4\int_0^1(1+\beta\xi)^4\sin(n\pi\xi)\sin(m\pi\xi)\,d\xi+\frac{\delta_{mn}}{2\alpha^4}\right)= \\ =\frac{pL^4}{EJ}\int_0^1(1+\beta\xi)^4\sin(m\pi\xi)\,d\xi. \quad (2.82)$$

where δ_{mn} is the Kronecker delta, i.e. $\delta_{mn}{=}1$ for $n{=}m$ and $\delta_{mn}{=}0$ for $n{\neq}m$. Now, it may be noted that the integrals on the left hand side of Eq. (2.82) are not trivial to be solved, but they may be derived by integration by parts. These have been performed in closed-form within a Mathematica [274] environment; however arising expressions are too lengthy to be reported here. Writing Eq. (2.80) for m from 1 to N leads to a linear system of equations, whose solution provides N unknown coefficients a_n.

As a third numerical approximate technique, the central-finite differences scheme treated in Bowles (1974) [42] has been considered, by a numerical implementation within Mathematica [274]. Each of these numerical methods obtains the solution by solving in the end a linear system of equations. Therefore, their accuracy has been checked by varying the size of the corresponding

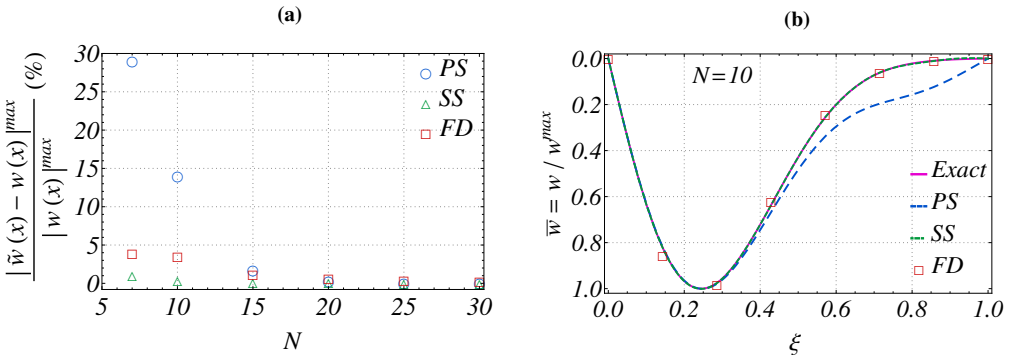

Figure 2.21: Maximum percentage relative errors of deflection (a) and deflection shapes (b) vs. dimension N of the solving system in the numerical solutions.

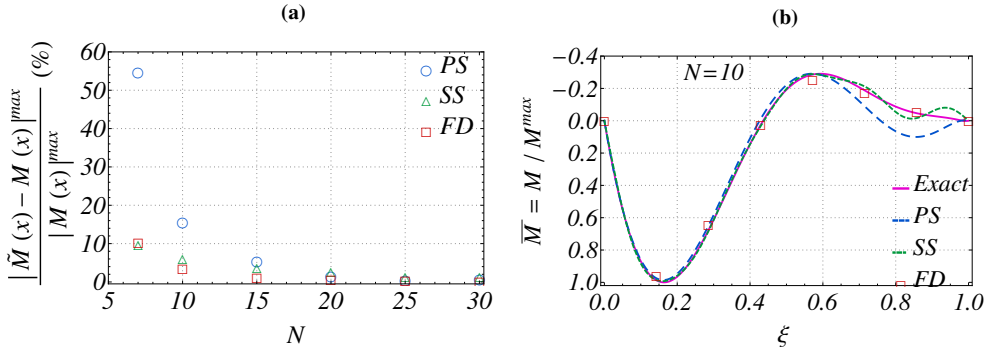

Figure 2.22: Maximum percentage relative errors of (a) and bending moment shapes (b) vs. dimension N of the solving system in the numerical solutions.

linear system, that is, number N of the solving equations. For the two methods based on series expansions, parameter N represents the number of considered terms in the truncated series, while in the FD approach it corresponds to the number of nodes plus two.

The simulations presented here are performed by assuming α and β equal to 0.177 (λL=4) and -0.9, respectively, a case in which quite complex deflection and bending moment shapes arise from the analytical solution (see Figs. 2.16c and 2.19c).

In Fig. 2.21a the percentage relative error of the deflection versus system size N is depicted, for the three numerical methods, with respect to the results from the analytical solution. The outcomes appear in good agreement with those of the analytical solution, for all the cases, while the achieved accuracy strongly depends on the type of the adopted numerical method.

It is possible to appreciate that the power series expansion (PS) looks the least reliable method, as it achieves good accuracy only for N approximately

higher than 15. The central-difference scheme (FD) proves to be the simplest and quickest procedure, although it allows to obtain only a discrete set of solution points. Moreover, its second-order convergence may be clearly observed in Fig. 2.21a. Sine series expansion (SS) turns out to be a very accurate method, although the implementation of this method is not that straightforward, since the solution of the non-trivial integrals commented above has been required.

The representations of the deflection shapes provided in Fig. 2.21b have been obtained with N equal to 10. Fig. 2.21b shows the agreement of the numerical methods with the exact solution. The percentage relative error of the bending moment versus size of the solving system N is investigated in Fig. 2.22a. As it may be expected, the accuracy provided by the numerical methods downgrades with respect to the description of the displacements. In more detail, both series expansions prove to be inadequate to predict the bending moment for N lower than 20, hence resulting in very lengthy expressions. On the other hand, it is important to highlight that the central-difference scheme remains sufficiently accurate, even for the representation of the bending moment. The discrepancies in the bending moment description provided by the numerical methods with respect to the exact solution are clearly represented in Fig. 2.22b for N equal to 10.

2.4 Closing chapter considerations

In this chapter, the static responses of finite Euler-Bernoulli elastic beams lying on a Winkler foundation with modulus of subgrade reaction assumed to vary in space have been analytically investigated. The exact closed-form parametric solutions of the underlying boundary value problems, characterized by a linear differential equations with variable coefficients, have been rigorously derived in full analytical form by the theory of ODE (as summarized in the chart of Figs. 2.15 and 2.4).

First, fundamental mathematical manipulations have been summarized and presented. Then, complete parametric analyses on the beam-foundation system response as a function of the characteristic mechanical parameters has been developed, with specific reference to explore the dependence of deflections and bending moments.

In the first analysis the analytical solution of the static elastic deflection of a free-free Euler-Bernoulli beam on a Winkler support with stiffness coefficient varying linearly along the axis of the beam and acted upon by a force and/or a torque at one of its edges has been explicitly examined. The solution has been again derived in closed-form, here by the aid of generalized hypergeometric functions. The (linear) space variation of the support elastic stiffness coefficient already allows to inspect space-variation effects on the structural re-

sponse, as well as to reproduce the limit case of a rigid beam on elastic support. Further, it agrees well with the case of a constant support elastic stiffness coefficient, whose solution has been also separately re-derived for completeness and comparison purposes.

Non-dimensional bending response curves have been depicted, displaying the main characteristic features of the behavior of the beam-foundation system. Shapes and amplitudes are ruled by the relative flexibility of the beam-foundation system at the upper beam extremum and by the stiffness ratio measuring how the elastic coefficient varies along the beam. Response curves may be inspected to visualize the maximum characteristic values of deflection and bending moment and shear.

In the second analysis a simply-supported beam subjected to a constant distributed load and a Winkler coefficient endowed with a minus four power variation along the beam axis has been studied. The outcomes of the achieved analytical solution, in terms of deflections and bending moments, are in perfect agreement with predictions from three independent reimplemented numerical methods. The advantage of owning the exact solution is evident, especially when the response has to be used to derive other quantities, as for the case of the bending moment derived by double differentiation from the deflection. The derived solution is fully consistent with an available theorem on existence and uniqueness of the solution.

The selected expression for the support elastic stiffness coefficient is able to represent manifold space-variation trends as well as to reproduce the limit case of the absence of foundation. Further, it agrees well with Hetenyi's solution for a constant support elastic stiffness coefficient. Deflection and bending moment non-dimensional curves versus non-dimensional spatial parameter have been presented, showing several characteristic features of the structural response. The shapes and amplitudes of these curves are controlled by the relative flexibility of the beam-foundation system evaluated at the left extreme of the beam and by the ratio describing how rapidly the elastic coefficient changes along the beam axis. Such dependence has been widely discussed in this study.

Curves which can be used to compute the maximum deflection and bending moment have been displayed for both considered problems. These curves may supply guidance for the practical design of beams on variable elastic Winkler support. Also, the reference analytical model derived here has been proven to constitute a powerful tool for the parametrization and interpretation of the structural response, and a reference analytical model appears undoubtedly more effective than a numerical one, especially for ensuing contexts of parameter identification or design purposes, also in terms of parametrization and interpretation of the achieved structural response.

Moreover, the derived exact analytical solution may constitute a benchmark reference for validating reliability and accuracy of alternative numerical ap-

proaches, which may be useful to solve more complicated problems, where analytical treatments may become unfeasible, especially in explicit closed-form.

Chapter 3

Transient formulation for finite beams under harmonic moving load

3.1 State of the art on moving load transient analysis

Concerning the analysis of beams lying on a damped or undamped Winkler elastic foundation, excited by a moving load, different approaches have been adopted so far. In case of linear foundations, one of the most common modelizations is to consider the steady-state response of infinite beams subjected to a constant magnitude moving load (see e.g. Kenney, 1954 [155], Frýba, 1972 [105], Froio et al., 2018 [102]), as well as to a moving load with harmonically-varying amplitude, as reported by Mathews (1958,1959) [189,190], Chonan (1978) [58] and Bogacz et al. (1989) [40].

In particular, Bogacz et al. (1989) [40] demonstrated that, given a certain frequency of loading, at critical conditions two of the four waves generated by the moving load propagate with a certain group velocity in the same direction of the moving force. If the load takes a velocity equal to the group velocity of one of these two waves, the energy is not transferred away from the load, but accumulates in its vicinity, leading to an infinite increase of the response of the beam. Such velocities for which an unbounded response occurs in the ideal undamped case are called critical velocities of an infinite beam.

Although steady-state solutions display an appealing simplicity, it is difficult to relate them to the response of finite beams. For instance, the steady-state solution for infinite beams on undamped elastic foundations indicates an unbounded response at the critical velocity. On the contrary, finite beams, acted upon by a moving load for a finite time, always display a bounded response. Nevertheless, structural vibrations of finite beams induced by a moving load may also become very high, when the velocity of the moving load attains a

certain characteristic value. Such velocity, again referred to as critical velocity in the literature, is defined as either the lowest between the modal resonant velocities of the system (Chen and Huang, 2003 [54]), the latter defined as the moving load velocity causing the maximum displacement for each modal coordinate, or the load velocity inducing the beam's highest deflections directed downward and/or upward (Dimitrovová and Varandas, 2009 [73]). In the present work the second definition will be considered, which can also be applied to nonlinear beam-foundation systems.

Moreover, for finite beams, the phenomenon of wave reflection at the boundaries occurs, leading to important increments of the beam displacements. A thorough explanation of the phenomenon of wave reflection for the transient response of a simply-supported Euler-Bernoulli beam and its strong influence on the maximum displacements attained by the beam at supercritical velocities is reported in the work of Steele (1967) [247]. The head wave front, moving with its group velocity, reflects from the far end before the load reaches the beam extreme. After the load departs from the beam, the head wave train remains in the system bouncing back and forth from the beam ends. The same occurs for the tail wave train, which displays a different group velocity. Due to these reflections, at certain times, the regions near the beam ends are exposed to the sum of incident and/or reflected portions of the wave trains, with several possible combinations. This implies increased values of the maximum displacements, about several times that related to the steady-state response of the infinite beam.

Chen and Huang (2003) [54] investigated the influence of the structural parameters and of the load frequency on the critical velocities of an Euler-Bernoulli or Timoshenko beam on a linear viscoelastic foundation by employing the dynamic stiffness matrix method derived in Chen (1987) [55], Chen and Sheu (1993) [57], Chen and Sheu (1993) [57] and Chen and Huang (2000) [53]. The authors showed that the minimum of the resonant curve for a finite beam coincides with the resonance condition of an infinite beam (critical velocity), while such minimum cannot be attained in general for a finite beam, since the set of feasible wave numbers of a finite beam is a countably infinite set of isolated values (discrete spectrum of the system's eigenvalues). Thus, the critical velocity for an infinite beam represents a lower bound for the critical velocity of the corresponding finite beam, proving that the velocity required to excite the resonance of an infinite beam is smaller than that of any finite one. Nevertheless, if the finite beam is sufficiently long, its lowest resonant velocity becomes very close to that of an infinite beam. A comparison between Euler-Bernoulli and Timoshenko models for practical values of the foundation stiffness, of the moving load velocity and of its frequency of oscillation revealed that the predictions from the two models were very close to each other.

Regarding the effect of an Harmonic Moving Load (HML), the results ob-

tained by Chen and Huang (2003) [54] showed the existence of two resonant curves which approach the curve obtained for a constant amplitude moving load, as the frequency of the harmonic amplitude of the moving load approaches zero. The relationship between the critical velocity and the frequency of oscillation of the load magnitude originates the bifurcation curves.

Dimitrovová and Varandas (2009) [73], analyzed the transient dynamic response of Euler-Bernoulli beams of finite length subjected to a moving constant force with sudden change of foundation stiffness at the mid-section. Such an abrupt change in the mechanical characteristics of the support may occur in several practical engineering applications. Two methods were proposed. One was based on the superposition of the global modes of vibration, obtained by using a finite integral transformation; the other one was based on linking together the analytical solutions of two separate parts of the structure, thanks to continuity conditions. The outcomes were expressed in terms of vertical displacement and were used for the determination of the critical velocities through a parametric analysis. In particular, it was shown that passing from a softer to a harder region, both critical velocities are clearly marked in the harder region and maximum dynamic displacements are amplified. This effect is instead not so evident by passing from a harder to a softer region. A generalization of this approach for beams resting on a piecewise homogeneous viscoelastic foundation is reported in Dimitrovová (2010) [73].

In a subsequent work, Dimitrovová and Rodrigues (2012) [72] presented parametric analyses aimed at obtaining the highest beam displacements as a function of the velocity of a load with constant amplitude moving uniformly along a simply-supported/almost infinite beam on a viscoelastic foundation, possibly composed of two subdomains accounting for abrupt changes in the foundation stiffness. The study was carried out by considering finite as well as infinite simply-supported beams, with both Euler-Bernoulli and Timoshenko-Rayleigh structural theories. In the considered case study, negligible differences between the two structural models were found, as in Chen and Huang (2003) [54]. Some interesting conclusions were outlined in that work, focused especially on the critical velocity and the effects of damping. For downward displacements at supercritical velocities and upward displacements at the full range of velocities, reflected waves imply that higher extreme values are achieved when the load is already off the structure. Pertaining to finite beams composed of two sub-domains, the harder sub-domain, which displays a higher critical velocity, acquires another displacement peak, which corresponds to the critical velocity of the softer sub-domain. It was also observed that extreme values in the first sub-domain are higher when the force is traveling over the second sub-domain than when it is traveling over the first sub-domain. Regarding the effect of damping, even a low level of damping is enough to smooth the resulting extreme displacement curves and to significantly decrease all the dis-

placements.

Amiri and Oyango (2010) [4] analyzed the vibrations induced by repeated concentrated loads of a constant magnitude, moving along simply-supported Euler-Bernoulli beams over an elastic foundation. The equation of motion, formulated with the superposition principle, was solved with the Fourier Sine transform. The effects of some important parameters, such as the foundation stiffness, the distance between the loads and the traveling speed were examined.

Besides analytical solutions and other numerical methods, in the past two decades the Finite Element Method (FEM) has been widely used for solving structural dynamic problems involving moving loads. For instance, Olsson (1991) [211] determined the dynamic response a simply-supported Euler-Bernoulli beam without support subjected to a constant amplitude moving load by the FEM and compared it with the analytical solution reported by Frýba (1972) [105]. Rieker (1996) [228] investigated the effects of mesh refinement on the accuracy of the finite element formulation. Beams subjected to a moving load, a moving mass or moving spring-mass system and with different boundary conditions were considered. The results showed more demanding requirements for the moving load dynamic problem with respect to those of the static analysis; in fact, the author proposed the following rule of thumb: the number elements used for a moving load analysis should be at least two to eight times the number used for a static analysis. Moreover, mesh refinement must be enhanced even further when the traveling speed increases or when the mass ratio between the load and the beam increases.

Among the copious studies involving beams without foundation, to the interested reader it is noteworthy to mention also the works of Abu-Hilal (2006) [1] and Wu and Gao (2015) [275], who investigated the dynamic response of two identical elastic homogeneous isotropic beams, parallel and connected continuously by a layer of elastic springs provided with viscous damping under a moving harmonic load, and of Kumar et al. (2015) [168] and Museros and Moliner (2017) [207], who studied the cancellation phenomenon characterizing the free vibration response of a simply-supported beam after the transition of a single concentrated moving load.

Combined with the FEM, the numerical direct integration in time appears one of the most common approaches for the solution of the equations of motion in the time domain. The FEM and Newmark method were applied successfully by Thambiratnam and Zhuge (1996) [250] for a constant amplitude moving load and by Kien and Hai (2006) [164], Kien (2008) [162] and Kien and Ha (2011) [163] for a harmonic moving load. The most interesting conclusion derived by these latter authors was that when the excitation frequency is lower than the fundamental frequency, an increment in axial force leads to an increment in the maximum dynamic deflection, while when the excitation

frequency is higher than the fundamental frequency, a reduction in maximum dynamic response is observed by increasing in the axial force. Further, Nguyen et al. (2017) [208] applied FEM and Newmark method in computing the vibration response of a bi-dimensional functionally graded Timoshenko beam excited by a moving concentrated load in order to highlight the effect of the material distribution and moving load velocity on the vibration characteristics of the beams.

Nevertheless, the support structure may reveal to be highly nonlinear, as for railway tracks due to the hardening mechanical characteristics of the ballast. For instance, the nonlinear elastic foundation model with linear plus cubic stiffness has been widely recognized as one of the most reliable and convenient modelizations for the dynamic analysis of tracks and pavements (Castro Jorge et al., 2015 [50]). Some of the studies dealing with such type of foundation are discussed below.

A simply-supported beam lying on a linear or nonlinear viscoelastic foundation subjected to a moving concentrated force was tackled by Ding et al. (2012) [74] and solved in space by the Galerkin method. The spatially-discretized equations of motion were solved in the time domain by means of fourth-order Runge Kutta method. The effects of foundation stiffness, boundary conditions, beam length and other parameters on the convergence rate were studied. It was found that the rate of convergence increased with the growing nonlinear stiffness of the foundation, but it decreased as the linear foundation stiffness and the damping coefficient increased. Furthermore, it was proven that the effects of the boundary conditions on the dynamic displacements became less relevant as the beam length increased.

Ansari et al. (2010,2011) [6,7] investigated the dynamics of simply-supported beams on a nonlinear viscoelastic foundation acted upon by a moving concentrated force. The nonlinear equation of motion of the Euler-Bernoulli beam was discretized with the Galerkin method and solved for different harmonics by implementing the Multiple Scales Method. The frequency response of different harmonics, the stability and the internal-external resonance conditions were studied. The frequency response curves for the first three harmonics revealed a jump phenomenon, which can be delayed by increasing the nonlinear stiffness, the foundation damping coefficient and the load magnitude. A sensitivity analysis proved that the first harmonics are more sensitive to the nonlinear component of the foundation stiffness, with respect to the damping factor and to the magnitude of the moving load.

Several authors adopted the FEM for the solution of dynamic problems involving nonlinear elastic foundations. Senalp et al. (2010) [236] analyzed the dynamic behavior of a simply-supported beam lying on a linear or nonlinear viscoelastic foundation subjected to a moving concentrated force in the subcritical range of velocity. The effects of moving load velocity and damping of the

system were found to be similar for linear and nonlinear elastic foundations. Castro Jorge et al. (2015) [50] took into account also supercritical velocities and considered also the presence of a discontinuity in space (two sub-domains) in the foundation modulus. The presence of damping was also taken into account. Critical velocities were determined and the effects of load intensity and foundation stiffness on both beam displacements and critical velocity were investigated. The results they presented were in agreement to those earlier shown by Dimitrovová and Varandas (2009) [73], Dimitrovová (2010) [68] and by Dimitrovová and Rodrigues (2012) [72], for a linear elastic foundation.

However, in practice, the support structure may also be highly nonlinear due to its asymmetric behavior in compression and in tension, even under small deformations, leading to a bilinear model of the foundation. The discrepancy in the beam analysis incurred from ignoring the effect of a bilinear behavior of the foundation may be relevant, because the reduced overall stiffness of the system may cause a consistent reduction of the value of the critical velocity (Castro Jorge et al., 2015 [49]). However, this aspect comes to complicate the analysis and makes it highly non-linear, since the location and extent of the regions of contact and separation is not known "a priori". As a result, only a limited number of studies dealing with a bilinear foundation appear to have been explored in the literature, mostly based on numerical methods. These are shortly reviewed below.

Studies involving tensionless or monolateral foundations (a special case of bilinear foundation with null tensile stiffness) have already appeared in the literature. For instance, Sapountzakis and Kampitsis (2011) [232] developed a Boundary Element Method (BEM) approach for the geometrical nonlinear response of shear deformable beams with simply or multiply connected constant cross-sections, traversed by moving loads as well as to axial loading, resting on a tensionless nonlinear three-parameter viscoelastic foundation and undergoing moderate large deflections under general boundary conditions.

Pertaining to bilinear foundations, a first analysis for deriving the static response of a finite Euler-Bernoulli beam was performed by Tsai and Westmann (1967) [255] through a Green function approach. Later, a computational method for the same problem was developed by Johnson and Kouskoulas (1973) [146]. Detailed transient dynamical FEM analyses of a simply-supported beam under a constant amplitude moving load may be found in the work of Castro Jorge et al. (2015) [49]. By varying load velocity, difference between foundation's moduli in compression and in tension and damping, several analyses were performed to determine the maximum upward and downward displacements of the beam, showing that displacements may become very important at the critical velocity, and also at lower velocities, as approaching a tensionless foundation case. Rodrigues et al. (2016) [229] extended this approach to a moving oscillator problem (see also Mazilu, 2013 [192]).

Hence, by several authors it has been reported that the value of the critical velocity for finite beams is influenced by the frequency of oscillation of the load magnitude and by the nonlinearity of the foundation. The aim of the present chapter is that of exploring this dependency in case of bilinear and cubic superlinear elastic foundations, thus extending the analyses presented in Castro Jorge et al. (2015) [49,50]. As previously exposed, prior studies involving beam-foundation systems acted upon harmonic moving loads demonstrated the existence of a bifurcation of the critical velocity into two distinct values, due to the harmonic variation of the moving load magnitude. Such bifurcation curves, but depicted for bilinear and cubic superlinear elastic foundations seem instead unprecedented in the scientific literature. However, this knowledge appears fundamental, also in terms of practical applications; for instance, when it looks necessary to choose between two possible design options of a vehicle, one which leads to exert forces on the tracks that are larger but display appreciably smaller frequencies or viceversa. By virtue of the present methodology and associated results, practical guidelines may be extrapolated towards handling such important design issues.

Therefore, the transient dynamic response of a simply-supported Euler-Bernoulli beam resting on a homogeneous in space Winkler nonlinear elastic foundation acted by a transverse concentrated moving load with harmonic-varying magnitude and constant velocity, is considered. Two types of nonlinearities of the support are considered with bilinear and cubic superlinear laws, respectively. The dynamic response is numerically obtained by using an autonomous FEM implementation coupled with a HHT-α method for the time integration (Hilber et al., 1977 [129]).

The purpose of the present chapter is two-fold. Firstly, this work aims at demonstrating the reliability, consistency and accuracy of the present implementation, described in Section 3.2, by the comparison of the obtained numerical critical velocities to earlier results reported by Castro Jorge et al. (2015) [49, 50] and by Chen and Huang (2003) [54]. Secondly, through a vast campaign of numerical simulations, the influence of the load velocity and of the load frequency on the maximum downward and upward displacements of the beam is investigated in Sections 3.3-3.4. By virtue of the obtained results, the critical velocities are determined as the load velocities inducing a peak of the beam's maximum displacements (as in Castro Jorge et al., 2015 [49]), and are plotted as a function of the load frequency. As outlined above, the effects of the load frequency on the critical velocity leads to multiple-branch maps. These curves are numerically computed from the outcomes of the FEM simulations and, then, reproduced by appropriate analytical fitting proposals with calibrated coefficients, providing simple and effective formulas to represent the critical velocity dependency on the load frequency.

Furthermore, regarding the bilinear foundation model, automated dedicated

computational strategies to handle the necessary and most appropriate space/ time discretization have been established and the dependence of the critical velocities on the ratio between the foundation's moduli in compression and in tension is also taken into account together with the load frequency. On the other hand, when considering a cubic superlinear constitutive law, the dependency of the critical velocities on the mean value of the harmonic moving load is also investigated, revealing the manifestation of three different critical velocities. The content of the present chapter stems from the outcomes of the research reported by Moioli (2016) [200] and Froio et al. (2016, 2017) [97, 100, 101].

3.2 Theoretical bases and FEM implementation

3.2.1 Problem formulation

Consider the idealized system shown in Fig. 3.1, consisting of a simply-supported beam of length L [m] lying on a Winkler nonlinear elastic foundation under the action of a concentrated force of magnitude $F(t)$ [N], harmonically oscillating in time t [s] with frequency Ω [rad/s] and moving with constant velocity v [m/s] along the beam. The force is assumed to be positive if directed upward. An Euler-Bernoulli beam model with Young modulus E [N/m^2], area moment of inertia J [m^4], cross-section area A [m^2] and mass density per unit volume ρ [kg/m^3], assumed constant along the beam, has been selected (thus, $\mu{=}\rho A$ [kg/m] is the mass per unit length of the beam). Viscous damping smeared onto both the beam and the foundation is assumed, with a constant damping coefficient c_d [Ns/m^2].

From these assumptions, by considering the dynamic equilibrium of a beam resting on such elastic support and undergoing transverse vibrations, the partial differential equation of motion describing the motion of the elastic beam-foundation system is

$$EJ\, w_x^{(4)}(x,t) + \mu\, w_t^{(2)}(x,t) + c_d\, w_t^{(1)}(x,t) + r(w) = F(t)\delta(x - vt) - \mu g; \quad (3.1)$$

where x is the axial coordinate ($0 < x < L$), with the origin fixed at the left end of the beam, t is the time variable ($0 < t < L/v$), with the origin at the instant on which the force starts its motion at the left extreme of the beam ($x{=}0$), $w(x,t)$ is the vertical deflection of the beam (positive if upward), and μg [N/m] is the beam's self-weight (g [N/kg] being the acceleration of gravity), and $r(w)$ [N/m] is the reaction force per unit length supplied by the elastic foundation. The concentrated moving load acting at time t at current position vt exciting the beam-foundation system is represented on the right hand side of Eq. (3.1) by Dirac delta function $\delta(\cdot)$.

One possible approach for obtaining the complete dynamic response of the system described by Eq. (3.1) consists of a spatial discretization of the struc-

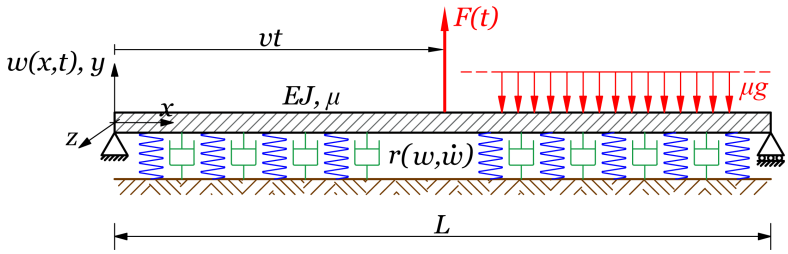

Figure 3.1: Simply-supported finite Euler-Bernoulli elastic beam lying on a nonlinear elastic foundation subjected to a moving load with variable amplitude.

ture by means of finite elements, followed by a temporal discretization of the resulting system of ordinary differential equations by a process of numerical integration. Thus, let the beam be discretized into a uniform mesh of finite elements of equal length h such as the one depicted in Fig. 3.2a.

Two degrees of freedom for each node are considered for the description of the beam displacements: the transverse displacement and the rotation around the axis normal to the plane of the sheet, resulting in a vector of four generalized coordinates $\mathbf{q}^e$ with components defined as in Fig. 3.2a. The generalized coordinates represent the weights of the linear combination of shape functions $\psi_i(x)$, which is used for approximating the field of transverse displacements $w(x) = \mathbf{\Psi}^e(x)\,\mathbf{q}^e$, being $\mathbf{\Psi}^e(x)$ the column vector containing the usual cubic Hermitian polynomials shape functions (Castro Jorge et al., 2015 [49]), whose expressions are the following:

$$\begin{aligned} \psi_1(x) &= 1 - 3\left(\frac{x}{h}\right)^2 + 2\left(\frac{x}{h}\right)^3; \quad & \psi_2(x) &= x - 2h\left(\frac{x}{h}\right)^2 + h\left(\frac{x}{h}\right)^3; \\ \psi_3(x) &= 3\left(\frac{x}{h}\right)^2 - 2\left(\frac{x}{h}\right)^3; & \psi_4(x) &= -h\left(\frac{x}{h}\right)^2 + h\left(\frac{x}{h}\right)^3. \end{aligned} \tag{3.2}$$

By means of such polynomial interpolation and by the application of the FEM, equation of motion (3.1), written for an arbitrary finite element of length h [m] in semi-discretized form and accounting for linear viscous damping, becomes

$$\mathbf{M}^e\,\ddot{\mathbf{q}}^e + \mathbf{C}^e\,\dot{\mathbf{q}}^e + \mathbf{K}_b^e\,\mathbf{q}^e + \mathbf{Q}_{f,nl}^e\left(\mathbf{q}^e\right) = \mathbf{F}^e + \mathbf{Q}^e; \tag{3.3}$$

where $\mathbf{M}^e$, $\mathbf{C}^e$ and $\mathbf{K}_b^e$ are the usual elementary mass, damping and stiffness matrices of a beam finite element, respectively. The effect of the nonlinear behavior of the foundation is represented by the element force vector

$$\mathbf{Q}_{f,nl}^e = \frac{\partial U_f}{\partial \mathbf{q}^e}; \tag{3.4}$$

where U_f is the elastic potential energy of the foundation.

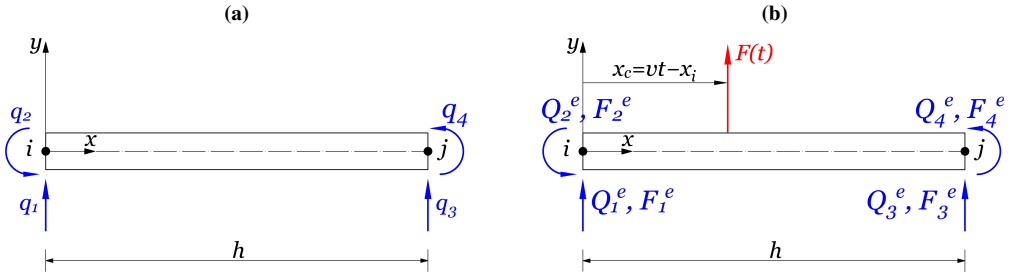

Figure 3.2: Nodal degrees freedom of an Euler-Bernoulli beam finite element on a bilinear elastic foundation (a) and generalized forces acting on a beam element (b).

Regarding to the right hand side of Eq. (3.3), vector of generalized forces $\mathbf{Q}^e$ describes the action of the neighboring finite elements and of the beam self-weight (constant distributed load), while $\mathbf{F}^e$ is the vector of equivalent external forces due to the moving load, which is defined as

$$\mathbf{F}^e = \begin{cases} F(t)\,\boldsymbol{\Psi}(x_c)^e & \text{if } 0 \leq x_c \leq h; \\ \mathbf{0} & \text{otherwise.} \end{cases} \tag{3.5}$$

In Eq. (3.5) $\boldsymbol{\Psi}(x_c)^e$ is the shape function vector evaluated at $x_c{=}vt{-}x_i^1$, where x_i^1 is the abscissa of the first node of the i-th finite element; thus coordinate x_c represents the position of the moving load at a particular time instant in the element reference frame (Rieker et al., 1996 [228], see Fig. 3.2b).

Then, by assembling the contributions from all of the finite elements and imposing the boundary conditions of zero transverse displacements at the two extreme nodes of the beam, the semi-discrete equations of motion derived from Eq. (3.1) become

$$\mathbf{M}\,\ddot{\mathbf{q}} + \mathbf{C}\,\dot{\mathbf{q}} + \mathbf{K}_b\,\mathbf{q} + \mathbf{Q}_{f,nl}(\mathbf{q}) = F(t)\boldsymbol{\Psi}\big(x_c(t)\big) - \mu g\,\mathbf{f}; \tag{3.6}$$

where $\mathbf{M}$ and $\mathbf{K}_b$ are the global structural mass and stiffness matrices of the beam, both symmetric and positive definite, $\mathbf{C}$ is the global viscous damping matrix of the beam-foundation system, $\mathbf{Q}_{f,nl}(\mathbf{q})$ is the global vector of the linear and nonlinear forces provided by the foundation and $\mathbf{f}$ are the equivalent force vectors due to unitary upward concentrated and distributed load, respectively; $\mathbf{q}$, $\dot{\mathbf{q}}$ and $\ddot{\mathbf{q}}$ are the global vectors of the generalized displacements, velocities and accelerations, respectively.

3.2.2 Description of the implemented algorithm

Semi-discretized equations of motion (3.6) derived in the previous section represent a coupled system of nonlinear ordinary second-order differential equations with constant coefficients, whose solution, given the initial conditions,

represents the transient response of the beam. The following homogeneous initial conditions are assumed

$$\mathbf{q}(0) = \mathbf{0}; \quad \dot{\mathbf{q}}(0) = \mathbf{0}; \tag{3.7}$$

meaning that the beam is initially at rest, with zero deflection and velocity at the instant when the force enters from the left support of the beam.

The numerical solution of the initial-value problem satisfying Eq. (3.6) in $t \in [0, \tau]$ has been achieved by a HHT-α implementation (see Hilber et al., 1977 [129]) coupled with a full Newton-Raphson method (see Belytschko and Hughes, 1983 [25], Bathe, 2006 [20]) at each time step. The length of the time interval for the moving load to go from one end to the other end of the beam is denoted by $\tau{=}L/v$ [s]. Let time span τ be subdivided into N equal time intervals $\Delta t{=}\tau/N$, such that $t_n{=}n\,\Delta t$.

An implicit formulation for the HHT-α method for nonlinear system (3.6) may be written as follows:

$$\mathbf{a}_{n+1} = \frac{2\beta-1}{2\beta}\,\mathbf{a}_n - \frac{1}{\beta\Delta t}\,\mathbf{v}_n + \frac{1}{\beta\Delta t^2}\,(\mathbf{d}_{n+1} - \mathbf{d}_n)\,; \tag{3.8a}$$

$$\mathbf{v}_{n+1} = \frac{2\beta-\gamma}{2\beta}\,\Delta t\,\mathbf{a}_n + \frac{\beta-\gamma}{\beta}\,\mathbf{v}_n + \frac{\gamma}{\beta\Delta t}\,(\mathbf{d}_{n+1} - \mathbf{d}_n)\,; \tag{3.8b}$$

$$\mathbf{r}(\mathbf{d}_{n+1}) = (1+\alpha)\mathbf{Q}_{f,nl}(\mathbf{d}_{n+1}) + \tilde{\mathbf{K}}(\mathbf{d}_{n+1})\,\mathbf{d}_{n+1} - \tilde{\mathbf{F}}(\mathbf{d}_n) = \mathbf{0}; \tag{3.8c}$$

where vectors $\mathbf{d}_n, \mathbf{v}_n$ and $\mathbf{a}_n$ stand for the approximations of $\mathbf{q}(t_n)$, $\dot{\mathbf{q}}(t_n)$ and $\ddot{\mathbf{q}}(t_n)$, respectively, derived from the numerical integration algorithm, while $\mathbf{r}(\mathbf{d}_{n+1})$ is the residue vector. In Eq. (3.8c), $\tilde{\mathbf{K}}$ is the effective stiffness matrix of the corresponding linear problem and $\tilde{\mathbf{F}}$ is the effective load vector, which take the following expressions:

$$\tilde{\mathbf{K}} = (1+\alpha)\left(\mathbf{K}_b + \frac{\gamma\mathbf{C}}{\beta\Delta t}\right) + \frac{\mathbf{M}}{\beta\Delta t^2}; \tag{3.9}$$

$$\tilde{\mathbf{F}} = \mathbf{F}(t_{n+\alpha}) + \alpha\,\mathbf{Q}_{f,nl}(\mathbf{d}_n) + \left(\alpha\mathbf{K}_b + \frac{\gamma(1+\alpha)}{\beta\Delta t}\mathbf{C} + \frac{\mathbf{M}}{\beta\Delta t^2}\right)\mathbf{d}_n + \\ + \left(\frac{\gamma-2\beta}{2\beta}\,(1+\alpha)\Delta t\,\mathbf{C} + \frac{1-2\beta}{2\beta}\,\mathbf{M}\right)\mathbf{a}_n + \left(\frac{\gamma(1+\alpha)-\beta}{\beta}\mathbf{C} + \frac{\mathbf{M}}{\beta\Delta t}\right)\mathbf{v}_n; \tag{3.10}$$

where $\mathbf{F}(t_{n+\alpha})$ is the right hand side of Eq. (3.6) computed at time instant $t_{n+\alpha}{=}t_n{+}\alpha\Delta t$. Thus, from Eqs. (3.8) the HHT-α method adopts the Finite Differences equations of the Newmark method, but the equations of motion are modified by introducing a parameter α, which represents a numerical lag in the stiffness, nonlinear and external forces.

The α parameter in Eqs. (3.8) allows for artificial high-frequency modal components to be removed from the structural response and to control the

amount of numerical damping: decreasing α increases the amount of numerical dissipation (α=0 reduces the HHT-α algorithm to the Newmark method). It is worthy to point out that this method provides numerical damping without degrading the order of accuracy and, furthermore, ensures an adequate dissipation for the higher modes, while guaranteeing that the lower modes are not too strongly affected (see Hilber et al., 1977 [129]). In fact, an accurate integration of low-frequency modes together with the suppression of spurious high-frequency responses is strongly desirable, since the spatial resolution of the high-frequency modes obtained from the FEM discretization is typically poor.

Eqs. (3.8a)-(3.8c) allow for the computation of three unknowns $\mathbf{d}_{n+1}$, $\mathbf{v}_{n+1}$ and $\mathbf{a}_{n+1}$, being assumed that $\mathbf{d}_n$, $\mathbf{v}_n$ and $\mathbf{a}_n$ are known from the previous step. For obtaining an approximate solution of the nonlinear system described by Eqs. (3.8), an equilibrium iteration sequence is required within each time step for finding current displacements $\mathbf{d}_{n+1}$.

Let one assume $\mathbf{d}_{n+1}^{(i)}$ to be a known approximation of $\mathbf{d}_{n+1}$ at the i^{th} iteration (i=0, 1, . . .). By applying a Newton-Raphson solution technique, the transient response of the nonlinear system at the $(i{+}1)^{\text{th}}$ iteration may be written as

$$\mathbf{d}_{n+1}^{(i+1)} = \mathbf{d}_{n+1}^{(i)} - \mathbf{S}^{-1}\big(\mathbf{d}_{n+1}^{(i)}\big)\,\mathbf{r}\big(\mathbf{d}_{n+1}^{(i)}\big); \tag{3.11}$$

where $\mathbf{S}\big(\mathbf{d}_{n+1}^{(i)}\big)$, is the Jacobian matrix (often called also global tangent stiffness matrix), defined as

$$\mathbf{S}\big(\mathbf{d}_{n+1}^{(i)}\big) = \left.\frac{\partial \mathbf{r}(\mathbf{d}_{n+1})}{\partial \mathbf{d}_{n+1}}\right|_{\mathbf{d}_{n+1}^{(i)}}. \tag{3.12}$$

The substitution of Eqs. (3.8c)-(3.9) into Eq. (3.12), leads to the expression of the tangent stiffness matrix:

$$\mathbf{S}\big(\mathbf{d}_{n+1}^{(i)}\big) = (1+\alpha)\left(\mathbf{K}_b + \mathbf{K}_{f,nl}^{(i)}\right) + \frac{1}{\beta \Delta t^2}\mathbf{M}; \tag{3.13}$$

where $\mathbf{K}_{f,nl}^{(i)}$=$\mathbf{K}_{f,nl}(\mathbf{d}_{n+1}^{(i)})$ is obtained by assembling the contributions from each finite element. The iterative process continues until an appropriate norm of the increment vector $\mathbf{d}_{n+1}^{(i+1)} - \mathbf{d}_{n+1}^{(i)}$ satisfies a convergence criterion. The algorithm described herein is resumed in synoptic form in the sketch provided in Fig. 3.3. The algorithm described above requires the selection of numerical parameters h, Δt, α, β, γ. A rigorous approach by which performing such a selection is presented in the following section.

SYNOPSIS OF THE IMPLEMENTED ALGORITHM

The implemented algorithm is composed of the following steps:

1. Set first time step at $n = 1$ and iteration counter at $i = 0$;
2. Initialization of acceleration vector given initial displacements and velocities: $\mathbf{a}_0 = \mathbf{M}^{-1}(\mathbf{F}_0 - \mathbf{K}\,\mathbf{d}_0 - \mathbf{C}\,\mathbf{v}_0)$;
3. Set iteration counter $i = 0$ for the Newton-Rapson algorithm;
4. Evaluation, assembly and factorization of tangent stiffness matrix $\mathbf{S}(\mathbf{d}_{n+1}^{(i)})$;
5. Evaluation of residual force vector $\mathbf{r}(\mathbf{d}_{n+1}^{(i)})$;
6. Solution of linear system $\quad \mathbf{d}_{n+1}^{(i+1)} = \mathbf{d}_{n+1}^{(i)} - \mathbf{S}^{-1}(\mathbf{d}_{n+1}^{(i)})\,\mathbf{r}(\mathbf{d}_{n+1}^{(i)})$;
7. Given a tolerance threshold ϵ, in the order of 10^{-12}, check for convergence on displacements by using the following criterion:
$$\left\|\mathbf{d}_{n+1}^{(i+1)} - \mathbf{d}_{n+1}^{(i)}\right\| \Big/ \left\|\mathbf{d}_{n+1}^{(i+1)}\right\| < \epsilon$$
   (a) If convergence is not met, set $i \leftarrow i + 1$, update displacement vector $\mathbf{d}_{n+1}^{(i)} \leftarrow \mathbf{d}_{n+1}^{(i+1)}$ and return to Step 3.
   (b) If convergence is met, proceed to Step 8.
8. Update converged displacement vector $\mathbf{d}_{n+1} \leftarrow \mathbf{d}_{n+1}^{(i+1)}$, generalized velocities $\mathbf{v}_{n+1}$ and generalized accelerations $\mathbf{a}_{n+1}$:
$$\mathbf{v}_{n+1} = \mathbf{v}_n + \Delta t(1-\gamma)\mathbf{a}_n + \frac{\gamma}{\beta\Delta t}\left(\mathbf{d}_{n+1} - \mathbf{d}_n - \Delta t\mathbf{v}_n\right) - \Delta t\gamma\left(\frac{1}{2\beta} - 1\right)\mathbf{a}_n;$$
$$\mathbf{a}_{n+1} = \frac{1}{\beta\Delta t^2}\left(\mathbf{d}_{n+1} - \mathbf{d}_\mathbf{n} - \Delta t\mathbf{v}_n\right) - \left(\frac{1}{2\beta} - 1\right)\mathbf{a}_n;$$
9. Assign obtained values to the final updated solution vectors:
$$\mathbf{q}_{n+1} \leftarrow \mathbf{d}_{n+1} \qquad \dot{\mathbf{q}}_{n+1} \leftarrow \mathbf{v}_{n+1} \qquad \ddot{\mathbf{q}}_{n+1} \leftarrow \mathbf{a}_{n+1}$$
10. Increment time step $n \leftarrow n + 1$, and return to Point 3 for the next time step.

Figure 3.3: Synoptic chart of the implemented algorithm for the nonlinear FEM transient analysis.

3.3 Dynamics of beams on Winkler bilinear elastic support

Consider the beam-foundation system represented in Fig. 3.1 where reaction force per unit length $r(w)$ supplied by the foundation is described by the bilinear law in Eq. (2.5). A zero-mean harmonically variable amplitude of the concentrated moving load acting at time t at current position vt is assumed, according to the following assumed harmonic law:

$$F(t) = \begin{cases} F\cos(\Omega t) & 0 < t \leq \tau; \\ 0 & t > \tau; \end{cases} \tag{3.14}$$

where F is the reference load magnitude, Ω is the angular frequency of the harmonic amplitude variation and time interval for the moving load to travel across the beam's span is denoted by $\tau = L/v$. Accordingly, the beam experiences forced vibrations in the time interval $(0,\ \tau]$ and free damped vibrations afterward.

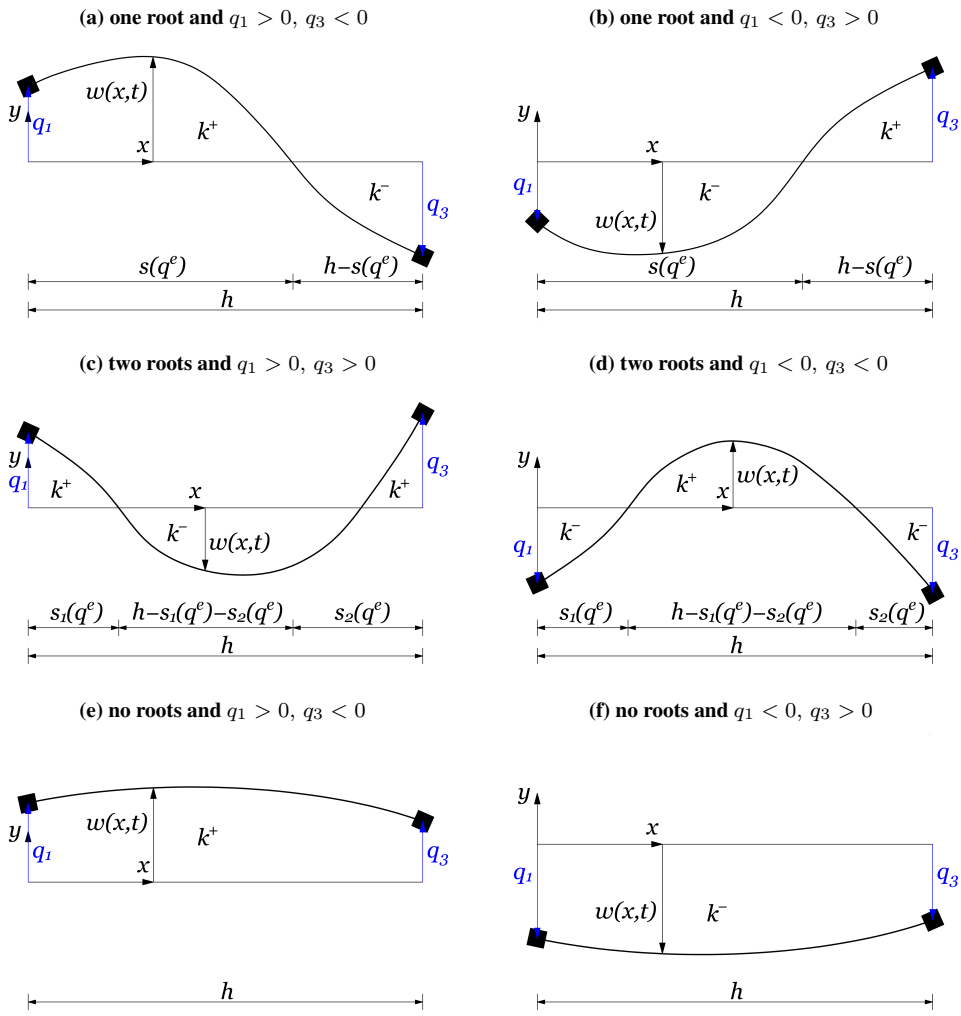

Figure 3.4: Interaction patterns between a beam finite element and the bilinear foundation with stiffnesses k^- and k^+ under compression and tension, respectively.

Although the effect of damping may also be considered in the present analysis, it has been neglected since it does not affect much the critical velocity of the beam-foundation system, as shown in numerous previous works (Castro Jorge et al., 2015 [49, 50]).

Previously-defined matrices and vectors in Section 3.2 have been obtained according to the work of Castro Jorge et al. (2015) [49]. Towards the FEM description of the bilinear behavior, six interaction patterns between a beam finite element and the underlying foundation are considered, as depicted in Fig. 3.4. The position of the transition point between compression and tension

Interaction patterns:	
$U_f^e = \frac{1}{2}\,\mathbf{q}^{e\,T}\,\mathbf{K}_{f,nl}^e(\mathbf{q}^e)\,\mathbf{q}^e$, $\mathbf{Q}_{f,nl} = \mathbf{K}_{f,nl}^e(\mathbf{q}^e)\,\mathbf{q}^e$	$\mathbf{K}_{f,nl}^e(\mathbf{q}^e) = \dfrac{\partial^2 U_f}{\partial \mathbf{q}^e \partial \mathbf{q}^e}$:
(a) one root and $q_1 > 0$, $q_3 < 0$	$k^+\mathbf{D}\big(0, s(\mathbf{q}^e)\big) + k^-\mathbf{D}\big(s(\mathbf{q}^e), h\big)$
(c) two roots and $q_1 > 0$, $q_3 > 0$	$k^+\Big(\mathbf{D}\big(0, s_1(\mathbf{q}^e)\big) + \mathbf{D}\big(h - s_2(\mathbf{q}^e), h\big)\Big) + k^-\mathbf{D}\big(s_1(\mathbf{q}^e), h - s_2(\mathbf{q}^e)\big)$
(e) no roots (linear foundation) and $q_1 > 0$, $q_3 > 0$	$k^+\mathbf{D}(0, h)$

Table 3.1: Expressions of the tangent stiffness matrix of the bilinear foundation for each beam-foundation pattern (interaction patterns (b),(d) and (f) may be derived using the expressions of patterns (a), (c) and (e), respectively, by exchanging k^- with k^+).

of the foundation, i.e. the points with null displacement, is labeled $s(\mathbf{q}^e)$ and is determined by setting to zero the cubic relation describing the displacement field within the local reference frame of each finite element ($0 < s(\mathbf{q}^e) < h$).

The considered interaction patterns account for a maximum of two transition points between the upward and the downward displacements. Nonetheless, two more interaction patterns are possible, besides those depicted in Fig. 3.4, because the deflection shape of the beam axis is described by a cubic polynomial. For these additional patterns there are three transition points between the upward and the downward displacements, corresponding to three roots of the cubic polynomial. However, in the numerical tests, an adequately refined mesh is always selected to allow for those two patterns to be precluded.

The expressions for the foundation internal force vector and the foundation tangent stiffness matrix, derived in the work of Castro Jorge et al. (2015) [49] for the six above-defined interaction patterns, are reported in Table 3.1, where, in order to simplify the notation, the following quantity is introduced:

$$\mathbf{D}(a,b) = \mathbf{N}^{-T}\int_a^b \mathbf{p}(x)\mathbf{p}(x)^{\mathrm{T}}\,dx\,\mathbf{N}^{-1}; \quad \mathbf{N} = \begin{bmatrix} 1 & 0 & 0 & 0 \\ 0 & 1 & 0 & 0 \\ 1 & h & h^2 & h^3 \\ 0 & 1 & 2\,h & 3\,h^2 \end{bmatrix}; \tag{3.15}$$

where $\mathbf{p}(x) = \{1\ x\ x^2\ x^3\}$.

3.3.1 Characteristic strategies of the numerical procedure

The solution algorithm for the implicit scheme, summarized in Fig. 3.3, requires assembling the global mass and stiffness matrices into a set of coupled algebraic equations and solving the system by a triangularization technique, such as the Choleski decomposition (MatLab [251]).

A peculiar feature of this approach is that a new tangent stiffness matrix has to be computed at each iteration within the time step and a new decomposition has to be performed on assembled tangent stiffness matrix $\mathbf{S}$. For this reason, appropriate space/time discretizations, i.e. values of mesh size h and time step Δt have to be accurately chosen, in order to optimize the computational effort.

Automated strategy for suitable space discretization

In general, mesh size h should be chosen such that all important vibration natural frequencies and mode shapes of the mathematical model are well approximated, and such number depends on the spatial distribution and frequency content of the loading. If not enough modes are considered, Eq. (3.6) is not enough accurately solved. On the other hand, there is no need to represent the higher frequency contributions because such contributions lead to an almost static response, which is already included in the direct integration step-by-step dynamic response calculations (Bathe, 1996 [20]).

The loading acting on the beam-foundation system is here represented by harmonic moving load $F\cos(\Omega t)\,\delta(x-vt)$, which varies both in space and time. Consequently, by performing a Fourier analysis (Buschman, 1996 [46]) of such dynamic load input, at this stage under the reasonable hypothesis of standard linear elastic behavior of the beam-foundation system (same stiffness in compression and in tension, i.e. $k^-{=}k^+{=}k$), the following expression of its Fourier decomposition $\mathcal{F}_n$ is obtained as

$$\mathcal{F}_n = \Omega + \frac{n\pi v}{L}; \tag{3.16}$$

that is a linear function of mode number n (recall that Ω is the frequency of the moving load amplitude variation). Therefore, Fourier analysis shows that the moving load frequency content is not bounded, but it increases linearly with the number of considered modes.

Let ω_n [rad/s] be the natural frequencies of the linear beam-foundation system, which for a linear Winkler foundation of coefficient k may be expressed by the following nonlinear function of mode number n (Dimitrovová and Varandas, 2009 [73]):

$$\omega_n = \sqrt{\left(\frac{n\pi}{L}\right)^4 \frac{EJ}{\rho A} + \frac{k}{\rho A}}; \tag{3.17}$$

evaluated here for the two limit cases $k{=}k^-$ and $k{=}k^+{=}0$, respectively. The comparison of natural frequencies ω_n with $\mathcal{F}_n$ in Eq. (3.16) allows to determine the nearest integer mode number $\bar{n}$ for which $\omega_n{<}\mathcal{F}_n$. The corresponding highest frequency of the system at $\bar{n}$, namely $\bar{\omega}{=}\omega_{\bar{n}}$, shown in Fig. 3.5,

has been depicted here for the worst considered case in the subsequent simulations (v=300 m/s, Ω=60 rad/s), according to the mechanical parameters of the adopted case study, which will be described in following Section 3.3.2.

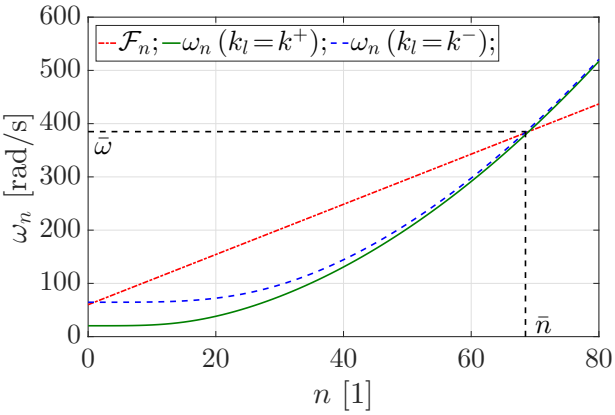

Figure 3.5: Evolution of frequency content of the harmonic moving load and natural vibration frequencies of the two limit beam-foundation systems as a function of the mode number

Hence, also in view of achieving a better convergence in the nonlinear procedure presented in Section 3.2.2, finite element mesh h is selected such that the smallest considered half-wavelength is described by at least four finite elements, that is

$$h \leq \frac{\lambda_{min}/2}{4} = \frac{L}{4\,\bar{n}}; \qquad \text{(Simply-supported beam);} \tag{3.18}$$

which, for a beam of lenght L=200 m (see following Section 3.3.2), corresponds to a spatial discretization composed of finite elements of a length of 0.5 m, i.e. 400 finite elements.

Automated strategy for suitable time discretization

Concerning aspects of numerical integration, the time span taken throughout the integration process corresponds to the amount of time along which the moving load is really acting along the beam, that is τ=L/v, plus one fifth of τ for free vibrations. In general, the numerical characteristics of the HHT-α method for linear elastic systems (Hilber and Hughes, 1978 [129]) are preserved for nonlinear systems. As proven by Chang (2008) [51], also for moderately nonlinear systems, if free parameters α, β and γ, which govern stability, accuracy and numerical damping of the algorithm, are chosen as follows:

$$-\frac{1}{3} \leq \alpha \leq 0; \quad \beta = \frac{1}{4}(1-\alpha)^2; \quad \gamma = \frac{1}{2} - \alpha; \tag{3.19}$$

the implicit HHT-α method constitutes an unconditionally stable and second-order accurate scheme (Hilber et al., 1977 [129]), characterized by favorable numerical dissipation and limited dispersion, without degrading the order of accuracy. By virtue of the unconditional stability of the numerical integration algorithm, time step Δt has to be chosen to yield an accurate and effective solution, i.e. it should be only small enough such that the response in all modes that significantly contribute to the total structural response is accurately calculated. In fact, by selecting a uniform time step for all the considered velocities does not represent an optimal choice, since it would lead to a huge and worthless computational effort, particularly at the low moving load velocities.

The accuracy of numerical integration schemes can be measured in terms of numerical dissipation (decay) and dispersion (period elongation or distortion). Since the HHT-α method guarantees a sufficient numerical dissipation if conditions in Eq. (3.19) are satisfied (Chang, 2008 [51]), an appropriate time step Δt to be adopted for the numerical simulations in order to limit dispersion may be estimated as follows:

$$\Delta t = (1 + P^*)\frac{\tilde{\Omega}^*(\Delta t)}{\omega^*}; \tag{3.20}$$

where P^* is the period distortion parameter associated with the maximum frequency to be represented $\omega^*{=}4\,\bar{\omega}$ (Bathe, 1996 [20]). In the previous equation, $\tilde{\Omega}^*(\Delta t)$ is the non-dimensional distorted counterpart of ω^* due to the numerical integration, which, consequently, makes it a function of selected time step Δt. More details on the calculation of $\tilde{\Omega}^*(\Delta t)$, which depends on both mechanical parameters of the structural system and numerical parameters of the HHT-α method, may be found in Hilber et al. (1977) [129], Belytschko and Hughes (1983) [25] and Chang (2008) [51]. Period distorsion P^* associated with the maximum frequency has been imposed to be less or equal than 5%, to warrant a sufficient accuracy. To evaluate time step Δt for each simulation, an automated calculation solving nonlinear Eq. (3.20) has been implemented, according to the computational procedure described in the above cited references.

When solving highly nonlinear problems, numerical dissipation has been found to improve the convergence of iterative equation solvers. However, since the addition of high-frequency dissipation should not induce a loss of accuracy nor introduce excessive algorithmic damping in the important low frequency modes, parameter α should not be too negative. Thus, the HHT-α parameter expressing the high-frequency numerical dissipation rate is chosen equal to $\alpha{=}{-}0.1$ (Hilber et al., 1977 [129]). Such choice is respectful of Eq. (3.19) and also in agreement with Castro Jorge et al. (2015) [50].

Concerning convergence properties of the Newton-Rapson scheme at each time step, if the initial solution is sufficiently close to the exact solution and if

the tangent stiffness matrix does not abruptly change, a local quadratic rate of convergence is attained (see Bathe, 1996 [20]). Such conditions are satisfied if both above selecting criteria for mesh size h and time step Δt, Eq. (3.18) and Eq. (3.20), respectively, are met.

The FEM program has been implemented within MatLab [251]. Despite for the large amplitudes and the high frequencies of oscillation of the response obtained for some combinations of the above-considered parameters, the algorithm always properly converged and allowed to produce the results of the massive computations illustrated in the next section.

3.3.2 Numerical results and discussion

Throughout this section, the main effects of the moving load velocity, of the frequency of the load harmonic-varying magnitude and of the ratio between the foundation's moduli in compression and in tension (stiffness ratio) on the maximum downward and upward displacements of the beam are outlined. In particular, after having detected the critical velocities of the system, as those specific moving load velocities at which maximum displacements are attained, their relationship with the amplitude frequency of the moving load and with the foundation stiffness ratio is explicitly depicted in appropriate bifurcation curves, described by fitted analytical proposals from the values of the critical velocity computed at different frequencies of the load variation.

(a)

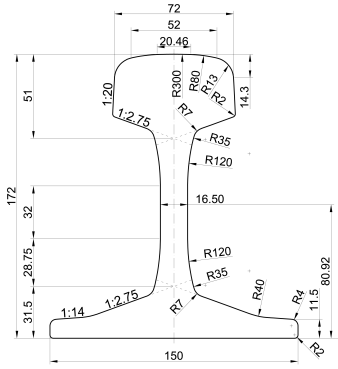

(b)

Mechanical properties			
Young's modulus	E	2.100×10^{11}	N/m^2
Cross-sectional area	A	7.684×10^{-3}	m^2
Area moment of inertia	J	3.055×10^{-5}	m^4
Mass per unit volume	ρ	7.800×10^{3}	kg/m^3

Figure 3.6: UIC60 rail profile **(a)** (dimensions in mm) and its corresponding mechanical properties **(b)**.

Beam response

The type of analyzed beam is a UIC60 rail (see Fig. 3.6a), one of the most diffused steel profiles in railway tracks; its mechanical properties are reported

in Fig. 3.6b. A beam length L of 200 m has been selected, in order to reasonably represent the limit case of a beam of an infinite length. The assumed load magnitude is $F{=}{-}83.4$ kN (the minus sign means a load acting downward), corresponding to a locomotive of the Thalys high-speed train (EU), which has a total axle mass of about 17000 kg (see Castro Jorge et al., 2015 [50]).

Computations are performed by assuming a constant value of the linear elastic Winkler coefficient in compression k^-, equal to 250×10^3 N/m^2 (Castro Jorge et al., 2015 [49]), while a variable value in tension k^+ is adopted according to the following definition:

$$k^+ = \kappa\, k^-, \qquad \kappa = \frac{k^+}{k^-}, \qquad 0 \leq \kappa \leq 1; \tag{3.21}$$

where stiffness ratio of the foundation κ is introduced as the ratio between the compression and tension foundation moduli. The range of κ defined in Eq. (3.21) is such that the constitutive law of the foundation varies between the two limit cases of linear elastic foundation ($k^+{=}k^-$, $\kappa{=}1$, symmetric behavior in compression and tension) and of tensionless foundation ($k^+{=}0$, $\kappa{=}0$).

Regarding the load frequency range, it depends on the stiffness coefficients of the foundation and on the mechanical characteristics of the rail profile. The present computations have been performed in a range of load frequency Ω from 0 to 60 rad/s, with intervals of 10 rad/s. For each of these frequencies of oscillation of the moving load amplitude, computations are performed for velocities of the moving load v varying between 10 m/s and 300 m/s, with a step variation of 1 m/s. Although the upper bound of the selected range of moving load velocity is clearly unattainable by today railway transportation vehicles, its adoption looks necessary in order to properly capture more than one critical velocity and to explore the whole solution range. This procedure is repeated for each considered stiffness ratio κ.

For illustration purposes, Figs. 3.7a-3.7c-3.7e depict the beam deflection profiles at three distinct time instants and corresponding three moving load positions ($vt{=}L/4,\ L/2,\ 3/4L$). The considered stiffness ratio of the foundation is $\kappa{=}0.2$, the moving load velocity is set at 30 m/s, the amplitude frequency is 30 rad/s (*subcritical regime*) and the time step is $\Delta t{=}3 \times 10^{-3} s$, apt to comply with Eq. (3.20). As expected, it can be observed that for the bilinear type of foundation, the beam exhibits higher upward beam displacements than downward ones, even though the mean loading is acting downward due to the applied beam self-weight. The results show that maximum displacements always occur beneath the moving load position and, at subcritical velocities of the moving harmonic load, the beam deflection clearly exhibits a wave character, while this is not observed for the case of a constant-amplitude moving load (Moioli, 2016 [200]). The wavelengths are similar both behind and ahead of the moving load position.

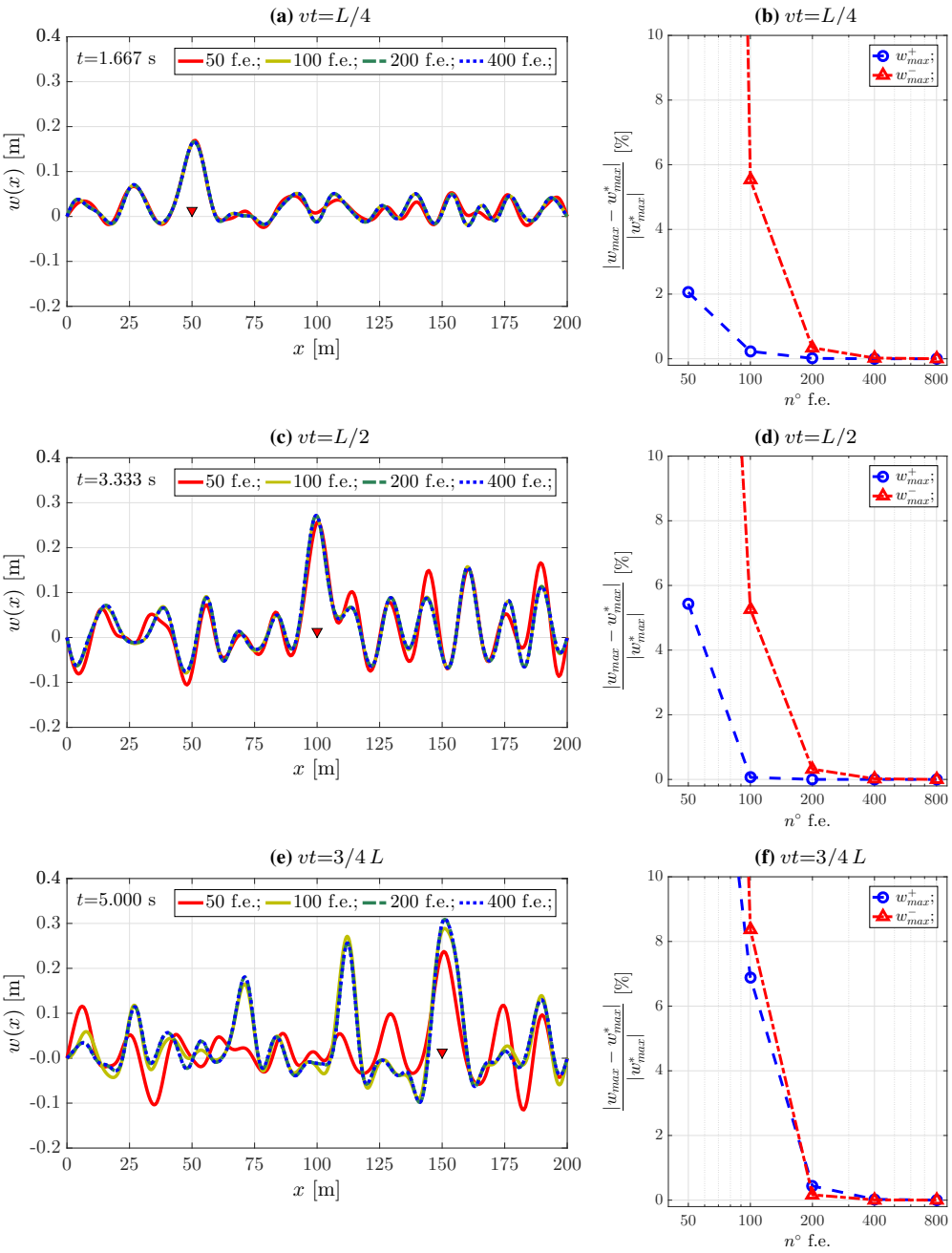

Figure 3.7: Left column: beam deflection at three different time instants, corresponding to three distinct positions of the load along the beam (specified by a red triangle): $L/4$=50 m (a), $L/2$=100 m (c) and $3/4\,L$=150 m (e). Right column: convergence study on maximum upward (w^+_{max}) and downward (w^-_{max}) displacements with respect to the number of adopted finite elements. Bilinear elastic foundation with κ=0.2. Results for a moving harmonic load with velocity v=30 m/s and frequency Ω=30 rad/s (subcritical regime). Time step Δt=$3 \times 10^{-3} s$.

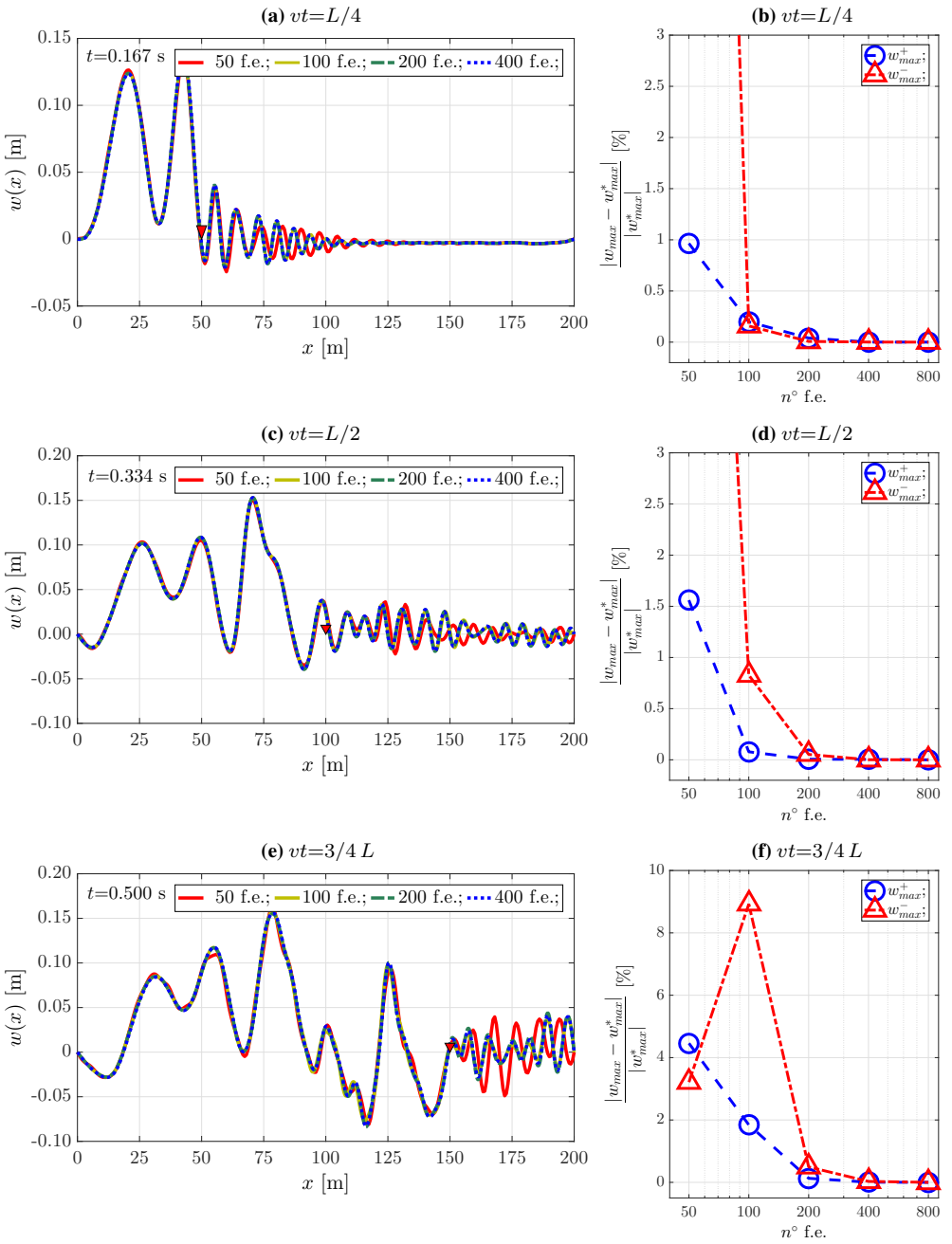

Figure 3.8: Left column: beam deflection at three different time instants, corresponding to three distinct positions of the load along the beam (specified by a red triangle): $L/4$=50 m (a), $L/2$=100 m (c) and $3/4\,L$=150 m (e). Right column: convergence study on maximum upward (w^+_{max}) and downward (w^-_{max}) displacements with respect to the number of adopted finite elements. Bilinear elastic foundation with κ=0.2. Results for a moving harmonic load with velocity v=300 m/s and frequency Ω=30 rad/s (supercritical regime). Time step Δt=$5 \times 10^{-4} s$.

The same type of representation in the *supercritical regime* (v=300 m/s) is provided by Figs. 3.8a-3.8c-3.8e. In this case, time step Δt=5 $\times$ $10^{-4}s$ is selected according to Eq. (3.20). Again, higher upward beam displacements with respect to the downward displacements are observed. In the supercritical regime, maximum displacements and larger waves are always located behind the moving load position, while the oscillations become smaller in amplitude and wave length ahead the moving load.

Figs. 3.7b-3.7d-3.7f and Figs. 3.8b-3.8d-3.8f depict the outcomes of the convergence study of the maximum upward (w^+_{max}) and downward (w^-_{max}) beam displacements for various mesh refinements at three distinct time instants, corresponding to the three moving load positions (vt=$L/4$, $L/2$, $3/4L$), for the subcritical (v=30 m/s) and the supercritical (v=300 m/s) regime, respectively. A very refined spatial discretization of 800 finite elements has been assumed as a target exact result. It can be seen that a mesh of 400 finite elements, would be the most appropriate choice to achieve an accurate and feasible solution, independently from the time instant. Nonetheless, if meshes composed by less than 400 finite elements are employed, the results may become inaccurate, but the algorithm does always converge.

3.3.3 Determination of the critical velocities

In this section, the effects of the load velocity, of the frequency of the harmonic-varying magnitude and of the ratio between the foundation's moduli in compression and in tension on the maximum downward and upward displacements of the beam are presented.

Given a value of the frequency of the harmonic-varying magnitude and of the ratio between the foundation's moduli, for each simulation performed at a certain value of the moving load velocity, the maximum upward (positive) and downward (negative) displacements of the beam are scored. Then, such outcomes of the FEM simulation are plotted as a function of the moving load velocity. From such curves the critical velocities of the beam-foundation system for a finite beam may be detected as the velocity of the moving load at which a maximum displacement is attained.

The relationship between beam maximum upward (w^+_{max}) and downward (w^-_{max}) displacements and load velocities, is shown in the sequence of graphs in Fig. 3.9, for various values of load amplitude frequency Ω and stiffness ratio κ. For each considered value of κ, it is noticeable that, as the amplitude of the moving load starts oscillating with frequency Ω, the critical velocities might be either one or two (bifurcation of the critical velocities), within the displayed range of velocities. This means that a harmonic load of a specific forced frequency causes a resonance effect at two different moving velocities, as illustrated by Chen and Huang (2003) [57] for a linear foundation.

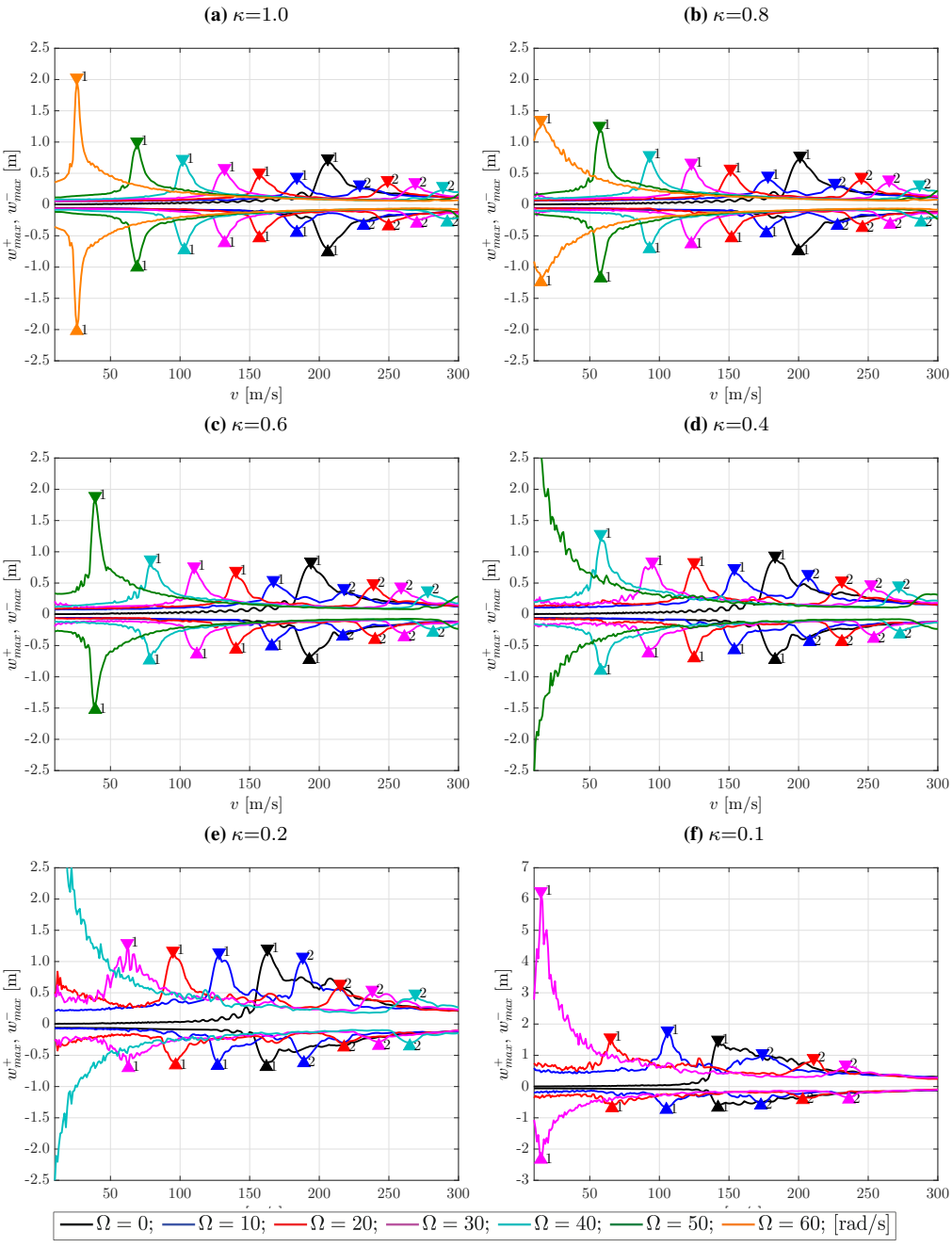

Figure 3.9: Representation of the beam maximum displacements as a function of load velocity v and frequency Ω for an undamped bilinear elastic foundation with compression stiffness k^{-}=250 kN/m^2 and tension stiffness k^{+}=κk^{-}. Load amplitude frequency Ω ranges from 0 rad/s to 60 rad/s. First peak: first critical velocity (1), second peak: second critical velocity (2).

		First critical velocity					Second critical velocity				
κ [1]	Ω [rad/s]	$v^+_{cr,1}$ [m/s]	$v^-_{cr,1}$ [m/s]	$v_{cr,1}$ [m/s]	$w^+_{m,1}$ [m]	$w^-_{m,1}$ [m]	$v^+_{cr,2}$ [m/s]	$v^-_{cr,2}$ [m/s]	$v_{cr,2}$ [m/s]	$w^+_{m,2}$ [m]	$w^-_{m,2}$ [m]
1.0	0	206.0	206.0	206.0	0.675	−0.701	-	-	-	-	-
	10	184.0	184.0	184.0	0.384	−0.387	229.0	232.0	230.5	0.262	−0.274
	20	157.0	157.0	157.0	0.450	−0.476	249.0	250.0	249.5	0.332	−0.287
	30	132.0	132.0	132.0	0.523	−0.552	269.0	270.0	269.5	0.292	−0.246
	40	102.0	103.0	102.5	0.665	−0.673	289.0	292.0	290.5	0.231	−0.226
	50	69.0	69.0	69.0	0.944	−0.943	-	-	-	-	-
	60	26.0	26.0	26.0	1.967	−1.961	-	-	-	-	-
0.8	0	201.0	200.0	200.5	0.724	−0.683	-	-	-	-	-
	10	178.0	177.0	177.5	0.403	−0.399	226.0	228.0	227.0	0.290	−0.282
	20	151.0	152.0	151.5	0.514	−0.479	245.0	246.0	245.5	0.384	−0.313
	30	123.0	123.0	123.0	0.607	−0.572	265.0	266.0	265.5	0.342	−0.264
	40	93.0	93.0	93.0	0.731	−0.650	287.0	288.0	287.5	0.261	−0.226
	50	57.0	58.0	57.5	1.197	−1.116	-	-	-	-	-
	60	15.0	15.0	15.0	1.297	−1.179	-	-	-	-	-
0.6	0	194.0	193.0	193.5	0.785	−0.672	-	-	-	-	-
	10	167.0	166.0	166.5	0.489	−0.454	218.0	217.0	217.5	0.357	−0.292
	20	140.0	140.0	140.0	0.631	−0.503	239.0	240.0	239.5	0.436	−0.351
	30	110.0	112.0	111.0	0.705	−0.583	259.0	261.0	260.0	0.387	−0.301
	40	79.0	78.0	78.5	0.813	−0.676	278.0	282.0	280.0	0.324	−0.238
	50	39.0	39.0	39.0	1.834	−1.463	-	-	-	-	-
0.4	0	183.0	183.0	183.0	0.873	−0.668	-	-	-	-	-
	10	154.0	154.0	154.0	0.673	−0.515	207.0	208.0	207.5	0.578	−0.381
	20	125.0	125.0	125.0	0.770	−0.641	231.0	231.0	231.0	0.476	−0.381
	30	95.0	92.0	93.5	0.781	−0.568	252.0	254.0	253.0	0.416	−0.331
	40	58.0	58.0	58.0	1.222	−0.844	272.0	273.0	272.5	0.399	−0.264
0.2	0	163.0	162.0	162.5	1.142	−0.627	-	-	-	-	-
	10	128.0	127.0	127.5	1.086	−0.605	188.0	189.0	188.5	1.020	−0.566
	20	95.0	97.0	96.0	1.114	−0.599	215.0	218.0	216.5	0.580	−0.314
	30	62.0	63.0	62.5	1.229	−0.640	238.0	243.0	240.5	0.483	−0.283
	40	-	-	-	-	-	269.0	265.0	267.0	0.426	−0.298
0.1	0	142.0	142.0	142.0	1.429	−0.611	-	-	-	-	-
	10	106.0	105.0	105.5	1.724	−0.673	174.0	173.0	173.5	1.002	−0.544
	20	65.0	66.0	65.5	1.503	−0.636	211.0	203.0	207.0	0.853	−0.363
	30	15.0	15.0	15.0	6.190	−2.273	234.0	236.0	235.0	0.636	−0.343
	40	-	-	-	-	-	260.0	259.0	259.5	0.496	−0.226

Table 3.2: Numerical values of critical velocities and maximum displacement amplitudes from the graphs in Fig. 3.9.

In particular, the higher critical velocity v_{cr2} increases and quickly moves toward the upper limit of the plot as the load frequency increases. Conversely, the lower critical velocity v_{cr1} decreases until reaching zero at a very high load frequency. The interpretation of this result is straightforward: in fact, it is well known that a fixed load oscillating at a certain frequency, called resonance frequency, causes the resonance of the beam-foundation system. Critical velocities for Ω=0 are in agreement with those obtained by Castro Jorge et al. (2015) [49].

From the observation of the graphs in Fig. 3.9, as expected, the progressive reduction of the foundation stiffness in tension, corresponding to a reduction of the global stiffness of the beam-foundation system, comes with (i) a shift in the position of both critical velocities toward lower values for all the load frequencies, in addition to (ii) an increase of the maximum deflection amplitudes, especially the upward one. It is also observed that the maximum displacements

may be already considerable for velocities well below the critical velocity. For an almost tensionless foundation ($\kappa \to 0$), the positive maximum displacements become extremely large (well above the range of validity of the geometrical linearity assumption). On the other hand, negative displacements keep practically the same values, consistently with the unaltered value of the compression stiffness of the foundation. Further, it may be noticed that at high frequencies the curves become much less smoother. The obtained numerical values of the critical velocities and the corresponding maximum upward and downward displacements are listed in Table 3.2.

In the following section, the obtained numerical values are employed to decipher the functional relationship existing between the critical velocities, the load frequency and the foundation stiffness ratio. In more detail, by appropriate analytical fitting proposals with calibrated coefficients, analytical bifurcation curves are defined in the critical velocities-load frequency plane, with parameters depending upon the foundation stiffness ratio.

3.3.4 Bifurcation curves of the critical velocities

The collected values of the critical velocities $v_{cr,j}$ ($j=1,2$) from the numerical simulations, reported in Table 3.2, are employed to provide a detailed description of the relationship between critical velocities $v_{cr,j}$, harmonic load frequency Ω and foundation stiffness ratio κ. Bifurcation curves representing the relationship between critical velocities and load frequency, for the various foundation stiffness ratios have been derived by an appropriate analytical fitting proposal using a parameter optimization performed within MatLab [251].

The analytical fitting expression has been proposed and adopted, for tracing both the lower and higher critical velocities, in the following simply and rather effective three-coefficient power-law form:

$$\frac{v_{cr,j}}{\overline{v}_{cr}} = a_1(\kappa)\left(1+(-1)^j \frac{\Omega/\omega_1}{a_2(\kappa)}\right)^{a_3}, \quad j=1,2; \quad a_1(\kappa)=\kappa^{b_1}; \quad a_2(\kappa)=\kappa^{b_2}; \tag{3.22}$$

where

$$\overline{v}_{cr} = \min_{n\in\mathbb{N}} \left\{ \frac{\omega_n L}{n\,\pi} \right\}; \qquad \omega_n = \sqrt{\left(\frac{n\,\pi}{L}\right)^4 \frac{EJ}{\rho A} + \frac{k}{\rho A}}; \tag{3.23}$$

are the critical velocity and the natural frequencies of a simply-supported beam lying on a classical linear elastic Winkler foundation ($\kappa=1$), respectively (ω_1 being the first natural frequency, i.e. ω_n for $n=1$ and $\kappa=1$). In Eq. (3.22) unknown parameters $a_1(\kappa)$, $a_2(\kappa)$, a_3 are apt to represent the intercepts with the ordinate and abscissa axes in Figs. 3.10-3.11 and the exponent of the power law, respectively. Latter parameter a_3 is taken constant at variable stiffness ratio κ.

Thus, parameters $a_1(\kappa)$ and $a_2(\kappa)$ assume the following clear and important physical meaning, at variable stiffness ratio κ:

- $a_1(\kappa)=\kappa^{b_1}$ describes the value of the critical velocity for a constant-amplitude moving load (i.e. with $\Omega=0$), and provides exact value $v_{cr}/\overline{v}_{cr}=1$ in the standard linear case ($\kappa=1$);
- $a_2(\kappa)=\kappa^{b_2}$ represents the value of the frequency ratio at resonance of a harmonic static load (i.e. such that $v_{cr}=0$), leading to a vanishing critical velocity of the beam-foundation system, and thus giving exact value $\Omega/\omega_1=1$ in the standard linear case ($\kappa=1$).

Then, two parameters $a_1(\kappa)$ and $a_2(\kappa)$ are in turn described by a power law relationship, in terms of exponent coefficients b_1 and b_2, respectively.

The formula for the critical velocities proposed in Eq. (3.22) shall provide a simple and effective analytical expression to represent the functional dependence between both $v_{cr,j}$ and Ω, κ. The adopted expression in Eq. (3.22), here for a bilinear foundation, results different from those earlier reported in Froio et al. (2017) [102] for a cubic superlinear foundation and is set here in a useful nondimensional form. Further, even more precise representations could be provided, but at the price of augmenting the number of underlying coefficients, here conveniently confined to three only.

The associated fitting procedure for obtaining three free parameters b_1, b_2, a_3, based on the data in Table 3.2, has lead to the following global fitting results:

$$b_1 = 0.1503 \simeq \frac{3}{20}, \qquad b_2 = 0.3067 \simeq \frac{3}{10}, \qquad a_3 = 0.7130 \simeq \frac{5}{7}; \quad (3.24)$$

where it appears that exponent $b_2 \simeq 0.30$ is about twice exponent $b_1 \simeq 0.15$, ruling the power law dependencies of parameters $a_1(\kappa)$ and $a_2(\kappa)$ (Fig. 3.12), while constant value a_3 is around 0.71, thus, as a rule of thumb, $a_3 \simeq 50/21$, $b_2 \simeq 100/21\, b_1$.

The curves retrieved with the analytical fitting expressions above are plotted in Figs. 3.10-3.11, in dimensional and nondimensional terms, respectively. The analysis of these figures reveals that the obtained curves fit rather accurately the outcomes of the numerical simulations, despite that only three unknown parameters appear in Eq. (3.22), thus proving the effectiveness of the predicted analytical proposals for critical velocities $v_{cr,j}$.

Fig. 3.13 additionally depicts the dependence of $v_{cr,j}$ on both Ω and κ in a three-dimensional plot, for the range of parameters considered in this study.

The comparison among the derived bifurcation curves reported in Fig. 3.10 and Fig. 3.11, proves that the critical velocities for the bilinear foundation, as expected, are lower than those obtained for a classical linear foundation with $k^+=k^-$. Although the effects of the load frequency on the critical velocities are similar for all the investigated foundation models, the slope of the

fitted curves in the neighborhood of Ω=0 increases as κ decreases. Therefore, small variations in moving load amplitude frequency Ω may lead to substantial changes in the critical velocities.

3.4 Dynamics of beams on cubic superlinear elastic Winkler support

In the present section the main effects of the velocity and the characteristic parameters of the harmonic-varying magnitude of the moving load on the displacements and on the critical velocities of the beam-foundation system are outlined. The methodology of the analysis is analoguos to the one described in the previous section.

Thus, consider the beam-foundation system represented in Fig. 3.1, where reaction force per unit length $r(w)$ supplied by the foundation is described by

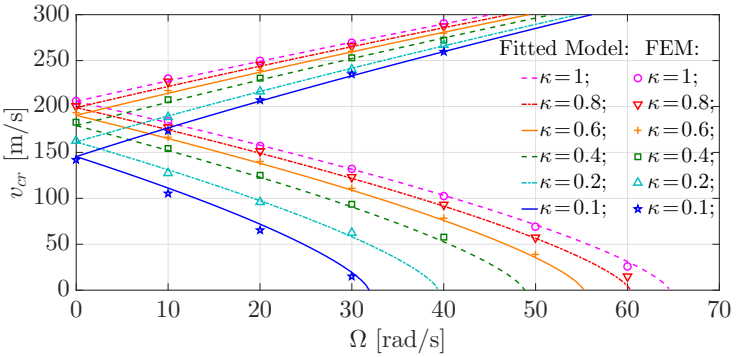

Figure 3.10: Bifurcation curves depicting the critical velocities as a function of the frequency of the load amplitude variation for an undamped bilinear elastic foundations with compression stiffness k^{-}=250 kN/m^2 and tension stiffness k^{+}=$\kappa\, k^{-}$. Results computed by the FEM implementation and fitted analytical curves. Global fittings in Eqs. (3.22)-(3.24) based on data from Table 3.2. $\overline{v}_{cr}$=205.6 m/s and ω_1=64.58 rad/s in Eq. (3.23). Dimensional representation.

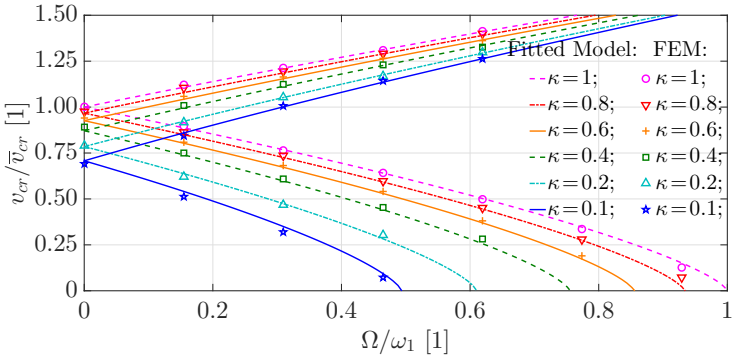

Figure 3.11: Same as Fig. 3.10. Fittings in Eqs. (3.22)-(3.24). Nondimensional representation.

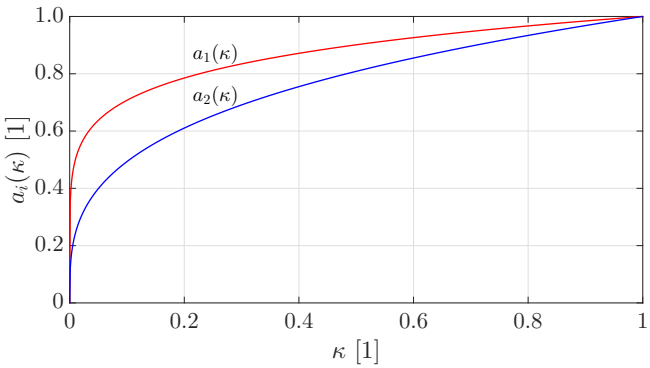

Figure 3.12: Physical parameters $a_1(\kappa)=\kappa^{b_1}$ and $a_2(\kappa)=\kappa^{b_2}$ as a power-law function of κ ($b_1=0.1503\simeq 0.15$, $b_2=0.3067\simeq 2b_1\simeq 0.30$).

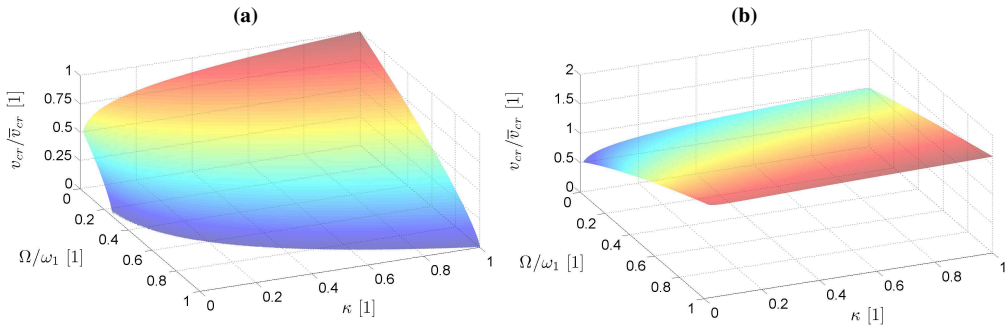

Figure 3.13: Variation of the first (a) and second (b) critical velocity versus frequency ratio Ω/ω_1 and stiffness ratio κ, according to the analytical fitting proposal in Eqs. (3.22)-(3.24).

the cubic superlinear law in Eq. (2.6). The concentrated moving load moves at a constant velocity along the beam, displaying a harmonic-varying magnitude in time t, defined in terms of mean value F_0, amplitude F and frequency of oscillation Ω, according to the following assumed law:

$$F(t) = \begin{cases} F_0 + F\sin(\Omega t) & 0<t\leq\tau; \\ 0 & t>\tau; \end{cases} \tag{3.25}$$

where $F_0=\alpha F$ and load ratio α describes the relative intensity between the constant and variable components of the moving load magnitude.

The response is calculated by the semi-discrete approach presented in Section 3.2: a classical FEM is employed to discretize the space domain, leading to the coupled system of linear second-order differential equations with constant coefficients in Eq. (3.6), while direct time integration through the HHT-α method is used to solve the problem in the time domain (see synoptic scheme

of the implemented algorithm in Fig. 3.3). The homogeneous initial conditions in Eq. (3.7) have been assumed and the beam's self-weight has not been taken into account because it seems not to affect much the dynamic response of the system due to the symmetric behavior of the nonlinear foundation in compression and in tension.

Thus, the differences between the problems considered in Section 3.3 are the type of foundation constitutive law and the nature of the external forcing function. The calculation of the nonlinear force vector and of the tangent stiffness matrix for the present case study have been implemented according to the work of Castro Jorge et al. (2015) [50]. The characteristic parameters of the beam are the same as those used in Section 3.3 (see Fig. 3.6b). The number of adopted finite elements is 200 (mesh size h=1 m), while the adopted time step is $\Delta t = \min\{10^{-3}\text{s}, h/(5v)\}$ in order to warrant a sufficient accuracy.

3.4.1 Validation of the FEM formulation for a constant amplitude moving load

A consistent validation comparison between the present numerical analyses, in terms of maximum upward and downward beam displacements versus load velocity, and analogous studies proposed in the literature is performed. In particular, results obtained by Castro Jorge et al. (2015) [50] for both linear and nonlinear foundation behaviors have been taken as reference outcomes, since their work has been lying at the basis of the present investigation. Since in the work of Castro Jorge et al. (2015) [50] the magnitude of the concentrated moving load was kept constant, such condition may be easily simulated by setting Ω=0 and α=1.

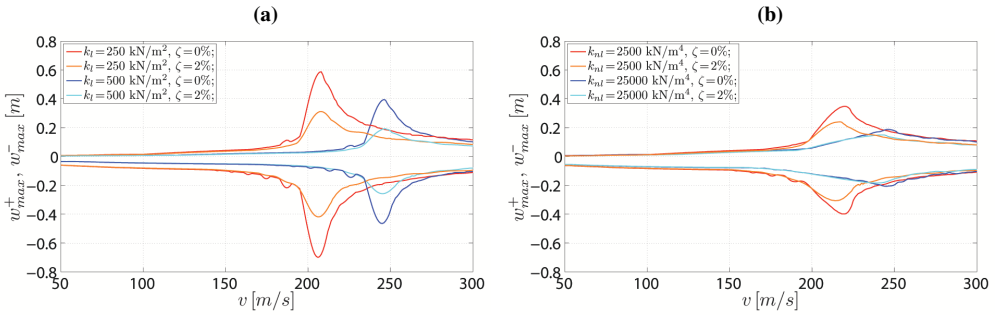

Figure 3.14: Representation of beam maximum displacements as a function of load velocity for linear (k_{nl}=0) (a) and nonlinear ($k_{nl}\neq$0 and k_l=250 kN/m^2) (b) elastic foundations.

First, a uniform linear elastic foundation is considered, with two different values of elastic Winkler coefficient equal to k_l=250 kN/m^2 and k_l = 500 kN/m^2, respectively. Both undamped and damped behaviors are taken into

account, assuming the damping factor ζ equal to 2%[1]. The results obtained for this case are shown in Fig. 3.14a. From the observation of these plots, the critical velocity may be clearly detected and the corresponding maximum (upward) and minimum (maximum downward) displacements are indicated in Table 3.3. It appears that the value of the critical velocity is weakly sensitive to the damping factor, while it affects more the magnitude of the maximum and minimum displacements. From Fig. 3.14a it appears that increasing the stiffness of the foundation causes a shift in the position of the critical velocities towards higher values, in addition to the expected effect of decreasing the deflection amplitudes.

The comparisons between the outcomes of the present work depicted in Fig. 3.14a and gathered in Table 3.3, if compared to those reported in Castro Jorge et al. (2015) [50], reveal a very good agreement, for both damped and undamped cases. Furthermore, in view of the results above, it may be noticed that a good degree of consistency has been also achieved with respect to the analytical solution proposed by Dimitrovová and Rodrigues (2012) [72].

	k_l=250 [kN/m^2]						k_l=500 [kN/m^2]					
	v_{cr} [m/s]			w_{max} [m]			v_{cr} [m/s]			w_{max} [m]		
ζ	PW	Ref. [50]	Err.	PW	Ref. [50]	Err.	PW	Ref. [50]	Err.	PW	Ref. [50]	Err.
0%	206	206	0.00	−0.700	−0.700	0.00	245	245	0.00	−0.465	−0.465	0.00
	208	208	0.00	0.587	0.587	0.00	246	246	0.00	0.395	0.395	0.00
2%	206	206	0.00	−0.419	−0.419	0.00	245	245	0.00	−0.258	−0.258	0.00
	208	208	0.00	0.312	0.312	0.00	246	246	0.00	0.192	0.192	0.00

Table 3.3: Maximum displacements and critical velocities for a linear foundation with stiffnesses k_l=250 kN/m^2 and k_l=500 kN/m^2. Percentage relative error of the present work (PW) with respect to Castro Jorge et al. (2015) [50].

	k_{nl}=2.5 × 10^3 [kN/m^4]						k_{nl}=2.5 × 10^4 [kN/m^2]					
	v_{cr} [m/s]			w_{max} [m]			v_{cr} [m/s]			w_{max} [m]		
ζ	PW	Ref. [50]	Err.	PW	Ref. [50]	Err.	PW	Ref. [50]	Err.	PW	Ref. [50]	Err.
0%	220	-	-	−0.400	−0.400	0.00	245	-	-	−0.204	−0.204	0.00
	220	-	-	0.350	0.349	0.00	246	-	-	0.186	0.186	0.00
2%	215	-	-	−0.306	−0.306	0.00	239	-	-	−0.183	−0.183	0.00
	217	-	-	0.242	0.242	0.00	242	-	-	0.150	0.150	0.00

Table 3.4: Maximum displacements and critical velocities for a cubic superlinear elastic foundation with k_{nl}=2.5 × 10^3 [kN/m^4] and k_{nl}=2.5 × 10^4 [kN/m^4] (k_l=250 kN/m^2). Percentage relative error of the present work (PW) with respect to Castro Jorge et al. (2015) [50].

Two examples of nonlinear foundations are also examined in Fig. 3.14b

[1]Mass proportional damping, with a damping factor defined according to Eq. (63) in Dimitrovová and Rodrigues (2012) [72].

(undamped and damped ζ=2% cases), one with a nonlinear component of foundation stiffness k_{nl}=2500 kN/m^4 and another with k_{nl}=25000 kN/m^4. The assumed linear component of foundation stiffness is k_l=250 kN/m^2 for both examples.

Comparing these plots to those depicted for a linear foundation, it can be seen that the addition of the nonlinear contribution to the foundation stiffness results in an increment of the critical velocities. Moreover, a decrease of the maximum upward and downward displacements is detected. The inclusion of damping brings a further decrease of the maximum displacements entity, together with a small decrease of the critical velocities. The values of critical velocities, maximum displacements and percentage relative errors upon the latter are reported in Table 3.4. For the nonlinear type of foundation the values of the critical velocities are not explicitly indicated by Castro Jorge et al. (2015) [50]. Nonetheless, the results obtained with the implemented method are matching the deflection curves and the maximum values of displacements reported in that work.

Hence, the comparison between the present results and the outcomes presented by Castro et al. (2015) [50] and by Dimitrovová and Rodrigues (2012) [72] reveals a very good agreement, providing a further verification of the reliability of the present finite element implementation.

3.4.2 Determination of the critical velocities

By assuming constant values of elastic coefficients of the foundation, for each load frequency Ω and ratio α=F_0/F, computations are performed for a moving load velocity varying between 10 m/s and 300 m/s, with a step variation of 1 m/s, recording, for each simulation, the maximum upward w^+_{max} and downward w^-_{max} displacements of the beam.

The frequency variation is chosen according to the stiffness coefficients of the foundation and the mechanical characteristics of the beam, and ranges from 0 to 30 rad/s, with intervals of 10 rad/s. The effect of damping has been neglected as in previous Section 3.3. Parameter α is varied in order to obtain the harmonic moving load magnitude trends depicted in Fig. 3.15.

The outcomes of the FEM simulations are plotted as a function of moving load velocity v in Fig. 3.16 and in Fig. 3.17, for the linear and the cubic superlinear foundation models, respectively. From the observation of Figs. 3.16a-3.17a, corresponding to a constant-magnitude moving load ($\Omega = 0$), one prominent peak can be observed, meaning that the beam-foundation system displays a single critical velocity; its value results independent of load ratio α, in case of a linear foundation model, while it increases with α for the cubic superlinear model. On the other hand, for both foundation models, it is noticeable that, as the magnitude of the moving load starts oscillating with frequency Ω,

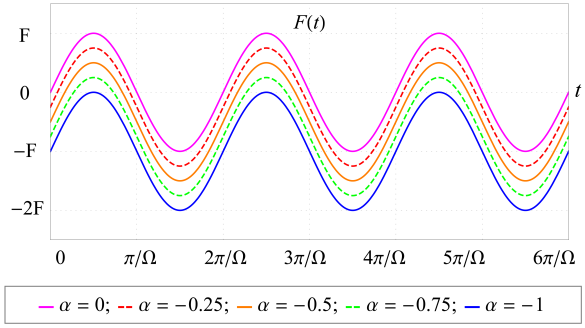

Figure 3.15: Harmonic moving load magnitude $F(t)$ within the selected range of values of α.

the peak bifurcates into two distinct peaks, for a zero-mean moving harmonic load (α=0) [97], or splits into three peaks, when the mean value of the moving load is different from zero ($\alpha \neq 0$).

In particular, two critical velocities tend to separate as the loading frequency increases, the lowest one (v_{cr1}) decreasing towards zero, the highest one (v_{cr3}), conversely, moving towards the upper limit of the plot. The central critical velocity (v_{cr2}) remains stationary for every Ω at the value corresponding to Ω=0. The effect of increasing the magnitude mean value (parameter α) is to further reducing v_{cr1} and at the same time increasing v_{cr2} and v_{cr3}, in the nonlinear case.

3.4.3 Bifurcation curves of the critical velocities

The extrapolated relationship between frequency Ω and critical velocities $v_{cr,j}$, j=1, 2, 3 is explicitly depicted in Fig. 3.18. Such threefold curves have been derived by appropriate analytical fitting proposals on the data collected from the numerical simulations. The following fitting expressions have been adopted for both considered types of foundation, linear and cubic superlinear:

$$v_{cr,j} = \sqrt{a_{0j} + a_{1j}\,\Omega + a_{2j}\,\Omega^2}, \quad j = 1, 3; \qquad v_{cr,2} = \sqrt{a_{02}}; \tag{3.26}$$

where each a_{ij} coefficient is implicitly depending on load ratio α. The associated fitting procedure based on a nonlinear least-squares regression, implemented in MatLab [251], with results in Table 3.5, has been performed by imposing additional constraints on the a_{ij} coefficients, as reported in Table 3.5 itself.

Comparing the curves retrieved for the nonlinear foundation (Fig. 3.18b) with the linear case (Fig. 3.18a), it is clear that the relationship between the critical velocities and the load frequency for linear and nonlinear elastic foundations displays similar features. Nonetheless, the curves for the nonlinear

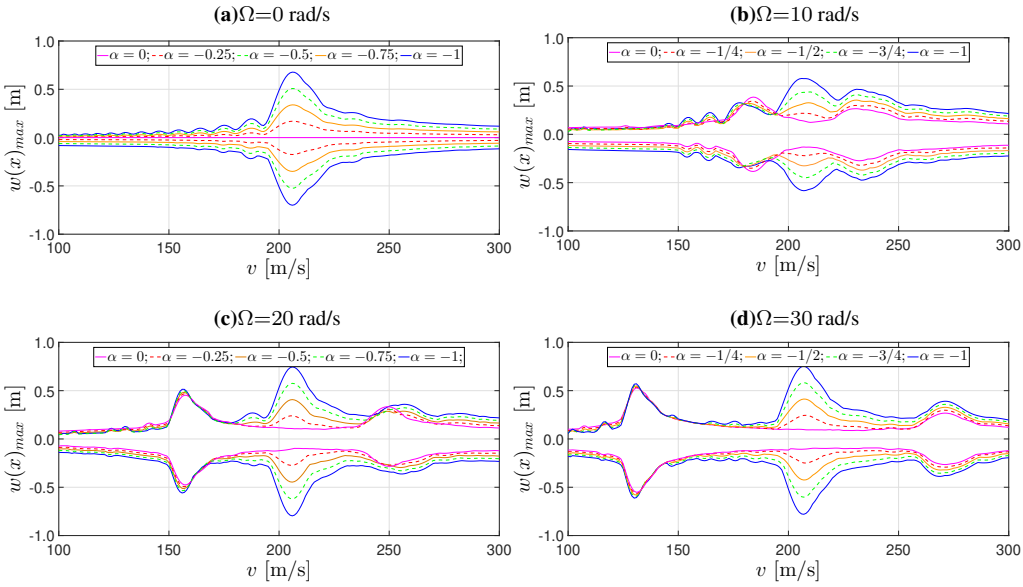

Figure 3.16: Representation of beam maximum displacements versus moving load velocity v and load ratio α=F_0/F for a linear elastic foundation with stiffness k_l=2.5 $\times$ 10^2 kN/m^2. Load frequency Ω ranges from 0 rad/s to 30 rad/s.

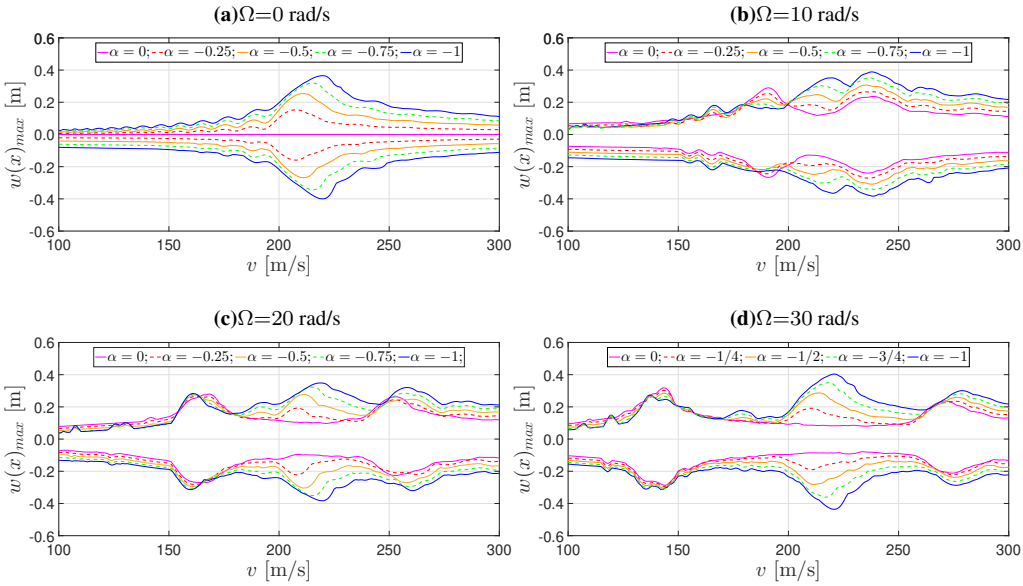

Figure 3.17: Representation of beam maximum displacements versus moving load velocity v and load ratio α=F_0/F for a nonlinear cubic elastic foundation with stiffnesses k_l=2.5 $\times$ 10^2 kN/m^2 and k_{nl}=2.5 $\times$ 10^3 kN/m^4. Load frequency Ω ranges from 0 rad/s to 30 rad/s.

foundation are slightly shifted upward, due to the increased global stiffness of the system.

Even though the determination of the coefficients in Eqs. (3.26) require a

significant amount of computational time, they explicitly show the critical velocities as a function of the load frequency, differently from the implicit formulation developed by Chen et al. (2003) [55]. Furthermore, the obtained models for the critical velocity/load frequency pairs are much simpler than their analytical counterparts proposed by Chen et al. (2003) [55], which involve cumbersome complex irrational fractions of polynomials containing the mechanical parameters of the system.

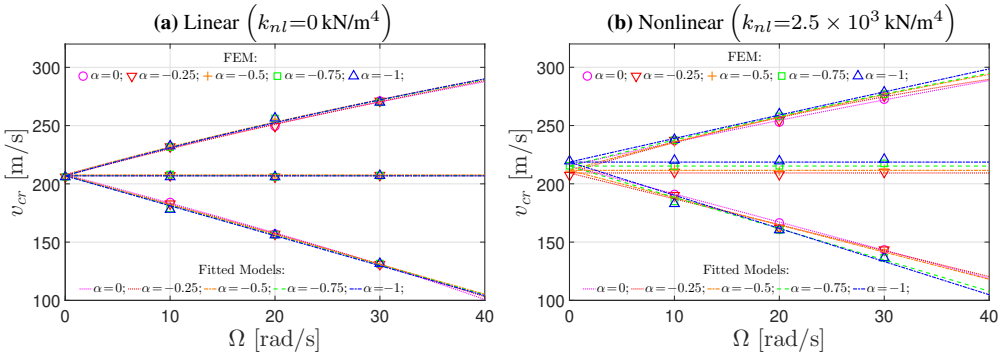

Figure 3.18: Critical velocities and load frequency three-branched curves for linear or cubic superlinear elastic foundations ($k_l = 2.5\times10^2$ kN/m^2). Results extracted from FEM results in Figs. 3.16-3.17 and fitted curves from predictions in Eq. (3.26).

Linear model

α	$a_{01}=a_{02}=a_{03}$ [m^2/s^2]	$a_{11}=-a_{13}$ [m^2/(rad s)]	a_{21} [m^2/rad^2]	a_{23} [m^2/rad^2]
0.00	$4.326\cdot10^4$	$-1.006\cdot10^3$	4.451	$-4.588\cdot10^{-1}$
-0.25	$4.283\cdot10^4$	$-1.008\cdot10^3$	5.054	$1.291\cdot10^{-1}$
-0.50	$4.312\cdot10^4$	$-1.063\cdot10^3$	6.552	$-9.597\cdot10^{-1}$
-0.75	$4.290\cdot10^4$	$-1.060\cdot10^3$	6.553	$-9.513\cdot10^{-1}$
-1.00	$4.280\cdot10^4$	$-1.063\cdot10^3$	6.605	$-7.281\cdot10^{-1}$

Nonlinear model

α	$a_{01}=a_{02}=a_{03}$ [m^2/s^2]	a_{11} [m^2/(rad s)]	a_{13} [m^2/(rad s)]	a_{21} [m^2/rad^2]	a_{23} [m^2/rad^2]
0.00	$4.641\cdot10^4$	$-1.041\cdot10^3$	5.833	$9.101\cdot10^3$	$2.910\cdot10^1$
-0.25	$4.380\cdot10^4$	$-9.305\cdot10^2$	4.942	$1.213\cdot10^3$	-5.272
-0.50	$4.475\cdot10^4$	$-9.890\cdot10^2$	5.465	$1.100\cdot10^3$	-1.501
-0.75	$4.632\cdot10^4$	$-1.156\cdot10^3$	7.207	$1.007\cdot10^3$	$2.157\cdot10^1$
-1.00	$4.780\cdot10^4$	$-1.244\cdot10^3$	8.093	$8.939\cdot10^3$	3.497

Table 3.5: Values of fitted a_{ij} coefficients according to Eq. (3.26).

3.5 Closing chapter considerations

In the first part of the present chapter, the dynamic transient response of a long finite, simply-supported beam, lying on linear or nonlinear elastic Winkler foundations, subjected to a concentrated load moving at a constant velocity along the beam, with harmonic-varying magnitude in time, has been numerically analyzed. A FEM implementation coupled with a HHT-α integration algorithm has been developed within MatLab [251] to determine the dynamic response of the beam-foundation system. Extensive numerical simulations by varying moving load velocity and amplitude frequency have been performed, providing several new outcomes about the mechanical behavior of the beam-foundation system.

The present FEM implementation has been first validated by comparing the gathered numerical responses with the results reported by Castro Jorge et al. (2015) [49, 50], in case of a constant amplitude moving load, providing outcomes that appear fully consistent with them. Multiple-branch numerical/analytical curves for the arising critical velocities have been derived, at variable mechanical parameters, by fitting the values of the critical velocities computed at different load frequencies through effective analytical interpolating proposals with calibrated coefficients, which may be employed for subsequent practical treatments.

Regarding the bilinear support case and a moving load with harmonic-varying magnitude characterized by null mean, bifurcation maps of the critical velocities have been obtained (Figs. 3.10-3.11). In fact, if the moving load magnitude is constant, only one critical velocity appears, and the present FEM implementation has been proven to provide results that are fully consistent to those earlier reported by Castro Jorge et al. (2015) [49]. Two critical velocities are instead observed for a harmonic moving load, independently from the foundation stiffness ratio. The two critical velocities tend to separate, one increasing, the other decreasing, as the moving load frequency increases, independently from the foundation stiffness ratio. Higher critical velocity v_{cr2} increases, starting from the value of the critical velocity obtained for a constant magnitude load. On the contrary, lower critical velocity v_{cr1} decreases, until it reaches zero for a frequency of the load equal to the first natural frequency of the beam.

A progressive decrease of the stiffness for the upward motions increases the positive (upward) displacements of the beam; the increase of the displacements is particularly important for a nearly vanishing tension stiffness, for which upward displacements may become so large that the hypothesis of geometrical linearity may become no longer valid. The moving load critical velocities also decrease when the foundations stiffness ratio decreases. Further, convergence studies on the maximum beam deflection demonstrate the high accuracy of the

retrieved results, for the adopted space discretization. In addition, for each simulation, an automated calculation is implemented to evaluate the time step for the numerical integration in order to optimize the computational effort.

Subsequently, a cubic superlinear elastic Winkler foundation and one harmonic moving load with not null mean magnitude have been taken into account. Several numerical simulations have been performed by varying moving load velocity, magnitude mean value and frequency, providing some interesting outcomes regarding the mechanical behavior of the beam-foundation system. If the moving load magnitude is constant, only one critical velocity appears, while two critical velocities are observed for a harmonic moving load with zero mean magnitude, one increasing, the other decreasing, as the moving load frequency increases. Three critical velocities are instead detected for a harmonic moving load with non-zero mean magnitude, which also depend on the moving load mean magnitude, in the nonlinear case. In the linear case (k_{nl}=0 kN/m^2) the obtained bifurcation curves show a very good agreement to those available from the analytical approaches by Chen et al. (2003) [55]. The relationship between the critical velocities and the moving load frequency has been portrayed in appropriate three-branch curves (Fig. 3.18). These curves have been achieved by fitting the values of the critical velocities computed at different load frequencies through effective analytical formulas (3.26), which may be assessed for practical treatments. An analytical discussion on the existence of the three peaks for moving load problems involving harmonic moving loads with non-zero mean magnitude will be the subjects of future developments.

Thus, the employed models for the description of the bifurcation curves are very appropriate for the considered nonlinear beam-foundation systems. The derived formulas are simple and possibly workable in practice; they may supply a guideline for the design of railway tracks when the magnitude of the moving load is oscillating in time. Furthermore, potential implications in practical design scenarios may be deduced from the study on the bilinear foundation case, especially in possibly lowering down the ranges of admissible vehicle velocities, as for a structural requirement or for preventing potential passenger discomfort.

It must be recognized that, in order to obtain a more realistic dynamic response of the system, some further improvements of the modelization could be made to obtain an even more detailed dynamic response of the beam-foundation system. A real vehicle spring-mass-damper system interacting with the beam should be considered, instead of a simple moving force. The geometrical linear hypothesis on the kinematics of the beam could be relaxed and a more complex constitutive law of the support, which would be both a nonlinear function of the beam displacements and with different behavior in compression and in tension, may be included. Real applications usually require extensions to infinite lenghts; it is then necessary to eliminate the effect of the supports,

by mitigating the perturbation induced by the reflection of the traveling waves. This could be achieved by implementing appropriate absorbing boundaries. These issues shall be the subject of future developments.

Chapter 4

Steady-state formulation for an infinite taut string on a Winkler elastic support under constant moving load

4.1 State of the art on moving-load steady-state analysis

As outlined in the previous chapter, many studies have been devoted in the literature to moving load problems, considering both different types of structures and kinds of loads, including also for various possible sources of nonlinearities. Concerning the analysis of infinite homogeneous beams lying on a damped or undamped Winkler elastic foundation, excited by a moving load, different approaches have been adopted so far. In case of homogeneous beam-foundation systems, one of the most common modelizations is to consider the steady-state response of infinite beams subjected to a constant magnitude moving load (see e.g. Kenney, 1954 [155], Frýba, 1972 [105]), as well as to a moving load with harmonically-varying amplitude, as reported by Mathews (1958,1959) [189,190], Chonan (1978) [58] and Bogacz et al. (1989) [40].

By assuming the homogeneity of the system in the direction of the moving load and a negligible influence of the transient motion regime, the problem may be analyzed in a moving reference frame attached to the position of the load, by using a space-time change of variables. The advantage of such a transformation in the moving reference frame is that the solution is obtained like for a fixed-load dynamic problem and, if the load amplitude is also taken constant in time, the stationary solution under steady-state conditions (*steady-state solution*) can be obtained as by solving a purely static problem (the solution is not dependent on the time variable).

Kenney (1954) [155] solved the case of an infinitely long Euler-Bernoulli elastic beam lying on a Winkler elastic foundation, i.e. a set of continuously-distributed, non-interconnected springs with a locally-constant stiffness, as explained in Chapter 2. The Author derived the analytical solution of the steady-state response for a constant-velocity moving load, by using a Green's function approach, accounting for viscous damping. According to the theory of harmonic flexural waves (see e.g. Graff, 1975 [116]), the velocity of propagation of free waves for the undamped case was obtained. Furthermore, it was shown that, in the limit case of no damping, if the velocity of the traveling load becomes equal to such a free wave or group velocity, displacements increase boundlessly, resulting in a resonance condition. In fact, as exposed by Simkins (1989) [239] for the analysis of gun tubes, the wave energy, which is transferred at the group velocity, concentrates on the load front (phase velocity) and continuously builds up the deformation near the front, as time progresses. Kenney (1954) [155] also showed that for a load velocity lower than the critical velocity (subcritical case), the largest wave amplitude occurs near the loading point, while, for a load velocity larger than the critical one (supercritical case), the waves moving ahead of the load become smaller in amplitude and in wavelength than those behind the load.

Mathews (1958) [189] and Achenbach and Sun (1965) [2] generalized Kenney's analytical solution for a moving load with harmonically varying amplitude and for a Timoshenko beam, respectively; a similar set of equations was derived by Jones and Buta (1964) [47], by investigating the steady-state response of cylindrical shells to a moving ring load. Chen et al. (2001) [56] obtained the bifurcation curves of the critical velocities in case of a harmonic moving load acting on an infinite compressed Timoshenko beam by using the dynamic stiffness method. In that context, a FEM approach to characterize such bifurcation curves for a nonlinear support has been developed by Froio et al. (2016) [99], as discussed in the previous chapter.

Kerr (1972) [157] has studied the effect of a compression axial force on an *undamped* beam-foundation system, which may be induced by a rise in temperature within the beam. It is shown that the action of the compression force progressively decreases to zero the value of the critical velocity, when it reaches the critical static buckling load of an infinite beam. In this sense, though the essence of that structural problem is different than that considered here, the action of a compression force in softening the model is analogous to the effect of the Pasternak foundation in stiffening the model.

A formal integral solution of the general dynamic problem of the transient and steady-state vibrations of an infinite Euler-Bernoulli beam on an elastic foundation has been obtained by both Stadler and Shreeves (1970) [246] and Sheehan and Debnath (1972) [237], by applying the joint Laplace and Fourier transforms. By assuming the beam as a two-dimensional elastic continuum,

Saito and Terasawa (1981) [230] derived the equations of motion of an elastic infinite beam supported by a Pasternak-type foundation and subjected to a moving load distributed on a narrow finite length. The Fourier transform technique was applied to compute the steady-state response, even though no analytical formulation of the solution was present. Numerical results revealed unimportant discrepancies between the two-dimensional elastic theory and the Euler-Bernoulli and Timoshenko beam theories.

The response of a uniform Timoshenko beam of infinite length placed on a generalized Pasternak viscoelastic foundation and subjected to a harmonic arbitrary distributed moving load was computed numerically by Kargarnovin and Younesian (2004) [151], by using the Fourier transform coupled with the Gaussian quadrature method. In a subsequent work, Younesian and Kargarnovin (2009) [281] considered the same problem, but with a stochastic variation of the Winkler modulus along the beam axis. Nonlinear problems involving an infinite beam on a Pasternak foundation seem rather limited in the literature; one example may be found in the work of Ding et al. (2013) [75], where the Adomian Decomposition method was applied to determine the dynamic response of the beam.

Regarding the steady-state response of infinite elastic plates on an elastic support under moving load, the interested reader may be referred to the works of Stadler (1971) [245] and of Watanabe (1981) [269]. Stadler (1971) [245] considered a Winkler support and derived the analytical solution of the steady-state response of the plate in integral form by using the Fourier transform. On the other hand, the problem of an elastic plate resting on an undamped Pasternak foundation under a concentrated load moving at a constant velocity along a straight line was analyzed by Watanabe (1981) [269]. By applying the double Fourier transform, the author derived a formal integral expression of the solution, by means of which he finally numerically computed the plate response. Thus, such a representation is not fully explicit in analytical terms and anyhow neglects the role of damping.

The analysis of the steady-state dynamic response of an infinite beam on a viscoelastic Winkler (or Winkler-Pasternak) foundation under a constant amplitude moving load shares many characteristics features, regarding both the determination of the solution and its physical manifestation, with the steady-state dynamic response of an infinite taut string lying on a viscoelastic Winkler support. Thus, as a preliminary approach towards the subsequent study of the infinite beam problem, it appears worthwhile to analyze first the problem of the taut string.

Very long *taut strings* are widely used as engineering components. Examples include overhead electrical power lines and mechanical guides. The theoretical formulation of the associated mechanical problem may be found in Graff (1975) [116]. The analysis of the linear and nonlinear steady-state

response of an infinite string-foundation system traveled by a moving load was studied by Yen and Tang (1970) [280], by using a perturbation technique; the authors focused their attention on the response characterizing the transition of an accelerating load crossing the wave propagation velocity in the string (critical velocity). Qualitative geometric analyses about the stationary response of an infinitely long string on linear and nonlinear viscoelastic foundations under moving load were performed by Metrikine (1994) [193] and Metrikine (2004) [194].

The transient response of an infinite taut string lying on an elastic foundation caused by an accelerating load crossing the critical velocity was investigated analytically by Gavrilov (1999) [107], by means of asymptotic expansion techniques. An alternative way of obtaining such a transition was presented by Wolfert and Dieterman (1997) [273], who considered a spatially piecewise constant foundation stiffness, for which a transition from subcritical into supercritical motion appeared, without modifying the moving load velocity.

In addition, it has also been shown that the string response depends crucially on the ratio between load velocity and critical velocity. If the load moves slower than the waves in the string, then the response is nearly symmetric with respect to the load position and decays exponentially with the distance from the load. On the other hand, if the load velocity exceeds the critical velocity, then the string exhibits a wave pattern behind the load, while it remains undeformed in front of it (Metrikine, 2004 [194]).

For the analysis of more complicated systems, where analytical methods might not be suitable, the design of numerical procedures, such as the Finite Element Method (FEM), would be strongly desirable. Unfortunately, when applying standard Galerkin Finite Element Method to moving load problems in a convected coordinate, serious difficulties arise. Attempts to apply a classical FEM approach based on a Galerkin scheme to the steady-state moving load problem have provided solutions that were corrupted by numerical instabilities and poor approximations of derivatives in the supercritical regime (Nguyen and Duhamel, 2006 [209]); in addition, it is well-known that any application of GFEM to non self-adjoint equations, such as e.g. the convection-dominated diffusion equation, results in a solution polluted by non-physical spurious oscillations, or "wiggles" (Johnson et al., 1984 [146]).

In other words, the convergence of a standard GFEM approximation noticeably deteriorates as the moving load velocity approaches and overcomes the critical velocity. In this context, Nguyen and Duhamel (2006) [209] proposed a method to obtain a stable stationary solution for the longitudinal vibration of beams under axial moving load, a differential problem finally equivalent to that of the taut string under transverse moving load, by combining the GFEM with the HHT-α method, thus resulting in a modified Taylor-Galerkin approach. Although the method provided quite accurate results at the price of a rather tricky

implementation, it is also characterized by a nonsymmetric resulting system of algebraic equations and, moreover, the validity of the approach depends on the setting of several user-tunable parameters, whose domains are unknown. Then, Nguyen and Duhamel (2008) [209] extended the same methodology to the nonlinear steady-state response of an infinite beam under moving harmonic loads.

In order to overcome these various drawbacks, a Least-Squares Finite Element Method approach (LSFEM, Jiang, 1998 [145]) may represent a valid alternative to classic GFEM. The LSFEM is a reliable and efficient class of FEMs with a unified formulation for the numerical solution of all types of linear PDEs, no matter whether the equations are elliptic, parabolic, hyperbolic or mixed, since its theoretical bases are rooted in the bounded inverse theorem for linear operators (Jiang, 1998 [143]). Therefore, as long as the problem displays a unique solution, the LSFEM can always determine a good approximate solution.

The application of the least-squares principles to the FEM leads to the definition of a quadratic least-squares functional $\mathcal{J}$ over a suitable function space $\mathcal{V}$. The differential equation governing the system is firstly recast to a first-order system by introducing additional, often physically motivated, variables; lowering the order of derivation of the problem is needed by the necessity of the least-squares method of working with functional spaces having smoother elements than those required by standard Galerkin method (Lin, 2009 [180]). Then, functional $\mathcal{J}$ is defined to be the sum of the squared L_2-norms of the residuals of each first-order differential equation. The exact solution must be the unique zero minimizer of the functional $\mathcal{J}$ over $\mathcal{V}$, obtained through the Euler-Lagrange equations. In practice, the least-squares FEM approximate solution is defined to be the minimizer of $\mathcal{J}$ over a suitable finite-dimensional subspace $\mathcal{V}_h$ of $\mathcal{V}$. A precursor analysis of this method was illustrated by Jespersen (1977) [141].

Although the research on these methods began in the early 1970s (for an overview see e.g. Eason, 1976 [80]), the LSFEM has become not that popular as for mixed Galerkin methods. However, the LSFEM encountered a revival in the 1990s, with the rising available computer performance, and many approaches were proposed and analyzed for different problems in fluid dynamics and solid mechanics. The monographs by Jiang (1998) [145] and Bochev and Gunzburger (2009) [38] and references reported therein provide a comprehensive survey on the scientific research in this LSFEM field.

The growing interest in developing LSFEM is due to its several theoretical and computational advantages characterize the LSFEM. A single piecewise polynomial, even discontinuous, space can be adopted for approximating all the involved variables, and, consequently, accurate approximations of all the unknowns can be simultaneously obtained. The LSFEM allows for circum-

venting well-known stability conditions such as the inf-sup or Ladyzhenskaya-Babŭska-Brezzi (LBB) condition arising in mixed-methods (see Ladyzhenskaya, 1969 [170], Babŭska, 1973 [14], Brezzi, 1974 [45]). Then, equal-order elements can be used, thus making programming much easier. Hence, stabilization terms and associated user-tunable parameters, which are prevalent in traditional schemes, are not needed inside the functional and, thus, they can be avoided.

The method, by construction, always yields sparse, symmetric and positive-definite algebraic discrete systems, for which robust and efficient iterative solvers exist (Zienkiewicz et al., 1974 [285]), such as preconditioned conjugate gradient methods, regardless of the grids and elements employed in the least-squares scheme. Therefore, the LSFEM recovers, in general settings, the advantageous features of the Rayleigh-Ritz method (Bochev and Gunzburger, 2006 [38]). In addition, the value of the least-squares functional of the approximate solution provides a practical and sharp a posteriori error estimator at no additional cost, applicable to adaptive mesh refinement algorithms. A bright review of the theory and formulations of least-squares variational principles and FEM may be found in Pontaza (2005) [217]. Further, trial functions are not required to satisfy any boundary conditions, which instead may be weakly imposed inside the functional, making the treatment of general complex boundary conditions more affordable.

By virtue of the above-listed advantages, over the past decades the use of least-squares principles in connection with finite element techniques has been extensively applied to numerical approximations in many different fields such as fluid dynamics: Jiang and Povinelli (1993) [142], Bochev and Gunzburger (1995) [36], Bochev et al. (2012) [39]; elasticity: Zienkiewicz et al. (1974) [285], Yang (2000) [276], Jou and Yang (2000) [149], Bramble et al. (2001) [43], Pontaza and Reddy (2005) [219], Moleiro et al. (2009) [201]; electromagnetism: Fix et al. (1979) [94], Monk and Wang (1999) [202]. For an overview on least-squares finite element methods, the interested reader may be referred to the review by Bochev and Gunzburger (1998) [37].

In the present chapter, a local Discontinuous Least-Squares Finite Element Method (DLSFEM) formulation is presented for the numerical solution of the steady-state response of a uniform infinite taut string resting on a viscoelastic foundation and traversed by a constant transverse point load, moving with a constant velocity along the string. In fact, since the LSFEM typically requires a rather strong regularity on the true solution, its standard application to the problem under consideration may result to be inappropriate in case of a moving concentrated force. Therefore, continuity requirements are relaxed by using discontinuous global shape functions at the point of application of the load, where both compatibility and equilibrium conditions are weakly enforced through a properly defined least-squares functional. Away from the point of ap-

plication of the load, the solution keeps regular and continuous, and standard continuous approximation spaces are employed.

Several papers have been devoted to investigations in the discontinuous least-squares framework. Cao and Gunzburger (1998) [48] used least-squares methods with discontinuous elements to treat interface problems. Gerritsma and Proot (2002) [109] derived a discontinuous least-squares spectral element method for a first-order ordinary differential equation. Bensow and Larson applied discontinuous LSFEMs to Div-Curl problems (Bensow and Larson, 2005 [26]) and to elliptic problems with boundary singularities (Bensow and Larson, 2005 [27]). Lin proposed a discontinuously discretized LSFEM for 1D (Lin, 2008 [180]) and 2D (Lin, 2009 [181]) singularly perturbed reaction-diffusion problems.

A second major difficulty of numerically solving steady-state problems in a moving coordinate system is that the problem is defined over an unbounded domain. In order to keep the computation feasible, the domain must be inevitably truncated to a finite computational domain and, consequently, completed by suitable artificial boundary conditions. The implementation of artificial boundary conditions cannot be neglected since the results of exterior problems over a finite region strongly depend on the proper treatment of the external boundaries. One of the most common approaches is to consider a bounded domain surrounded by a boundary layer which, by virtue of its augmented absorbing properties, artificially absorbs waves propagating outwards from the bounded domain (radiation condition or radiation damping). Thus, when the wave enters the absorbing layer, it is attenuated by absorption and it decays in a very fast way. The drawback of such an approach is that, whenever there is a transition from one media to another one, waves generally reflect and the transition from a non-absorbing to an absorbing material makes no exception. In order to simulate a problem originally defined on an unbounded domain, a steady-state PML technique in moving coordinates has been considered, thus balancing the geometric truncation of the original unbounded domain.

Hence, in order to eliminate numerical difficulties that may arise when trying to simulate steady-state responses at supercritical velocity regimes and to avoid the need of either special treatments or user-tunable parameters associated to stabilization terms, the objective of the present chapter is to derive and implement a DLSFEM-PML method for the string-foundation interaction problem under moving load, for providing a unitary and robust computational tool endowed of a general validity, within the whole space of variation of the characteristic mechanical parameters of the taut string-foundation system and thus reaching the most possible general level of analysis.

Further, as concerning to the local DLSFEM formulation, the convergence of the method is rigorously demonstrated in matrix form, as opposed to previous works reported in the literature, *here assessing the Least-Squares FEM*

being valid for any linear ordinary differential equation of any order, written as a first-order differential system, within a complex-valued function space framework, if the original mathematical problem is well-posed. This shall constitute a main achievement of this work in computational terms. Thanks to such an important property, this numerical technique will be also applied in the next chapter dealing with the steady-state vibration of an infinite beam. The theoretical results are also demonstrated for the physical problem under consideration, by comparing the obtained numerical results with an available analytical solution (Metrikine, 2004 [194]).

In addition, as concerning to the PML implementation, for the first time the PML absorbing boundary conditions is successfully formulated and implemented within a Least-Squares FEM context and its effectiveness has been proven through several numerical examples, where the rate of convergence of both H^1 and L^2-norms of the error is shown to be coherent with the derived theoretical a priori error estimates.

The layout of the chapter is as follows. In Section 4.2 the steady-state first-order formulation governing the string motion in a convected coordinate is introduced, along with the interface conditions at the point of application of the load and the conditions at infinity; then the analytical solution, taken from the literature (Metrikine, 2004 [194]), is reported for further information. In order to treat such far-field conditions, the differential equation governing the PML is further derived. Then, the DLSFEM formulation is presented in Section 4.4. Coercivity in the H^1-norm of the derived sesquilinear form is proven. By virtue of this property, a priori uniform error estimates in both L^2- and H^1-norms are established, thus assuring the convergence of the DLSFEM approximation. Numerical experiments involving the complete normalized steady-state response of the taut string-foundation system (deflection and slope) by the DLSFEM defined in Section 4.4 constitutes the main subject of Section 4.6. These numerical results are compared to the outcomes of an available analytical solution, in order to support the statements of Section 4.4 and to validate the application of the PML. Finally, main conclusions of the work are resumed in closing Section 4.7. The discussion of the achievements of the present chapter may be also found in Froio et al. (2019) [103].

4.2 Theoretical bases and analytical solution

In this section, the differential problem of an infinite taut string supported by a viscoelastic foundation is introduced and the corresponding analytical solution is presented.

Consider a taut string, of an infinite length and supported by a viscoelastic foundation, as briefly sketched in Fig. 4.1, endowed with right-handed sys-

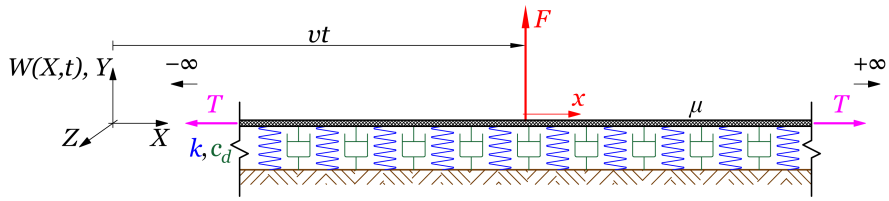

Figure 4.1: Infinite taut string resting on a viscoelastic Winkler foundation under a constant transverse load F moving at constant velocity v along the string.

tem of rectangular coordinates (X,Y,Z) and time variable t [s]; the X-axis (longitudinal axis) is taken along the undeformed string axis, while the Y-axis (transverse vertical axis) and the Z-axis (transverse horizontal axis) are perpendicular to it; the positive direction of the Y-axis is taken vertically upward. The positive direction for measuring string slopes is conformal to typical usage, i.e. according to a right-handed screw rule. The thickness of the cross-section of the string is small and negligible, thus making the problem one-dimensional. The taut string is traversed by a transverse constant concentrated load F [N], positive if upward, moving from $-\infty$ to $+\infty$ at a constant velocity v [m/s]. The load is taken upward for the derivation of the equations; it will finally acts downward in the final presented applications.

In such a reference frame, by neglecting geometric non-linearity of the displacements of the string, which looks of secondary importance for the model under investigation, the equation of motion describing the vertical vibration of the taut string under the moving concentrated load is represented by the following second-order PDE (see e.g. Graff, 1975 [116]):

$$\mu\, W_t^{(2)}(X,t) - T\, W_X^{(2)}(X,t) + c_d\, W_t^{(1)}(X,t) + k\, W(X,t) = F\, \delta(X - vt); \quad (4.1)$$

where μ [kg/m] is the mass per unit length of the string, T [N] is the given constant tension of the string, k [N/m^2] is the Winkler stiffness coefficient, c_d [Ns/m^2] is the viscous damping coefficient per unit length of the foundation; all such characteristic parameters are assumed to be constant in both space and time. Moreover, the unknown transverse displacement of the string induced by the acting moving load has been labeled as $W(X,t)$ [m] (positive in the Y direction); finally, F on the right-hand side of Eq. (4.1) is the constant magnitude of the concentrated moving load, v is its moving velocity and $\delta(\cdot)$ is the Dirac delta function. If F and c_d are both assumed to be zero, Eq. (4.1) constitutes the one-dimensional dispersive wave equation, also known as Klein-Gordon equation (Salsa, 2008 [231]).

By assuming steady-state conditions, i.e. supposing that the effects of transients due to the initial conditions during the first evolution of the system become negligible at later stages, it is possible to directly correlate string transverse displacement $W(X,t)$ to the character of forcing action $F\,\delta(X - vt)$

acting on the infinite string. This means that, under steady-state conditions, $W(X,t)$ can be assumed to display the following form:

$$W(X,t) = W_0\, w(X - vt); \tag{4.2}$$

where $w(X-vt)$ is a dimensionless steady-state displacement of the string, measured at locations X–vt [m] relative to moving load position vt, and W_0 [m] is a normalization factor, to be defined later. Hence, the definition in Eq. (4.2) characterizes the solution $W(X,t)$ as a *"travelling wave"* (Salsa, 2008 [231]), moving at velocity v.

Furthermore, since the string-support system displays homogeneous characteristics, it is customary to introduce the following new real independent variable:

$$x = X - vt; \qquad -\infty < x < +\infty; \tag{4.3}$$

representing a moving reference frame attached to the position of the moving load, which reduces original PDE Eq. (4.1), with $W(X,t)$ as in Eq. (4.2), into an ODE. The same change of variables will be applied for the case of an infinite beam in the next chapter. Now, from the change of variables defined in Eq. (4.3), Eq. (4.2) reads

$$W(X,t) = W_0\, w(x); \tag{4.4}$$

and the application of the chain rule of differentiation to Eq. (4.4), with x defined in Eq. (4.3), yields:

$$W_X^{(2)} = W_0\, w_x^{(2)}(x), \;\; W_t^{(1)} = -W_0\, v\, w_x^{(1)}(x), \;\; W_t^{(2)} = W_0\, v^2\, w_x^{(2)}(x). \tag{4.5}$$

The substitution Eqs. (4.4) and (4.5) into Eq. (4.1) and rearrangement of all terms leads to the following second-order ODE in unknown steady-state normalized displacement $w(x)$:

$$\left(v^2 - v_0^2\right) w_x^{(2)}(x) - \frac{c_d\, v}{\mu}\, w_x^{(1)}(x) + \frac{k}{\mu}\, w(x) = 0; \tag{4.6a}$$

$$[\![w(x)]\!]_0 = 0; \tag{4.6b}$$

$$[\![w_x^{(1)}(x)]\!]_0 = \frac{F}{W_0\, \mu\, (v^2 - v_0^2)}; \tag{4.6c}$$

where

$$v_0 = \sqrt{\frac{T}{\mu}}; \tag{4.7}$$

is the propagation velocity of transverse waves in the string [m/s] and

$$[\![\psi]\!]_a = \psi(a^+) - \psi(a^-); \tag{4.8}$$

denotes the jump difference between the limits from the two sides of any arbitrary function ψ at point $x{=}a$.

Accordingly, the normalized steady-state slope may be defined as:

$$\theta(x) = \frac{\Theta(X - vt)}{\Theta_0} = \frac{W_X^{(1)}(X - vt)}{\Theta_0} = \frac{W_0}{\Theta_0}\, w_x^{(1)}(x) = w_x^{(1)}(x). \tag{4.9}$$

By choosing $\Theta_0{=}W_0$ as the normalization factor for the slope, $\theta(x)$ is directly expressed as the derivative of unknown function $w(x)$, $\theta(x){=}w_x^{(1)}(x)$. Eq. (4.6a) governs the vertical motion of the supported string everywhere but in the point of loading, whereas Eqs. (4.6b)-(4.6c) represent the continuity condition for the string displacement and the balance of vertical forces at the point of loading, respectively.

Notice that Dirac delta function in Eq. (4.1) has been transferred to Eq. (4.6c) for the purposes of the forthcoming numerical developments. Eqs. (4.6) are supplemented by the following far-field conditions:

$$\lim_{x \to \pm\infty} w(x) = \lim_{x \to \pm\infty} w_x^{(1)}(x) = 0; \tag{4.10}$$

providing that at an infinite distance to the left, as well as to the right, of moving load F, the transverse displacement of the string and its derivative (slope) shall vanish.

The analytical solution of Eqs. (4.6), endowed with far-field conditions in Eq. (4.10) may be distinguished in two different cases as follows (Metrikine (2004) [194]):

1. $v{<}v_0$:

$$\hat{w}(s) = \frac{F}{W_0\,\mu\,(v^2 - v_0^2\,)}\frac{e^{q_1 s}}{q_2 - q_1}, \qquad \text{if } s < 0; \tag{4.11}$$

$$\hat{w}(s) = \frac{F}{W_0\,\mu\,(v^2 - v_0^2\,)}\frac{e^{q_2 s}}{q_2 - q_1}, \qquad \text{if } s \geq 0; \tag{4.12}$$

$$\hat{\theta}(s) = \frac{F}{W_0\,\mu\,(v^2 - v_0^2\,)}\frac{q_1\, e^{q_1 s}}{q_2 - q_1}, \qquad \text{if } s < 0; \tag{4.13}$$

$$\hat{\theta}(s) = \frac{F}{W_0\,\mu\,(v^2 - v_0^2\,)}\frac{q_2\, e^{q_2 s}}{q_2 - q_1}, \qquad \text{if } s \geq 0; \tag{4.14}$$

2. $v{>}v_0$:

$$\hat{w}(s) = \frac{F}{W_0\,\mu\,(v^2 - v_0^2\,)}\frac{e^{q_1 s} - e^{q_2 s}}{q_2 - q_1}, \qquad \text{if } s < 0; \tag{4.15}$$

$$\hat{w}(s) = 0, \qquad \text{if } s \geq 0; \tag{4.16}$$

$$\hat{w}(s) = \frac{F}{W_0\,\mu\,(v^2 - v_0^2\,)}\frac{q_1\, e^{q_1 s} - q_2\, e^{q_2 s}}{q_2 - q_1}, \qquad \text{if } s < 0; \tag{4.17}$$

$$\hat{\theta}(s) = 0, \qquad \text{if } s \geq 0; \tag{4.18}$$

where the normalizing factors for representing the normalized steady-state response are now chosen as follows:

$$W_0 = \Theta_0 = \left| \frac{F}{\mu\,(v^2 - v_0^2\,)} \right|; \tag{4.19}$$

in order to consistently obtain $\hat{F}{=}{-}1$ in Eqs. (4.6), whereas q_1 and q_2 are the roots of the following characteristic polynomial:

$$\mu\big(v^2 - v_0^2\big)q^2 - c_d v\, q + k = 0. \tag{4.20}$$

Notice that when $v{=}v_0$ (critical condition), resonance occurs, in the sense that the amplitude of the traveling waves increases without bound, as dictated by the vanishing denominator in Eqs. (4.11)-(4.15).

4.3 Numerical modelization over infinite domains

Infinite or unbounded domains are often encountered in mathematical models in various fields of applied mechanics and engineering. Infinite domains are spatial domains of an infinite measure, i.e. domains in $\mathbb{R}$ or in $\mathbb{R}^N$, which display an infinite extension. An infinite domain is usually considered as a replacement of a medium surrounding the region of physical interest and extending very far away from it, so far that the effect of any boundary conditions imposed on the boundary of such a medium do not affect the sought response within the region of interest. Mathematical problems defined on infinite domains are usually called "*exterior problems*" or "*infinite domain problems*". Such problems frequently arise in practice, but less consideration has been devoted to them, with respect to classical boundary value problems.

Examples of exterior problems are: problems in earthquake engineering, where the infinite domain is the earth and the region of interest is the region around a structure and/or around a seismic source; problems in acoustics, where the infinite domain is the air and the region of interest is the region around the acoustic source; problems in structural mechanics involving wide beams or plates, where the infinite domain is represented by the portion of the structural element far from the applied loads; and problems in fluid dynamics or aerodynamics related to the flow around an obstacle, where the infinite domain is constituted by the undisturbed flow field of the fluid.

In general, analytic treatments of problems defined on infinite domains are usually easier to be tackled with respect to corresponding problems with a finite geometry (Givoli, 1992 [110]). On the contrary, the application of well-known numerical techniques to problems defined on large or infinite domains, such as

Finite Element Method (FEM) and Finite Differences (FD), becomes impossible or poses serious difficulties, when used in a straightforward manner, since the most common numerical methods require a finite computational domain.

Thus, the infinite domain has to be truncated by introducing an artificial boundary, on which some boundary conditions have to be specified, in order to complete the "*truncated problem*". The infinite domain may be truncated so that the "infinity" boundary condition is imposed on the boundary of a large domain, but deciding "how wide is large" is a difficult problem and the usual approach is that of trial and error. Further, in general, this does not represent a very safe choice, since the results of the analysis will predict some interaction between the region of interest and the boundary conditions, which is totally spurious. Thus, the only feasible alternative is to properly modify the usual boundary conditions by introducing special features, so that this would be effective in handling infinite domains.

Many techniques have been developed toward this purpose since the 1970s (Givoli, 1992 [110]). Among those, it is worth to mention Absorbing Boundary Conditions (ABC), or equivalently Non-Reflecting Boundary Conditions (NRBC), Perfectly Matched Layers (PML), boundary integral methods, infinite elements, absorbing layer methods and various other techniques including mapping techniques, filtering and damping schemes, sub-structuring and domain decomposition methods. Some of the main methods and relative notable research works from the literature are briefly discussed in the following. For a more comprehensive literature review on the subject, the interested reader may be referred to the works discussed below and the references reported therein.

One of the first methods to replace the infinite domains by finite domains was to map the infinite domain into a finite one by means of a smooth mapping, and then to numerically solve the problem in the finite domain (De Hoog and Weiss, 1979 [64]); however, since the mapping cannot be bounded in this case, the resulting mapped problem contains singular points in its finite domain. Such an approach is seldom used in practice because numerical approximations about a singularity entail tricky numerical problems. Whenever the solution oscillates moving towards infinity, mapping techniques are ineffective and alternate approaches must be developed for treating the computational boundaries (Engquist and Majda, 1979 [85], Givoli, 1992 [110]).

Linear boundary value problems may be solved by the Boundary Integral method, according to which the problem is first reformulated as a Fredholm integral equation on the boundary of the domain, owing to the use of exact fundamental solutions, and then numerically solved. One well-known numerical method for solving Fredholm integral equations is the Boundary Element Method (BEM), by which the integral equation on the boundary is solved with an approach similar to that of the FEM. For problems posed on unbounded

domains, the BEM may be very appropriate, as opposed to the FEM, since it enables one to eliminate the infinite domain before any computation starts. Nevertheless, the BEM needs a regular domain and rather simple linear governing equations, for which exact fundamental solutions are known. On the other hand, the FEM is far more general. It can handle variable coefficients, anisotropic materials and various nonlinearities, because it does not rely on the availability of an analytic fundamental solution (Givoli, 1992 [110]). Further, the limitations of the BEM may be relaxed through a coupled FEM-BEM approach. In this method the capabilities of the FEM to handle complex governing differential equations are combined with the advantages of the BEM when treating infinite domains, although, in this case, the elimination of the infinite domain is only performed in an approximate manner.

Still in the FEM context, infinite domains are sometimes approximately taken into account by using infinite elements. An infinite element (Bettess, 1977 [30]), is similar to usual finite elements except for some nodes placed at infinity or at a large but finite distance. The infinite element formulations have followed two main lines of development: the application of decay functions in conjunction with the ordinary shape function (decay function infinite elements or displacement descent elements) and the mapping the element from finite to infinite domain (mapped infinite elements or coordinate ascent elements).

In case of decay function infinite elements, the finite element shape functions are retained and then multiplied by a decay function, which is chosen to mimic the asymptotic behavior of the solution at infinity, thus providing a reasonable reflection of the physics. This requires appropriate shape functions which are defined up to infinity and tend to the finite value in a suitable way. Second, it requires a means of integration over the unbounded domain (Bettess, 1984 [31]). For instance, a natural choice for the decay function, and the first to be used, was the exponential decaying function. This has the advantage that it decays to zero faster than any polynomial and so dominates the polynomial behavior as the spatial coordinate is large and ensures convergence towards zero as x increases.

On the other hand, mapped infinite elements use conventional shape functions are used to describe the variation of the field variable, whereas the geometry is mapped from a finite to an infinite domain using growth shape functions in the infinite direction (Zienkiewicz et al., 1983 [284]). In this case, two mappings are usually needed, one for the shape function and one for the integration formula.

Research on infinite elements continues to be an on-going topic, see e.g. Biermann (2009) [33] and Erkal et al. (2015) [88]. For more details on infinite element techniques the interested reader is referred to Astley (2000) [9].

The most diffused strategy of simulating infinite domain problems is to introduce an artificial finite boundary and to consider the problem only on the en-

closed finite domain, thus imposing some "appropriate" boundary conditions on the artificial boundary, devised in order to compensate for the truncation of the infinite domain. As it has been shown by several authors, the overall accuracy and performance of numerical algorithms, as well as interpretation of the results, strongly depend on the proper choice of such supplementary conditions (de Hoog and Weiss, 1979 [65], Tsynkov, 1998 [257]) and they should be posed in a way so that they express well the behavior at infinity of the actual solution (Markowich, 1982 [188]).

Hence, an artificial boundary condition is a special condition imposed on the introduced boundary in order to complete the statement of the problem on the truncated domain (i.e. to make there the solution unique) and to ensure that no (or little) spurious wave reflection occurs at the boundary. For almost any exterior problem there are many different ways of formulating artificial boundary conditions (see e.g. the review of Tsynkov, 1998 [257] and Givoli, 2004 [112]), all of which display their specific strengths and weaknesses. There are two necessary requirements which the additional boundary conditions must ensure, namely the solvability of the truncated problem (well-posedness of the finite boundary value problem) and the equivalence between the latter and the original well-posed problem for the infinite domain, meaning that the solutions to the two problems (finite and infinite) agree on the finite domain that is common to the two formulations (Hagstrom and Keller, 1987 [119]).

Thus, the original problem over an infinite domain is replaced by a problem over a finite domain, with an artificial boundary condition on the introduced artificial boundary, so that, if such a condition is properly designed, the original problem is well approximated by the finite domain problem. The problem is not trivial, because the artificial boundary condition has the difficult task of accurately representing the solution in the omitted infinite domain. In fact, boundary conditions may be thought as *a mathematical model for the rest of the universe* (Givoli, 1992 [110]). As underlined by Givoli (2004) [112], it results very difficult to find a single artificial boundary condition that is sufficiently general and which after discretization leads to a scheme which is stable, accurate, efficient and easy to be implemented.

Artificial boundary conditions may be divided into two main groups: local and non-local ones. The local conditions are almost all approximate and thus approximately account for the omitted domain. Most local artificial boundary conditions perform very well either with a sufficiently large computational domain, which, of course, is opposed to their early scope, or in case of a high suitability of the boundary condition for the specific problem at hand. Non-local artificial boundary conditions are more complicated, but usually they are more accurate and guarantee good results with a small computational domain. In addition, some of them are exact.

In devising accurate and efficient numerical methods towards the approx-

imate solution of exterior problems involving linear and nonlinear ODEs, local asymptotic boundary conditions based on projection were suggested by de Hoog and Weiss (1980) [65] (and references quoted therein). The authors examined the rate of convergence of the solution of the "finite" problem to that of the original "infinite" problem, as the interval length of the finite problem tends to infinity, and describe the supplementary boundary conditions for which this rate becomes optimal. Such a condition, namely the projection condition, should be derived by a previous asymptotic analysis on the eigenvalues of the Jacobian matrix of the right-hand sides of the first-order system of ODEs, evaluated at infinity, but imposed at a finite point. This approach was formalized by Lentini and Keller (1980) [175] and by Markowich (1982) [188], who developed a general theory of existence, uniqueness and approximation of bounded solutions of linear and nonlinear exterior problems over a semi-infinite domain.

The asymptotic boundary condition for the infinite interval problem of a general linear second-order ODE was derived by Kadalbajoo and Rama (1986) [150]. Asymptotic boundary conditions for the solution of a second-order linear differential problem posed on an infinite interval were illustrated by Kanth and Reddy (2003) [223], by using a fourth-order finite difference method, and by Ibdah et al. (2014) [132], through a fourth-order spline collocation approach.

Croft (1992) [62] proposed a strategy to solve a second-order linear boundary value problem on unbounded domain based on convergence acceleration techniques. The strategy exploits information contained in a sequence of solutions obtained on bounded domains in order to exploit the information contained therein to improve these solutions rather than continue increasing the interval of integration until convergence has been achieved. Fazio (1996) [91] considered boundary value problems on infinite intervals governed by a third-order ODE depending on several parameters and treated it by formulating the original problem as a free BVR, where the truncated boundary is an unknown free boundary and has to be determined as part of the solution.

In the context of wave problems (second-order hyperbolic PDEs), terms "absorbing" or "non-reflecting" are commonly used instead of word "artificial" to designate conditions apt to simulate the so-called radiation condition, which states that waves at infinity are outgoing. The simplest ABC, namely the Sommerfield radiation condition imposed at the truncated boundary, produces large spurious reflections in many cases (Givoli, 1992 [110]). Approximate local boundary conditions were derived for instance by Bayliss and Turkel (1980) [22], for the wave-like equation, and by Bayliss et al. (1982) [21], for the Helmholtz equation, based on a known truncated asymptotic expansion in powers of r^{-1} of the solution valid for large distances, r being the radial coordinate. The obtained boundary conditions generally involve derivatives of

an order greater than or equal to the order of the differential equation, and still lead to spurious reflections.

Engquist and Majda (1977, 1979) [85, 86] formulated exact reflectionless radiating conditions, simultaneously non-local in both space and time, thus useless for practical problems, and approximated such conditions in sequence by local ones of increasing order, in terms of pseudo-differential operators and rational Padé expansions. Such low-order absorbing boundary conditions have became well-known, especially for the second-order ones, which are still commonly used today.

Higdon (1994) [128] proposed a sequence of local ABCs of an increasing order, for the dispersive wave equation, which exactly absorb all the waves that propagate with certain phase velocities at specific angles of incidence. Higdon showed that several ABCs which had been previously proposed were special cases of his conditions, with an appropriate choice of the involved parameters. The Higdon NRBCs are very general, namely they apply to a variety of wave propagation problems and in all spatial dimensions. Moreover, they can be used, without any difficulty, for wave problems in dispersive and stratified media.

Higdon's ABCs, although powerful by virtue of their capability of obtaining solutions with unlimited accuracy, are characterized by intrinsic computational complications. In fact, their complexity rapidly increases with the system's order, since they involve higher order normal and temporal derivatives, which poses obvious disadvantages. Higher order normal derivatives are problematic, because they are not compatible with standard FD schemes or low-order finite elements. High time derivatives are also disadvantageous, in that they require the use of high-order time discretizations and the storage of the whole solution history. Thus, the original implementation of the Higdon NRBCs turns out to be limited to lower orders of derivation.

More recently, higher-order local ABCs have been introduced, which, despite being of an arbitrarily higher-order, do not involve higher derivatives, owing to the use of specially defined auxiliary variables. Givoli and Neta (2003) [115] reformulated the sequence of Higdon's ABCs for time-dependent wave problems, by introducing special auxiliary variables on the truncated boundary, in addition to the physical ones. Such auxiliary variables eliminate the need of any higher-order derivatives beyond the second order, thus making the ABCs amenable for standard FD or FEM discretizations.

Exact non-local artificial conditions try to incorporate the exact far-field conditions at the cost of non-local boundary conditions, which are more complicated. On the other hand, they are usually more accurate and guarantee good results with a small computational domain. An example of non-local artificial conditions may be found in Han and Wu (1992) [121], who derived exact artificial boundary conditions of the exterior problem for the equations of

linear elasticity and obtained their finite element approximation on a bounded domain.

The Dirichlet-to-Neumann (DtN) method leads to exact non-local artificial boundary conditions. After having introduced the artificial boundary, the governing equations of the problem (usually a simplified version of them), are analytically solved within the exterior residual domain. From the solution, an exact relation which maps the solution (Dirichlet datum) and its derivatives (Neumann datum) on the artificial boundary, called the DtN boundary condition, is deduced and employed for the numerical calculations inside the retained computational domain, where the same solution is obtained as in the original infinite domain problem. In case of 1-D problems the DtN boundary condition turns out to be local (a mixed Robin-type condition), whereas the DtN boundary condition is non-local in the multidimensional case.

Keller and Givoli (1989) [154] showed how to explicitly obtain the exact DtN boundary condition on an artificial boundary for the reduced wave equation and for Laplace's equation in infinite domains, in conjunction with the FEM. Givoli and Keller (1989) [113] applied the same approach for various elliptic boundary value problems (linear elastostatics, beams and cylindrical shells). Regarding dynamical analyses, the DtN method was applied to time-harmonic two-dimensional elastodynamics in infinite domains by Givoli and Keller (1990) [114] and to time dependent problems by Givoli (1992) [111]. In the latter case, the serious drawbacks originating from the non-locality in time as well as in space of the DtN boundary condition, were solved by first discretizing the problem in time, resulting in a sequence of boundary value problems in an infinite domain, which were solved by the DtN method.

An alternative method for the analysis of unbounded elastic or visco-elastic media for Soil-Structure Interaction (SSI), the Damping-Solvent Extraction Method (DSEM), devised by Song and Wolf (1994) [243], seeks to simulate approximately the radiation condition by using artificial material damping (usually linear hysteretic), to attenuate both outgoing and reflected waves, and then extracting the artificial damping in order to remove its undesirable effects. Basu and Chopra (2002) [18] improved the DSEM and addressed some issues related to the influence of the computational parameters (domain size, mesh density and artificial damping) upon the DSE performances through two classical model problems, for which (semi-)analytical solutions are available, concluding that the DSEM is merely able to decrease the adequate domain size, particularly for high frequencies, by using a large value of artificial damping. Further investigations by Hajiabadi and Lotfi (2012) [120] lead to the conclusion that the ability of the DSE method consists in making possible to relax the mesh density requirement for the far-field region (depending on the excitation frequency) of the considered bounded domain rather than a method in which a smaller domain size is required.

4.3.1 Perfectly Matched Layer

Among the broad framework of numerical schemes for treating artificial boundary conditions, in the more recent past, besides to the previously discussed high-order ABCs methods, the Perfectly Matched Layer (PML) have emerged as especially powerful. A Perfectly Matched Layer (PML) is an artificial absorbing layer model for linear wave equations that absorbs, almost perfectly, outgoing waves, thus minimizing any spurious wave reflection from the interface and from the boundary. The PML effect may be described by the following two actions: (i) reduction of the amplitude of the incident waves and (ii) delay of the wave propagation.

The concept of a PML seems to have been first introduced by Berenger (1994) [28], for the absorption of electromagnetic waves, a context where it has been widely used (Singer and Turkel, 2004 [240]), but it has been also employed together with standard finite elements to simulate transient wave propagation in elastic media (see e.g. Basu and Chopra, 2003 [19], Matzen, 2011 [191]), and specifically inside cables resting on elastic supports (dispersive wave equation) by Lancioni (2012) [172]. The PML technique has been also very recently applied to wave propagation problems in moving coordinates by Madsen and Krenk (2017) [184], who analyzed the transient dynamic response of a multi-layer 2D half-space subjected to moving loads, by means of a standard displacement-based FEM formulation.

The present section describes the so-called Perfectly Matched Layer approach for absorbing out-going stationary waves propagating from a finite taut string. In fact, the previously stated problem can be numerically solved by FEM techniques, as long as the infinite one-dimensional domain is replaced by a finite domain $\Omega{=}(-x_2, x_2)$, being a bounded, open, connected subset of $\mathbb{R}$. Let subset $\Omega_N{=}(-x_1, x_1)$ be the finite domain of interest, i.e. the region where an accurate approximation of the steady-state response is sought (see Fig. 4.2). Let complementary set $\Omega_{PML}{=}\Omega \setminus \Omega_N$ be the PML region surrounding the finite domain of interest, as illustrated in Fig. 4.2, showing two side regions $(-x_2, -x_1)$ and (x_1, x_2), both of length $x_2 - x_1$. Inside PML domain Ω_{PML} a complex-valued stretching coordinate transformation $s(x)$, $s(x)$ being an injective function, is introduced as follows (Basu and Chopra, 2003 [19], Matzen, 2011 [191]):

$$s(x) = \int_0^x \sigma(u)\, du; \qquad s_x^{(1)}(x) = \sigma(x) = 1 + g(x) + \mathrm{i}\, h(x); \tag{4.21}$$

where $\sigma(x)$ is the stretching function (Madsen and Krenk, 2017 [184]); non-dimensional attenuation functions $g(x),\ h(x)$ are continuous, real-valued, positive and monotonically increasing, with $g(x){=}h(x){=}0$ in Ω_N, thus retaining original unstretched coordinate x inside computational domain of interest Ω_N $(-x_1{\leq}x{\leq}x_1)$. In particular, $g(x)$ imposes an attenuation on evanescent waves

and $h(x)$ on propagating waves (Basu and Chopra, 2003 [19]); in Eq. (4.21) i is the imaginary unit, which makes the stretching complex-valued. Indeed, a complex stretching becomes crucial here to achieve a full PML effectiveness on the propagating waves, see e.g. Singer and Turkel (2004) [240].

Thereafter, by imposing inverse coordinate transformation $x{=}x(s)$ in Eq. (4.6a) the resulting steady-state transformed equation of motion becomes:

$$\frac{v^2-v_0^2}{\hat{\sigma}(s)}\left(\frac{\hat{w}_s^{(1)}(s)}{\hat{\sigma}(s)}\right)_s^{(1)} - \frac{c_d\, v}{\mu}\,\frac{\hat{w}_s^{(1)}(s)}{\hat{\sigma}(s)} + \frac{k}{\mu}\,\hat{w}(s) = 0; \tag{4.22}$$

$$\frac{v^2-v_0^2}{\hat{\sigma}^2(s)}\,\hat{w}_s^{(2)}(s) - \left(\left(v^2-v_0^2\right)\frac{\hat{\sigma}_s^{(1)}(s)}{\hat{\sigma}^2(s)} + \frac{c_d\, v}{\mu}\right)\frac{\hat{w}_s^{(1)}(s)}{\hat{\sigma}(s)} + \frac{k}{\mu}\,\hat{w}(s) = 0; \tag{4.23}$$

where auxiliary function $\hat{\sigma}(s)$ and transformed displacement $\hat{w}(s)$ are introduced such that $\hat{\sigma}{=}\sigma(x)$ and $\hat{w}(s){=}w(x)$, respectively. Hence, the spatial coordinate transformation in Eq. (4.21) acts on Eq. (4.6a) in such a way that Eq. (4.23) appears as a governing equation with variable coefficients. For this reason, a PML may be also interpreted as a particular artificial medium with space-dependent inertial and damping material properties, depending on the coordinate stretching function, which enhance the dispersive and dissipative characteristics of the layer.

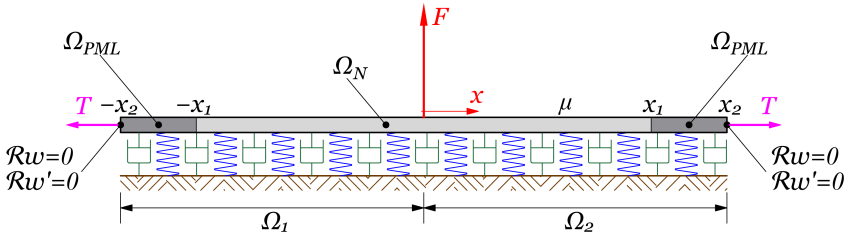

Figure 4.2: Geometrical scheme of computational domain of interest Ω_N, truncated by PML layer Ω_{PML}. Boundary conditions on normalized displacement w, w' apply to their real parts ($\Re\,{\cdot}{=}\mathrm{Re}(\cdot)$).

Such a transformation is introduced only in two layers surrounding the computational domain of interest where the special features of the absorbing boundary condition are demanded, while the transformation degenerates to an identity inside Ω_N ($g(x){=}h(x){=}\,0$). Thus, the response attenuation occurs only over the two PML regions (Fig. 4.2). Attenuation functions $g(x)$ and $h(x)$ take the following similar forms (Basu and Chopra (2003) [19]):

$$g(x) = G\left(\frac{|x|-x_1}{x_2-x_1}\right)^r, \qquad h(x) = H\left(\frac{|x|-x_1}{x_2-x_1}\right)^r; \tag{4.24}$$

where r is a positive integer exponent ($r{\geq}1$) and G, H are two non-dimensional parameters apt to control the amount of attenuation imposed inside the PML.

Therefore, the dissipation properties of the PML region are governed by parameters G, H, r, and by its width $x_2 - x_1$.

Notice that transformation provided by Eq. (4.21), needed for converting exterior problem (4.6)-(4.10) into a boundary value problem affordable by a FEM approach, makes Eq. (4.23) a linear ODE with variable complex-valued coefficients. Hence, following treatments need to be developed within a complex-valued function space.

4.3.2 First-order differential system

From a practical standpoint, it is better to develop a LSFEM formulation allowing the use of C^0 basis interpolation functions, in order to reduce the higher regularity requirements of the LSFEM. This is accomplished by transforming the governing second-order differential equation governing the string-foundation system into an equivalent first-order system, and constructing the least-squares functional using the L_2 norms of the first-order system residuals. Such a reduction implies the introduction of additional independent variables within the formulation. Nonetheless, this transformation may be useful, since such auxiliary variables may represent physically meaningful ones, as in the framework of mixed formulations.

Accordingly, governing scalar equation Eq. (4.23), valid inside both Ω_N ($g(x)=h(x)=0$) and Ω_{PML} ($g(x), h(x)>0$), may be split into a coupled pair of first-order ordinary differential equations, by considering two independent variables, namely, normalized transverse displacement $\hat{w}$ and slope $\hat{\theta}$:

$$\hat{w}'_s(s) - \hat{\theta}(s) = 0 \qquad \text{in } \Omega; \tag{4.25a}$$

$$a(s)\,\hat{\theta}'_s(s) + b(s)\,\hat{\theta}(s) + c(s)\,\hat{w}(s) = 0 \qquad \text{in } \Omega; \tag{4.25b}$$

where the variable coefficients in Eq. (4.25b) take the following form:

$$a(s) = \frac{v^2 - v_0^2}{\hat{\sigma}^2(s)}, \quad b(s) = \frac{-c_d\, v}{\mu\,\hat{\sigma}(s)}\left(1 + \frac{\mu}{c_d\, v}\,\frac{v^2 - v_0^2}{\hat{\sigma}^2(s)}\,\hat{\sigma}'(s)\right), \quad c(s) = \frac{k}{\mu}. \tag{4.26}$$

For convenience, first-order differential system (4.25) may be expressed in compact notation, together with loading point conditions of Eqs. (4.6b)-(4.6c), as specified below:

$$\hat{\mathbf{w}}'_s(s) + \mathbf{A}(s)\,\hat{\mathbf{w}}(s) = \mathbf{0}; \qquad \text{in } \Omega; \tag{4.27a}$$

$$[\![\hat{\mathbf{w}}]\!]_0 = \left[\, 0 \quad F/\big(W_0\,\mu(v^2 - v_0^2)\big) \,\right]^{\intercal}; \tag{4.27b}$$

where $\hat{\mathbf{w}}(s) = [\, \hat{w}(s) \quad \hat{\theta}(s) \,]^{\intercal}$ is the column vector of variables and $\mathbf{A}(s)$ is the

coefficient matrix, defined as

$$\mathbf{A}(s) = \begin{bmatrix} 0 & -1 \\ \dfrac{c(s)}{a(s)} & \dfrac{b(s)}{a(s)} \end{bmatrix}. \tag{4.28}$$

Finally, the previous system governing the motion of the system inside Ω is supplemented by homogeneous boundary conditions on $\partial\Omega$:

$$\Re\,\hat{\mathbf{w}} = \mathrm{Re}(\hat{\mathbf{w}}) = \mathbf{0} \qquad \text{on } \partial\Omega. \tag{4.29}$$

where $\Re\,\hat{\mathbf{w}}$ is the real part of vector $\hat{\mathbf{w}}$.

Eq. (4.1) is elliptic at subcritical moving load velocities ($v<v_0$), whereas it becomes hyperbolic when the moving load velocity gets supercritical ($v>v_0$). In the following sections, the numerical solution of problem (4.27)-(4.29) is developed, based on a Discontinuous Least-Squares FEM approach. The advantage of such a numerical discretization method is that it is characterized by a unified formulation for the numerical solution of all types of partial differential equations, without any special treatment for hyperbolic and mixed-type problems (Jiang, 1998 [145]).

Thus, the present attempt completes previous literature derivations, by providing a unitary and robust numerical tool from which the steady-state moving load response can be obtained for each combination of the characteristic mechanical parameters of the taut string-foundation system, without stabilization terms and associated user-tunable parameters.

4.4 Discontinuous Least-Squares Finite Element Method

In this section, the formulation of the Discontinuous Least-Squares Finite Element Method (DLSFEM) for problem (4.27)-(4.29) is introduced. Although the presence of only one moving load has been assumed in writing Eqs. (4.27), the possible action of multiple moving loads is considered within the formulation, in order to bring the discussion to a more general tone. In setting up the discontinuous formulation, the so-called discontinuous least-squares functional is derived and minimized. In addition, the corresponding norm-equivalence of the discontinuous functional is demonstrated, which is fundamental for the ensuing error analysis in Section 4.5. This is illustrated in the following.

4.4.1 Function spaces notation

In order to provide a proper formulation of the Least-Squares FEM for system (4.25) the needed function spaces must be introduced. By using standard notations and definitions, let $(\cdot,\cdot)_{0,\Omega}$ and $\|\cdot\|_{0,\Omega}$ denote the inner product and

norm on the Hilbert space $L_2(\Omega)$=$H^0(\Omega)$ of square integrable complex-valued functions, respectively. Let $\Re\, z$=Re(z) point out the real part of a complex-valued function z.

Define $H^m(\Omega)$ the classical Sobolev space of all square integrable complex-valued functions with square integrable distributional derivatives up to order m (see e.g. Oden and Demkowicz (2010) [210]); their associated inner product $(\cdot,\cdot)_{m,\Omega}$ and norm $\|\cdot\|_{m,\Omega}$ are also introduced. Vector-valued fields and their associated function spaces are denoted by bold face symbols. Thus, given two n-dimensional vectors $\mathbf{u}(s)$ and $\mathbf{v}(s)$, the corresponding inner product and norms take the form:

$$(\mathbf{u},\mathbf{v}) = \int_\Omega \mathbf{u}(s)^*\,\mathbf{v}(s)\,\mathrm{d}s = \int_\Omega \sum_{i=1}^{n} \overline{u_i(s)}\; v_i(s)\,\mathrm{d}s; \tag{4.30}$$

$$\|\mathbf{v}\|_{0,\Omega} = (\mathbf{v},\mathbf{v})_{0,\Omega}^{\frac{1}{2}}; \tag{4.31}$$

where $\overline{v_i(s)}$ is the complex conjugate of $v_i(s)$ and superscript $(\,\cdot\,)^*$ denotes the conjugate transpose operator. The following function spaces are needed to be further introduced:

$$\begin{aligned} H_0^1(\Omega) &= \left\{v \in H^1(\Omega) :\ \Re\, v = 0 \text{ on } \partial\Omega\right\};\\ {}_n\boldsymbol{H}_0^1(\Omega) &= \left[H_0^1(\Omega)\right]^n = H_0^1(\Omega)\times H_0^1(\Omega)\times\ldots\times H_0^1(\Omega) \qquad (n \text{ times}); \end{aligned}$$

which are Sobolev spaces with corresponding squared norm

$$\|\mathbf{v}\|_{1,\Omega}^2 = \sum_{i=1}^{n} \|v_i\|_{0,\Omega}^2 + \|v_i'\|_{0,\Omega}^2 \qquad \mathbf{v}\ \in\ \boldsymbol{H}_0^1(\Omega). \tag{4.32}$$

Space $H_0^1(\Omega)$ consists of functions having null real trace on boundary $\partial\Omega$, i.e. vanishing on its boundary. Then, without ambiguity, symbol $\|\cdot\|_{1,\Omega}$ will be used to denote norms in both $H_0^1(\Omega)$ and ${}_n\boldsymbol{H}_0^1(\Omega)$.

Since the solution of (4.27)-(4.29) is expected of a low regularity only at the loading points, it is natural to use the computationally expensive discontinuous elements only in these zones and use continuous elements in smooth regions. To this scope, let $\mathcal{O}$=$\{\Omega_j\}_{j=1}^{P}$ be a collection of open disjoint subsets of domain Ω such that Ω=$\bigcup_j \Omega_j$. Let $\mathcal{E}$ be the union of the boundaries of all subsets Ω_j associated with $\mathcal{O}$, and let $\mathring{\mathcal{E}}$=$\mathcal{E}\cap\Omega$ be the set of all the interior edges contained in Ω. Collection $\mathcal{O}$ must be such that $\mathring{\mathcal{E}}$ coincides with the finite set of $P-1$ loading points of the infinite string where concentrated moving loads F_j are applied. Then, the following fragmented Sobolev spaces are introduced:

$$H_0^1(\mathcal{O}) = \left\{w \in L_2(\Omega) :\ w \in H^1(\Omega_j)\ \forall\ j = 1,\ldots,P,\ \Re\, w = 0 \text{ on } \partial\Omega\right\};$$

$$ {}_n\boldsymbol{H}_0^1(\mathcal{O}) = \left[H_0^1(\mathcal{O})\right]^n = H_0^1(\mathcal{O}) \times H_0^1(\mathcal{O}) \times \ldots \times H_0^1(\mathcal{O}) \quad (n \text{ times}); $$

with corresponding squared norm

$$ \|\mathbf{v}\|_{1,\mathcal{O}}^2 = \sum_{j=1}^{P} \sum_{i=1}^{n} \|v_i\|_{0,\Omega_j}^2 + \left\| v_{i\,s}^{(1)} \right\|_{0,\Omega_j}^2 \qquad \mathbf{v} \in \boldsymbol{H}_0^1(\mathcal{O}). \tag{4.33} $$

4.4.2 Least-Squares functional

According to known LSFEM literature (Jiang, 1998 [145], Bochev and Gunzburger, 1998 [37]), the method consists in an unconstrained minimization problem within a certain function space $\mathcal{V}$, as follows:

$$ \text{Find} \quad \hat{\mathbf{w}} \in \mathcal{V} \quad \text{such that} \quad \hat{\mathbf{w}} = \underset{\mathbf{v} \in \mathcal{V}}{\arg\min}\ \mathcal{J}(\mathbf{v}, \mathbf{f}); \tag{4.34} $$

where the quantity to be minimized is a specifically designed positive definite least-squares functional $\mathcal{J} : \mathcal{V} \to \mathbb{R}$, whose solution (the minimizer) represents the unknown response of the differential problem. Functional $\mathcal{J}$ is devised by measuring the squared residuals in terms of the L_2-norm of the governing differential equations (4.27a) and of the interface conditions (Bensow and Larson, 2005 [27], Lin, 2009 [181]), such as those arising at the loading points of the problem under consideration (4.27b). The following formulation is traced within this mathematical setting, but with the peculiarity of developing it into a complex-valued function space framework.

Thus, define a function space $\mathcal{V}$ for problem (4.27)-(4.29) by

$$ \mathcal{V} = {}_2\boldsymbol{H}_0^1(\mathcal{O}) = H_0^1(\mathcal{O}) \times H_0^1(\mathcal{O}); \tag{4.35} $$

and let e_j be the j^{th} element of $\mathring{\mathcal{E}}$. Quadratic least-squares functional $\mathcal{J}$ for problem (4.27)-(4.29) is defined as follows:

$$ \begin{aligned} \mathcal{J}(\mathbf{v}, \mathbf{f}) &= \frac{1}{2} \sum_{j=1}^{P} \left\| \mathbf{v}_s' + \mathbf{A}\mathbf{v} \right\|_{0,\Omega_j}^2 + \frac{1}{2} \sum_{j=1}^{P-1} \mathbf{r}_{e_j}^*(\mathbf{v}, \mathbf{f}_j) \mathbf{A}_{e_j}^H \mathbf{A}_{e_j}^H \mathbf{r}_{e_j}(\mathbf{v}, \mathbf{f}_j), \\ \mathbf{r}_{e_j}(\mathbf{v}, \mathbf{f}_j) &= [\![\mathbf{v}]\!]_{e_j} - \mathbf{f}_j, \qquad\qquad \mathbf{v} \in \mathcal{V},\ \mathbf{f}_j \in L_2(\Omega); \end{aligned} \tag{4.36} $$

where $\mathbf{A}_{e_j}^H = (\mathbf{A}_{e_j} + \mathbf{A}_{e_j}^*)/2$ is the Hermitian part of matrix $\mathbf{A}$ in Eq. (4.28), evaluated at j^{th} edge e_j, while

$$ \mathbf{f}_j = \left[0 \quad F_j / \left(W_0\, \mu (v^2 - c_0^2) \right) \right]^{\intercal}; \tag{4.37} $$

is a 2D-vector representing both the continuity requirement of displacement response $\hat{w}$ and the j^{th} jump discontinuity of slope $\hat{\theta}$ due to the action of j^{th} applied force F_j inside functional $\mathcal{J}(\mathbf{v}, \mathbf{f})$ of Eq. (4.36).

Problems (4.27)-(4.29) and (4.34) are equivalent in the sense that the unique solution of the first-order system, augmented by the corresponding interface and boundary conditions, is the unique zero minimizer $\hat{\mathbf{w}}$ of functional $\mathcal{J}(\mathbf{v}, \mathbf{f})$. Basically, the least-squares functional may be viewed as an "artificial" energy, e.g. an externally defined convex quadratic functional that plays the same role, for LSFEM, as the true physical energy does for Rayleigh-Ritz methods (Bochev and Gunzburger, 2006 [38]).

Notice that boundary conditions (4.29) have been assumed both *essential* as they explicitly appear in the variational formulation, i.e., in the definition of $\mathcal{V}$. This is simply a choice, since boundary conditions could be equivalently made *natural*, by imposing them inside functional $\mathcal{J}(\mathbf{v}, \mathbf{f})$.

A necessary condition so that $\hat{\mathbf{w}} \in \mathcal{V}$ may be a minimizer of real functional $\mathcal{J}(\mathbf{v}, \mathbf{f})$ in Eq. (4.36) is that its first variation vanishes at $\hat{\mathbf{w}}$, that is

$$\delta\mathcal{J} = \lim_{\eta \to 0} \frac{\mathrm{d}}{\mathrm{d}\eta} \mathcal{J}(\hat{\mathbf{w}} + \eta\, \mathbf{v}, \mathbf{f}) = 0 \quad \forall\, \mathbf{v} \in \mathcal{V}; \tag{4.38}$$

which, after some mathematical manipulations, can be equivalently written in the form $S(\hat{\mathbf{w}}, \mathbf{v}) = L(\mathbf{v})$, as follows

$$\begin{aligned} &\Re\left(\hat{\mathbf{w}}'_s + \mathbf{A}\,\hat{\mathbf{w}},\ \mathbf{v}'_s + \mathbf{A}\,\mathbf{v}\right)_{0,\mathcal{O}} + \\ &\quad + \Re \sum_{j=1}^{P-1} [\![\mathbf{v}]\!]^*_{e_j} \mathbf{A}^H_{e_j} \mathbf{A}^H_{e_j} [\![\hat{\mathbf{w}}]\!]_{e_j} = \Re \sum_{j=1}^{P-1} [\![\mathbf{v}]\!]^*_{e_j} \mathbf{A}^H_{e_j} \mathbf{A}^H_{e_j} \mathbf{f}_j \quad \forall\, \mathbf{v} \in \mathcal{V}; \end{aligned} \tag{4.39}$$

where $S(\hat{\mathbf{w}}, \mathbf{v})$ is a symmetric sesquilinear form (or Hermitian form) and $L(\mathbf{v})$ is a linear functional. Thus, minimization problem (4.34) leads to the following variational equation:

$$\text{Find} \quad \hat{\mathbf{w}} = [\,\hat{w} \quad \hat{\theta}\,]^T \in \mathcal{V} \quad \text{such that} \quad S(\hat{\mathbf{w}}, \mathbf{v}) = L(\mathbf{v}) \quad \forall\, \mathbf{v} \in \mathcal{V}. \tag{4.40}$$

The single most important prerequisite for the success of LSFEM in recovering all the desirable properties of the Rayleigh-Ritz setting, thus assuring existence, uniqueness and stability of the solution of LSFEM formulation (4.40), is to ensure that sesquilinear form $S(\hat{\mathbf{w}}, \mathbf{v})$ defines an equivalent inner product on underlying Hilbert space $\mathcal{V}$ and functional $\mathcal{J}$ defines an equivalent norm on $\mathcal{V}$ (Bochev and Gunzburger, 2006 [38]).

In fact, if the functional is norm-equivalent within the minimization space, then the resulting unconstrained minimization problem is strongly *coercive*, or, equivalently, the least-squares functional generates a sesquilinear form that is continuous and $\mathcal{V}$-elliptic in a properly defined subspace of $\mathcal{V}$ and, therefore, standard finite element theory can be applied (Jiang, 1998 [145]). The norm-equivalence of the least-squares functional defined by Eq. (4.36) corresponds to the following condition being satisfied.

Theorem 1 - Norm-equivalence of least-squares functional.
There exist positive constants S_1 and S_2, independent of $\mathbf{v}$*, such that*

$$S_1 \left\|\mathbf{v}\right\|_{1,\mathcal{O}}^2 \leq 2\left|\mathcal{J}(\mathbf{v},\mathbf{0})\right| = \left|S(\mathbf{v},\mathbf{v})\right| \leq S_2 \left\|\mathbf{v}\right\|_{1,\mathcal{O}}^2 \qquad \forall\ \mathbf{v}\in\mathcal{V}. \quad (4.41)$$

Proof. Suppose that $a_0(s)$, $a_1(s),\ldots,a_{n-1}(s)$ are n piecewise continuous complex-valued functions in domain of interest Ω, and consider a general homogeneous linear differential equation of order n in the standard form:

$$\hat{w}_s^{(n)}(s) + \sum_{k=0}^{n-1} a_k(s)\hat{w}_s^{(k)}(s) = 0; \quad (4.42)$$

where superscript $(\,\cdot\,)^{(k)}$ denotes the order of the spatial derivative with respect to s. Eq. (4.42) may be rearranged into the following system of n first-order differential equations (see Coddington and Levinson, 1955 [61]):

$$\hat{\mathbf{w}}_s'(s) + \mathbf{A}(s)\,\hat{\mathbf{w}}(s) = \mathbf{0} \qquad \text{in } \Omega; \quad (4.43a)$$

$$\mathbf{A}(s) = \begin{pmatrix} 0 & -1 & 0 & \cdot & 0 \\ 0 & 0 & -1 & \cdot & 0 \\ \cdot & \cdot & \cdot & \cdot & \cdot \\ 0 & 0 & 0 & \cdot & -1 \\ a_0(s) & a_1(s) & a_2(s) & \cdot & a_{n-1}(s) \end{pmatrix}; \quad \hat{\mathbf{w}}(s) = \begin{pmatrix} \hat{w}(s) \\ \hat{w}_s^{(1)}(s) \\ \cdot \\ \hat{w}_s^{(n-2)}(s) \\ \hat{w}_s^{(n-1)}(s) \end{pmatrix}; \quad (4.43b)$$

Given the previous definitions of vector $\hat{\mathbf{w}}(s)$ and matrix $\mathbf{A}(s)$ the following steps apply.

Consider first the *right inequality* in Eq. (4.41). Let $\mathbf{v},\hat{\mathbf{w}}\in\mathcal{V}$; then, it is possible to write

$$\begin{aligned}
\left|S(\hat{\mathbf{w}},\mathbf{v})\right| = \Bigg|\sum_{j=1}^{P}\Big(&\Re(\mathbf{v}',\hat{\mathbf{w}}')_{0,\Omega_j} + \Re(\mathbf{v}',\mathbf{A}\hat{\mathbf{w}})_{0,\Omega_j} + \Re(\mathbf{A}\mathbf{v},\hat{\mathbf{w}}')_{0,\Omega_j} \\
&+ \Re(\mathbf{A}\mathbf{v},\mathbf{A}\hat{\mathbf{w}})_{0,\Omega_j}\Big) + \sum_{j=1}^{P-1}\Re\,[\![\mathbf{v}]\!]_{e_j}^{*}\mathbf{A}_{e_j}^{H}\mathbf{A}_{e_j}^{H}[\![\hat{\mathbf{w}}]\!]_{e_j}\Bigg| \leq \\
\leq \Bigg|\Re\sum_{j=1}^{P}&(\mathbf{v}',\hat{\mathbf{w}}')_{0,\Omega_j}\rho_{1,j}\Big((\mathbf{v}',\hat{\mathbf{w}})_{0,\Omega_j} + (\mathbf{v},\hat{\mathbf{w}}')_{0,\Omega_j}\Big) \\
&+ \rho_{1,j}^2(\mathbf{v},\hat{\mathbf{w}})_{0,\Omega_j}\Bigg| + \rho_2^2\left\|\mathbf{v}\right\|_{1,\mathcal{O}}\left\|\hat{\mathbf{w}}\right\|_{1,\mathcal{O}} \leq \\
\leq \Bigg|\max_j\{1,\rho_{1,j}^2\}&\Big((\mathbf{v}',\hat{\mathbf{w}}')_{0,\mathcal{O}} + (\mathbf{v},\hat{\mathbf{w}})_{0,\mathcal{O}}\Big) \\
+\max_j\{\rho_{1,j}\}&\Big((\mathbf{v}',\hat{\mathbf{w}})_{0,\mathcal{O}} + (\mathbf{v},\hat{\mathbf{w}}')_{0,\mathcal{O}}\Big)\Bigg| + \rho_2^2\left\|\mathbf{v}\right\|_{1,\mathcal{O}}\left\|\hat{\mathbf{w}}\right\|_{1,\mathcal{O}};
\end{aligned} \quad (4.44)$$

where the following constants have been defined

$$\rho_{1,j} = \max_k \Big\{ \max_{s\in\Omega_j} \big\{ \lambda_k\big(\mathbf{A}\big) \big\} \Big\}; \tag{4.45a}$$

$$\rho_2^2 \;\; = \max_k \Big\{ \max_j \big\{ \beta_{\mathbf{v}j}\beta_{\hat{\mathbf{w}}j}\, \lambda_k^2\big(\mathbf{A}_{e_j}^H\big) \big\} \Big\} (P-1); \tag{4.45b}$$

and $\lambda_k\big(\mathbf{A}\big)$ stands for the eigenvalues of matrix $\mathbf{A}(s)$. If matrix $\mathbf{A}_{e_j}^H$ is discontinuous at edge e_j, the average value between the limits of $\mathbf{A}_{e_j}^H$ from the two sides of the edge may be employed. Since only finite discontinuities are allowed, the following inequalities apply for each jump discontinuity in Eq. (4.44):

$$\big|\, [\![\mathbf{v}]\!]_{e_j} \,\big| \le \beta_{\mathbf{v}j}\, \|\mathbf{v}\|_{1,\mathcal{O}}\,, \qquad \beta_{\mathbf{v}j} > 0; \tag{4.46a}$$

$$\big|\, [\![\hat{\mathbf{w}}]\!]_{e_j} \big| \le \beta_{\hat{\mathbf{w}}j}\, \|\hat{\mathbf{w}}\|_{1,\mathcal{O}}\,, \qquad \beta_{\hat{\mathbf{w}}j} > 0. \tag{4.46b}$$

Thus, by applying the Cauchy-Schwarz inequality (Oden and Demkowicz (2010) [210]), one gets

$$\begin{aligned}
\big|S(\hat{\mathbf{w}},\mathbf{v})\big| \le \Big| \max_j\{1,\rho_{1,j}^2\}(\mathbf{v},\hat{\mathbf{w}})_{1,\mathcal{O}} \,+ \max_j\{\rho_{1,j}\}\Big((\mathbf{v}',\hat{\mathbf{w}})_{0,\mathcal{O}} \,+ \\
+\,(\mathbf{v},\hat{\mathbf{w}}')_{0,\mathcal{O}}\Big)\Big| + \rho_2^2\, \|\mathbf{v}\|_{1,\mathcal{O}}\, \|\hat{\mathbf{w}}\|_{1,\mathcal{O}} \le \\
\le \max_j\big\{\big|\rho_{1,j}\big|\big\}\Big(\|\mathbf{v}'\|_{0,\mathcal{O}}\|\hat{\mathbf{w}}\|_{0,\mathcal{O}} + \|\mathbf{v}\|_{0,\mathcal{O}}\|\hat{\mathbf{w}}'\|_{0,\mathcal{O}}\Big) + \\
+\max_j\{1,\rho_{1,j}^2\}\|\mathbf{v}\|_{1,\mathcal{O}}\|\hat{\mathbf{w}}\|_{1,\mathcal{O}} + \rho_2^2\, \|\mathbf{v}\|_{1,\mathcal{O}}\|\hat{\mathbf{w}}\|_{1,\mathcal{O}} \le \\
\le \max_j\big\{1,\, 2|\rho_{1,j}|,\, \rho_{1,j}^2,\, \rho_2^2\big\}\, \|\mathbf{v}\|_{1,\mathcal{O}}\|\hat{\mathbf{w}}\|_{1,\mathcal{O}} \le \\
\le S_2\, \|\mathbf{v}\|_{1,\mathcal{O}}\|\hat{\mathbf{w}}\|_{1,\mathcal{O}} \qquad\qquad \forall\;\, \mathbf{v},\hat{\mathbf{w}} \in \mathcal{V};
\end{aligned} \tag{4.47}$$

where the maximum is performed over all P subsets Ω_j associated with partitioning $\mathcal{O}$. Then, sesquilinear form $\big|S(\hat{\mathbf{w}},\mathbf{v})\big|$ is continuous.

Now, consider the *left inequality* in Eq. (4.41). Let $\tilde{S}(\mathbf{v},\mathbf{v}) = \big\|\mathbf{v}'+\mathbf{A}\mathbf{v}\big\|_{0,\mathcal{O}}^2$. Since the eigenvalues of Hermitian matrix $\mathbf{A}_{e_j}^H$ are real, it is possible to write

$$\begin{aligned}
\big|S(\mathbf{v},\mathbf{v})\big| = \Big| \sum_{j=1}^{P} \big\|\mathbf{v}'+\mathbf{A}\mathbf{v}\big\|_{0,\Omega_j}^2 + \sum_{j=1}^{P-1} \Re\, [\![\mathbf{v}]\!]_{e_j}^*\, \mathbf{A}_{e_j}^H \mathbf{A}_{e_j}^H [\![\mathbf{v}]\!]_{e_j} \Big| \ge \\
\ge \Big| \sum_{j=1}^{P} \big\|\mathbf{v}'+\mathbf{A}\mathbf{v}\big\|_{0,\Omega_j}^2 + \sum_{j=1}^{P-1} \min_k\big\{\, \lambda_k^2\big(\mathbf{A}_{e_j}^H\big)\big\}\, \big|[\![\mathbf{v}]\!]_{e_j}\big|^2 \Big| \ge \\
\ge \tilde{S}(\mathbf{v},\mathbf{v}) \ge \sum_{j=1}^{P} \big\|\mathbf{v}'\big\|_{0,\Omega_j}^2 + \big\|\mathbf{A}\mathbf{v}\big\|_{0,\Omega_j}^2 - 2\big|(\mathbf{v}',\mathbf{A}\mathbf{v})_{0,\Omega_j}\big| \ge \\
\ge \big\|\mathbf{v}'\big\|_{0,\mathcal{O}}^2 + \big\|\mathbf{A}\mathbf{v}\big\|_{0,\mathcal{O}}^2 - 2\,\big\|\mathbf{v}'\big\|_{0,\mathcal{O}}\big\|\mathbf{A}\mathbf{v}\big\|_{0,\mathcal{O}};
\end{aligned} \tag{4.48}$$

where the last inequality holds true by virtue of the Cauchy-Schwarz inequality. Consequently, the following Gårding type inequality (Brenner and Scott, 2008 [44]) is established

$$\begin{aligned}\tilde{S}(\mathbf{v},\mathbf{v})+K\|\mathbf{v}\|_{0,\mathcal{O}}^2 &\geq \|\mathbf{v}'\|_{0,\mathcal{O}}^2 - 2\,\|\mathbf{v}'\|_{0,\mathcal{O}}\|\mathbf{A}\mathbf{v}\|_{0,\mathcal{O}}+\|\mathbf{A}\mathbf{v}\|_{0,\mathcal{O}}^2+\\ &+\left(\frac{1}{1-C_1}-\frac{1}{1-C_1}\right)\|\mathbf{v}\|_{0,\mathcal{O}}^2+K\|\mathbf{v}\|_{0,\mathcal{O}}^2 \geq\\ &\geq C_1\|\mathbf{v}'\|_{0,\mathcal{O}}^2+\left(K+\bar{\lambda}^2-\frac{1}{1-C_1}\right)\|\mathbf{v}\|_{0,\mathcal{O}}^2+\\ &+\left(\sqrt{1-C_1}\|\mathbf{v}_s'\|_{0,\mathcal{O}}-\frac{1}{\sqrt{1-C_1}}\|\mathbf{v}\|_{0,\mathcal{O}}\right)^2 \geq\\ &\geq C_1\|\mathbf{v}'\|_{0,\mathcal{O}}^2+C_2\|\mathbf{v}\|_{0,\mathcal{O}}^2 \geq C_3\|\mathbf{v}\|_{1,\mathcal{O}}^2;\end{aligned} \tag{4.49}$$

where $0{\leq}C_1{\leq}1$, K is an arbitrary big positive number such that $C_2{=}K+\bar{\lambda}^2-(1-C_1)^{-1}$ in the previous expression results positive, and $\bar{\lambda}^2$ is defined as follows:

$$\begin{aligned}\|\mathbf{A}\mathbf{v}\|_{0,\mathcal{O}}^2 &= \sum_{j=1}^{P}\int_{\Omega_j}\mathbf{v}^*\mathbf{A}^*\mathbf{A}\,\mathbf{v}\,\mathrm{d}s \geq\\ &\geq \min_k\Big\{\min_{s\in\mathcal{O}}\{\,\lambda_k^2(\mathbf{A})\,\}\Big\}\|\mathbf{v}\|_{0,\mathcal{O}}^2=\bar{\lambda}^2\,\|\mathbf{v}\|_{0,\mathcal{O}}^2;\end{aligned} \tag{4.50}$$

with $C_3{=}\min\{C_1,C_2\}$. Without loss of generality, let one assume $K{\geq}1$, so that

$$C_3\|\mathbf{v}\|_{1,\mathcal{O}}^2 \leq \tilde{S}(\mathbf{v},\mathbf{v})+K\|\mathbf{v}\|_{0,\mathcal{O}}^2 \leq K\Big(\tilde{S}(\mathbf{v},\mathbf{v})+\|\mathbf{v}\|_{0,\mathcal{O}}^2\Big); \tag{4.51}$$

and, hence, letting $C_4{=}C_3/K$

$$C_4\|\mathbf{v}\|_{1,\mathcal{O}}^2 \leq \tilde{S}(\mathbf{v},\mathbf{v})+\|\mathbf{v}\|_{0,\mathcal{O}}^2. \tag{4.52}$$

By defining now a vector function $\mathbf{z}(s)$ such that

$$\tilde{S}(\mathbf{z},\mathbf{v})=(\mathbf{v},\mathbf{v})_{0,\mathcal{O}}=\|\mathbf{v}\|_{0,\mathcal{O}}^2; \tag{4.53}$$

and by substituting Eq. (4.53) into Eq. (4.52), one ends up with

$$\begin{aligned}
C_4\|\mathbf{v}\|_{1,\mathcal{O}}^2 &\leq \tilde{S}(\mathbf{v},\mathbf{v})+\tilde{S}(\mathbf{z},\mathbf{v}) = \tilde{S}(\mathbf{v}+\mathbf{z},\mathbf{v}) = \\
&\leq \Re((\mathbf{z}+\mathbf{v})'+\mathbf{A}(\mathbf{z}+\mathbf{v}),\mathbf{v}'+\mathbf{A}\mathbf{v})_{0,\mathcal{O}} \leq \\
&\leq \left|(\mathbf{z}'+\mathbf{v}',\mathbf{v}'+\mathbf{A}\mathbf{v})_{0,\mathcal{O}}\right|+\left|(\mathbf{A}(\mathbf{z}+\mathbf{v}),\mathbf{v}'+\mathbf{A}\mathbf{v})_{0,\mathcal{O}}\right| \leq \\
&\leq \left(\|\mathbf{z}'+\mathbf{v}'\|_{0,\mathcal{O}}+\max_j\{|\rho_{1,j}|\}\|\mathbf{z}+\mathbf{v}\|_{0,\mathcal{O}}\right)\|\mathbf{v}'+\mathbf{A}\mathbf{v}\|_{0,\mathcal{O}} \leq \\
&\leq 2\max\left\{1,\max_j\{|\rho_{1,j}|\}\right\}\|\mathbf{z}+\mathbf{v}\|_{1,\mathcal{O}}\|\mathbf{v}'+\mathbf{A}\mathbf{v}\|_{0,\mathcal{O}} = \\
&= C_5\|\mathbf{z}+\mathbf{v}\|_{1,\mathcal{O}}\|\mathbf{v}'+\mathbf{A}\mathbf{v}\|_{0,\mathcal{O}} \leq \\
&\leq C_5\left(\|\mathbf{z}\|_{1,\mathcal{O}}+\|\mathbf{v}\|_{1,\mathcal{O}}\right)\|\mathbf{v}'+\mathbf{A}\mathbf{v}\|_{0,\mathcal{O}} \leq \\
&\leq C_6\|\mathbf{v}\|_{1,\mathcal{O}}\|\mathbf{v}'+\mathbf{A}\mathbf{v}\|_{0,\mathcal{O}};
\end{aligned} \tag{4.54}$$

Thus,

$$C_7\|\mathbf{v}\|_{1,\mathcal{O}} = \frac{C_4}{C_6}\|\mathbf{v}\|_{1,\mathcal{O}} \leq \|\mathbf{v}'+\mathbf{A}\mathbf{v}\|_{0,\mathcal{O}} \tag{4.55}$$

and by squaring inequality (4.55) and by letting $S_1{=}C_7^2$, it can be concluded that

$$S_1\|\mathbf{v}\|_{1,\mathcal{O}}^2 \leq \|\mathbf{v}'+\mathbf{A}\mathbf{v}\|_{0,\mathcal{O}}^2 = \tilde{S}(\mathbf{v},\mathbf{v}) \leq |S(\mathbf{v},\mathbf{v})|. \tag{4.56}$$

Hence, $\left|S(\hat{\mathbf{w}},\mathbf{v})\right|$ is a coercive sesquilinear form. This completes the proof. □

The above theorem states that functional $\mathcal{J}(\mathbf{v},\mathbf{0})$ is norm-equivalent to the $\mathcal{V}$-norm or, equivalently, that sesquilinear form $S(\hat{\mathbf{w}},\mathbf{v})$ is continuous and coercive on $\mathcal{V}\times\mathcal{V}$. The immediate and important consequence of that is the existence and uniqueness of a weak solution, which can be established through the application of the Riesz representation theorem in the form of the Lax-Milgram lemma (Jiang, 1998 [145]). A second likewise mathematical interpretation of inequalities (4.41) was given by Jiang (1998) [143]: the left inequality means a bounded below differential operator in Eq. (4.27a) and, therefore, the existence of a continuous inverse operator in $\mathcal{V}$; the right inequality indicates that the differential operator is continuous.

Hence, by proving Theorem 1, the immediate consequence is the well-posedness of least-squares variational problem (4.40), meaning that it provides a unique and stable solution, which is a crucial requirement for the numerical implementation. To the best of the author's knowledge, such proof is characterized by an innovative arrangement in matrix form, allowing for demonstrating the applicability and validity of Discontinuous Least-Squares FEM for *any linear ordinary differential problem of any order (rewritten as a first-order system)*, with interface conditions in a general complex-valued function space,

provided that the original mathematical problem is well-posed. Based on Theorem 1, useful a priori error estimates will also be derived in following Section 4.5.

4.4.3 Finite element approximation

The finite element approximation of the steady-state response of the vibrating string under moving load is obtained by either restricting (4.40) to a finite-dimensional subspace $\mathcal{V}_h$ of the infinite dimensional space $\mathcal{V}$. Let mesh $\mathcal{T}_h$ be the union of all shape regular tessellations on Ω_j with refinement level h (mesh size), e.g. an indexed collection of N_e intervals $\{I_i = [n_{1,i}, n_{2,i}]\}_{1\leq i\leq N_e}$, with non-zero measure forming a partition of Ω. The mesh may possibly display a variable mesh size h_i, and in this case h is set as:

$$h = \max_{0\leq i\leq N} \{\, h_i\}. \tag{4.57}$$

There are no restrictive compatibility conditions on the discrete spaces, so, for each of the primary variables, the same finite element subspace is chosen. Let $\mathbb{P}_1$ denote the space of linear algebraic polynomials with complex coefficients in one variable. The approximating finite element space $\mathcal{V}_h \subset \mathcal{V}$ associated with $\mathcal{T}_h$ is defined as

$$\mathcal{V}_h = \big\{\mathbf{v}_h \in {}_2\boldsymbol{H}_0^1(\mathcal{O}) : \forall i \in \{1,\ldots,N_e\}, v_{h\,j}|_{I_i} \in \mathbb{P}_1\big\}; \tag{4.58}$$

that is, the vector space of 2D-vector functions whose components are piecewise linear complex-valued polynomials allowing for a discontinuity along interelement edges $e_j \in \mathring{\mathcal{E}}$. Then, by restricting the function space to $\mathcal{V}_h$, the following discrete least-squares variational problem (Ritz-Galerkin approximation) may be formulated:

$$\text{Find } \hat{\mathbf{w}}_h = [\,\hat{w}_h \;\; \hat{\theta}_h]^{\mathsf{T}} \in \mathcal{V}_h \text{ such that } S(\hat{\mathbf{w}}_h, \mathbf{v}_h) = L(\mathbf{v}_h)\;\forall\; \mathbf{v}_h \in \mathcal{V}_h \subset \mathcal{V}. \tag{4.59}$$

Thanks to inclusion $\mathcal{V}_h \subset \mathcal{V}$, Theorem 1 remains valid when $S(\hat{\mathbf{w}}, \mathbf{v})$ is restricted to $\mathcal{V}_h \times \mathcal{V}_h$. Consequently, such a confirming discretization of weak problem (4.40) into weak problem (4.59) automatically gives rise to a well-posed FEM (Ern and Guermond, 2004 [89]).

According to the usual finite element approach, let ϕ_j be a basis of $\mathcal{V}_h$ such that $\hat{w}_j = \hat{w}(s_j)$ and $\hat{\theta}_j = \hat{\theta}(s_j)$ are the nodal values of function $\hat{w}(s)$ and $\hat{\theta}(s)$, respectively, where s_j represent the nodes of mesh $\mathcal{T}_h$ (identical shape functions for each component of $\hat{\mathbf{w}}$). Then, by writing

$$\hat{\mathbf{w}}_h = \sum_{j=0}^{N_e} \hat{\mathbf{W}}_j\, \phi_j = \sum_{j=0}^{N_e} [\,\hat{w}_j \quad \hat{\theta}_j]^T\, \phi_j; \tag{4.60}$$

variational problem (4.59) generates the following system of linear algebraic equations:

$$\mathbf{K}\,\hat{\mathbf{W}} = \mathbf{F} \qquad\qquad \hat{\mathbf{W}}, \mathbf{F} \in \mathbb{C}^{2(N_e+1)}; \tag{4.61}$$

where $K_{ij}{=}S(\phi_i, \phi_j)$, $\hat{W}_j$ and $F_i{=}L(\phi_i)$ are the the global stiffness matrix, the global generalized displacement vector and the global force vector, respectively. Since the sesquilinear form in Eq. (4.59) is symmetric and coercive, matrix $\mathbf{K}$ associated with problem (4.59) is Hermitian and positive definite. Thus the weak discrete problem has a unique solution.

Furthermore, the equivalence of sesquilinear forms to inner products also implies that the discrete solutions are projections of exact solutions onto the approximating space with respect to the norms generated by the sesquilinear form itself, i.e. approximations are quasi-optimally accurate, as it is shown the in following section.

4.5 Error estimates

As least-squares methods share similar variational foundations with classical Rayleigh-Ritz principles, a fundamental property of the least-squares method is that quasi-optimal error estimates in the energy norm can be obtained, that is $\hat{\mathbf{w}}_h$ is the orthogonal projection of exact solution $\hat{\mathbf{w}}$ with respect to energy inner product $S(\cdot,\cdot)$. Thanks to Theorem 1, in the present section such a priori error estimates for the DLSFEM are analyzed.

Let $\hat{\mathbf{w}}$ and $\hat{\mathbf{w}}_h$ be the solutions of variational problems (4.40) and (4.59), respectively. Let one begin by observing the fundamental orthogonality relation between $\hat{\mathbf{w}}$ and $\hat{\mathbf{w}}_h$. Subtracting (4.40) from (4.59) implies

$$S(\hat{\mathbf{w}} - \hat{\mathbf{w}}_h, \mathbf{v}_h) = 0 \qquad \forall\, \mathbf{v}_h \in \mathcal{V}_h. \tag{4.62}$$

Then, by Theorem 1 and by the previous equation, it results

$$\begin{aligned} S_1 \left\|\hat{\mathbf{w}} - \hat{\mathbf{w}}_h\right\|^2_{1,\mathcal{O}} \leq\; & S(\hat{\mathbf{w}} - \hat{\mathbf{w}}_h, \hat{\mathbf{w}} - \hat{\mathbf{w}}_h) = S(\hat{\mathbf{w}} - \hat{\mathbf{w}}_h, \hat{\mathbf{w}} - \mathbf{v}_h) \leq \\ & \leq S_2 \left\|\hat{\mathbf{w}} - \hat{\mathbf{w}}_h\right\|_{1,\mathcal{O}} \left\|\hat{\mathbf{w}} - \mathbf{v}_h\right\|_{1,\mathcal{O}} \quad \forall\, \mathbf{v}_h \in \mathcal{V}_h; \end{aligned} \tag{4.63}$$

and, consequently, a standard FEM error estimate still holds even for DLSFEM

$$\left\|\hat{\mathbf{w}} - \hat{\mathbf{w}}_h\right\|_{1,\mathcal{O}} \leq \frac{S_2}{S_1} \inf_{\mathbf{v}_h \in \mathcal{V}_h} \left\|\hat{\mathbf{w}} - \mathbf{v}_h\right\|_{1,\mathcal{O}}; \tag{4.64}$$

where S_1 and S_2 are the coercivity and the continuity constants of $S(\cdot,\cdot)$ on $\mathcal{V}$, respectively, as in Theorem 1.

This result corresponds to well-known Céa type error estimate (Brenner and Scott, 2008 [44]) and represents the basic error estimate for the finite element interpolation theory of well-posed problems (Ern and Guermond, 2004 [89]).

In fact, inequality (4.64) says that the numerical error is quasi-optimal in the energy norm, in the sense that it only differs by a constant from the best possible solution in the space. In other words, the error results proportional to the best it can be using the subspace $\mathcal{V}_h$ (Brenner and Scott, 2008 [44]).

In order to derive a more concrete estimate for the error based on constructing an interpolation of $\hat{\mathbf{w}}$ in $\mathcal{V}_h$, let $\hat{\mathbf{w}}_h{=}I_h^m\,\hat{\mathbf{w}}$ be a standard finite element interpolation of $\hat{\mathbf{w}}$. Then, from Bramble-Hilbert Lemma (Brenner and Scott, 2008 [44]), the error in interpolating a function $\hat{\mathbf{w}} \in H^{m+1}(I_i)$ is

$$\|\hat{\mathbf{w}} - I_h^m\,\hat{\mathbf{w}}\|_{q,I_i} \leq \hat{C} h_i^{m+1-q} |\hat{\mathbf{w}}|_{m+1,I_i}; \tag{4.65}$$

where $|\cdot|_{m+1,I_i}$ is the H^{m+1}-seminorm on I_i. As a result, by considering a linear interpolation ($m{=}1$), there exist two positive constants $\hat{C}_1$ and $\hat{C}_2$ such that

$$\left\|\hat{\mathbf{w}} - I_h^1\,\hat{\mathbf{w}}\right\|_{0,I_i} \leq \hat{C}_1 h_i^2 |\hat{\mathbf{w}}|_{2,I_i}; \tag{4.66}$$

$$|\hat{\mathbf{w}} - I_h^1\,\hat{\mathbf{w}}\,|_{1,I_i} \leq \hat{C}_2 h_i\,|\hat{\mathbf{w}}|_{2,I_i}; \tag{4.67}$$

and by summing over all the finite elements, it results

$$\left\|\hat{\mathbf{w}} - I_h^1\,\hat{\mathbf{w}}\right\|_{0,\mathcal{O}} \leq \widetilde{C}_1 h^2 |\hat{\mathbf{w}}|_{2,\mathcal{O}}; \tag{4.68}$$

$$|\hat{\mathbf{w}} - I_h^1\,\hat{\mathbf{w}}\,|_{1,\mathcal{O}} \leq \widetilde{C}_2\,h\,|\hat{\mathbf{w}}|_{2,\mathcal{O}}; \tag{4.69}$$

Hence, with near optimality established in Eqs. (4.64) and interpolation error estimate available by combining Eqs. (4.68)-(4.69) the final convergence of the present DLSFEM in a complex-valued function space is established

$$\|\hat{\mathbf{w}} - \hat{\mathbf{w}}_h\|_{0,\mathcal{O}} \leq C_1 h^2; \tag{4.70}$$

$$\|\hat{\mathbf{w}} - \hat{\mathbf{w}}_h\|_{1,\mathcal{O}} \leq C_2 h; \tag{4.71}$$

where positive constants C_1 and C_2 are independent of $\hat{\mathbf{w}}$ and of mesh parameter h. A priori error estimates (4.70)-(4.71) imply that the uniform rate of convergence of the least-squares method with equal-order finite elements is of order two in L_2-norm and one of order one in H^1-norm, respectively. Such rates of convergence are optimal since the rate predicted is as high as the interpolation can reach (Jiang, 1998 [143]). Analogous rates was obtained by Cao and Gunzburger (1998) [48] for second-order elliptic boundary value problem having interfaces due to discontinuous media properties. The same rates of convergence have been derived here for a general boundary value problem of arbitrary type and order having discontinuous response, in a complex-valued function space.

In order to validate a priori error estimates (4.70)-(4.71), numerical examples will be presented in the following section for the specific problem of the infinite taut string under moving load, whose formulation have been already discussed in Section 4.2.

4.6 Numerical simulations and outcomes

In this section, the moving load problem exposed in Section 4.2 is solved by the developed DLSFEM (Section 4.4), based on the above-mentioned theoretical results characterizing the formulation, discussed in Section 4.5, and by the application of the PML, presented in Section 4.3.1. The DLSFEM code has been implemented within a MatLab environment [251]. In the current implementation, a uniform mesh size $h_i{=}h$ has been adopted.

Gauss-Legendre quadrature rules have been employed for computing global stiffness matrix $K_{ij}{=}S(\phi_i, \phi_j)$, owing to the complexity of the expressions involved in the definition of coefficient matrix $\mathbf{A}(s)$ in Eqs. (4.26)-(4.28). As already highlighted by Zienkiewicz et al. (1974) [285] and Jiang (1998) [143], the order of the numerical integration is crucial for the success of a LSFEM implementation. In fact, if the order of the Gaussian quadrature is too high, the least-squares method amounts to solving an extremely overdetermined system; in other words, the latter occurrence corresponds to try forcing too many residual equations to become zero at Gauss points with too few adjustable unknowns (Jiang, 1998 [143]), thus leading to an inaccurate and underestimated solution (*locking phenomenon*). Therefore, a reduced integration based on a 1-point Gauss-Legendre quadrature rule is employed in the present implementation. A high-order (3-point) Gauss-Legendre quadrature rule is used to calculate the norms of the numerical errors, which hereby causes no competitive extra-errors in the numerical integration.

Notice that, if a 2-point quadrature integration scheme (full numerical integration) is considered, analogous results may be obtained for the case of a rapidly decaying response (highly-damped system and/or subcritical velocity); on the other hand, when trying to simulate almost undamped supercritical motion regimes, locking phenomena may become very important and a very refined mesh should be used for obtaining the same accuracy attainable with a reduced integration on a rough mesh. Thus, reduced integration or alternatively p-refinement (Pontaza and Reddy, 2005 [219]) would be needed for obtaining a DLSFEM performing always rather well in the whole space of variation of the characteristic mechanical parameters of the taut string-foundation system. However, the adopted reduced integration already provides consistent and satisfactorily accurate results.

The considered dimensions for the problem already sketched in Fig. 4.2 are $x_1{=}50$ m and $x_2{=}55$ m, so that the size of each PML is $1/20$ of the size of Ω_N, that is a much smaller PML layer than the computational domain of interest, providing an effective reduction of the computational cost in the modelization of far-field conditions (4.10). In the present implementation, quadratic polynomial attenuation functions $g(x)$, $h(x)$ are employed, i.e. $r{=}2$ is chosen in Eq. (4.24), while various different values of imposed attenuation parame-

ters G, H are considered in the analyses; in particular the same magnitude of both attenuation functions is assumed (i.e. $G{=}H$).

Reference mechanical properties of the string-foundation system			
String tension	T	15	kN
Mass per unit length of the string	μ	1.1	kg/m
Elastic stiffness of the foundation springs	k	250	kN/m^2

Table 4.1: Reference mechanical properties of the string-foundation system (taken from Metrikine (2004) [194]).

The assumed mechanical properties of the cable-foundation system have been taken from Metrikine (2004) [194] and are listed in Table 4.1. The load is taken acting downward ($F{<}0$). The normalizing factors for representing the normalized steady-state response are as in Eq. (4.19). Moreover, the following non-dimensional real characteristic system parameters α, ζ are introduced:

$$\alpha = \frac{v}{v_0}; \qquad \zeta = \frac{c_d}{2\sqrt{k\mu}}; \tag{4.72}$$

to express the effect of moving load velocity (α) and of structural damping (ζ). In the following numerical investigation, several different values of system parameters α and ζ will be considered.

The steady-state solution in convected moving coordinate (solution of Eqs. (4.6)-(4.10)) can explicitly be found in closed form (Metrikine, 2004 [194], see Appendix B). The analytical solution shows that there may exist two different states, depending on the relation between the load velocity and the wave velocity within the string-foundation system: (i) the subcritical regime ($v{<}v_0$) determines an evanescent wave, symmetric with respect to the moving load position and rapidly decaying, moving away from the load; (ii) the supercritical regime ($v{>}v_0$) generates a propagating wave behind the load and no response in front of the load position.

Whenever the moving load velocity results equal to the propagation velocity of transverse waves in the string (also called "characteristic" or "critical" velocity of the linear string theory), $v{=}v_0$, resonance occurs, that is large amplitude string responses are predicted even if load intensity is kept small, and, therefore such large amplitude responses may obviously lead to invalidate the basic assumptions of a linear string theory.

The analytical solution of Eqs. (4.6)-(4.10), relative to the infinite string, is rigorously different from the exact solution of a finite domain problem (4.27)-(4.29) where estimates (4.70)-(4.71) are referred to. Thus, in order to compute the error norms in (4.70)-(4.71), in the following it is assumed that the numerical solution of Eqs. (4.27)-(4.29) approximates the exact solution of an infinite string problem over the finite computational domain of interest Ω_N,

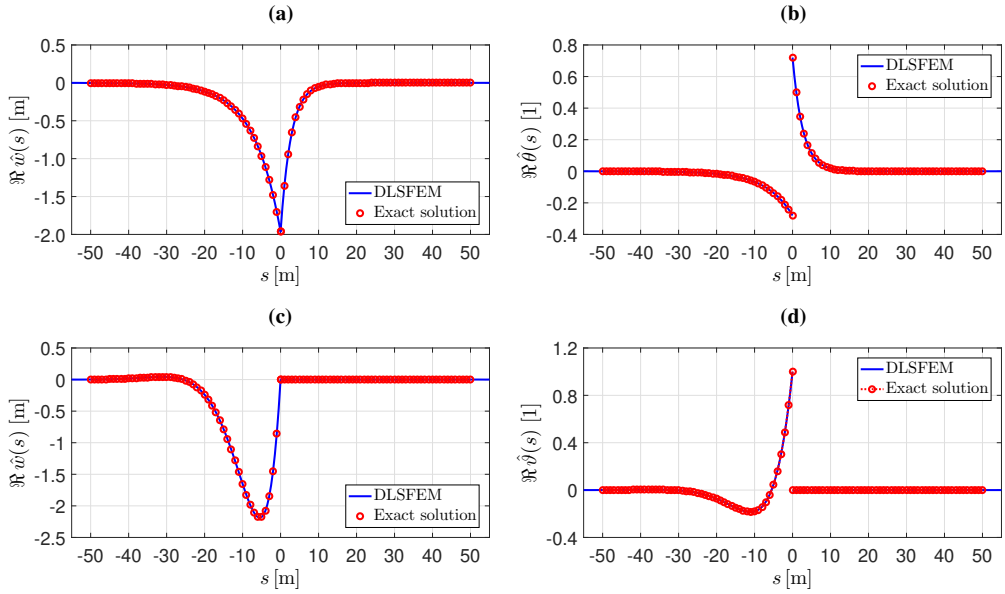

Figure 4.3: Comparison between DLSFEM-PML numerical results and analytical solution (ζ=0.5, G=H=10). Normalized deflection $\hat{w}$, left column: α=0.7 (a); α=1.3 (c); and normalized rotation $\hat{\theta}$, right column: α=0.7 (b); α=1.3 (d). For the reference mechanical parameters, see Table 4.1.

and, consequently the error norms are evaluated on $\mathcal{O}_N$=$\mathcal{O} \cap \Omega_N$, instead as on $\mathcal{O}$. As a matter of fact, this assumption holds true in so far as the solution naturally rapidly decays before reaching the boundaries, so that the influence of the boundary reflections may be neglected. Moreover, the obtained theoretical a priori error estimates pertain only to the DLSFEM application, hence not accounting for other sources of perturbations, such as the use of numerical integration or the employment of the PML to simulate an unbounded domain.

Accordingly, estimates (4.70)-(4.71) are firstly verified for a highly damped string-foundation system, in order to obtain a rapidly decaying solution both in the subcritical (α=0.7) and in the supercritical (α=1.3) regime, as shown in Fig. 4.3, where both normalized real displacement $\Re\,\hat{w}$ and normalized real rotation $\Re\,\hat{\theta}$ are displayed. Numerical computations have been performed with a mesh size of h=0.5 m. The comparisons displayed in Fig. 4.3 show that the numerical results obtained from the proposed finite element formulation fit very well with the analytical solution, even if the mesh density is rather rough. Although apparently the employment of the PML could be also avoided in this case, because the response itself rapidly decays down to zero, moving away from the load position, an effective stretching has been still set in the PML (G=H=10); in fact, the PML indeed also acts on evanescent waves, thus improving the global convergence of the approximation, as illustrated as

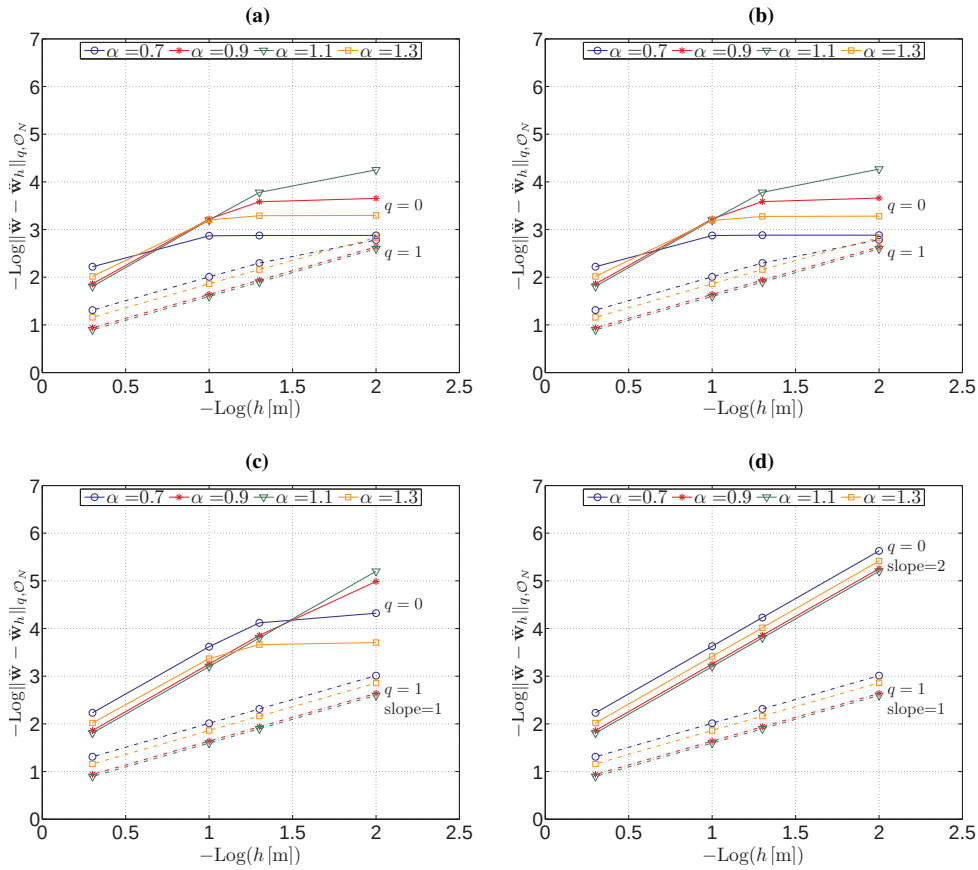

Figure 4.4: Convergence of DLSFEM-PML in L_2- (q=0, continuous line) and H^1-norms (q=1, dot-dashed line), at variable moving load velocity v, for a damped system (ζ=0.5) with respect of amplitudes G=H of the attenuation functions of the PML: G=H=10^{-2} (a); G=H=10^{-1} (b); G=H=10 (c); G=H=10^2 (d). Norms are evaluated on the computational domain of interest.

follows.

The L_2- and H^1-norm of the error are provided in log-log plot against mesh size h in Fig. 4.4. By inspecting the graphs it may be observed that the error in the L_2-norm ($\|\hat{\mathbf{w}} - \hat{\mathbf{w}}_h\|_{0,\mathcal{O}}$) is strongly influenced by the presence or not of the PML. In fact, if a slight stretching is imposed in the PML layer (small amplitudes of the attenuation functions, Figs. 4.3a-4.3b), corresponding to a non-appropriate modelization of the far-field conditions, the L_2-norm does not respect the theoretical estimate in Eqs. (4.70). On the other hand, by introducing a more effective PML layer, the error in the L_2-norm progressively reaches a convergence rate of 2, hence respectful of the theoretical estimate in Eqs. (4.70).

Conversely, the error in the H^1-norm ($\|\hat{\mathbf{w}} - \hat{\mathbf{w}}_h\|_{1,\mathcal{O}}$) appears always of or-

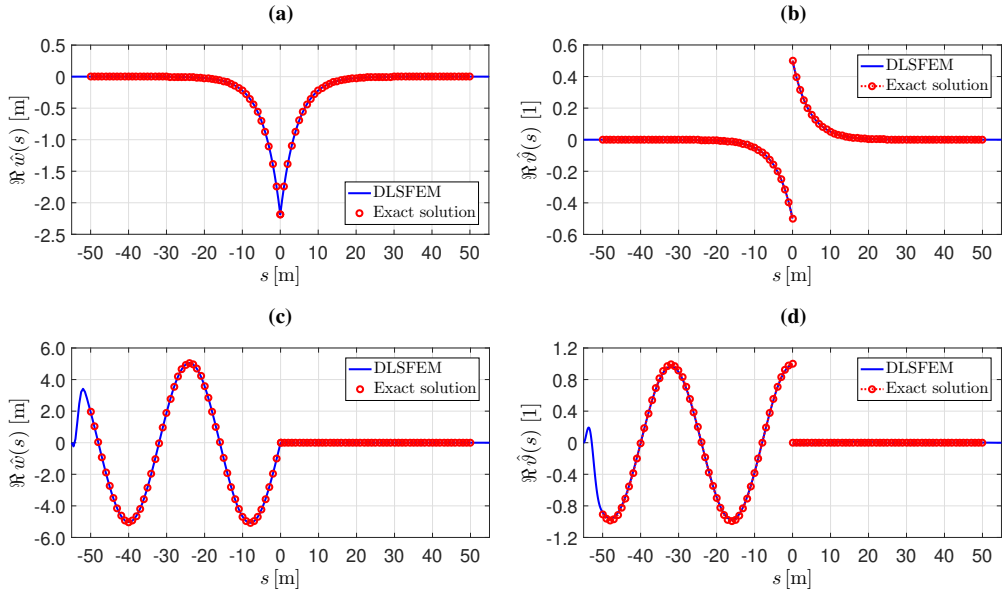

Figure 4.5: Comparison between DLSFEM-PML numerical results and analytical solution (ζ=0.001, G=H=10 in the left PML and G=10, H=0 in the right PML). Normalized deflection: α=0.7 (a); α=1.3 (c); and normalized rotation: α=0.7 (b); α=1.3 (d). For the reference mechanical parameters, see Table 4.1.

der $O(h)$, thus verifying estimate (4.71) independently from the presence or not of the PML, thanks to the natural decay of the evanescent waves for a highly-damped taut string-foundation system.

A more challenging case study is represented by a nearly undamped system (ζ=0.001), for which a suitable absorbing boundary conditions is mandatory. A graphical representation of the complete normalized response (deflection, slope) is displayed in Figs. 4.5, again both in the subcritical (α=0.7) and in the supercritical (α=1.3) regime. The numerical computations have been performed with h=0.5 m. In this case a value of G=H=10 has been set in the left PML, while G=10 and H=0 in the right PML. By observing the graphs in Fig. 4.3 the very good agreement between the DLSFEM responses and the analytical ones may be appreciated, again by using a few finite elements. In addition, it may be noticed that when the wave enters the PML, it is attenuated by absorption and it decays in a very fast way and that the response attenuation occurs only over the PML regions.

The effect of the PML on the error in log-log plot against mesh size h is illustrated in Fig. 4.6. In the subcritical regime of velocities (evanescent waves) the error in the L_2-norm is again influenced by the presence or not of the PML, and, in fact, the theoretical a priori L_2-convergence rate is only reached in Fig. 4.6d for the smaller velocity (blue curve). Hence, the previously discussed

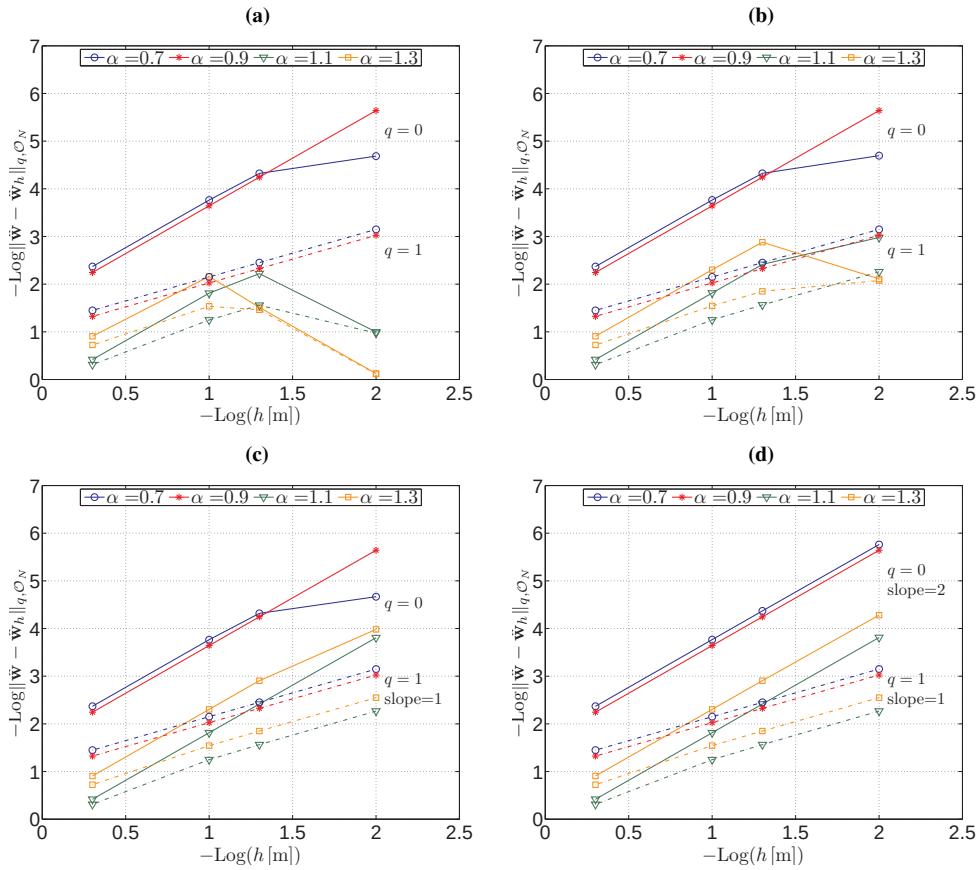

Figure 4.6: Convergence of DLSFEM-PML in L_2- ($q=0$, continuous line) and H^1-norms ($q=1$, dot-dashed line), at variable moving load velocity v, for a nearly undamped system ($\zeta = 0.001$) with respect of amplitudes $G{=}H$ of the attenuation functions of the PML: (a) $G{=}H{=}10^{-2}$; (b) $G{=}H{=}10^{-1}$; (c) $G{=}H{=}1$; (d) $G{=}H{=}10$. Norms are evaluated on the computational domain of interest.

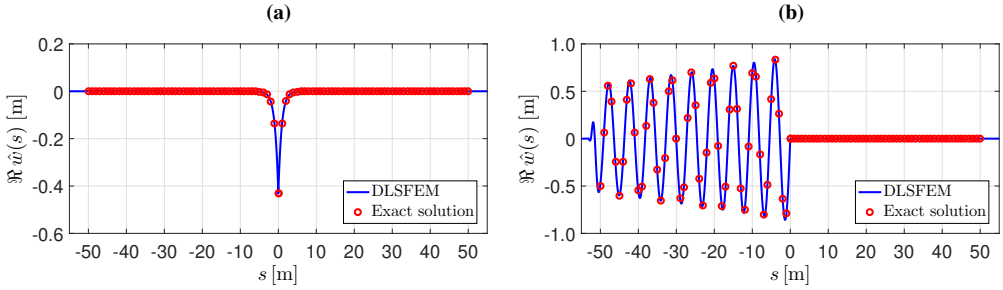

Figure 4.7: Comparison between DLSFEM-PML numerical results and analytical solution as approaching the critical velocity for a nearly undamped system ($\zeta{=}0.001$, $G{=}H{=}10$ in the left PML and $G{=}10$, $H{=}0$ in the right PML). Normalized deflection: $\alpha{=}0.99$ (a) and $\alpha{=}1.01$ (b). For the reference mechanical parameters, see Table 4.1.

observations for the high-damped case are confirmed even for the nearly undamped system. An insufficient amount of attenuation in the PML leads to inconsistent errors in the supercritical regime, as revealed by the green and yellow curves in Figs. 4.6a-4.6b. By looking at Figs. 4.6c-4.6d, that is by increasing the magnitude of the attenuation, the performance of the DLSFEM substantially improves, until reaching the expected rates of convergence established in Eqs. (4.70)-(4.71). Thus, as expected, either the higher the moving load velocity or the smaller the damping, the higher is the demanded capacity of the PML in absorbing the stationary propagating wave.

Numerical experiments have also been performed for an even more challenging configuration of the mechanical parameters, by considering the nearly undamped case (ζ=0.001) with two values of velocity ratio α, one just subcritical, α=0.99 and one just supercritical, α=1.01, thus very close to critical value α=1. This is to inspect the limits up to which the formulation can be successfully pushed.

The numerical results in terms of normalized deflection are presented in Fig. 4.7, still showing a very good agreement with respect to the target solution. Therefore, although, as expected, by approaching the critical configuration, namely α=1, ζ=0, the performance of the DLSFEM is expected to deteriorate, such a drop of performance is fairly limited, even for almost critical configurations, so that the range of α in which this methods performs well is rather wide. In fact, a smaller, but not so much, mesh size (h=0.2 m) has been employed, in order to obtain the very accurate numerical outcomes depicted in Fig. 4.7. This should be conceived as a point of force of the present formulation.

4.7 Closing chapter considerations

In the present investigation, a local Discontinuous Least-Squares FEM (DLSFEM) formulation with a PML implementation is developed for the numerical solution of the steady-state dynamic response of a homogeneous infinite taut string resting on a uniform elastic foundation and subjected to a constant transverse point load moving with a constant velocity along the string. The characterization of the steady-state response can be considered as a static problem in the moving coordinate.

Based on the expected jump discontinuities of the exact solution, continuity requirements are locally relaxed by using discontinuous global shape functions at the loading points, where both compatibility and equilibrium conditions are weakly enforced through a properly defined least-squares functional. Otherwise, the solution keeps regular and continuous away from the loading points, where a standard continuous piecewise-linear approximation is employed.

The present derived and implemented DLSFEM formulation provides a unitary and robust numerical tool, from which the steady-state moving load response can be obtained in the whole space of variation of the characteristic mechanical parameters of the taut string-foundation system, thus requiring neither special treatments nor user-tunable parameters associated to stabilization terms, which are prevalent in traditional schemes. Although the presence of only one moving load has been assumed in the analyzed problem, a more general DLSFEM formulation has been developed, by considering the possible treatment of multiple moving loads.

The continuity and coercivity of the discontinuous functional has been rigorously demonstrated (see Theorem 1 in Section 4.4) by an innovative arrangement in matrix form, valid *for any linear ordinary differential problem of any order*, with complex-valued coefficients (rewritten as a first-order system), with interface conditions, thus advancing and completing previous literature derivations. On this basis, theoretical a priori error estimates have been consistently derived for the finite element approximation, asserting that the uniform rate of convergence of the present DLSFEM with equal-order finite elements is of order two in L_2-norm and of order one in H^1-norm.

In order to simulate a problem originally defined on an unbounded domain, an effective steady-state PML technique in moving coordinates is implemented, thus balancing the geometric truncation of the original unbounded domain. Quadratic polynomials have been considered for both the attenuation functions of the considered PML scheme. The stationary Perfectly-Matched Layer (PML) technique in moving coordinates, analyzed and discussed thoroughly in the present chapter, has been successfully implemented within the DLSFEM formulation, to accurately simulate far-field conditions of the original exterior problem into an appropriate boundary value problem.

The validation of the derived theoretical results, together with the effectiveness of the PML as a valuable absorbing layer, have been proven through several numerical examples, for the moving load physical context of interest, in which the obtained numerical results have been compared with an available analytical solution from the literature, for an infinite taut string. Numerical evidences have confirmed that the method reveals to be truly capable of accurately capturing the prescribed jumps at the loading points. At supercritical velocities, when the action of the PML becomes mandatory to provide the sought response, it is shown that the present DLSFEM-PML turns out rather robust, stable and convergent, even for a very slightly damped system, if a sufficient amount of attenuation imposed by the PML is selected. Even in this latter case, the rate of convergence of both H^1-norm and L_2-norm of the error is shown to be coherent with the derived theoretical a priori error estimates.

For all the above mentioned reasons, the developed and implemented DLSFEM-PML formulation shall be considered as rather innovative in the ded-

icated field. It is the author's belief that an analogous approach could be developed for other moving load problems, such as those pertaining to beams and plates. Therefore, for future developments of this study, which actually provided an underlying main motivation to pursue the present numerical formulation of a problem already endowed with a closed-from explicit analytical solution for benchmark reference, there appears a commitment to extend the present approach to other moving source problems, both in the linear and the nonlinear contexts.

Chapter 5

Steady-state response of an infinite beam on a Pasternak elastic support under constant moving load

5.1 Theoretical bases

As disclosed in previous Chapter 4, in the present chapter a homogeneous infinite Euler-Bernoulli elastic beam of constant cross-section resting on a uniform Pasternak elastic foundation is analyzed. The infinite beam is subjected to a constant transverse point load moving with a constant velocity along the beam. Smeared structural viscous damping is accounted for. A steady-state solution response is sought, derived and interpreted in terms of all the involved characteristic structural parameters of the beam-foundation system, through both an analytical explicit closed-form solution and a numerical modelization, analogous to the one developed in Chapter 4 for determining the steady-state vibrations of a taut string. After these general premises, detailed analytical and numerical studies directly related to the specific subject of the present work are briefly discussed below, to further motivate the problem statement, to outline the developed method for the analytical solution and to highlight the differences and novelties of the present work with respect to previous important research contributions on the subject.

Kerr (1972) [158], a main reference in the present mathematical framing of the underlying differential problem, studied the effect of a compressive axial force on an *undamped* beam-foundation system, which may be induced by a rise of temperature within the beam. It was shown that the action of the compressive force progressively decreases to zero the value of the critical ve-

locity, when it reaches the critical static buckling load of an infinite beam. In this sense, though the essence of that structural problem is different than that considered here, the action of a compression force in softening the model is analogous to the effect of the Pasternak foundation in strengthening it.

Some authors have derived the analytical solution for the steady-state vibrations of an infinite beam on a Pasternak foundation, in analogy with the analysis proposed by Kenney (1954) [155] and Kerr (1972) [158]. Mallik et al. (2006) [186] and Basu and Kameswara Rao (2013) [17] based their derivation on a priori assuming an exponential form of the solution, while a Fourier transform technique was employed by Cao and Zhong (2008) [48] and Uzzal et al. (2012) [259], to find out the analytical solution for some solution cases. A purely numerical approach based of a Fast Fourier Transform technique (FFT) was instead employed by Evcan and Hayir (2013) [90], who numerically analyzed the undamped beam displacement response at subcritical moving load velocities.

In further details, Mallik et al. (2006) [186] derived the variation of the dynamic amplification factor of maximum settlement, uplift and bending moment of the beam as a function of load velocity, by evidencing an analogy with the frequency response curve of a SDOF system. The critical velocity of the beam-foundation system under moving load plays the same role of the resonance frequency of the SDOF system, leading to an unbounded response. In addition, the effect of viscous damping on the dynamic amplification factor becomes very similar in both cases.

Cao and Zhong (2008) [48] presented the effect of the velocity of the moving load and of the Pasternak modulus on the dynamic displacement response. In such a work, damping was not taken into account, and consequently only a subcritical range of velocities was considered, as in Evcan and Hayir (2013) [90]. The maximum deflection of the beam, placed always beneath the load, increased slightly at growing load velocity, and rather significantly by reducing the Pasternak modulus.

Parametric analyses were also obtained by Uzzal et al. (2012) [259], who described the variation of the beam deflection and of the bending moment with respect to different velocity ratios, Pasternak moduli and foundation stiffnesses. As a rather unexpected occurrence, the reported results seemed to display some differences with respect to the response earlier depicted by Mallik et al. (2006) [186].

Basu and Kameswara Rao (2013) [17] investigated deflection, bending moment, shear force and contact pressure for a load moving at subcritical and supercritical velocities, for different damping ratios. The dependence of the critical velocity and of the critical damping, namely the amount of damping for which the wavelength of the wave propagating behind the load becomes infinite, on the foundation parameters was also investigated.

Even though analytical and numerical solutions have been determined in the studies above, their application seems to have been limited to certain combinations of beam and foundation stiffness parameters, and some considered just the undamped case. In fact, no previous proposals considered the possibility of a considerable Pasternak modulus G_P, e.g. $G_P > \sqrt{4kEJ}$, where EJ is the beam bending stiffness and k is the Winkler support coefficient. However, as already noticed by Razaqpur and Shah (1991) [225], since the stiffnesses of the beam or of the support may widely vary, values $G_P > \sqrt{4kEJ}$ may apply and, hence, a full solution range may be needed for the moving load problem. Moreover, the investigation on "high" values of G_P has indeed led to reveal a second branch in the critical damping curve, depicted later in the chapter in Fig. 5.6, each branch corresponding to a specific traveling wave pattern, shifting from propagating to evanescent wave, either in front (left branch) or behind (right branch) the moving load position, thus showing an important new feature of the present analytical solution.

In order to provide an analytical tool endowed of a general validity, the first objective of the present chapter is to analyze all possible instances of the characteristic system parameters and to analytically derive a universal explicit formulation for the steady-state response, by a rigorous Fourier transform approach. Such an approach avoids the need of using distinct expressions of the final analytical solution, like as it was proposed in previous research works. Through a complete mathematical treatment, a comprehensive classification of all solution cases is achieved in the chapter, according to the values of the characteristic system parameters, which determine the nature of the poles of the Fourier transform of the solution. By virtue of such a classification, an "a priori" characterization about how the beam-foundation steady-state response shape changes according to the paths followed in the space of the system parameters, by varying load velocity, Pasternak shear modulus and damping coefficient, is developed. Characteristic features of the steady-state response such as critical velocity and critical damping are rigorously derived and interpreted. A unified analytical representation of the solution is also obtained and then adopted to plot, inspect and interpret the associated structural response.

The present analysis focuses on the various mathematical steps of the derivation and on their implications in the external manifestation of the achieved steady-state solution. The motivation of the present research work is to provide a whole complete and general solution, seemingly lacking in the several contributions dispersed in the literature, accounting all together for the presence of Pasternak modulus, structural viscous damping and the other characteristic mechanical parameters of the beam-foundation system, possibly varying over all their range of existence, thus becoming useful for reference and validation of numerical implementations of moving load problems, in all possible parameter and solution ranges. Such a derivation is conceived as to be rigorous and

self-contained, so that the reader may follow all the truly needed and available steps. This has led to one of the main results of the chapter, as condensed in the synoptic chart later shown in Fig. 5.4 (and solution regions in Fig. 5.2), complementing the previous contributions above. Such an achievement would allow readers to analytically plot and inspect the analytical solution, at variable system parameters (i.e. by independently reproducing the trends that will be depicted in following Figs. 5.8-5.12), without wondering much about the various underlying solution cases.

Moreover, by the continuous advances in computer technology and the raising demand of effectively solving more complicated modelizations, accounting also for various sources of possible nonlinearities, robust numerical methods should be developed, especially for the cases where no analytical solutions may be found (see e.g. Eftekhari, 2016 [82]). The Least-Squares Finite Element Method (Jiang, 1998 [145]) developed in the previous chapter shall constitute a rather general numerical method for finding an approximate solution to a broad class of physical problems. Among the applications in structural mechanics, Zienkiewicz et al. (1974) [285] proposed a LSFEM formulation for the plane elasto-static response of slender beams and plates. Jou and Yang (2000) [149] and Yang (2000) [276] proposed a finite element method based on least-squares principles for approximating the solution to a Timoshenko beam problem and of a circular arch problem with shear deformation, respectively, avoiding the locking phenomenon as the thickness of the beam tends to zero and achieving optimal order error estimates for all the unknown variables.

Jiang (2002a,b) [142, 144] analyzed the static problem of plane elasticity and bending of thin plates (Kirchhoff plate theory) by the LSFEM to accommodate all kinds of equal-order interpolations for quadrilateral elements, such that the two formulations may cooperate together for solving shell problems. A mathematical analysis of this numerical method was provided by Duan et al. (2009) [77]. Further, a LSFEM approach for the bending of thin and thick isotropic plates (Mindlin plate theory) using high-order nodal expansions to span the finite element spaces was presented by Pontaza and Reddy (2004) [218]. Then, the same authors extended such LSFEM formulation to the numerical analysis of shear-deformable shell structures (Pontaza and Reddy, 2005 [219]), the formulation being robust with regard to membrane- and shear-lockings and yielding highly accurate results for displacements as well as stresses (or stress resultants). Moleiro et al. (2009) [201] developed two LSFEM models for the static and free vibration analyses of laminated composite plates, considering the first-order shear deformation theory with generalized displacements and stress resultants as independent variables.

Since the considered moving load problem displays a jump discontinuity in the shear force at the point where the moving load is acting, the continuity requirements on the trial space may be relaxed by using discontinuous global

shape functions at such a point. Hence, a local DLSFEM numerical approach represents a valid computational tool by which obtaining an accurate approximation for the response of a beam under moving load, following the same approach earlier pursued in Chapter 4 in case of a taut string.

As discussed in Chapter 4, the numerical solution to exterior problems represents a source of numerical troubles and a suitable ABC has to be introduced in order to simulate the original problem posed on an unbounded domain. In the previous chapter, a Perfectly Matched Layer (PML) technique has been described in detail and implemented together with the DLSFEM, within a second-order differential context (taut string on visco-elastic foundation). Previous studies have confirmed the successful application of PML techniques for acoustic, elastodynamics, and electromagnetic wave-propagation problems, which are characterized by PDEs with second-order derivatives in space. Besides, the application of Perfectly Matched Layers for flexural waves inside beams, involving fourth-order PDEs, are seemingly limited to a few very recent results, and characterized by rather conflicting outcomes. To the author's best knowledge, first attempts in the application of a PML as an absorbing layer for studying wave propagation in beams were undertaken by Lancioni (2012) [171], who highlighted some convergence and stability problems relative to the numerical outcomes.

On the other hand, Arbabi and Farzanian (2014) [8] proposed a numerical implementation of a standard PML technique for the equation of motion of a beam, leading to a nonlinear classic Galerkin FEM (GFEM) formulation, solved by a Newmark algorithm along with a Newton-Raphson iteration at each time step. However, the results reported by these authors to validate their model were rather limited and, according to their implementation, a nonlinear procedure seemed to be always needed to solve even a linear problem. In a more recent work, Morvaridi and Brun (2016) [204] actually combined the use of a PML with the insertion of additional boundary conditions, which shall be nothing as asymptotic boundary conditions (Lentini and Keller, 1980 [174]) or Dirichlet to Neumann (DtN) conditions (Givoli, 1992 [110], Andersen et al., 2001 [5]), but written within the PML transformed domain. Hence, the latter added boundary conditions shall make that PML strategy not a "pure" one and truly appear as those assuring the outward waves not to be reflected. A new, true, effective PML technique for a fourth-order differential problem is originally derived here, in the present fourth-order context of beam vibration.

Hence, the second purpose of the present study is to derive a robust and efficient computational tool for numerically simulating the steady-state response in convected coordinate of an infinite beam on a Pasternak visco-elastic foundation under a constant transverse moving load. Therefore, a local Discontinuous Least-Squares Finite Element Method (DLSFEM) with appropriate PML is formulated and implemented. The numerical method is characterized by

highly accurate results for the displacements as well as the rotations, and for the bending moments and the shear forces, and is endowed of a general validity in the whole space of variation of the characteristic mechanical parameters of the beam-foundation system. The convergence of the method has already been discussed in the previous chapter.

Despite for the similarity of the numerical approach, the present investigated beam response constitutes a completely different differential problem (of a fourth-order) with respect to that of the taut string (second-order) and involves a totally different, new, PML formulation. In fact, a new, effective fourth-order PML technique is proposed here for handling the issue of spurious reflections and non-evanescence of the flexural waves at the truncated boundaries of the finite computational domain of slender beams apt to describe the transverse steady-state response under moving load. Specifically, this shall be conceived as a "pure" PML approach, in the sense of both eliminating the reflections and making the progressive waves to become evanescent on an unbounded domain, without recurring to additional ad-hoc boundary conditions (as instead attempted by Morvaridi and Brun, 2016 [204]). To the best of the author's knowledge, this approach represents a wholly innovative contribution, filling the gap between the existing absorbing boundary and PML approaches for handling flexural waves.

The effectiveness of the PML technique, of the theoretical results attached to the DLSFEM formulation and of their practical validity is proven for the physical moving load problem under consideration, by comparing the obtained numerical results with the analytical solution for the steady-state condition derived in the first part of the present chapter, showing a full agreement and a perfect match.

An overview on the structure of the chapter is as follows. In the continuation of the present section, the steady-state formulation governing an infinite Euler-Bernoulli elastic beam resting on a Pasternak foundation in convected coordinate is introduced, along with the interface conditions at the point of application of the load and the conditions at infinity. In Section 5.2 a complete Fourier transform approach developed for deriving the analytical solution is reported. After the determination of the general parametric form of the poles of the Fourier transform of the solution, the analytical solution is finally derived in exact closed form by inverting the Fourier transform, according to a universal solution representation. The singular cases of critical velocity and critical damping are also derived and analyzed. In Section 5.3, normalized curves of the complete steady-state response of the beam-foundation system (deflection, rotation, bending moment and shear force) are represented, and their dependence on the characteristic parameters of the dynamical system is discussed.

Regarding the numerical formulation, the discussion on the ineffectiveness of standard PML techniques for treating far-field conditions of fourth-order

ODEs and the derivation of a new effective PML and the corresponding differential equation are delivered in Section 5.4. Next, Section 5.5 is devoted to the present DLSFEM-PML formulation and implementation (within a Matlab environment) and to the outcomes gathered from numerical simulations involving the complete normalized steady-state response of the beam-foundation system (deflection, slope, bending moment and shear). Such numerical results are compared to the outcomes of the above-mentioned analytical solution, in order to support the statements of Section 4.4 in terms of uniform error estimates in both L^2- and H^1-norms and to validate the application of the present DLSFEM-PML approach. Finally, main concluding remarks are resumed in closing Section 5.6. The achievements of the present chapter may also be found in Froio et al. (2017,2019) [102, 104].

5.1.1 Problem formulation

Consider an infinite Euler-Bernoulli elastic beam lying on a Pasternak viscoelastic foundation, as sketched in Fig. 5.1, endowed with a right-handed system of rectangular coordinates (X,Y,Z) and a time variable t [s]; the X-axis (longitudinal axis) is taken along the beam axis while the Y-axis (transverse vertical axis) and the Z-axis (transverse horizontal axis) are assumed to coincide with the principal axes of inertia of the beam cross-section; the positive direction of the Z-axis is taken vertically upward. The positive direction for measuring beam slopes (cross-section rotations) is conformal to typical usage, i.e. according to the right-handed screw rule. A positive bending moment indicates tensile stresses in the bottom of the beam and positive shear indicates that the left side of the beam tends to rise. The infinite beam lying on an elastic foundation is traversed by a constant force F [N], positive if upward, moving from $-\infty$ to $+\infty$ at a constant velocity v [m/s]. Load is taken upward for the derivation of the equations; it will finally act downward in the final presented applications.

In such a reference frame, the of motion describing the transverse deflection $w{=}w(X,t)$ of the elastic beam on a Pasternak viscoelastic support, within

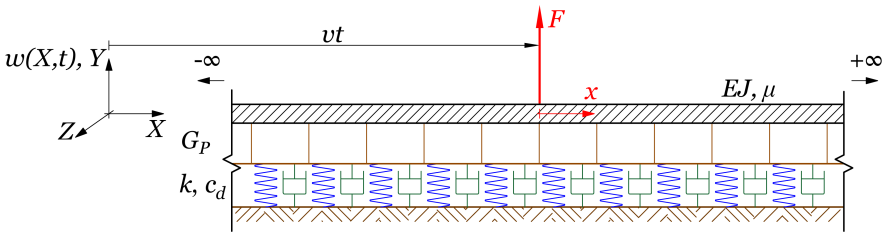

Figure 5.1: Infinite Euler-Bernoulli elastic beam resting on a viscoelastic Pasternak foundation under a uniform load F moving at constant velocity v along the beam.

an infinitesimal strain framework, is represented by the following fourth-order PDE (see e.g. Mallik et al., 2006 [186]):

$$EJ\, w_X^{(4)} + \mu\, w_t^{(2)} - G_P\, w_X^{(2)} + c_d\, w_X^{(1)} + k\, w = F\delta(X - vt); \qquad (5.1)$$

where E [N/m^2] is the elastic modulus of the material, J [m^4] is the central moment of inertia of the beam cross-section around the Y-axis and μ [kg/m] is the mass per unit length of the beam, i.e. the three characteristic mechanical parameters of the beam; also, regarding the elastic foundation, according to standard notation as reported in Wang et al. (2005) [268], k [N/m^2] is the elastic stiffness of the distributed foundation springs, named also modulus of subgrade reaction or Winkler foundation modulus (first stiffness parameter of the Pasternak elastic foundation) and G_P [N] is the Pasternak shear modulus of the interconnecting shear layer (second stiffness parameter of the Pasternak elastic foundation), namely the further two parameters of the elastic support; c_d [Ns/m^2] is the viscous damping coefficient per unit length of the beam-foundation system; all such characteristic parameters are assumed to be constant in both space and time. Moreover, the unknown transverse deflection of the beam induced by the acting moving load has been labeled as $w(X,t)$ [m] (positive in the Y direction); finally, F [N] on the right-hand side of Eq. (5.1) is the constant magnitude of the concentrated moving load, v [m/s] is its velocity and $\delta(\cdot)$ is the Dirac delta function.

By assuming steady-state conditions, i.e. supposing that the effects of transients due to the initial conditions during the first evolution of the system are negligible at later stages, it is possible to directly correlate beam transverse displacement $w(X,t)$ to the character of forcing action $F\delta(X-vt)$ acting on the infinite beam. In other words, this means that, under steady-state conditions, $w(X,t)$ can be assumed to display the following form (see e.g. Kenney, 1954 [155] and Frýba, 1972 [105]):

$$w(X,t) = w_0 \hat{w}(X - vt); \qquad (5.2)$$

where $\hat{w}(X-vt)$ is a dimensionless steady-state deflection of the beam, measured at locations $X-vt$ [m] relative to the position vt of the moving load, and w_0 [m] is a normalizing factor, to be defined later. Hence, the definition in Eq. (5.2) characterizes the solution $w(X,t)$ as a *"traveling wave"*, moving at velocity v.

Furthermore, since the beam-support system displays homogeneous characteristics, it becomes suitable to rewrite PDE (5.1), with $w(X,t)$ as in Eq. (5.2), with respect to a moving reference frame attached to the position of the moving load, by introducing the following new non-dimensional real independent variable:

$$s = \lambda(X - vt) = \lambda\, x; \qquad -\infty < s < +\infty; \qquad (5.3)$$

where variable x is the corresponding dimensional counterpart ($-\infty<x<+\infty$) and

$$\lambda = \left(\frac{k}{4EJ}\right)^{1/4} \quad [\mathrm{m}^{-1}] \tag{5.4}$$

is the so-called wave number (Graff, 1975 [116]) of the corresponding static problem (v=0), for a Winkler elastic foundation (G_P=0), namely 2π times the inverse of the wavelength of the resulting static displacement function, represented in space as a function of λX. Then, its inverse λ^{-1} [m] is also frequently referred to as the characteristic length of the infinite beam (Hetényi, 1946 [125]). In the following analytical derivations, non-dimensional moving coordinate s will be employed, while dimensional moving coordinate x will be used for the subsequent numerical approach.

Now, from the change of variables defined in Eq. (5.3), Eq. (5.2) reads

$$w(X,t) = w_0\,\hat{w}(s); \tag{5.5}$$

and the chain rule of differentiation on Eq. (5.5), with s defined in Eq. (5.3), yields:

$$w_X^{(k)}(X,t) = w_0\lambda^k\hat{w}_s^{(k)}(s), \qquad w_t^{(k)}(X,t) = (-1)^k w_0\lambda^k\hat{w}_s^{(k)}(s). \tag{5.6}$$

Substituting Eqs. (5.5) and (5.6) into PDE (5.1), by taking into account the following characteristic property of the Dirac delta function (Buschman, 1996 [46]):

$$\delta(X-vt) = \delta(x) = \lambda\delta(s); \tag{5.7}$$

and rearranging all terms, Eq. (5.1) leads to the following fourth-order ODE in the unknown steady-state non-dimensional displacement $\hat{w}(s)$:

$$\lambda^4 EJ\,\hat{w}_s^{(4)}(s)+\lambda^2(\mu v^2-G_P)\,\hat{w}_s^{(2)}(s)-\lambda v c_d\,\hat{w}_s^{(1)}(s)+k\,\hat{w}(s) = \frac{\lambda F}{w_0}\delta(s). \tag{5.8}$$

The far-field boundary conditions relative to ODE Eq. (5.8) are specified by stipulating that at an infinite distance to the right, as well as to the left, of moving load F, the beam deflection and its derivatives shall vanish:

$$\lim_{s\to\pm\infty}\hat{w}_s^{(k)}(s) = 0; \quad k = 0,1,2,3. \tag{5.9}$$

Hence, the advantage of transforming the equation of motion into a moving reference frame is that the steady-state solution becomes time invariant, i.e. it may be obtained as by solving a purely static problem, since the time variable has explicitly disappeared.

For the purposes of the forthcoming analytical developments and ensuing discussion, the following two non-dimensional real characteristic parameters α, β are introduced:

$$\alpha = \frac{\mu v^2 - G_P}{4\lambda^2 EJ} = \frac{v^2 - G_P/\mu}{\sqrt{4kEJ}/\mu} = \frac{v^2 - G_P/\mu}{v_{cr,W}^2} = \left(\frac{v}{v_{cr,W}}\right)^2 - g_p; \tag{5.10}$$

$$\beta = \frac{v c_d}{\lambda^3 EJ} = 8\,\frac{v}{v_{cr,W}}\,\zeta \geq 0; \tag{5.11}$$

where parameters

$$g_P = \frac{G_P}{\mu v_{cr,W}^2} = \frac{G_P}{\sqrt{4kEJ}}; \qquad \zeta = \frac{c_d}{2\sqrt{k\mu}}; \tag{5.12}$$

are the non-dimensional Pasternak modulus of the foundation and the damping ratio, respectively, and where

$$v_{cr,W} = 2\lambda\sqrt{\frac{EJ}{\mu}} = \sqrt[4]{\frac{4kEJ}{\mu^2}} \tag{5.13}$$

is the critical velocity of the moving load problem for a Winkler elastic foundation, i.e. for G_P=0 (see e.g. Kenney, 1954 [155]), as re-derived in the subsequent sections.

By virtue of such mathematical definitions of α and β, ODE (5.8) finally becomes

$$\hat{w}_s^{(4)}(s) + 4\alpha\,\hat{w}_s^{(2)}(s) - \beta\,\hat{w}_s^{(1)}(s) + 4\,\hat{w}(s) = \hat{F}\,\delta(s); \tag{5.14}$$

where

$$\hat{F} = \frac{F}{\lambda^3 EJ w_0} \tag{5.15}$$

is a non-dimensional amplitude of the moving load.

Consequently, non-dimensional steady-state rotation, bending moment and shear force, as a function of nondimensional variable s, may be written in terms of the following relations:

$$\hat{\theta}(s) = \frac{\theta(X-vt)}{\theta_0} = \frac{1}{\theta_0} w_X^{(1)}(X-vt) = \frac{w_0\lambda}{\theta_0}\hat{w}_s^{(1)}(s) = \hat{w}_s^{(1)}(s); \tag{5.16a}$$

$$\hat{M}(s) = \frac{M(X-vt)}{M_0} = \frac{EJ}{M_0} w_X^{(1)}(X-vt) = \frac{EJ w_0\lambda^2}{M_0}\hat{w}_s^{(2)}(s) = \hat{w}_s^{(2)}(s); \tag{5.16b}$$

$$\hat{S}(s) = \frac{S(X-vt)}{S_0} = \frac{EJ}{S_0} w_X^{(1)}(X-vt) = \frac{EJ w_0\lambda^3}{S_0}\hat{w}_s^{(3)}(s) = \hat{w}_s^{(3)}(s); \tag{5.16c}$$

where

$$\theta_0 = \lambda\, w_0, \quad M_0 = \lambda^2 EJ\, w_0, \quad S_0 = \lambda^3 EJ\, w_0 \tag{5.17}$$

are chosen normalization factors for rotation, bending moment and shear force, respectively, so that $\hat{\theta}(s)$, $\hat{M}(s)$ and $\hat{S}(s)$ are directly expressed as the derivatives of unknown $\hat{w}(s)$. These will be set at a later stage.

Hence, it appears that the steady-state response of the beam-support system is mathematically ruled by non-dimensional parameters α, β in Eqs. (5.10)-(5.11). The explicit analytical solution of Eq. (5.14) for some combinations

of parameters α, β has been already conjectured in the literature, as earlier discussed in the Introduction. In the following sections, an accurate analysis of the general solution of Eq. (5.14), parametrized with respect to α, β, is developed, based on a rigorous derivation by a full Fourier transform approach, giving rise to a universal parametric representation.

Thus, the present attempt fully completes previous literature derivations and explores new solution instances that may be obtained for some given values of non-dimensional physical parameters α, β, outlining a unitary, comprehensive general formulation of the analyzed steady-state moving load response of a beam-Pasternak foundation system.

5.1.2 Comments on the definition of the characteristic system parameters

Possible alternative definitions of the characteristic parameters that rule the analytical problem are feasible, based on the involved mechanical parameters (EJ, μ; k, G_P; c and v). In particular, by inspecting Eqs. (5.10)-(5.14) three main characteristic parameters appear to rule the beam-foundation system response (G_P, c and v, or their non-dimensional counterparts g_P, ζ and $v/v_{cr,W}$). The definition of α in Eq. (5.10) is consistent with that provided by Frýba (1972) [105] for a Winkler foundation (G_P=0), so that when G_P=0 the two definitions come up to coincide. Consequently, in order to achieve a differential equation containing two parameters only, parameter β in Eq. (5.11) has been defined as a function of both damping ratio and velocity ratio. This choice allows for a 2D representation of the solution domain in terms of two parameters α, β as done in Fig. 5.2, instead of a 3D representation on the above-mentioned three physical parameters. The links between the former and the latter representation will be extensively illustrated in Fig. 5.7.

The present "mathematical" definition goes to the core of the analytical derivation, allowing for a true decoupling of effects in mathematical terms and referring to the source differential equation (see final differential Eq. (5.14)). Thus, the above definitions constitute those leading to the simplest mathematical inspection, also for its physical implications, entailing the minimum number of parameters governing the system response. In fact, whatever choice of the parameters based on physical considerations will lead to three independent parameters governing the system (as shown in Eqs. (5.10)-(5.11)), thus making it more intricate the a "priori" analysis of the possible evolutions of the system. In this sense, α, β shall be conceived as "mathematical" parameters, more than "physical" parameters, apt to rule the solution regimes in fourthcoming Fig. 5.2, and relevant outcoming solution characteristics, without impeding to appreciate physical implications in subsequent Fig. 5.7, as shown in the following sections.

5.2 Analytical solution

5.2.1 Application of the Fourier transform

The analytical solution to Eq. (5.14) with far-field conditions in Eq. (5.9) may be derived by the application of the Fourier integral transform, by starting from the following fundamental definitions:

$$\hat{W}(q) = \int_{-\infty}^{\infty} \hat{w}(s) e^{-\mathrm{i}sq}\, ds; \quad \hat{w}(s) = \frac{1}{2\pi} \int_{-\infty}^{\infty} \hat{W}(q) e^{\mathrm{i}sq}\, dq; \tag{5.18}$$

where $s,\ q \in \mathbb{R}$, i is the imaginary unit, $\hat{W}(q)$ is the Fourier transform of $\hat{w}(s)$, and, conversely, $\hat{w}(s)$ is the inverse Fourier transform of $\hat{W}(q)$. By applying Fourier transform (5.18) to Eq. (5.14), the expression of the Fourier transform $\hat{W}(q)$ of $\hat{w}(s)$ may be represented as

$$\hat{W}(q) = \frac{\hat{F}}{q^4 - 4\alpha q^2 - \beta \mathrm{i} q + 4} = \frac{\hat{F}}{P(q)}; \tag{5.19}$$

where

$$P(q) = q^4 - 4\alpha q^2 - \beta \mathrm{i} q + 4 \tag{5.20}$$

is a fourth-order polynomial with complex coefficients, whose roots (system poles) take a main role in the subsequent derivation of $\hat{w}(s)$, since they represent the four isolated singularities of Fourier transform $\hat{W}(q)$.

The solution to Eq. (5.14) is then obtained by using inverse Fourier transform in Eq. (5.18), namely by inverting $\hat{W}(q)$ in Eq. (5.19):

$$\hat{w}(s) = \frac{\hat{F}}{2\pi} \int_{-\infty}^{+\infty} \frac{e^{\mathrm{i}sq}}{P(q)}\, dq \;=\; \frac{\hat{F}}{2\pi} \lim_{R \to +\infty} \int_{-R}^{R} \frac{e^{\mathrm{i}sq}}{P(q)}\, dq; \tag{5.21}$$

where R is an auxiliary real parameter, useful to perform the infinite integration through a limit process as $R \to \infty$.

The most widely-used technique for evaluating the complex integral in the inverse transform of Eq. (5.18), with $\hat{W}(q)$ given by Eq. (5.19), namely for resolving Eq. (5.21), is through a contour integration (Duffy, 2004 [78]). In that method, an integration along the real axis is converted into a closed contour integration in the complex plane, by adding a semicircle, of an infinite radius in the limit, which, together with the real axis, forms a closed integration path. Then, by an *analytic continuation* of variable q into the entire complex plane ($q \in \mathbb{C}$), the integral in Eq. (5.21) may be expressed as

$$\lim_{R \to +\infty} \int_{-R}^{R} \frac{e^{\mathrm{i}sq}}{P(q)}\, dq \;=\; \lim_{R \to +\infty} \left(\oint_{\mathcal{C}} \frac{e^{\mathrm{i}sq}}{P(q)}\, dq - \int_{\mathcal{C}_R} \frac{e^{\mathrm{i}sq}}{P(q)}\, dq \right); \tag{5.22}$$

where $\mathcal{C}_R$ is a semicircle centered on the origin of the complex plane, either in the upper ($\mathcal{C}_R^+$) or lower ($\mathcal{C}_R^-$) half-plane and $\mathcal{C}$=$\mathcal{C}_R \cup (-R, R)$ is a closed curve, obtained by joining semicircle $\mathcal{C}_R$ and segment $(-R, R)$ on the real axis (see Fig. 5.3, later shown).

The integrals in Eq. (5.22) converge because the integrand is a *meromorphic* function, namely an everywhere regular function in the complex plane, except for a finite number of points, called *poles*, where the integrand diverges to infinity (see e.g. Bak and Newman, 2010 [15]). Since exponential $e^{\mathrm{i}sq}$ and fourth-order polynomial $P(q)$ are *entire* functions, i.e. functions that are anywhere analytic in the complex plane, the poles of the integrand coincide with the roots of polynomial $P(q)$ defined in Eq. (5.19).

Furthermore, it may be verified that when radius R finally goes to infinity, the integral along semicircle $\mathcal{C}_R$ in Eq. (5.22) vanishes. In fact, by the triangle inequality, the absolute value of $P(q)$ in Eq. (5.19) is bounded from below as follows:

$$\left|P(q)\right| \geq \left|q^4\right| - \left|-4\alpha q^2\right| - \left|-\beta \mathrm{i} q\right| - \left|4\right| = \left|q^4\right| - 4\left|\alpha q^2\right| - \beta\left|q\right| - 4; \quad (5.23)$$

and for $q \in \mathcal{C}_R$, i.e. for $|q|$=R, one gets

$$\left|P(q)\right|_{q\in\mathcal{C}_R} \geq R^4\left(1 - \frac{4\left|\alpha\right|}{R^2} - \frac{\beta}{R^3} - \frac{4}{R^4}\right) = m_R. \quad (5.24)$$

As a result, the modulus of the integrand of the integral along semicircle $\mathcal{C}_R$ in Eq. (5.22) is bounded from above as follows:

$$\left|\frac{e^{\mathrm{i}sq}}{P(q)}\right| = \frac{\left|e^{\mathrm{i}s(a+ib)}\right|}{|P(q)|} = \frac{\left|e^{-bs}\right|}{|P(q)|} \leq \frac{1}{m_R} = \begin{cases} \text{for } q \in \mathcal{C}_R^+, & \text{if } s > 0; \\ \text{for } q \in \mathcal{C}_R^-, & \text{if } s < 0; \end{cases} \quad (5.25)$$

where a and b are the real and imaginary parts of q, respectively. Finally, the application of Jordan's lemma (see e.g. Duffy, 2004 [78]) leads to the above stated vanishing result:

$$\begin{aligned} 0 \leq \lim_{R\to+\infty}\left|\int_{\mathcal{C}_R}\frac{e^{\mathrm{i}sq}}{P(q)}\,dq\right| &\leq \lim_{R\to+\infty}\frac{2R}{m_R}\int_0^{\pm\frac{\pi}{2}} e^{-2sR\theta/\pi}d\theta \leq \\ &\leq \lim_{R\to+\infty}\frac{\pi}{m_R\left|s\right|}\left(1-e^{-|s|R}\right) = 0. \end{aligned} \quad (5.26)$$

Consequently, according to Cauchy's Residue Theorem (Bak and Newman, 2010 [15]), one may write:

$$\begin{aligned} \hat{w}(s) &= \frac{\hat{F}}{2\pi}\lim_{R\to+\infty}\int_{-R}^{R}\frac{e^{\mathrm{i}sq}}{P(q)}\,dq = \frac{\hat{F}}{2\pi}\lim_{R\to+\infty}\oint_{\mathcal{C}}\frac{e^{\mathrm{i}sq}}{P(q)}\,dq = \\ &= \frac{\hat{F}}{2\pi}\left(\pm 2\pi\mathrm{i}\sum_{k=1}^{n}\mathrm{Res}\left\{\frac{e^{\mathrm{i}sq}}{P(q)}; q_k\right\}\right) = \pm\mathrm{i}\hat{F}\sum_{k=1}^{n}\mathrm{Res}\left\{\frac{e^{\mathrm{i}sq}}{P(q)}; q_k\right\}; \end{aligned} \quad (5.27)$$

where $\mathrm{Res}\{f; q_k\}$ denotes the residue of function f at pole q_k, namely the coefficient of the minus-one power term of the power series expansions (known also as Laurent expansions) of f centered at q_k; n is the number of isolated singularities (poles) q_k placed inside closed curve $\mathcal{C}$, the plus or minus sign depending on whether the orientation of $\mathcal{C}$ is counterclockwise or clockwise, respectively. Specifically, the residue for a pole of order m may be evaluated according to the subsequent formula (Duffy, 2004 [78]):

$$\mathrm{Res}\Big\{ f(q); q_k \Big\} = \frac{1}{(m-1)!} \lim_{q \to q_k} \Big((q-q_k)^m f(q) \Big)_q^{(m-1)}. \tag{5.28}$$

Since the integral in Eq. (5.27) depends on the location of the zeros of polynomial $P(q)$ in the complex plane, it is evident how the characteristic system parameters α, β, which are contained in the expressions of such roots, may imply different manifestations of the steady-state solution. The derivation of the expressions of the poles as a function of the system parameters and the complete determination of the universal analytical solution in explicit form are carried out in the following section.

5.2.2 Inversion of the Fourier transform

Parametric location of the poles

Fourth-order polynomial denominator $P(q)$ reported in Eq. (5.19) displays four zeros in the complex plane. To classify the nature of these roots as a function of real non-dimensional parameters α, β it is more suitable to analyze real-coefficient polynomial

$$\hat{P}(r) = P(\mathrm{i}r) = r^4 + 4\alpha r^2 + \beta r + 4 \tag{5.29}$$

in complex variable $r{=}{-}iq$ (Achenbach and Sun, 1965 [2]). Let Δ be the discriminant of $\hat{P}(r)$, i.e. the product of the squares of the differences of the roots of $\hat{P}(r){=}0$ (see e.g. Rees, 1922 [226]).

Since the roots are a priori unknown, the following theorem reported by Rees (1922) [226] turns out to be useful. Denoting by r_k the roots of $\hat{P}(r)$ and by r'_k the roots of the first-order derivative of $\hat{P}(r)$, namely $\hat{P}'(r)$, one has

$$\begin{aligned} \Delta(\alpha,\beta) &= \prod_{k=1}^{4} \prod_{j>k} (r_k - r_j)^2 = 4^4 \prod_{k=1}^{4} \hat{P}(r'_k) = \\ &= 16384 \left(\alpha^2 - 1\right)^2 - 256\alpha \left(\alpha^2 - 9\right)\beta^2 - 27\beta^4; \end{aligned} \tag{5.30}$$

where the final expression of $\Delta(\alpha,\beta)$ may be readily verified within Mathematica [274].

Four distinct roots	Case 1	$\Delta > 0,\ \alpha < -1$	$r_1 = b_1;\ \ r_2 = b_2;$ $r_3 = b_3;\ \ r_4 = b_4;$	$q_1 = b_1\mathrm{i};\ \ q_2 = b_2\mathrm{i};$ $q_3 = b_3\mathrm{i};\ \ q_4 = b_4\mathrm{i};$
	Case 2	$\Delta < 0,\ \forall\, \alpha$	$r_1 = b_1;\ \ r_2 = b_2;$ $r_3 = b_3 + a_3\mathrm{i};$ $r_4 = b_3 - a_3\mathrm{i};$	$q_1 = b_1\mathrm{i};\ \ q_2 = b_2\mathrm{i};$ $q_3 = -a_3 + b_3\mathrm{i};$ $q_4 = a_3 + b_3\mathrm{i};$
	Case 3	$\Delta > 0,\ \alpha > -1$	$r_1 = b_1 + a_1\mathrm{i};$ $r_2 = b_1 - a_1\mathrm{i};$ $r_3 = b_3 + a_3\mathrm{i};$ $r_4 = b_3 - a_3\mathrm{i};$	$q_1 = -a_1 + b_1\mathrm{i};$ $q_2 = a_1 + b_1\mathrm{i};$ $q_3 = -a_3 + b_3\mathrm{i};$ $q_4 = a_3 + b_3\mathrm{i};$
At least two coincident roots	Case 4	$\Delta = 0,\ \alpha < -1$	$r_1 = b_1;\ \ r_2 = b_2;$ $r_3 = r_4 = b_3;$	$q_1 = b_1\mathrm{i};\ \ q_2 = b_2\mathrm{i};$ $q_3 = q_4 = b_3\mathrm{i};$
	Case 5	$\Delta = 0,\ \alpha > -1$	$r_1 = b_1;\ \ r_2 = b_1;$ $r_3 = b_3 + a_3\mathrm{i};$ $r_4 = b_3 - a_3\mathrm{i};$	$q_1 = q_2 = b_1\mathrm{i};$ $q_3 = -a_3 + b_3\mathrm{i};$ $q_4 = a_3 + b_3\mathrm{i};$
	Case 6	$\beta = 0,\ \alpha \geq 1$ $(\Delta \geq 0)$	$r_1 = a_1\mathrm{i};\ \ r_2 = -a_1\mathrm{i};$ $r_3 = a_3\mathrm{i};\ \ r_4 = -a_3\mathrm{i};$	$q_1 = -a_1;\ \ q_2 = a_1;$ $q_3 = -a_3;\ \ q_4 = a_3;$

Table 5.1: Classification of the nature of roots r_k of $\hat{P}(r)$ and q_k of $P(q)$ as a function of characteristic system parameters α, β; real-valued a_i, b_i define real and imaginary parts of the roots.

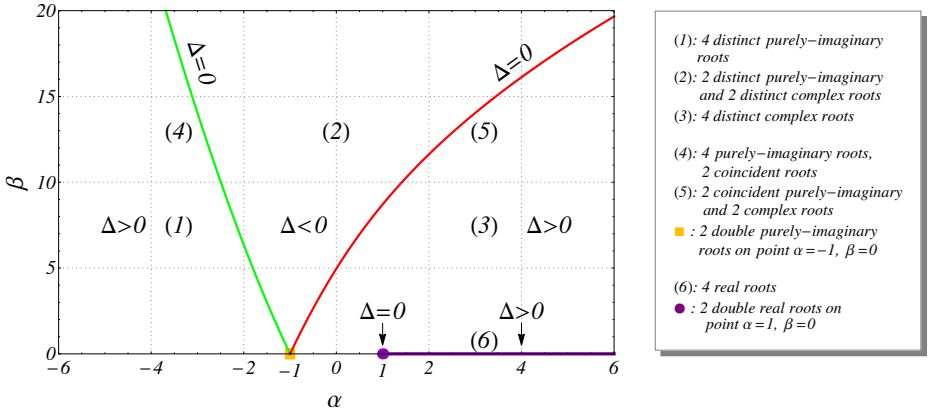

Figure 5.2: Graphical representation of the solution regions in the domain of real nondimensional system parameters α, β with the same type of q_k roots.

The sign of discriminant Δ is a fundamental feature to determine the nature of the poles. In fact, according to a theorem reported by Dickson (1914) [66], the four roots of quartic equation $\hat{P}(r)=0$ with real coefficients and discriminant Δ take the form reported in Table 5.1. Consequently, by multiplying roots r_k by imaginary unit i, it is straightforward to characterize the form of roots q_k of denominator $P(q)$, also listed in Table 5.1.

A graphical representation of the nature of roots q_k of $P(q)$ as a function of

characteristic parameters α and β is depicted in Fig. 5.2, where a subdivision of the parametric space into different subdomains is pointed out. Such a partition is fundamental for characterizing the behavior of the beam-foundation response, as it will be outlined in following Section 5.3.

Parametric expression of the poles

As exposed in Subsection 5.2.1, the key feature for the inversion of the Fourier transform in Eq. (5.18) is the characterization of the nature of poles q_k as a function of characteristic parameters α, β. In this section, exact symbolic expressions of these roots are provided.

By virtue of the analysis in Subsection 5.2.2, based on the discriminant of fourth-order polynomial $P(q)$, roots q_k may be written in the subsequent general form:

$$q_1 = -a_1 + \mathrm{i}b_1; \quad q_2 = a_1 + \mathrm{i}b_2; \quad q_3 = -a_3 + \mathrm{i}b_3; \quad q_4 = a_3 + \mathrm{i}b_4; \tag{5.31}$$

where a_1, a_3 and b_1, b_2, b_3, b_4 are six real coefficients, labeling the real and imaginary parts of roots q_k, respectively. In order for q_k to be a root of polynomial $P(q)$, above-defined coefficients a_i and b_i have to be related to the coefficients of $P(q)$.

The definition of such relationships may be accomplished by Vieta's formulas (see e.g. Vinberg, 2003 [266]), which relate the coefficients of polynomial $P(q)$ to sums and products of its roots, as follows:

$$\sum_{1\leq i\leq 4} q_i = 0; \tag{5.32a}$$

$$\sum_{1\leq i<j\leq 4} q_i q_j = -4\alpha; \tag{5.32b}$$

$$\sum_{1\leq i<j<k\leq 4} q_i q_j q_k = -\mathrm{i}\beta; \tag{5.32c}$$

$$\sum_{1\leq i<j<k<l\leq 4} q_i q_j q_k q_l = 4. \tag{5.32d}$$

By using other auxiliary real constants A_i, defined as:

$$A_1 = a_1^2 + b_1 b_2; \quad A_2 = b_1 + b_2; \quad A_3 = a_3^2 + b_3 b_4; \quad A_4 = b_3 + b_4; \tag{5.33}$$

and according to Table 5.1, which implies one of the following three occurrences:

$$a_1 = a_3 = 0 \ \text{ or } \ a_1 = 0 \text{ and } b_3 = b_4 \ \text{ or } \ a_1, a_3 \neq 0 \text{ and } b_1 = b_2,\ b_3 = b_4; \tag{5.34}$$

the system of Eqs. (5.32) becomes:

$$A_2 + A_4 = 0; \tag{5.35a}$$

$$A_1 + A_3 + A_2 A_4 = 4\alpha; \tag{5.35b}$$
$$(A_1 A_4 + A_2 A_3)\mathrm{i} = -\beta\mathrm{i}; \tag{5.35c}$$
$$A_1 A_3 = 4. \tag{5.35d}$$

The solution of the nonlinear system of Eqs. (5.35) may be expressed as:

$$A_1 = \frac{A_4^2}{2} + 2\alpha - \frac{\beta}{2A_4}; \qquad A_2 = -A_4; \qquad A_3 = \frac{A_4^2}{2} + 2\alpha + \frac{\beta}{2A_4}; \tag{5.36}$$

where coefficient A_4 comes by solving the following sixth-order polynomial equation:

$$A_4^6 - 8\alpha A_4^4 + 16(\alpha^2 - 1)A_4^2 - \beta^2 = 0; \tag{5.37}$$

which may be further recast into a third-order polynomial equation:

$$t^3 - 8\alpha t^2 + 16(\alpha^2 - 1)t - \beta^2 = 0; \tag{5.38}$$

by defining auxiliary variable $t{=}A_4^2$. Since, by definition, A_4 in Eqs. (5.33) is a real number, only positive values of t have to be taken into account amongst the three solutions of Eq. (5.38). The discriminant of the cubic polynomial in Eq. (5.38), evaluated in accordance to Dickson (1914) [66], is exactly the quantity Δ reported in Eq. (5.30), expressing the discriminant of the quartic polynomial in Eq. (5.29). Following a theorem reported by Dickson (1914) [66], a cubic polynomial equation with real coefficients has always at least a real root, independently from the sign of its discriminant; furthermore, at least one positive root must exist since constant term $-\beta^2$ in Eq. (5.38) is negative.

The choice of the sign of $A_4{=}\pm\sqrt{t}$ is arbitrary and not significant towards the derivation of the solution, since it induces only an exchange of values between roots q_1, q_2 and q_3, q_4. In the following, a plus sign is considered; thus, A_4 is a non-negative real number. The explicit expression of quantity $A_4{=}\sqrt{t}$ has been derived within Mathematica [274], where Cardan's formula is implemented by a built-in function, and takes the following final form:

$$A_4(\alpha,\beta) = \frac{1}{\sqrt{3}}\sqrt{\frac{16(\alpha^2+3)}{f(\alpha,\beta)} + f(\alpha,\beta) - 8\alpha}; \tag{5.39a}$$

$$f(\alpha,\beta) = \sqrt[3]{\frac{27}{2}\beta^2 + 64\alpha(\alpha^2-9) + 3\frac{\sqrt{3}}{2}\sqrt{-\Delta(\alpha,\beta)}}. \tag{5.39b}$$

It may be shown that expressions in Eqs. (5.39) always lead to a real non-negative coefficient A_4. Then, the final expressions of unknown coefficients a_1, a_3, b_1, b_2, b_3, b_4 become:

$$a_1 = \begin{cases} 0 & \text{if } 4A_1 - A_4^2 = A_4^2 + 8\alpha - 2\beta/A_4 \le 0; \\ \dfrac{1}{2}\sqrt{4A_1 - A_4^2} & \text{otherwise } \ (\Delta > 0,\ \alpha \le -1); \end{cases} \tag{5.40a}$$

$$a_3 = \begin{cases} 0 & \text{if } 4A_3 - A_4^2 = A_4^2 + 8\alpha + 2\beta/A_4 \leq 0; \\ \dfrac{1}{2}\sqrt{4A_3 - A_4^2} & \text{otherwise } \ (\Delta < 0;\ \Delta > 0,\ \alpha \geq -1); \end{cases} \tag{5.40b}$$

$$b_{1,2} = -\frac{1}{2}\left(A_4 \mp \sqrt{4a_1^2 - 4A_1 + A_4^2} \right); \tag{5.40c}$$

$$b_{3,4} = \frac{1}{2}\left(A_4 \mp \sqrt{4a_3^2 - 4A_3 + A_4^2} \right); \tag{5.40d}$$

where the choice between the two alternatives for a_1 and a_3, prescribed by Eqs. (5.40a) and (5.40b), respectively, is determined by the sign of the quantity under square root. Since $A_4{=}\sqrt{t}$ is, by definition, a non-negative quantity, from Eqs. (5.31) and Eqs. (5.40) it results that roots q_1, q_2 are always placed in the lower half-plane of the complex plane, while roots q_3, q_4 are located in the upper half-plane.

The possible loci of the roots in the complex plane arising from the above analysis are represented in Fig. 5.3, where contour paths explained earlier in Subsection 5.2.1 are also depicted.

It is noteworthy to mention that the possibility of a vanishing A_4 represents a singular case in the above derivation, meaning that the roots of $P(q)$ cannot be represented by Eqs. (5.40). This occurrence corresponds to the appearance of four real roots, as it will be shown in following Subsection 5.2.3. The derivation of the final analytical solution by contour integration now follows.

Derivation of the universal analytical solution

According to the graphical representation of the poles (Table 5.1) provided in Figs. 5.3a-5.3c and given Eq. (5.28), the residues of the integrand in Eq. (5.27) for non-coincident poles (poles of first-order) are computed as:

$$\text{Res}\left\{ \frac{e^{\mathrm{i}sq}}{P(q)}; q_k \right\} = \frac{e^{\mathrm{i}sq_k}}{P'(q_k)} = e^{\mathrm{i}sq_k} \prod_{j=1,\, j\neq k}^{4} (q_k - q_j)^{-1}; \tag{5.41}$$

and then the final non-dimensional deflection solution becomes

$$\hat{w}^-(s) = \mathrm{i}\hat{F}\, \frac{(q_2{-}q_4)(q_3{-}q_2)e^{\mathrm{i}q_1 s} - (q_1{-}q_3)(q_4{-}q_1)e^{\mathrm{i}q_2 s}}{(q_1{-}q_2)(q_1{-}q_3)(q_2{-}q_3)(q_1{-}q_4)(q_2{-}q_4)}, \quad \text{for } s \leq 0; \tag{5.42a}$$

$$\hat{w}^+(s) = \mathrm{i}\hat{F}\, \frac{(q_3{-}q_1)(q_3{-}q_2)e^{\mathrm{i}q_3 s} - (q_4{-}q_2)(q_4{-}q_1)e^{\mathrm{i}q_4 s}}{(q_3{-}q_4)(q_1{-}q_3)(q_2{-}q_3)(q_1{-}q_4)(q_2{-}q_4)}, \quad \text{for } s \geq 0. \tag{5.42b}$$

By further rearranging terms in Eq. (5.42), the non-dimensional deflection solution may be written as follows:

$$\hat{w}(s) = \hat{w}^-(s) = \frac{\hat{F}}{B_5}\, \frac{B_2 e^{-(a_1\mathrm{i}+b_1)s} - B_1 e^{(a_1\mathrm{i}-b_2)s}}{B_1\, B_2}, \quad \text{for } s \leq 0; \tag{5.43a}$$

$$\hat{w}(s) = \hat{w}^+(s) = \frac{\hat{F}}{B_6} \frac{B_4 e^{-(a_3\mathrm{i}+b_3)s} - B_3 e^{(a_3\mathrm{i}-b_4)s}}{B_3\, B_4}, \quad \text{for } s \geq 0; \tag{5.43b}$$

where coefficients B_i, introduced to further simplify the notation, are defined as

$$B_1 = (q_1 - q_3)(q_4 - q_1) = \frac{\beta}{A_4} + A_4^2 - A_4 B_5; \tag{5.44a}$$

$$B_2 = (q_3 - q_2)(q_2 - q_4) = \frac{\beta}{A_4} + A_4^2 + A_4 B_5; \tag{5.44b}$$

$$B_3 = (q_1 - q_3)(q_2 - q_3) = \frac{\beta}{A_4} - A_4^2 - A_4 B_6; \tag{5.44c}$$

$$B_4 = (q_1 - q_4)(q_2 - q_4) = \frac{\beta}{A_4} - A_4^2 + A_4 B_6; \tag{5.44d}$$

$$B_5 = -(q_1 - q_2)\mathrm{i} = \mathrm{i}\sqrt{A_4^2 + 8\alpha - 2\beta/A_4}; \tag{5.44e}$$

$$B_6 = -(q_3 - q_4)\mathrm{i} = \mathrm{i}\sqrt{A_4^2 + 8\alpha + 2\beta/A_4}; \tag{5.44f}$$

and the coefficients involved in the exponential functions have been written as:

$$a_1\mathrm{i} + b_1 = -\frac{A_4 - B_5}{2}; \tag{5.45a}$$

$$a_1\mathrm{i} - b_2 = \frac{A_4 + B_5}{2}; \tag{5.45b}$$

$$a_3\mathrm{i} + b_3 = \frac{A_4 + B_6}{2}; \tag{5.45c}$$

$$a_3\mathrm{i} - b_4 = -\frac{A_4 - B_6}{2}; \tag{5.45d}$$

where coefficient A_4 has been defined in Eqs. (5.39). From the expressions of the solution in Eqs. (5.43), the steady-state solution turns out proportional to $\hat{F}$ (thus to the moving load amplitude F), as it was expected from the linearity of the source differential equation.

By combining Eqs. (5.43)-(5.44)-(5.45), the final universal non-dimensional solution of the steady-state vibration of the infinite beam in explicit form is given by

$$\hat{w}(s) = \hat{w}^-(s) = \frac{\hat{F}}{B_5} \frac{B_2 e^{(A_4-B_5)s/2} - B_1 e^{(A_4+B_5)s/2}}{B_1\, B_2}, \quad \text{for } s \leq 0; \tag{5.46a}$$

$$\hat{w}(s) = \hat{w}^+(s) = \frac{\hat{F}}{B_6} \frac{B_4 e^{-(A_4+B_6)s/2} - B_3 e^{-(A_4-B_6)s/2}}{B_3\, B_4}, \quad \text{for } s \leq 0; \tag{5.46b}$$

Notice that when coefficient B_5 becomes purely imaginary, that is when $\Delta>0$ and $\alpha\geq-1$, the half of its absolute value ($|B_5|/2$) represents the frequency of oscillation of the wave propagating backward with respect to the moving load ($\hat{w}^-(s)$). Instead, when B_5 is real, no propagation of waves appears behind the moving load, but the response is described by the difference of two exponentially decaying functions (evanescent wave). Accordingly, the same features characterize the response of the part of the beam placed on the right of the moving load ($\hat{w}^+(s)$), in terms of coefficient B_6; in fact, if B_6 becomes purely imaginary ($\Delta<0$ or $\Delta>0$ and $\alpha\geq-1$), $|B_6|/2$ represents the frequency of oscillation of the wave propagating forward from the moving load.

The final achieved analytical representation of the steady-state response is

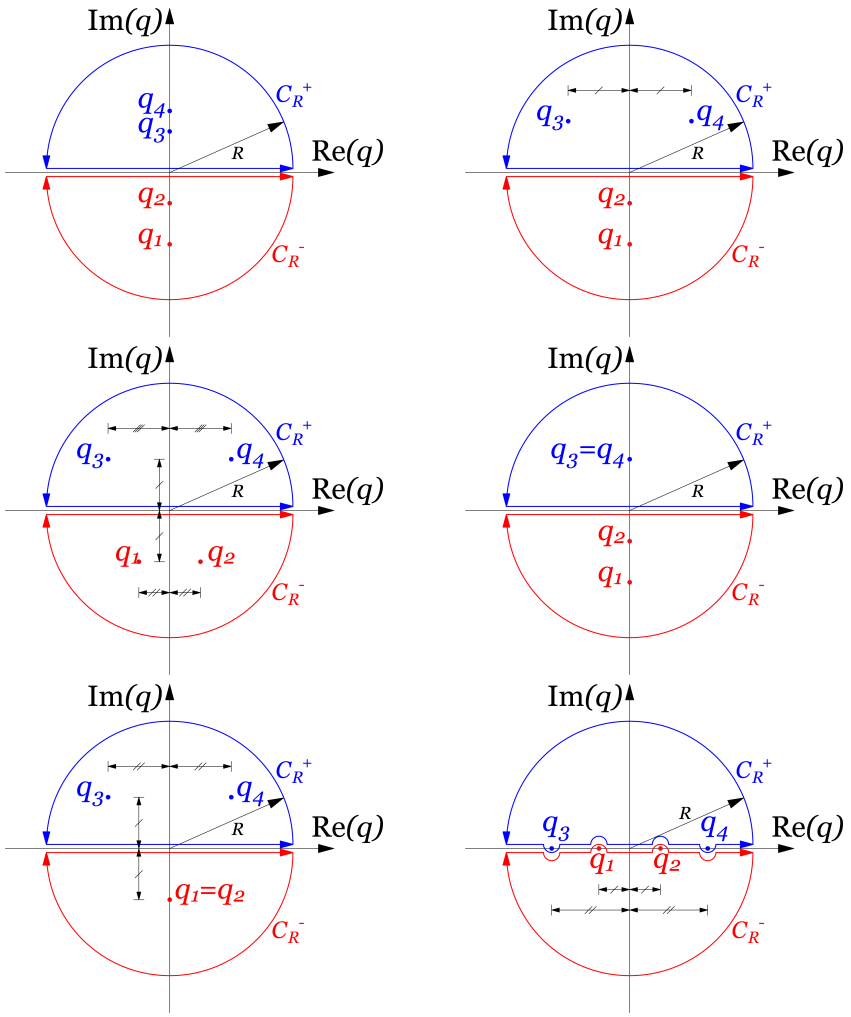

Figure 5.3: Poles q_k in the complex plane (Case 1 (a); Case 2 (b); Case 3 (c); Case 4 (d); Case 5 (e); Case 6 (f)).

SYNOPSIS OF THE STEADY-STATE ANALYTICAL SOLUTION

Definitions

- $s = \lambda(x - vt); \quad \lambda = \sqrt[4]{\dfrac{k}{4EJ}};$
- $w(s) = w_0 \hat{w}(s); \quad \hat{F} = \dfrac{F}{\lambda^3 EJ w_0};$
- $\alpha = \dfrac{v^2 - G_P/\mu}{v_{cr,W}^2}; \quad \beta = \dfrac{v c_d}{\lambda^3 EJ}; \quad v_{cr,W} = \sqrt[4]{\dfrac{4kEJ}{\mu^2}};$

Governing differential equation and boundary conditions

- $\hat{w}_s^{(4)}(s) + 4\alpha \hat{w}_s^{(2)}(s) - \beta \hat{w}_s^{(1)}(s) + 4\hat{w}(s) = \hat{F}\delta(s), \quad -\infty < s < \infty;$
- $\lim_{s \to \pm\infty} \hat{w}(s) = 0; \quad \lim_{s \to \pm\infty} \hat{w}^{(1)}(s) = 0;$

General solution ($\Delta \neq 0$)

- $\hat{w}(s) = \hat{w}^-(s) = \dfrac{\hat{F}}{B_5} \dfrac{B_2 e^{(A_4 - B_5)s/2} - B_1 e^{(A_4 + B_5)s/2}}{B_1 B_2}, \quad for\ s \leq 0;$
- $\hat{w}(s) = \hat{w}^+(s) = \dfrac{\hat{F}}{B_6} \dfrac{B_4 e^{-(A_4 + B_6)s/2} - B_3 e^{-(A_4 - B_6)s/2}}{B_3 B_4}, \quad for\ s \geq 0;$

where:

- $B_1 = \dfrac{\beta}{A_4} + A_4^2 - A_4 B_5; \quad B_2 = \dfrac{\beta}{A_4} + A_4^2 + A_4 B_5; \quad B_5 = \mathrm{i}\sqrt{A_4^2 + 8\alpha - 2\beta/A_4};$
- $B_3 = \dfrac{\beta}{A_4} - A_4^2 - A_4 B_6; \quad B_4 = \dfrac{\beta}{A_4} - A_4^2 + A_4 B_6; \quad B_6 = \mathrm{i}\sqrt{A_4^2 + 8\alpha + 2\beta/A_4};$
- $A_4(\alpha, \beta) = \dfrac{1}{\sqrt{3}} \sqrt{\dfrac{16(\alpha^2 + 3)}{f(\alpha, \beta)} + f(\alpha, \beta) - 8\alpha};$
  - $f(\alpha, \beta) = \sqrt[3]{\dfrac{27}{2}\beta^2 + 64\,\alpha(\alpha^2 - 9) + 3\dfrac{\sqrt{3}}{2}\sqrt{-\Delta(\alpha, \beta)}};$
    - $\Delta(\alpha, \beta) = 16384\left(\alpha^2 - 1\right)^2 - 256\,\alpha\left(\alpha^2 - 9\right)\beta^2 - 27\beta^4$

Figure 5.4: Synoptic chart of the universal steady-state analytical solution of the beam-Pasternak foundation system. Corresponding responses are plotted in Figs. 5.8-5.11.

resumed in synoptic form in the sketch provided in Fig. 5.4, where all the necessary ingredients are included. The representation and interpretation of such achieved analytical steady-state solution is going to be presented and discussed in detail in Section 5.3, but, first, singular cases of the dynamic response are further commented in Section 5.2.3 below.

Notice that, despite for these singular cases, the achieved analytical solution provides a universal representation for all the regular solution instances, namely Cases (1), (2) and (3) with $\Delta \neq 0$ in Fig. 5.2. This is a main achievement of the present derivation, with respect to the previous cited attempts from the existing literature.

From the final expression of the solution in Eqs. (5.46), it is straightforward to derive the normalized response characteristics (Eqs. (5.16)) at the point underneath the load ($s{=}0$), which take the following analytical representations:

$$\hat{w}(0){=}\hat{F}\,\frac{B_2{-}B_1}{B_1B_2B_5}=2\hat{F}\,\frac{A_4}{B_1B_2}=\hat{F}\,\frac{2A_4^3}{2A_4^6{+}8\alpha A_4^4{+}\beta^2}; \tag{5.47a}$$

$$\hat{\theta}(0){=}\hat{F}\,\frac{B_2(A_4{-}B_5){-}B_1(A_4{+}B_5)}{2B_1B_2B_5}=\hat{F}\,\frac{A_4\beta}{2A_4^6{+}8\alpha A_4^4{+}\beta^2}; \tag{5.47b}$$

$$\hat{M}(0){=}\hat{F}\,\frac{B_2(A_4{-}B_5)^2-B_1(A_4{+}B_5)^2}{4B_1B_2B_5}=\hat{F}\,\frac{-A_4^3\,(A_4^2{+}4\alpha)}{2A_4^6{+}8\alpha A_4^4{+}\beta^2}; \tag{5.47c}$$

$$\hat{S}(0^-){=}\hat{F}\,\frac{B_2(A_4{-}B_5)^3{-}B_1(A_4{+}B_5)^3}{8B_1B_2B_5}{=}\frac{\hat{F}}{2}\left(\frac{A_4\beta(A_4^2{+}4\alpha)}{2A_4^6{+}8\alpha A_4^4{+}\beta^2}{-}1\right); \tag{5.47d}$$

$$\hat{S}(0^+){=}\hat{F}\,\frac{B_3(A_4{-}B_6)^3{-}B_4(A_4{+}B_6)^3}{8B_3B_4B_6}{=}\frac{\hat{F}}{2}\left(\frac{A_4\beta(A_4^2{+}4\alpha)}{2A_4^6{+}8\alpha A_4^4{+}\beta^2}{+}1\right). \tag{5.47e}$$

which will be used in the later illustrations in Section 5.3.

5.2.3 Singular cases

The analytical solution in Eq. (5.46), provided in parametric form, is able to represent the response of the system everywhere in the domain of system parameters α and β, except for two singular situations (Cases (4)-(5) and Case (6) in Table 5.1 and Figs. 5.2-5.3):

- the first considered singular instance corresponds to Case (6), namely $\Delta{\geq}0$, with $\alpha{\geq}1$ and $\beta{=}0$, and is referred to the occurrence in which coefficient A_4 becomes null (situation which also includes the case when coefficients $B_i,\ i{=}1,2,3,4$, may vanish);
- the second considered singular situation occurs when B_5 or B_6, which appear in the denominators of $\hat{w}^-(s)$ and $\hat{w}^+(s)$, respectively, become null; from their definitions given in Eqs. (5.44e) and (5.44f), B_5 or B_6 may become null if and only if poles $q_1,\ q_2$ and $q_3,\ q_4$ come to coincide, respectively, that is if $\Delta{=}0$ (Cases (4)-(5)).

For these two specific occurrences, treated in the following, the solution has to be derived independently from Eq. (5.46), leading to the derivation of the *critical velocity* and of the *critical damping* for a beam-Pasternak foundation system, respectively.

Undamped supercritical stage and critical velocity

As earlier mentioned in Subsection 5.2.2, the singular case of $A_4(\alpha,\beta)$ becoming null must be separately treated from the above derived general formulation.

As it may be checked from Eqs. (5.39), this situation occurs for $\beta{=}0$ and $\alpha{\geq}1$, corresponding to Case (6) in Table 5.1 and Figs. 5.2-5.3. The resulting expressions of the four real roots of $P(q)$ become:

$$q_1 = -a_1 = -\sqrt{2}\sqrt{\alpha - \sqrt{\alpha^2 - 1}}; \quad q_2 = a_1 = \sqrt{2}\sqrt{\alpha - \sqrt{\alpha^2 - 1}}; \quad \text{(5.48a)}$$

$$q_3 = -a_3 = -\sqrt{2}\sqrt{\alpha + \sqrt{\alpha^2 - 1}}; \quad q_4 = a_3 = \sqrt{2}\sqrt{\alpha + \sqrt{\alpha^2 - 1}}. \quad \text{(5.48b)}$$

In deriving the non-dimensional solution of Eq. (5.14) in case of real roots, the first step is to avoid the singularity on the integration path by deforming the contour in a small, semicircular path (indentation) either above or below the poles (in the sense of Cauchy principal value, see Duffy 2004 [78]). Such an indentation will include or exclude a singularity from the contour of integration, depending on whether the overall closure of the contour is above or below the real axis. The indentations of the paths represented in Fig. 5.3f are determined in continuity with the representation in Fig. 5.3c, i.e. by including the same poles, having now null imaginary parts ($\beta{=}0$), within the corresponding contours.

Then, the non-dimensional solution of Eq. (5.14) for this singular case is obtained as:

$$\hat{w}^-(s) = -\mathrm{i}\hat{F}\,\frac{e^{-\mathrm{i}a_1 s} - e^{\mathrm{i}a_1 s}}{-2a_1(a_1^2 - a_3^2)} = \hat{F}\,\frac{\sin(a_1 s)}{a_1(a_1^2 - a_3^2)}, \quad \text{for } s \leq 0; \quad \text{(5.49a)}$$

$$\hat{w}^+(s) = \mathrm{i}\hat{F}\,\frac{e^{-\mathrm{i}a_3 s} - e^{\mathrm{i}a_3 s}}{-2a_3(a_3^2 - a_1^2)} = \hat{F}\,\frac{\sin(a_3 s)}{a_3(a_1^2 - a_3^2)}, \quad \text{for } s \geq 0. \quad \text{(5.49b)}$$

Eqs. (5.49) show that resonance occurs as α approaches 1 ($a_1{=}a_3{=}\sqrt{2}$, double pole on the real axis), in the sense that the amplitude of the traveling waves, which increases without bound, can no longer be defined. The nonexistence of the solution may be also justified by the nonexistence of the integral in Eq. (5.21) for $\alpha{=}1$:

$$\hat{w}(s) = \frac{\hat{F}}{2\pi}\int_{-\infty}^{+\infty}\frac{e^{\mathrm{i}sq}}{P(q)}\,dq = \frac{\hat{F}}{2\pi}\int_{-\infty}^{+\infty}\frac{e^{\mathrm{i}sq}}{(q-\sqrt{2})^2(q+\sqrt{2})^2}\,dq; \quad \text{(5.50)}$$

even in the sense of Cauchy principal value, as it was shown by Buta and Jones (1964) [47] and by Achenbach and Sun (1965) [2].

By inverting Eq. (5.10), with $\alpha{=}1$, the velocity of the moving load at which such instability occurs, i.e. the critical velocity for a beam-Pasternak founda-

tion system, is obtained as

$$
\begin{aligned}
v_{cr,_P} &= \sqrt{v_{cr,_W}^2 + \frac{G_P}{\mu}} = v_{cr,_W}\sqrt{1+g_P} = \\
&= v_{cr,_W}\sqrt{1+\sqrt{\frac{G_P}{k}}\sqrt{\frac{G_P}{EJ}}} = v_{cr,_W}\sqrt{1+\lambda^2\frac{G_P}{k}};
\end{aligned}
\tag{5.51}
$$

where g_P and $v_{cr,_W}$ were defined in Eq. (5.12) and Eq. (5.13), respectively. The expression of the critical velocity in Eq. (5.51) is the same as that reported by Kerr (1972) [158], by Mallik (2006) [186] and by Basu and Kameswara Rao (2013) [17]. Eq. (5.51) reveal three different interpretation trends for Pasternak/Winkler critical velocity ratio $v_{cr,_P}/v_{cr,_W}$, as illustrated in Fig. 5.5 and discussed below.

Indeed, a graphical description of the Pasternak/Winkler critical velocity ratio, expressed as a function of the stiffness parameters of the beam-foundation system according to the three expressions in the second line of Eq. (5.51), is provided in Fig. 5.5. In particular, as it can be appreciated in Fig. 5.5a, the critical velocity for a beam-Pasternak foundation system is represented by an increasing function of parameter g_P in Eq. (5.12), i.e. of Pasternak modulus G_P, and results always larger than that for a Winkler beam-foundation system, which may be taken as a sub-case by setting $G_P{=}0$.

A graphical description of the Pasternak/Winkler critical velocity ratio, expressed as a function of the stiffness parameters of the beam-foundation system according to Eq. (5.51), is shown in Fig. 5.5. The Pasternak/Winkler critical velocity ratio depending on the ratios between Pasternak modulus G_P and both Winkler foundation coefficient k and beam bending stiffness EJ, respectively. Given the high initial steepness of the curves in these plots, the velocity ratio grows rather quickly, even for small values of the Pasternak/Winkler coefficient ratio, meaning that the threshold of the critical velocity may be raised by considering even only a little amount of shear interaction between the foundation springs. Thus, the shear interaction linked to G_P leads to a beneficial effect in structural terms by increasing the critical velocity, since the whole model stiffness is increased.

Finally, from a further observation of the graphs in Figs. 5.5c, where the ratio between the two critical velocities has been represented for feasible physical ranges of wave number λ and foundation moduli ratio G_P/k, it is possible to appreciate that the ratio of velocities increases in a weakly nonlinear fashion, with respect to foundation moduli ratio G_P/k. In addition, for compliant beams (high values of λ) it increases more than for stiff beams (small values of λ).

For $\alpha{>}1$ and $\beta{=}0$, both waves are described by finite-amplitude undamped harmonic oscillations, violating the far-field boundary conditions in Eq. (5.9),

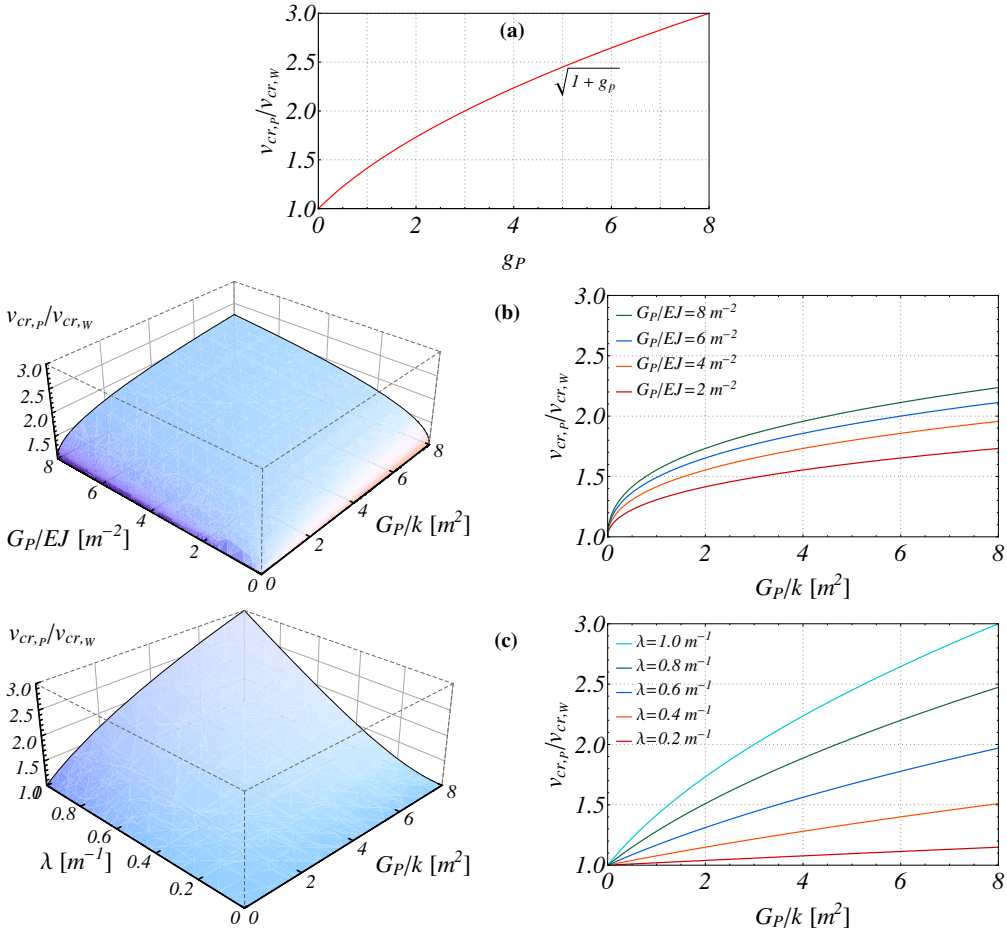

Figure 5.5: Representation of Pasternak/Winkler critical velocity ratio as a function of: (**a**) non-dimensional Pasternak modulus $g_P{=}G_P/\sqrt{4kEJ}$; (**b**) foundation moduli ratio G_P/k and Pasternak modulus/bending stiffness ratio G_P/EJ; (**c**) foundation moduli ratio G_P/k and wave number λ.

which state a zero response at $\pm\infty$. Hence, the undamped response of the beam-foundation system at the supercritical velocities cannot be evaluated by the present approach, namely the beam never attains a steady-state condition for the ideal undamped case. The case $\alpha{>}1$ and $\beta{=}0$ (corresponding to the purple line in Fig. 5.2) is thus consistent with Kerr's (1972) [158] conclusion that, for $v{=}0$ (static case), $-G_P$, which corresponds to an axial compressive force in the analysis of Kerr, has to be smaller than $\sqrt{4kEJ}$ (buckling), and even smaller if the velocity is not null. Moreover, notice that, when there is an even slight amount of viscous damping, Kerr's restriction does not apply, since the system is able to dissipate energy by virtue of its infinite extension. Therefore, a physical realistic solution exists in whole region (3) of Fig. 5.2,

that is, suddenly, this restriction on G_P (and also v) does not apply, no matter how negatively large G_P is, in region (3), arbitrarily close to half-line (6).

Critical damping

By looking at the classification reported in Table 5.1, the situation for which two poles come to coincide or, in other words a pole of second-order appears, is determined by the discriminant Δ in Eq. (5.30) becoming zero. Such occurrence may appear twice, either for $q_1{=}q_2$, i.e. for $B_5{=}0$ (Case (5), $\Delta{=}0$ and $\alpha{>}{-}1$, red curve in Fig. 5.2), or for $q_3{=}q_4$, i.e. for $B_6{=}0$ (Case (4), $\Delta{=}0$ and $\alpha{<}{-}1$, green curve in Fig. 5.2).

Such two cases describe the transition from an evanescent wave to a propagating leftward wave ($\hat{w}^-(s)$), Case (5), or to a propagating rightward wave ($\hat{w}^+(s)$), Case (4), respectively. Indeed, since these special responses are characterized by a zero frequency of oscillation, their wavelength becomes infinite. This condition arises in the case of *critical damping* (Basu and Kameswara Rao, 2013 [17]).

The critical damping condition may be determined from the expression of $\Delta(\alpha,\beta)$ in Eq. (5.30) by solving the polynomial equation $\Delta(\alpha,\beta){=}0$ (biquadratic in β) with respect to β, which, by considering only real and non-negative values of β in Eq. (5.11), gives

$$\beta_{cr,P} = \frac{8\sqrt{2}}{3\sqrt{3}}\sqrt{\alpha(9-\alpha^2)+\sqrt{(\alpha^2+3)^3}}; \tag{5.52}$$

and which, rewritten in terms of the physical parameters of the system, provides the expression of the critical damping coefficient for a Pasternak elastic foundation:

$$\begin{aligned} c_{d\,cr,P} = {} & 2\sqrt{k\mu}\cdot\frac{\sqrt{2}}{3\sqrt{3}}\frac{v_{cr,W}}{v}\cdot \\ & \cdot\sqrt{\left(\frac{v^2-G_P/\mu}{v_{cr,W}^2}\right)\left(9-\left(\frac{v^2-G_P/\mu}{v_{cr,W}^2}\right)^2\right)+\left(\left(\frac{v^2-G_P/\mu}{v_{cr,W}^2}\right)^2+3\right)^{\frac{3}{2}}}; \end{aligned} \tag{5.53}$$

where $2\sqrt{k\mu}$ represents a reference critical damping coefficient of a classical spring-mass system (see Eq. (5.12)).

As already noticed by Frýba (1972) [105] for a Winkler-type foundation ($G_P{=}0$), Eq. (5.53) points out that, in addition to the mechanical parameters of the beam-Pasternak foundation system, the critical damping coefficient depends also upon moving load velocity v. Notice that, for $G_P{=}0$, the value of the critical damping coefficient of a Winkler foundation is recovered (see

Fryba, 1972 [105]):

$$c_{d\,cr,W} = 2\sqrt{k\mu}\,\cdot\,\frac{\sqrt{2}}{3\sqrt{3}}\sqrt{\left(9-\left(\frac{v}{v_{cr,W}}\right)^4\right)+\left(\frac{v_{cr,W}}{v}\right)^2\left(\left(\frac{v}{v_{cr,W}}\right)^4+3\right)^{\frac{3}{2}}}. \tag{5.54}$$

Furthermore, for a Winkler foundation (G_P=0, thus $\alpha\geq 0$) or for a Pasternak elastic foundation subjected to the condition $G_P>\sqrt{4kEJ}$ (equivalent to $\alpha>-1$), given a certain damping coefficient c_d, there exists only one value of moving load velocity for which such value of damping becomes critical; this corresponds to a leftward beam response ($s<0$) characterized by a null frequency (B_5=0) and a corresponding infinite wavelength.

Within such a situation, by applying Eq. (5.28), the residue of the integrand in Eq. (5.27) for coincident poles (poles of second-order) can be computed as ($j\neq k\neq l$):

$$\text{Res}\left\{\frac{e^{\mathrm{i}sq}}{(q-q_j)(q-q_k)(q-q_l)^2};q_l\right\}=\frac{q_j+q_k-2q_l+(q_j-q_l)(q_k-q_l)\mathrm{i}s}{(q_l-q_j)^2(q_l-q_k)^2}e^{\mathrm{i}sq_l}. \tag{5.55}$$

According to the graphical representation of the poles provided in Fig. 5.3d and to Eq. (5.55), the critically damped non-dimensional deflection solution for this singular case becomes for $s\leq 0$:

$$\hat{w}^-_{\beta_{cr}}(s)=-\mathrm{i}\hat{F}\,\frac{q_3+q_4-2q_1+(q_3-q_1)(q_4-q_1))\mathrm{i}s}{(q_1-q_3)^2(q_1-q_4)^2}\,e^{\mathrm{i}sq_1},\quad \text{for } s\leq 0; \tag{5.56}$$

and, by a further manipulation:

$$\hat{w}^-_{\beta_{cr}}(s)=\hat{F}\,\frac{2A_4-B_1 s}{B_1^2}\,e^{\frac{A_4}{2}s},\quad \text{for } s\leq 0; \tag{5.57}$$

where A_4 and B_1 are still given in Eq. (5.39) and Eq. (5.44a), respectively.

As an interesting new insight of the present derivation, for a Pasternak elastic foundation with $\alpha<-1$, the formula in Eq. (5.53) provides the opportunity for a second possible moving load velocity value at which a critical damping may be attained, pertaining this time to the rightward wave ($s>0$, B_6=0). The expression of the solution in this case, represented in the complex plane in Fig. 5.3e, is given as follows for $s\geq 0$:

$$\hat{w}^+_{\beta_{cr}}(s)=\mathrm{i}\hat{F}\,\frac{q_1+q_2-2q_3+(q_1-q_3)(q_2-q_3)\mathrm{i}s}{(q_1-q_3)^2(q_2-q_3)^2}\,e^{\mathrm{i}sq_3},\quad \text{for } s\geq 0; \tag{5.58}$$

and then its final expression becomes

$$\hat{w}^+_{\beta_{cr}}(s)=\hat{F}\,\frac{2A_4+B_3 s}{B_3^2}\,e^{-\frac{A_4}{2}s},\quad \text{for } s\geq 0; \tag{5.59}$$

where A_4 and B_3 are still given in Eq. (5.39) and Eq. (5.44c), respectively.

These occurrences are illustrated in Fig. 5.6a, where the two-branch curves of critical damping ratio $\zeta_{cr,P}=c_{d\,cr,P}/2\sqrt{k\mu}$ for a Pasternak foundation versus velocity ratio $v/v_{cr,W}$ are depicted. Then, given an arbitrary value of damping, represented in Fig. 5.6a by a black dashed horizontal line, there exist two distinct values of velocity for which such a value of damping becomes critical, for the forward wave ($\alpha<-1$) and for the backward wave ($\alpha>-1$), respectively. Notice that while such second occurrence had been provided by the formula derived by Basu and Kameswara Rao (2013) [19], the first one was not. In fact, Eq. (5.52) generalized the formula derived by Basu and Kameswara Rao (2013) [19] for the critical damping ratio, by also providing the first branch of the critical damping curve, by virtue of general character of the present formulation. The dependence of $\zeta_{cr,P}$ on velocity ratio $v/v_{cr,W}$ and non-dimensional Pasternak modulus g_P is also shown in Fig. 5.6b.

Therefore, on both branches of the critical damping curve, one of the two functions describing the beam-Pasternak foundation response is represented by an exponentially decaying function times a linear function of normalized position from the moving load.

Finally, case $\alpha=-1$, leading to two pairs of double purely-imaginary poles, implies that two new forms (5.57) and (5.59) exist simultaneously.

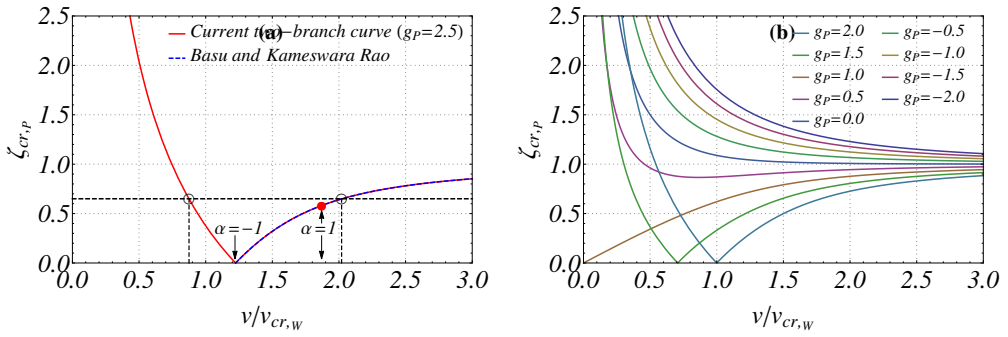

Figure 5.6: Two-branch curve of critical damping ratio $\zeta_{cr,P}$ as a function of velocity ratio $v/v_{cr,W}$ (**a**). At a given non-zero value of damping, as that marked by a dashed horizontal line, there always appear two values of velocity for which such damping becomes critical, one for the forward wave (left branch, $\alpha<-1$) and the other for the backward wave (right branch, $\alpha>-1$). The red dot marks the value of critical damping at the critical velocity ($\alpha=1$). Critical damping ratio curves as a function of both velocity ratio $v/v_{cr,W}$ and non-dimensional Pasternak modulus g_P (**b**).

5.3 Results and interpretation

The explicit universal analytical solution in Eq. (5.46) reveals that the steady-state response of the beam non-proportionally depends upon both two charac-

teristic parameters α, β defined in Section 5.1.1. According to their definitions provided in Eqs. (5.10) and (5.11), the two parameters are in turn functions of moving load velocity v. By combining such definitions, it results that the parametric variation of α and β with the moving load velocity may be represented by parabolas with horizontal axes in the α, β parametric plane.

The expression of such parabolas may be written in explicit form as follows:

$$\alpha = \left(\frac{\sqrt{k\mu}/4}{c}\right)^2 \beta^2 - \frac{G_P}{\sqrt{4kEJ}} = \frac{1}{64\zeta^2}\,\beta^2 - g_P; \tag{5.60}$$

where non-dimensional Pasternak modulus of the foundation g_P, defined in Eq. (5.12), determines the position of the parabola's vertex, and damping ratio ζ, also defined in Eq. (5.12), controls the steepness of the parabolas.

Such representation is useful to recognize the type of steady-state response, according to the nature of the poles, which depend on parameters α, β (Fig. 5.2), i.e. as a function of the characteristic physical parameters of the beam-Pasternak foundation system, as shown in Fig. 5.7. There, the two branches characterized by a null discriminant (Δ=0) have been represented with a dot-dashed curve. The adopted ranges of parameters employed for the parametric analysis illustrated below have been represented in Fig. 5.7.

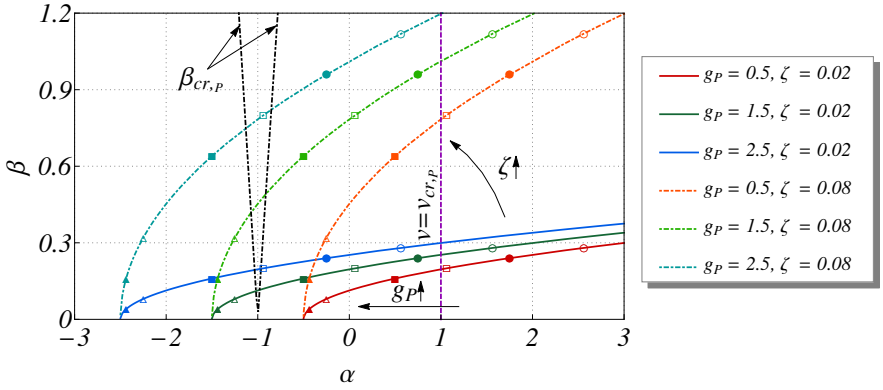

Figure 5.7: Graphical representation of the parabolic parametric variation of beam-foundation system parameters α, β as a function of normalized Pasternak modulus g_P, damping ratio ζ and moving load velocity v: ▲ v=0.50 $v_{cr,W}$, △ v=0.75 $v_{cr,W}$, ■ v=1.00 $v_{cr,W}$, □ v=1.25 $v_{cr,W}$, ● v=1.50 $v_{cr,W}$, ○ v=1.75 $v_{cr,W}$. Recall that, from Fig. 5.5, $v_{cr,P}$=$v_{cr,W}\sqrt{1+g_P}$ at α=1, as marked by the vertical dashed line. For the reference mechanical parameters see Table 5.2.

The analysis reported in Subsection 5.2.2 has illustrated that if point (α, β) lies below either the green curve or the red curve in Fig. 5.2, namely within fields (1) and (3) in Fig. 5.2, both backward and forward waves are either evanescent or propagating away from the load (source), respectively; on the other hand, if the (α, β) point is placed in the region above both curves, namely

within region (2) of the parametric space in Fig. 5.2, the backward wave becomes evanescent, while the forward wave is propagating. Furthermore, as the (α, β) point approaches the purple half-line in Fig. 5.2, namely region (6), which is characterized by $A_4{=}0$, the exponential decay, ruled by A_4, becomes smaller and smaller; consequently, the range of s with non-negligible wave amplitude is expected to grow, producing waves with very large spatial extension.

To verify the above mentioned a priori considerations and to accurately investigate the effect of the characteristic parameters of the system on the response behavior, a parametric study can be carried out, at this stage, as reported in the following.

5.3.1 Response characteristics along the beam

The assumed mechanical properties of the beam-foundation system are again those listed in Table 5.2. The load is taken acting downward ($F{<}0$). The normalizing factor for representing the normalized steady-state response is now chosen as follows:

$$w_0 = \frac{F}{\lambda^3 EJ}; \tag{5.61}$$

in order to consistently obtain $\hat{F}{=}{-}1$ in Eq. (5.46).

Reference mechanical properties of the beam-Pasternak foundation system			
Young's modulus	E	210	GPa
Central moment of inertia	J	3055×10^{-8}	m^4
Mass per unit length	μ	60	kg/m
Winkler foundation modulus	k	250	$\mathrm{kN/m}^2$
Wave number (Winkler foundation)	λ	3141×10^{-4}	m^{-1}
Reference damping coefficient (spring-mass system)	$2\sqrt{k\mu}$	7746	$\mathrm{Ns/m}^2$

Table 5.2: Reference mechanical properties of the beam-Pasternak foundation system, assumed for the representations in Figs. 5.8-5.11.

A graphical representation of the complete normalized response (deflection, cross-section rotation, bending moment, shear force) is provided in Figs. 5.8-5.11, for various values of velocity of the moving load (v), non-dimensional Pasternak modulus (g_P) and damping ratio (ζ). The considered range of velocities is sufficiently broad, namely it goes from 0.5 to 1.75 times the critical velocity of a beam resting on a Winkler elastic foundation ($v_{cr,W}$). Two values of damping factor have been selected, one indicating a lightly damped system ($\zeta{=}2\%$) and the other a moderately damped system ($\zeta{=}8\%$). Three values of normalized Pasternak modulus have been taken into account ($g_P{=}0.5,\ 1.5,\ 2.5$), in order to show how this parameter may affect the response of the system.

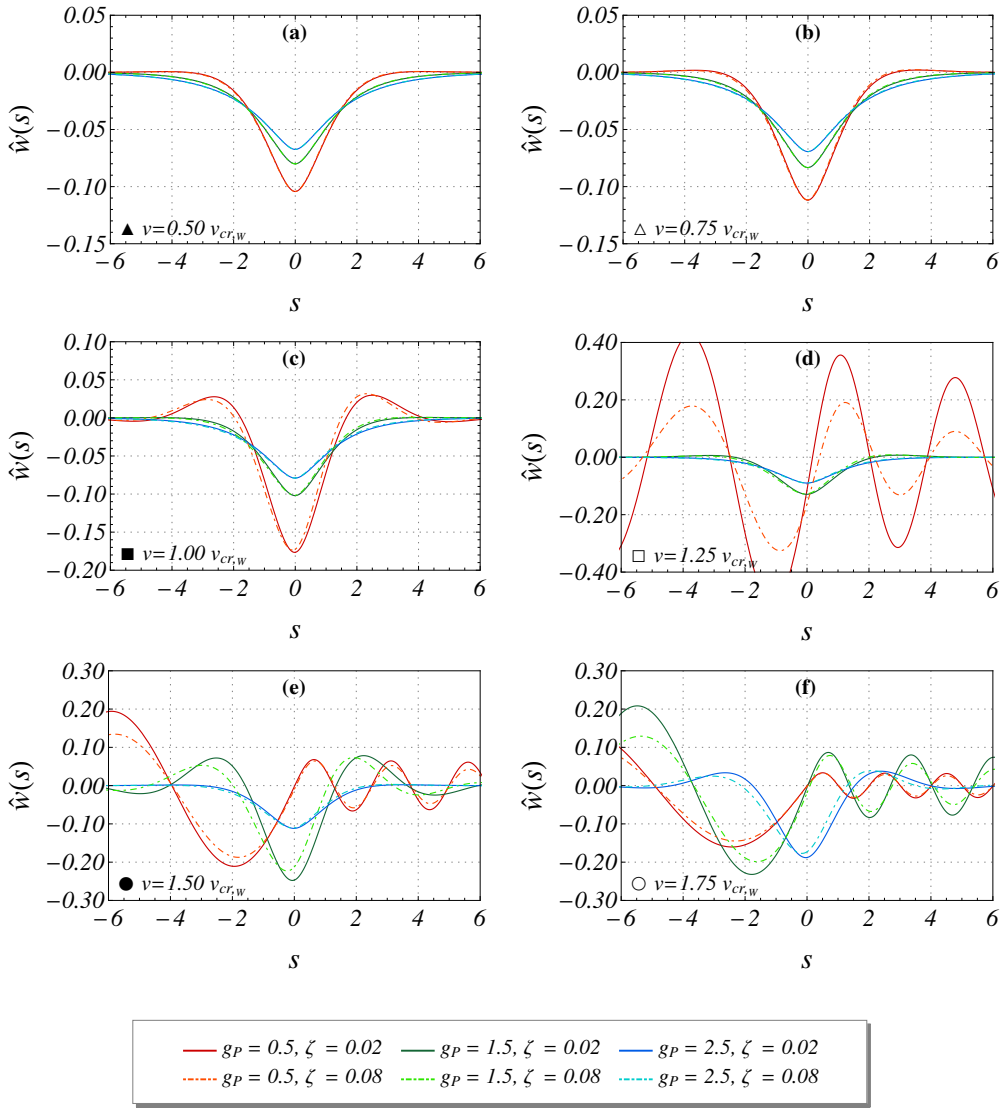

Figure 5.8: Normalized deflection $\hat{w}(s)$ for various values of normalized Pasternak modulus g_P and damping ratio ζ at variable moving load velocity v: **(a)** ▲ v=0.50 $v_{cr,W}$; **(b)** △ v=0.75 $v_{cr,W}$; **(c)** ■ v=1.00 $v_{cr,W}$; **(d)** □ v=1.25 $v_{cr,W}$; **(e)** ● v=1.50 $v_{cr,W}$; **(f)** ○ v=1.75 $v_{cr,W}$. For the reference mechanical parameters see Table 5.2.

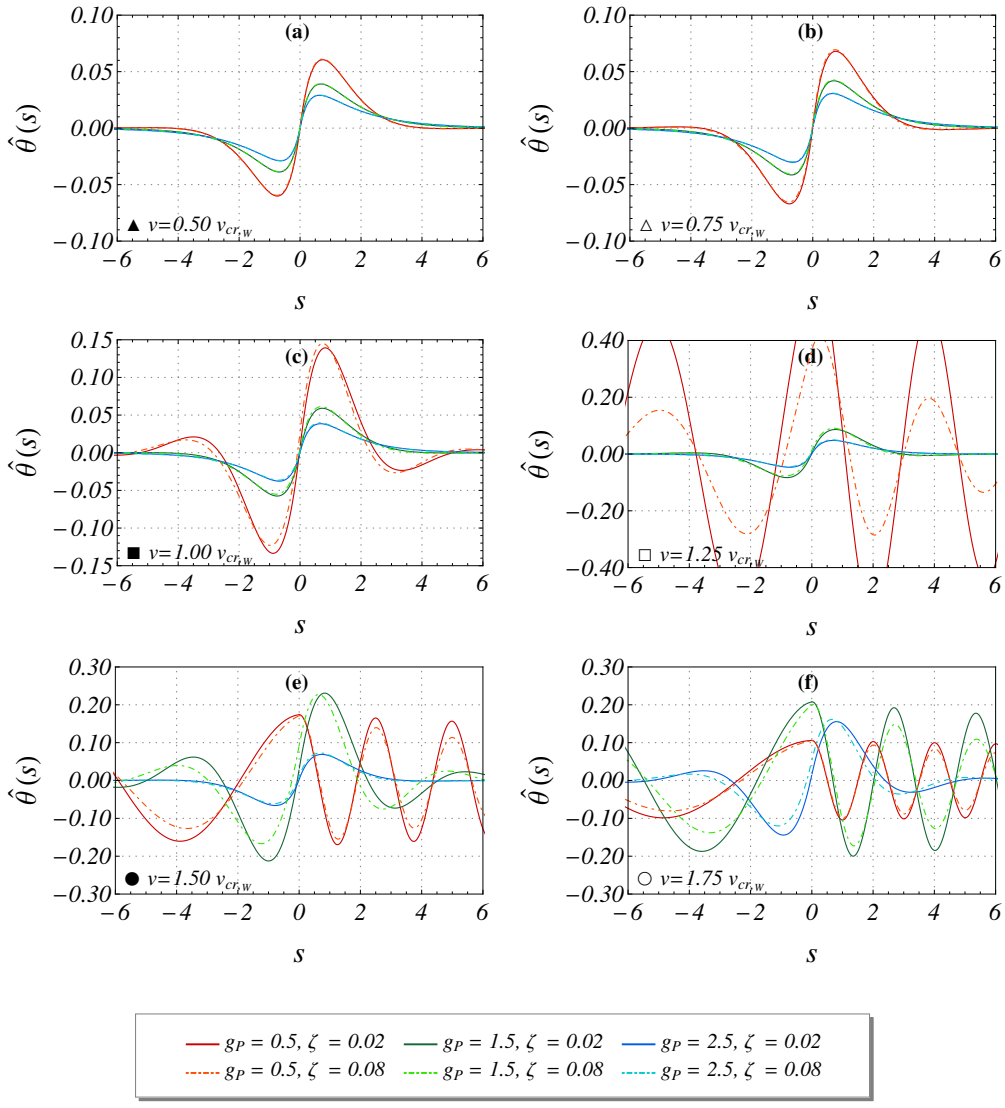

Figure 5.9: Normalized rotation $\hat{\theta}(s)$ for various values of normalized Pasternak modulus g_P and damping ratio ζ at variable moving load velocity v: **(a)** ▲ v=0.50 $v_{cr,W}$; **(b)** △ v=0.75 $v_{cr,W}$; **(c)** ■ v=1.00 $v_{cr,W}$; **(d)** □ v=1.25 $v_{cr,W}$; **(e)** ● v=1.50 $v_{cr,W}$; **(f)** ○ v=1.75 $v_{cr,W}$. For the reference mechanical parameters see Table 5.2.

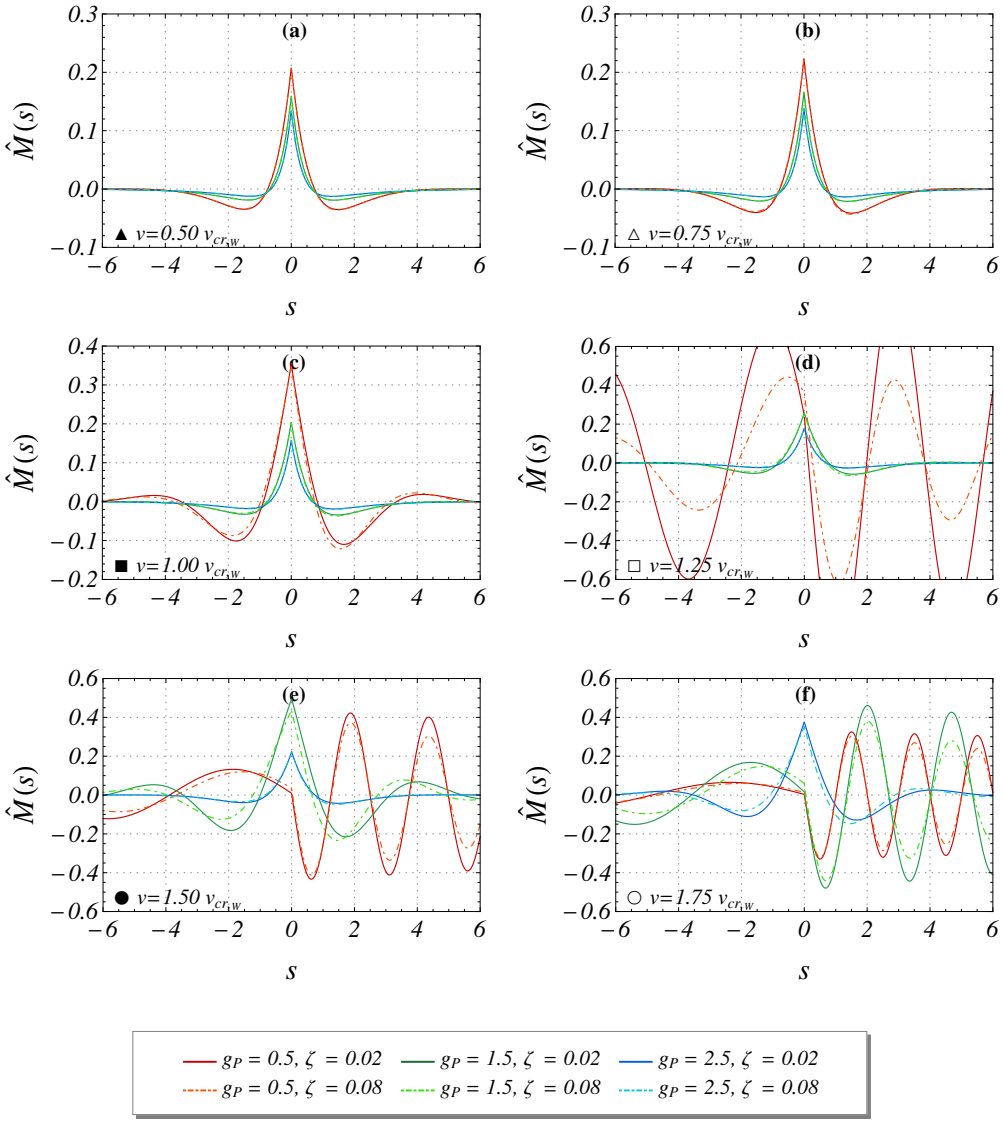

Figure 5.10: Normalized bending moment $\hat{M}(s)$ for various values of normalized Pasternak modulus g_P and damping ratio ζ at variable moving load velocity v: **(a)** ▲ v=0.50 $v_{cr,W}$; **(b)** △ v=0.75 $v_{cr,W}$; **(c)** ■ v=1.00 $v_{cr,W}$; **(d)** □ v=1.25 $v_{cr,W}$; **(e)** ● v=1.50 $v_{cr,W}$; **(f)** ○ v=1.75 $v_{cr,W}$. For the reference mechanical parameters see Table 5.2.

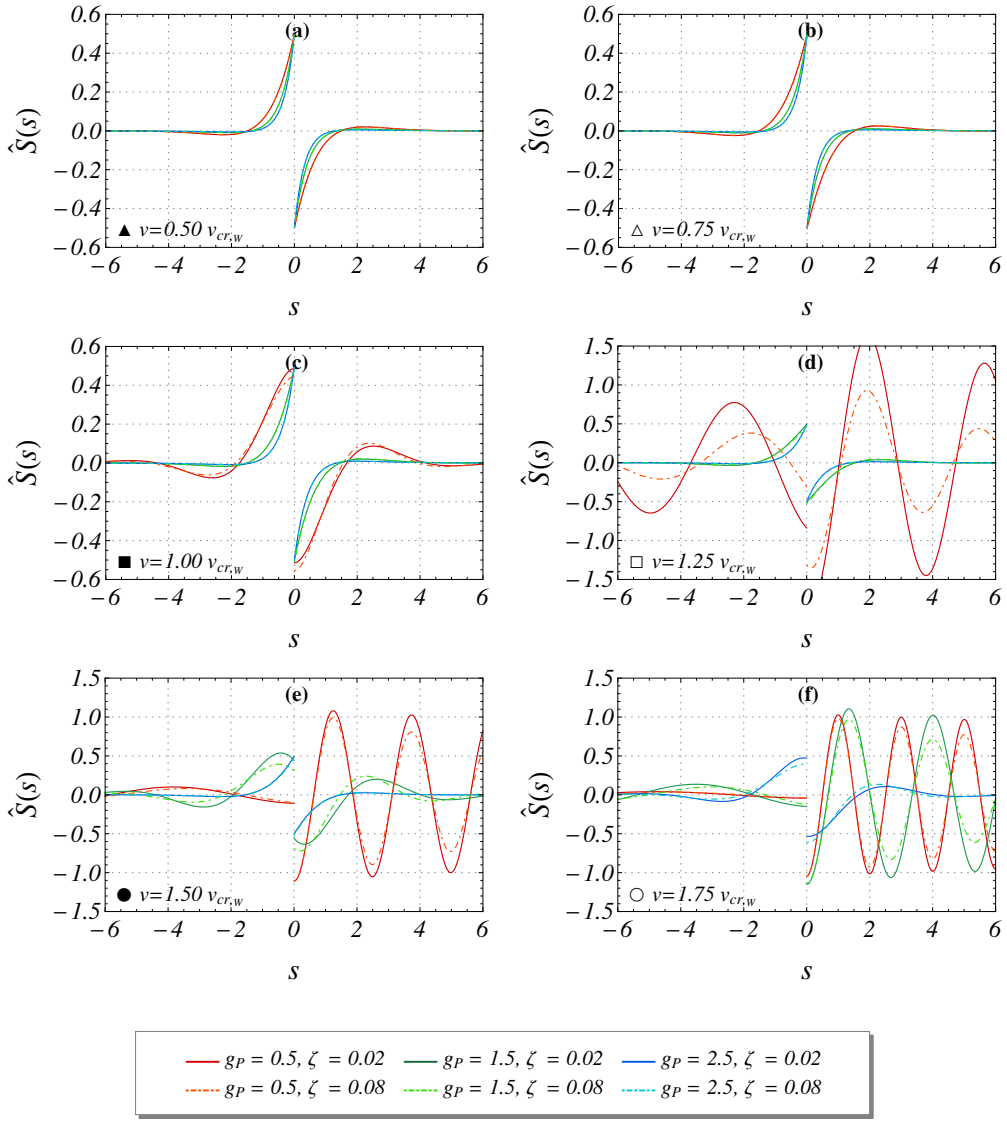

Figure 5.11: Normalized shear force $\hat{S}(s)$ for various values of normalized Pasternak modulus g_P and damping ratio ζ at variable moving load velocity v: **(a)** ▲ v=0.50 $v_{cr,W}$; **(b)** △ v=0.75 $v_{cr,W}$; **(c)** ■ v=1.00 $v_{cr,W}$; **(d)** □ v=1.25 $v_{cr,W}$; **(e)** ● v = 1.50 $v_{cr,W}$; **(f)** ○ v = 1.75 $v_{cr,W}$. For the reference mechanical parameters see Table 5.2.

By observing the curves depicted in Figs. 5.8-5.11, some common features of all the represented quantities may be underlined. First, by considering values of α approximately lower than 0.5, corresponding to either a low velocity or a high Pasternak modulus, damping does not affect much the steady-state response, which turns out essentially symmetric with respect to the moving load position. On the contrary, for larger values of α, damping is shown to be more influential, both in reducing the amplitudes of both waves and in changing their phase; in fact, in this case the response becomes noticeably non-symmetric. Secondly, in the presence of propagating waves, by increasing the velocity of the moving load, the frequency of oscillation of the backward wave decreases (i.e. by having a larger wavelength), while the contrary occurs for the forward wave.

As expected by the definition of α given in Eq. (5.10), for $\alpha>0$ the effect of the Pasternak modulus may be conceived as to be equivalent to converting the actual moving load velocity into a lower apparent velocity, with the Pasternak modulus being null (Winkler foundation). In addition, when the load velocity is near to the critical velocity ($\alpha=1$), for instance for the empty square marker on the red line in Fig. 5.7, the amplitude of the corresponding response quantities grows sharply (see red curves in Figs. 5.8d-5.9d-5.10d-5.11d).

By analyzing the normalized deflection shown in Figs. 5.8a-5.8f, for either low velocity or high Pasternak modulus (roughly speaking for $\alpha<0.5$), the results display a downward maximum displacement occurring beneath the moving load position ($s=0$), analogously to Fig. 5 reported by Kerr's (1972) [158], while as the velocity increases or the Pasternak modulus decreases, the maximum displacements, of the same amount both downward and upward, appear for a negative value of s, since displacements are larger behind than ahead of the moving load position. Such occurrence does not appear in the plots of the cross-section rotations, shown in Figs. 5.9a-5.9f, where a very slight difference between the amplitudes of the two waves may be observed.

Looking at the variations of the normalized bending moment and shear force, the maximum is again placed under the moving load for approximately $\alpha<0.5$, while for larger α a different trend may be captured, with respect to that of the deflection: the maximum values appear on the right of the moving load, that is for $s>0$. As expected, the bending moment plots in Figs. 5.10a-5.10f are continuous and exhibit a kink at the load position ($s=0$), whereas the shear force curves consistently display a jump discontinuity there.

5.3.2 Response characteristics at the point underneath the moving load

Figs. 5.12a-5.12c display the normalized response characteristics at the point underneath the load ($s=0$) provided in Eqs. (5.47), as a function of the moving load velocity, for various values of non-dimensional Pasternak modulus and

damping ratio. These results, in terms of deflection, may be compared to those by Watanabe (1981) [269], relative to the response of an infinite plate, for the undamped case only.

From the observation of these plots, an infinite response may be observed in correspondence of the critical velocity, when approaching the ideal undamped case; on the other hand, a finite peak of response is always displayed in the presence of damping. Regarding the effect of the Pasternak modulus, the already discussed effect of increasing the critical velocity is confirmed also by these latter representations.

Notice that for $\hat{F}<0$ (moving load acting downward), the normalized deflection results always negative ($\hat{w}(0)<0$) as the velocity grows, while both normalized rotation and bending moment remain always positive ($\hat{\theta}(0)<0$, $\hat{M}(0)<0$). The normalized left shear force ($S(0^-)$), initially positive, decreases progressively as the velocity increases, until it changes sign while approaching the supercritical range. On the other hand, the normalized right shear force ($S(0^+)$) remains always negative and for a moving load velocity getting close to the supercritical range its value is even larger than the moving load amplitude, in order to guarantee equilibrium with the left shear force. In case of a zero velocity (static configuration) the load is equally distributed among the left and right shear forces, while in correspondence of the limit situation of velocity going to infinity the load is totally sustained by the shear force acting on the right part of the beam ($S(0^+)$).

The plots of the normalized displacement and bending moment are characterized by an increasing amplitude as the velocity approaches the critical velocities, and by a very steep decrease towards null values at the post-critical conditions. Conversely, the normalized rotation and left and right shear forces display large increments before the critical velocity, and more slowly decrements after passing such a critical value.

In the present analysis, the influence of velocity, damping ratio and Pasternak modulus has been studied. The structural parameters of the beam and the Winkler foundation modulus have been taken as fixed. If one would attempt a parametric analysis involving the latter parameters, it is important to underline that they shall induce a double effect, because they affect not only the normalized response, but also the adopted normalization factors (λ, w_0, θ_0, M_0, S_0). Therefore, in order to analyze the physical sensitivity of the steady-state solution upon variations of such parameters, a non-normalized response or a different type of normalization should be considered.

5.4 Effective Perfectly Matched Layer

In the following a formulation and implementation for numerically solving the moving load problem ruled by Eq. (5.8) with far-field conditions in Eq. (5.9) is developed. Towards this scope, the present section describes an effective Perfectly Matched Layer approach for absorbing out-going stationary waves propagating from a finite elastic beam (fourth-order problem). In fact, the previously stated problem can be numerically solved by FEM techniques, as long as the infinite one-dimensional domain is again replaced by a finite do-

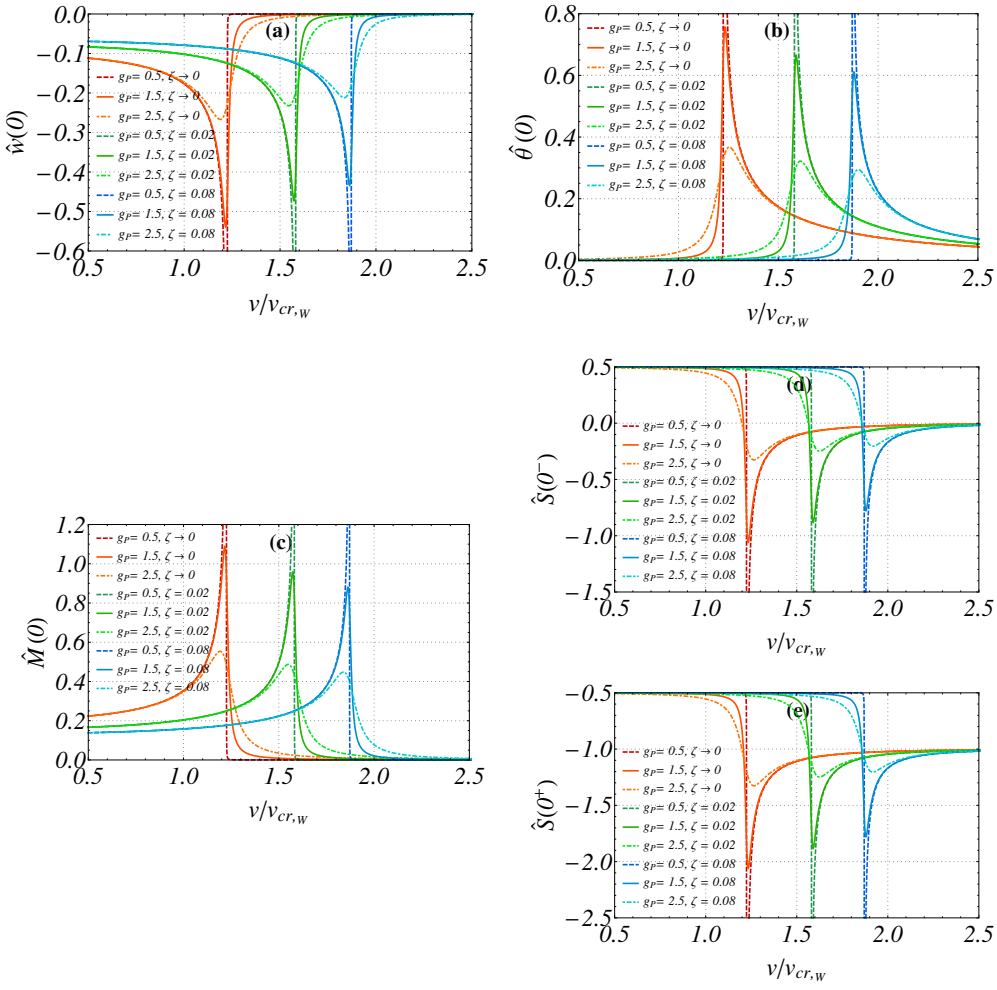

Figure 5.12: Variation of normalized deflection $\hat{w}(0)$ (a), rotation $\hat{\theta}(0)$ (b), bending moment $\hat{M}(0)$ (c) and shear forces $\hat{S}(0^-)$, $\hat{S}(0^+)$ (d), (e) at the point underneath the load (s=0), for various values of normalized Pasternak modulus g_P and damping ratio ζ, at variable moving load velocity v. For the reference mechanical parameters see Table 5.2.

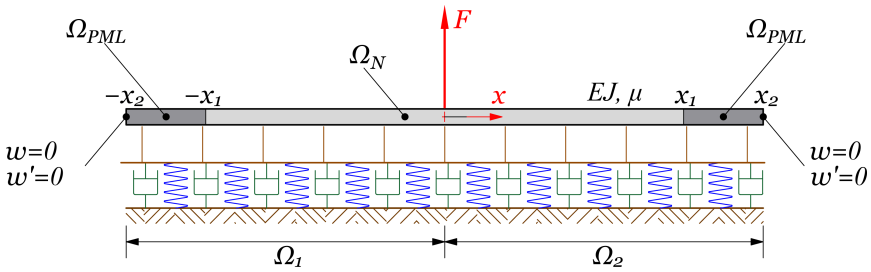

Figure 5.13: Geometrical scheme of computational beam domain of interest Ω_N, truncated by PML layer Ω_{PML}

.

main $\Omega{=}(-x_2, x_2)$, being a bounded, open, connected subset of $\mathbb{R}$.

Similarly to Chapter 4, let subset $\Omega_N{=}(-x_1, x_1)$ be the finite domain of interest, i.e. the region where an accurate approximation of the steady-state beam response is sought (see Fig. 5.13). Let complementary set $\Omega_{PML}{=}\Omega \setminus \Omega_N$ be the PML region surrounding the finite domain of interest, as illustrated in Fig. 5.13, showing two side regions $(-x_2, -x_1)$ and (x_1, x_2), both of length $x_2{-}x_1$ (coordinates $x_1,\ x_2$ are taken here both positive, as evident in Fig. 5.13). The following presentation in the first subsection forms a necessary background for the subsequent new developments reported in the second subsection.

5.4.1 Classic Perfectly Matched Layer

An explanation of why the classic PML approach, employed in Section 4.3.1 in the context of the taut string problem, is effective in simulating the behavior of the solution of an exterior problem, is provided in the present section. In addition, the justification of the inefficacy of a classic PML approach as an artificial boundary condition for the fourth-order beam problem is also addressed here.

The effect of the application of the transformation in Eq. (4.21) to Eq. (4.6a) leads to Eq. (4.23), whose analytical solution results as follows

$$\hat{w}(s) = \begin{cases} C_1\, e^{\eta_1\, s} + C_2\, e^{\eta_2\, s}, & \text{if } -x_1 < s < x_1 \\ C_1\, e^{\eta_1\, x(s)} + C_2\, e^{\eta_2\, x(s)}, & \text{otherwise;} \end{cases} \tag{5.62}$$

where $e^{\eta_i\,(\cdot)}$ $(i{=}1, 2)$ are the two fundamental solutions, η_1, η_2 represent the roots of the corresponding characteristic equation (4.20) and C_1, C_2 are the arbitrary integration constants.

In order the PML to be truly needed, it is assumed the roots to be in a complex conjugate pair $\eta_2{=}\overline{\eta}_1$(supercritical motion regime, Metrikine, 2004 [194]), which means that the solution exhibits a progressive wave pattern behind the

load with wavelength and spatial decay ruled by the imaginary and real part of η_1, respectively; the real part is assumed to be small, thus inducing a limiting spatial decay of the exponential functions. Under the condition of no divergence at infinity, the expression of exact solution $\hat{w}(s)$ results as follows (Metrikine, 2004 [194]):

$$\hat{w}(s) = 2\mathrm{i}\,\tilde{C}_1\, e^{\eta_1^R\, s}\sin\big(\eta_1^I\, s\big), \qquad 2\mathrm{i}\,\tilde{C}_1 \in \mathbb{R}; \tag{5.63}$$

where

$$\eta_1^R = \Re(\eta_1), \qquad \eta_1^I = \Im(\eta_1) \tag{5.64}$$

are the real and imaginary parts of root η_1, respectively, and $\tilde{C}_1$ is an arbitrary imaginary constant which depends on the moving load amplitude.

Now, let one consider the effect of the application of the PML for $s{<}{-}x_1$ (left PML). The variation of complex arguments $\eta_i\, x(s)$ ($i{=}1,2$) inside the left PML of the exponential functions has been displayed in a graph in Fig. 5.14a, where the effect of the amount of imaginary stretching $h(x)$, ruled by parameter H, on the arguments of the corresponding fundamental solutions has been depicted ($G{=}0$, $r{=}2$). By looking at Fig. 5.14a it may be noticed that the trends of the exponential functions in Eq. (5.62) is modified, similarly to a gradual rotation and a scaling of the positions of roots η_1, η_2. The effect of the domain termination in the PML with a support leads to the following condition:

$$\hat{w}(-x_2) = C_1\, e^{\eta_1\, x(-x_2)} + C_2\, e^{\eta_2\, x(-x_2)} = 0; \tag{5.65}$$

from which the following estimate of the solution is obtained

$$\hat{w}(s) = C_1\left(e^{\eta_1\, x(s)} + \epsilon\right) \simeq C_1\, e^{\eta_1\, x(s)}, \qquad |\epsilon| \to 0; \tag{5.66}$$

the latter approximation holding true since $|C_2|{\to}0$ as rapidly as $x(-x_2)$, and consequently $|e^{\eta_2\, x(-x_2)}|$, approach infinity, as shown in Fig. 5.14a. Thus, inside the unstretched domain, the real part of the obtained response becomes

$$\Re\big(\hat{w}(s)\big) = \hat{w}^R(s) = e^{\eta_1^R\, s}\Big(C_1^R\cos\left(\eta_1^I\, s\right) - C_1^I\sin\left(\eta_1^I\, s\right)\Big); \tag{5.67}$$

thus including the exact formula of Eq. (5.63) as a subcase by setting $C_1^R{=}0$ and $C_1^I{=}{-}2\mathrm{i}\,\tilde{C}_1$, the latter conditions naturally arising by the solution to the problem in the unstretched domain.

Hence, the effectiveness of a PML for systems described by second-order differential equations has been proved to be based on two occurrences. The first one is the cancellation of one of the two components of the fundamental solution ($|C_2|{\to}0$), thus preventing any combination of two fundamental solutions $e^{\eta_i\,(\,\cdot\,)}$ ($i{=}1,2$), i.e. the cause of possible reflections at the truncated boundary. The second important evidence is the absence of any loss in the

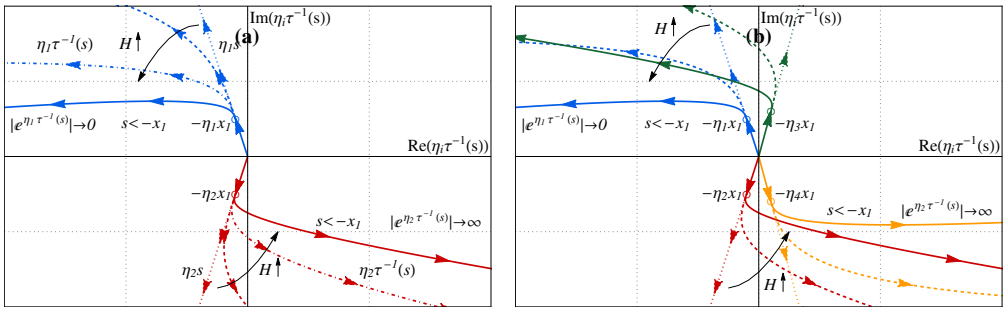

Figure 5.14: Effect of the application of complex coordinate transformation $x(s)=\tau^{-1}(s)$ of Eq. (4.21) (classic PML) in case of two poles (2^{nd}-order ODE) (a) and of four poles (4^{nd}-order ODE) (b).

sought solution as a result of the elimination of one part of the fundamental solution; in fact, due to the particular complex conjugate nature of the roots, both fundamental solutions represent exactly the same wave pattern. However, notice that this is not the case when applying the PML to fourth-order differential equations.

Now by considering the case of the steady-state vibration response of an elastic infinite beam on a Pasternak visco-elastic support in dimensional moving coordinate $x=X-vt$ $(-\infty<x<+\infty)$, one ends up with the following fourth-order ODE in the unknown steady-state normalized displacement $\hat{w}(x)$:

$$\hat{w}_x^{(4)}(x)+\frac{\mu v^2-G_P}{EJ}\,\hat{w}_x^{(2)}(x)-\frac{vc}{EJ}\,\hat{w}_x^{(1)}(x)+\frac{k}{EJ}\,\hat{w}(x)=0; \tag{5.68a}$$

$$[\![w_x^{(i)}(x)]\!]_0=0, \quad i=0,1,2; \tag{5.68b}$$

$$[\![w_x^{(3)}(x)]\!]_0=\frac{F}{w_0 EJ}=\hat{F}; \tag{5.68c}$$

where the coefficient of second derivative $\hat{w}^{(2)}(s)$ in the previous equation may also be written as follows:

$$\frac{\mu v^2-G_P}{EJ}=2\sqrt{\frac{k}{EJ}}\left(\frac{v^2-G_P/\mu}{v_{cr,W}^2}\right)=2\sqrt{\frac{k}{EJ}}\left(\frac{v^2}{v_{cr,W}^2}-g_P\right); \tag{5.69}$$

with the corresponding definition of symbols previously provided in the previous sections of the present chapter. Eq. (5.68a) governs the vertical motion of the supported beam everywhere but in the point of loading, whereas Eqs. (5.68b)-(5.68c) represent the continuity condition for the beam displacement and the balance of vertical forces at the point of loading, respectively, thus substituting the effect of Dirac delta function in Eq. (5.1).

Let one assume again the four poles to be in complex conjugate pairs $\eta_2{=}\overline{\eta}_1$, $\eta_4{=}\overline{\eta}_3$, as shown in Fig. 5.14b, which means that the solution exhibits a progressive wave pattern both ahead and behind the load, which should be transformed into evanescent waves (fastly decaying) before reaching the truncated boundary by a PML technique. By applying the transformation in Eq. (4.21), the homogeneous solution to fourth-order ODE (5.68a) takes the form:

$$\hat{w}(s) = \begin{cases} \displaystyle\sum_{i=1}^{4} C_i \, e^{\eta_i \, s}, & \text{if } -x_1 < s < x_1 \\ \displaystyle\sum_{i=1}^{4} C_i \, e^{\eta_i \, x(s)}, & \text{otherwise;} \end{cases} \tag{5.70}$$

where $e^{\eta_i \, (\cdot)}$ ($i{=}1,\ldots,4$) are the four fundamental solutions and C_i are the arbitrary integration constants. By considering again the behavior of the solution for $s{<}{-}x_1$, the fundamental solutions relative to η_1, η_2 should be kept (decaying to zero for $s{\to}{-}\infty$), thus C_1, $C_2{\neq}0$, while those depending on η_3, η_4 should be discarded, namely $C_3{=}C_4{=}0$, (exploding by moving towards $-\infty$) in order to obtain a bounded response. However, this is not truly the case.

In fact, by observing Fig. 5.14b, the coordinate transformation inside the PML ($s{<}{-}x_1$), governed as before by the amount of imaginary stretching $h(x)$ ($G{=}0$, $r{=}2$), induces again, as expected, a progressive rotation and variation of the scale of the arguments of the four fundamental solutions. The effect of the domain truncation and the imposition of a fixed boundary condition, leads to the following couple of equations:

$$\hat{w}(-x_2) = \sum_{i=1}^{4} C_i \, e^{\eta_i \, x(-x_2)} = 0; \tag{5.71a}$$

$$\hat{w}'(-x_2) = \sum_{i=1}^{4} C_i \, \eta_i \, e^{\eta_i \, x(-x_2)} = 0. \tag{5.71b}$$

By means of analogous considerations for the second-order ODE case, from the solution to Eqs. (5.71) at truncated boundary $s{=}{-}x_2$, constants of integration C_2, C_4 are almost vanishing, while the two kept fundamental solutions result those relative to roots η_1, η_3, which is not what was initially sought. As a consequence, an exponentially increasing fundamental solution due to η_3 remains in the final solution, giving rise to the instability problems described in the literature (Lancioni, 2012 [171]). The same happens for the right PML ($s{>}x_1$).

Therefore, for fourth-order problems, a classic PML is never able to cancel both exponentially increasing fundamental solutions at the same time, since a coordinate transformation involving only the independent variable only pro-

duces a global rotation of all the arguments of the exponential fundamental solutions.

5.4.2 New Perfectly Matched Layer

As exposed in the previous subsection, a classic PML is not suited for continuously transforming beam progressive waves to evanescent waves in the right way, that is by continuously moving roots η_i, gathered at complex conjugate pairs, at the same time away from the imaginary axis (decay increase) and possibly close to the real axis (frequency reduction).

Thus, instead of an affine transformation of the roots in the complex plane, a transformation which would actually suit such a scope can be newly represented by a *projective transformation (homography or collineation)* inside the PML, as follows:

$$\mathcal{P} : \eta_i\, x = \eta_i^R\, x + \mathrm{i}\, \eta_i^I\, x \;\rightarrow\; \eta_i^R\, a(x) + \mathrm{i}\, \eta_i^I\, b(x) = z_i(x), \quad i = 1, 2, 3, 4; \tag{5.72}$$

where $a(x)$, $b(x)$ are two real-valued functions which govern the projective transformation, the first one being more than linearly increasing while the second one being at least linearly increasing as x, but possibly decreasing from a certain value of x forward inside the PML.

In addition, functions $a(x)$, $b(x)$ have to be chosen such that the following perfectly matched conditions at the interfaces $\pm x_0$ between Ω_N and Ω_{PML} must be fulfilled

$$\hat{w}_x^{(i)}(\pm x_1^-) = \hat{w}_x^{(i)}(\pm x_1^+); \qquad i = 0, 1, 2, 3. \tag{5.73}$$

In order to accomplish the above fundamental requirements, possible convenient analytical expressions for $a(x)$, $b(x)$ are here originally proposed in the following forms:

$$a(x) = (1 - \chi_a)\, x + \chi_a \left(1 + A\, \frac{x_1}{|x|}\, d(x)^4\right) x; \tag{5.74a}$$

$$b(x) = (1 - \chi_b)\, x + \chi_b \left(1 + \sum_{k=1}^{3} \frac{B^k}{k!}\, d(x)^k\right) x\, e^{-B\, d(x)}; \tag{5.74b}$$

where flags χ_a, χ_b are equal to zero if $x \in \Omega_N$ or equal to one, when the projection inside the PML is active, if $x \in \Omega_{PML}$, A, B are two non-dimensional parameters controlling the amount of projective transformation and

$$d(x) = \frac{|x| - x_1}{x_2 - x_1} \tag{5.75}$$

is the normalized distance within the PML region, coherently with Fig. 5.13.

Increasing function $a(x)$ defined in Eq. (5.74a) has been derived by adding to original linear function x, valid on the computational domain of interest Ω_N, an increasing polynomials function of x, fulfilling conditions (5.72). On the other hand, the derivation of the expression of function $b(x)$ is slightly more involved, since a decreasing function is expected. Thus, a pure polynomial function cannot be employed. For this reason, the combination of a polynomial and an exponentially decaying function have been selected for function $b(x)$ as shown in Eq. (5.74b) in order to both verify conditions (5.72) and obtain a globally decreasing function $b(x)$. Other forms for functions $a(x)$, $b(x)$ may be certainly admissible, as long as the above dictated requirements would be fulfilled. The adopted prescriptions allow to derive consistent results, as revealed by the subsequent numerical outcomes.

The effect of such a transformation may be appreciated in Fig. (5.15a). Function $a(x)$ rules the decay properties of the fundamental solutions, while function $b(x)$ governs their frequencies of oscillation. Notice that, in order to provide a complete description of the projection transformation in Eq. (5.72), both functions $a(x)$ and $b(x)$ have been conceived and presented in Eqs. (5.74). Nevertheless, since the most important required effect is constituted by the high decay or increase of the fundamental solutions before reaching the boundary, the effect of function $a(x)$ by itself reveals to be already sufficient for minimizing the reflections (see Fig. (5.15b)), thus appropriately simulating the far-field conditions. Thus, flag χ_a=1 is always turned on inside Ω_{PML}.

On the other hand, the effect of function $b(x)$, consisting of a reduction of the frequency of the response inside Ω_{PML}, albeit further beneficial for the final numerical outcomes, results to be nonessential for the success of the PML implementation. Then, for simplicity, $b(x)$=x will be also assumed in the sequel inside the Ω_{PML} (i.e. flag χ_b is turned off: χ_b=0 for $x \in \Omega_{PML}$). Thus, despite the completeness of the transformation provided in Eqs. (5.72)-(5.74),

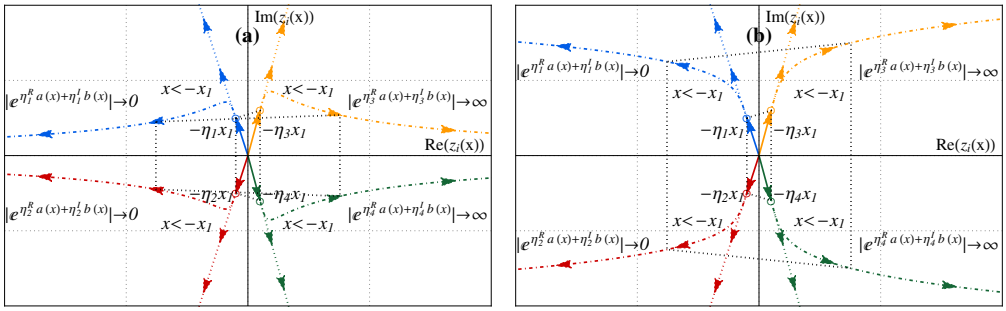

Figure 5.15: Two examples of the effect of the application of the projective transformation in Eq.(5.72) in case of four poles for $a(x)$ as in Eq. (5.74a) and $b(x)$ as in Eq. (5.74b): χ_a=1 (A<0) and χ_b=1 (B>0) (a), χ_a=1 (A<0) and χ_b=0 ($b(x)$=x) (b).

the discussion from this point on will focus only on the major effect induced by function $a(x)$.

Thereafter, the imposition of projective transformation $\mathcal{P}$ to the fundamental solutions of the homogeneous version of Eq. (5.68a) leads to the following steady-state transformed equation of motion:

$$\hat{w}_x^{(4)}(x)+c_3(x)\hat{w}_x^{(3)}(x)+c_2(x)\hat{w}_x^{(2)}(x)+c_1(x)\hat{w}_x^{(1)}(x)+c_0(x)\hat{w}(x)=0; \quad (5.76)$$

each variable coefficient defined by the Cramer rule (Ince, 1978 [133]):

$$c_{i-1}(x) = -\frac{\Delta_i}{\Delta}; \quad (5.77)$$

where Δ is the Wronskian, i.e. the determinant of fundamental matrix $\mathbf{D}$ defined as follows:

$$\Delta = \det\ \mathbf{D}; \qquad D_{ij} = \left(e^{z_j(x)}\right)_x^{(i-1)}; \quad (5.78)$$

and Δ_i is obtained from Δ by replacing the i^{th} row of Δ with row vector $\left(e^{z_j(x)}\right)_x^{(4)}$ (i=1,...,4). Recall that functions $z_i(x)$ are the arguments of the fundamental solutions after projection, as defined in Eq. (5.72). Thus, the projective transformation in Eq. (5.72) acts in such a way that Eq. (5.76) appears as a linear governing equation with variable coefficients.

Notice that the projective transformation provided by Eq. (5.72), needed for obtaining a good approximation of exterior problem (5.68a)-(5.9) by a boundary value problem affordable through a FEM approach, makes Eq. (5.76) a linear ODE with variable real-valued coefficients, as opposed to the case of a standard PML, for which variable complex-valued coefficients are obtained. This is due to the fact that the projective transformation, as it has been introduced, maintains the original complex conjugate structure of the arguments of the exponential functions.

5.4.3 First-order differential system

In order to develop a LSFEM formulation allowing the use of C^0 basis interpolation functions, thus reducing the higher regularity requirements of the LSFEM, the governing fourth-order differential equation is transformed into an equivalent first-order system, and the least-squares functional is composed using the L_2 norms of the first-order system residuals. Such a reduction, which implies the introduction of additional independent variables within the formulation, may be useful, if such auxiliary variables may represent physically meaningful ones, as in the framework of mixed formulations.

Consequently, let one introduce other three independent variables, namely, normalized steady-state rotation $\hat{\theta}(x)$, bending moment $\hat{M}(x)$ and shear

force $\hat{S}(x)$, defined as follows:

$$\hat{\theta}(x) = \frac{\theta(x)}{\theta_0} = \frac{w_0}{\theta_0}\hat{w}_x^{(1)}(x) = \hat{w}_x^{(1)}(x); \tag{5.79a}$$

$$\hat{M}(x) = \frac{M(x)}{M_0} = \frac{EJw_0}{M_0}\hat{w}_x^{(2)}(x) = \hat{w}_x^{(2)}(x); \tag{5.79b}$$

$$\hat{S}(x) = \frac{S(x)}{S_0} = \frac{EJw_0}{S_0}\hat{w}_x^{(3)}(x) = \hat{w}_x^{(3)}(x); \tag{5.79c}$$

where parameters

$$\theta_0 = w_0, \quad M_0 = EJw_0, \quad S_0 = EJw_0; \tag{5.80}$$

are chosen as normalization factors for rotation, bending moment and shear force, respectively, so that $\hat{\theta}(x)$, $\hat{M}(x)$ and $\hat{S}(x)$ are directly expressed as the derivatives of unknown $\hat{w}(x)$. Normalizing factor w_0 in Eq. (5.80) is chosen according to Eq. (5.61) in Section 5.3.

Thanks to the above definitions, governing scalar equation Eq. (5.76), valid inside Ω, may be split into four first-order ordinary differential equations:

$$\hat{w}_x^{(1)}(x) - \hat{\theta}(x) = 0 \qquad \text{in } \Omega; \tag{5.81a}$$

$$\hat{\theta}_x^{(1)}(x) - \hat{M}(x) = 0 \qquad \text{in } \Omega; \tag{5.81b}$$

$$\hat{M}_x^{(1)}(x) - \hat{S}(x) = 0 \qquad \text{in } \Omega; \tag{5.81c}$$

$$\hat{S}_x^{(1)}(x) + c_3(x)\,\hat{S} + c_2(x)\,\hat{M}(x) + c_1(x)\,\hat{\theta}(x) + c_0(x)\,\hat{w}(x) = 0 \qquad \text{in } \Omega; \tag{5.81d}$$

and, for convenience, first-order differential system (5.81) may be expressed in compact notation, together with loading point conditions of Eqs. (5.68b)-(5.68c), as specified below:

$$\hat{\mathbf{w}}_x^{(1)}(x) + \mathbf{A}(x)\,\hat{\mathbf{w}}(x) = \mathbf{0}; \qquad \text{in } \Omega; \tag{5.82a}$$

$$[\![\hat{\mathbf{w}}]\!]_0 = \begin{bmatrix} 0 & 0 & 0 & \hat{F} \end{bmatrix}^\intercal; \tag{5.82b}$$

where $\hat{\mathbf{w}}(x) = [\,\hat{w}(x) \;\; \hat{\theta}(x) \;\; \hat{M}(x) \;\; \hat{S}(x)\,]^\intercal$ is the column vector of variables and $\mathbf{A}(x)$ is the coefficient matrix, defined as

$$\mathbf{A}(x) = \begin{bmatrix} 0 & -1 & 0 & 0 \\ 0 & 0 & -1 & 0 \\ 0 & 0 & 0 & -1 \\ c_0(x) & c_1(x) & c_2(x) & c_3(x) \end{bmatrix}. \tag{5.83}$$

Finally, the previous differential system governing the motion of the structural system inside Ω is supplemented by homogeneous boundary conditions on $\partial\Omega$:

$$\hat{w} = \hat{\theta} = 0, \qquad \text{on } \partial\Omega; \tag{5.84}$$

equivalent to the imposition of clamped-clamped beam extrema.

In the following sections, the numerical solution to problem (5.82)-(5.84) is developed, based on a DLSFEM-PML approach. The present attempt completes previous literature derivations, by providing a unitary and robust numerical tool from which the steady-state moving load response can be obtained for each combination of the characteristic mechanical parameters of the beam-foundation system, without stabilization terms and associated user-tunable parameters.

5.5 Numerical solution

5.5.1 Least-Squares functional

In this section, the Discontinuous Least-Squares Finite Element Method (DLSFEM) formulated for the taut string problem in Chapter 4 is extended to problem (5.82)-(5.84), by taking advantage of its general formulation. Although the presence of only one moving load has been assumed in writing Eqs. (5.82), the possible action of multiple moving loads is again considered within the formulation.

Let one define a function space $\mathcal{V}$ for problem (5.82)-(5.84) by

$$\mathcal{V} = {}_2\boldsymbol{H}^1_0(\mathcal{O}) \times {}_2\boldsymbol{H}^1(\mathcal{O}) = H^1_0(\mathcal{O}) \times H^1_0(\mathcal{O}) \times H^1(\mathcal{O}) \times H^1(\mathcal{O}); \quad (5.85)$$

and let e_j be the j^{th} element of the collection of subset $\mathring{\mathcal{E}}$, according to its definition given in Section 4.4.1. Quadratic least-squares functional $\mathcal{J} : \mathcal{V} \to \mathbb{R}$ for problem (5.82)-(5.84), devised by measuring the squared residuals in terms of the L_2-norm of the governing differential equations (5.82a) and of the interface conditions (5.82b), is defined as follows

$$\mathcal{J}(\mathbf{v}, \mathbf{f}) = \frac{1}{2}\sum_{j=1}^{P} \left\| \mathbf{v}^{(1)}_x + \mathbf{A}\mathbf{v} \right\|^2_{0,\mathbf{F},\Omega_j} + \frac{1}{2}\sum_{j=1}^{P-1} \mathbf{r}^{\intercal}_{e_j}(\mathbf{v}, \mathbf{f}_j)\mathbf{A}^{\intercal}_{e_j}\mathbf{F}\,\mathbf{A}_{e_j}\mathbf{r}_{e_j}(\mathbf{v}, \mathbf{f}_j); \quad (5.86a)$$

$$\mathbf{r}_{e_j}(\mathbf{v}, \mathbf{f}_j) = [\![\mathbf{v}]\!]_{e_j} - \mathbf{f}_j, \qquad \mathbf{v} \in \mathcal{V},\ \mathbf{f}_j \in L_2(\Omega); \quad (5.86b)$$

where $\mathbf{A}_{e_j}$ is matrix $\mathbf{A}(x)$ in Eq. 5.83 evaluated at j^{th} edge e_j, while

$$\mathbf{f}_j = \begin{bmatrix} 0 & 0 & 0 & -\hat{F} \end{bmatrix}^{\intercal}; \quad (5.87)$$

is a 4D-vector representing both the continuity requirements of the response, except for the j^{th} jump discontinuity of normalized shear force $\hat{S}$ due to the action of j^{th} applied force F_j inside functional $\mathcal{J}(\mathbf{v}, \mathbf{f})$ of Eq. (5.86a).

Moreover, since generally in structural mechanics problems, the displacements are numerically very small compared to the forces, in coherent units, the

squares of the residuals of the equations involving generalized force variables may be large compared to those containing generalized displacements in the least-squares functional. To handle these magnitude differences, the residuals in Eq. (5.86b) have been properly turned non-dimensional to make the equations numerically comparable by multiplying them by a proper scaling matrix

$$\mathbf{F} = \begin{bmatrix} 1 & 0 & 0 & 0 \\ 0 & \lambda^{-2} & 0 & 0 \\ 0 & 0 & \lambda^{-4} & 0 \\ 0 & 0 & 0 & \lambda^{-6} \end{bmatrix}; \tag{5.88}$$

with λ [m^{-1}] as in Eq. (5.4).

It is assumed that problem (5.82)-(5.84) is well posed, thus a unique solution exists, which corresponds to the unique zero minimizer $\hat{\mathbf{w}}$ of functional $\mathcal{J}(\mathbf{v}, \mathbf{f})$. Boundary conditions (5.84) have been assumed both essential as they explicitly appear in the definition of $\mathcal{V}$.

A necessary condition so that $\hat{\mathbf{w}} \in \mathcal{V}$ may be a minimizer of real functional $\mathcal{J}(\mathbf{v}, \mathbf{f})$ in Eq. (5.86a) is that its first variation vanishes at $\hat{\mathbf{w}}$, that is

$$\delta\mathcal{J} = \lim_{\eta \to 0} \frac{\mathrm{d}}{\mathrm{d}\eta} \mathcal{J}(\hat{\mathbf{w}} + \eta\, \mathbf{v}, \mathbf{f}) = 0 \quad \forall\, \mathbf{v} \in \mathcal{V}; \tag{5.89}$$

which, after some mathematical manipulations, can be equivalently written in the form $B(\hat{\mathbf{w}}, \mathbf{v}) = L(\mathbf{v})$, as follows

$$\begin{aligned} \left(\mathbf{v}_x^{(1)} + \mathbf{A}\mathbf{v},\ \hat{\mathbf{w}}_x^{(1)} + \mathbf{A}\hat{\mathbf{w}}\right)_{0,\mathcal{O}} + \sum_{j=1}^{P-1} [\![\mathbf{v}]\!]_{e_j}^{\intercal}\, \mathbf{A}_{e_j}^{\intercal}\, \mathbf{F}\, \mathbf{A}_{e_j}\, [\![\hat{\mathbf{w}}]\!]_{e_j} = \\ = \sum_{j=1}^{P-1} [\![\mathbf{v}]\!]_{e_j}^{\intercal}\, \mathbf{A}_{e_j}^{\intercal}\, \mathbf{F}\, \mathbf{A}_{e_j}\, \mathbf{f}_j \qquad \forall\, \mathbf{v} \in \mathcal{V}; \end{aligned} \tag{5.90}$$

where $B(\hat{\mathbf{w}}, \mathbf{v})$ is a symmetric bilinear form and $L(\mathbf{v})$ is a linear functional. Thus, minimization problem (5.89) leads to the following variational equation:

$$\text{Find } \hat{\mathbf{w}} = [\,\hat{w}\ \ \hat{\theta}\ \ \hat{M}\ \ \hat{S}\,]^{\intercal} \in \mathcal{V} \text{ such that } B(\hat{\mathbf{w}}, \mathbf{v}) = L(\mathbf{v})\ \ \forall\, \mathbf{v} \in \mathcal{V}. \tag{5.91}$$

Norm-equivalence property of least-squares functional $\mathcal{J}(\mathbf{v}, \mathbf{0})$, asserted by Theorem 1, states that bilinear form $B(\mathbf{v}, \hat{\mathbf{w}})$ is continuous and coercive on $\mathcal{V} \times \mathcal{V}$, thus ensuring the well-posedness of least-squares variational problem (5.91) is guaranteed, which is a crucial requirement for the numerical implementation.

5.5.2 Finite element approximation

The finite element approximation of the steady-state response of the vibrating beam on Pasternak viscoelastic foundation under moving load is obtained by restricting Eq. (5.91) to a finite-dimensional subspace $\mathcal{V}_h$ of infinite dimensional space $\mathcal{V}$. The approximating finite element space $\mathcal{V}_h \subset \mathcal{V}$ associated with mesh $\mathcal{T}_h$, is defined as

$$\mathcal{V}_h = \left\{ \mathbf{v}_h \in {}_2\boldsymbol{H}_0^1(\mathcal{O}) \times {}_2\boldsymbol{H}^1(\mathcal{O}) : \forall i \in \{1, \ldots, N_e\}, v_{h\,j}|_{I_i} \in \mathbb{P}_1 \right\}; \quad (5.92)$$

that is, the vector space of 4D-vector functions whose components are piecewise linear polynomials allowing for a discontinuity along interelement edges $e_j \in \mathring{\mathcal{E}}$. Then, by restricting the function space to $\mathcal{V}_h$, the following discrete least-squares variational problem may be formulated:

$$\text{Find } \hat{\mathbf{w}}_h = [\hat{w}_h\ \hat{\theta}_h\ \hat{M}_h\ \hat{S}_h]^\intercal \in \mathcal{V}_h \text{ such that } S(\hat{\mathbf{w}}_h, \mathbf{v}_h) = L(\mathbf{v}_h)\ \ \forall\, \mathbf{v}_h \in \mathcal{V}_h. \quad (5.93)$$

Thanks to inclusion $\mathcal{V}_h \subset \mathcal{V}$, Theorem 1 remains valid when $S(\hat{\mathbf{w}}, \mathbf{v})$ is restricted to $\mathcal{V}_h \times \mathcal{V}_h$. Consequently, such a confirming discretization of weak problem (5.91) into weak problem (5.93) automatically gives rise to a well-posed FEM (Ern and Guermond, 2004 [89]), as well as in Chapter 4.

According to the usual finite element approach, let ϕ_j be a basis of $\mathcal{V}_h$ such that $\hat{w}_j = \hat{w}(x_j)$, $\hat{\theta}_j = \hat{\theta}(x_j)$, $\hat{M}_j = \hat{M}(x_j)$ and $\hat{S}_j = \hat{S}(x_j)$ are the nodal values of function $\hat{w}(x)$, $\hat{\theta}(x)$, $\hat{M}(x)$ and $\hat{S}(x)$, respectively, where x_j represent the nodes of mesh $\mathcal{T}_h$ (identical shape functions for each component of $\hat{\mathbf{w}}$). Then, by writing

$$\hat{\mathbf{w}}_h = \sum_{j=0}^{N_e} \hat{\mathbf{W}}_j\, \phi_j = \sum_{j=0}^{N_e} [\,\hat{w}_h\ \ \hat{\theta}_h\ \ \hat{M}_h\ \ \hat{S}_h]^\intercal\, \phi_j; \quad (5.94)$$

variational problem (5.93) generates the following system of linear algebraic equations:

$$\mathbf{K}\,\hat{\mathbf{W}} = \mathbf{F} \qquad\qquad \hat{\mathbf{W}}, \mathbf{F} \in \mathbb{R}^{4(N_e+1)}; \quad (5.95)$$

where $K_{ij} = S(\phi_i, \phi_j)$, $\hat{W}_j$ and $F_i = L(\phi_i)$ are the the global stiffness matrix, the global generalized displacement vector and the global force vector, respectively. Since the bilinear form in Eq. (5.93) is symmetric and coercive, matrix $\mathbf{K}$ associated with problem (5.93) is symmetric and positive definite. Thus the weak discrete problem has a unique solution.

Based on the analysis presented in Section 4.5, the obtained a priori error estimates (4.70)-(4.71) also hold for the present DLSFEM formulation. Numerical examples will be presented in the following section, in order to confirm the validity of a priori error estimates (4.70)-(4.71) also for the specific problem of the infinite beam on Pasternak viscoelastic foundation under moving load presented in Section 5.1.

5.5.3 Numerical simulations and outcomes

In the present section, the formulated DLSFEM-PML implementation presented in Sections 5.4.2 and 5.5.1-5.5.2 is employed to solve the moving load problem exposed in Section 5.1 and to verify the above-mentioned theoretical results characterizing the formulation, considering several different values of characteristic system parameters $v/v_{cr,_P}$ and ζ in the following numerical investigation. The DLSFEM-PML code has been implemented within a MatLab environment [251] and a uniform mesh size $h_i{=}h$ has been adopted for the current simulations.

The considered dimensions for the problem sketched in Fig. 5.13 are $x_1{=}50$ m and $x_2{=}60$ m, so that the size of each PML is $1/10$ of the size of Ω_N, that is a much smaller PML layer than the computational domain of interest, providing an effective reduction of the computational cost in the modelization of far-field conditions (5.9). In order to investigate the effectiveness of the new PML ruled by the projective transformation in Eq. (5.72), different values of parameter A in Eq. (5.74a) have been considered in the analyses; in particular, the same amount of A with opposite signs is assumed for both PMLs, namely negative and positive for the left and right PML, respectively.

Global stiffness matrix $K_{ij}{=}S(\phi_i, \phi_j)$ has been computed by means of Gauss-Legendre quadrature rules, in order to overcome the complexity of analytically integrating the terms containing the expressions of coefficient matrix $\mathbf{A}(x)$ in Eqs. (5.77)-(5.83). A 1-point reduced integration is considered in the present implementation, while a high-order (3-point) Gauss-Legendre quadrature rule is employed to compute the error norms, thus not introducing competitive extra-errors in the numerical integration.

It is important to underline that, if a 2-point quadrature integration scheme (full numerical integration) is chosen, accurate results may be obtained for the case of a rapidly decaying response (highly-damped system and/or subcritical velocity), while, on the contrary, the locking phenomenon may become very important when trying to push to almost undamped supercritical motion regimes, where an excessively refined mesh should be employed for obtaining the same accuracy attainable with a reduced integration and a rough mesh. Therefore, reduced integration or alternatively high-order expansions and full integration (p-refinement, Pontaza and Reddy, 2005 [219]) are needed for truly minimizing the least-squares functional. Actually, the adopted reduced integration proves to produce consistent and rather accurate numerical outcomes in the whole space of variation of the characteristic mechanical parameters of the beam-foundation system.

The assumed mechanical properties of the beam and the Winkler foundation modulus are reported in Table 5.2. The load is taken acting downward ($F{<}0$).

The analytical solution relative to an infinite beam, is rigorously different

from the exact solution pertinent to that of a finite domain problem (5.82)-(5.84), where estimates (4.70)-(4.71) are referred to. Thus, for computing the error norms in (4.70)-(4.71), in the following it is assumed that the numerical solution to Eqs. (5.82)-(5.84) approximates the exact solution to an infinite beam problem over the finite computational domain of interest Ω_N, and, consequently the error norms are evaluated on $\mathcal{O}_N{=}\mathcal{O} \cap \Omega_N$, instead as on $\mathcal{O}$, just as in Chapter 4. In addition, the obtained theoretical a priori error estimates pertain only to the DLSFEM application, hence they do not account for other sources of perturbations, such as the use of numerical integration or the employment of the PML to simulate an unbounded domain, which, however accurate, always represents an approximation of the far-field conditions.

The complete normalized response (deflection, rotation, bending moment, shear force) is shown in Figs. 5.16-5.17 and in Figs. 5.19-5.20, for non-dimensional Pasternak modulus $g_P{=}0.5$, and for two values of moving load velocity v and damping ratio ζ. The considered range of velocities is sufficiently broad, namely it goes from 0.7 to 1.3 times critical velocity $v_{cr,_P}$. Two selected values of damping ratio are chosen, one indicating a highly damped system ($\zeta{=}0.5$) and the other an almost undamped system ($\zeta{=}0.001$), to investigate the spread of the arising characteristic features.

Estimates (4.70)-(4.71) are firstly verified for a highly damped beam-foundation system ($\zeta{=}0.5$), providing a rapidly decaying response both in the subcritical ($v{=}0.7\, v_{cr,_P}$) and in the supercritical ($v{=}1.3\, v_{cr,_P}$) regime, as shown in Figs. 5.16-5.17. Numerical computations have been performed with a mesh size of $h{=}0.1$ m. The displayed comparisons show that the numerical results obtained from the proposed DLSFEM-PML formulation fit very well with the analytical solution, even if the mesh density is rather rough.

Although apparently the employment of the PML could also be avoided in this case, because the response itself rapidly decays down to zero, moving away from the load position, an effective stretching has been still set in the PML ($A{=}\pm\, 4 \times 10^2$), in order to demonstrate that its application does not downgrade the accuracy of the numerical outcomes, in cases when its action would not be strictly demanded.

The L_2- and H^1-norm of the error are provided in log-log plots against mesh size h in Fig. 5.18. By inspecting the graphs it may be observed that the error in the L_2-norm ($\|\hat{\mathbf{w}} - \hat{\mathbf{w}}_h\|_{0,\mathcal{O}}$) is almost unaffected by the amount of parameter A, that is by the presence or not of the PML. This due to the fact that the solution already rapidly decays to zero before reaching the boundary, and thus reflections are consequently negligible.

A more challenging case study is represented by a nearly undamped system ($\zeta{=}0.001$), for which a suitable absorbing boundary conditions is mandatory. A graphical representation of the complete normalized response is displayed in Figs. 5.19-5.20, again both in the subcritical ($v{=}0.7\, v_{cr,_P}$) and in the

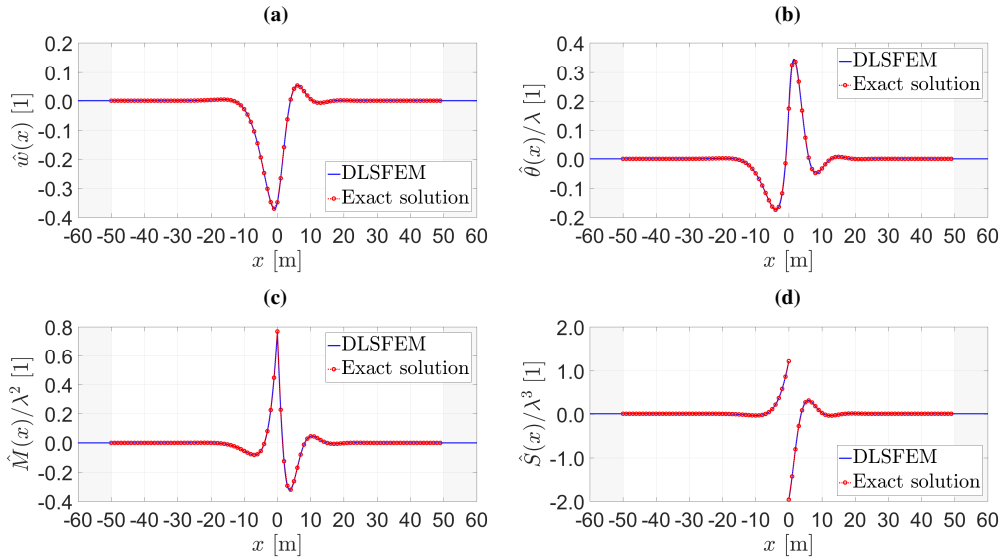

Figure 5.16: Comparison between DLSFEM-PML numerical results and analytical solution (g_P=0.5, ζ=0.5, v=0.7 $v_{cr,P}$, A=$\pm\,4\times10^2$). Normalized deflection $\hat{w}$ (a), rotation $\hat{\theta}$ (b), bending moment $\hat{M}$ (c), shear force $\hat{S}$ (d). For the reference mechanical parameters, see Table 5.2.

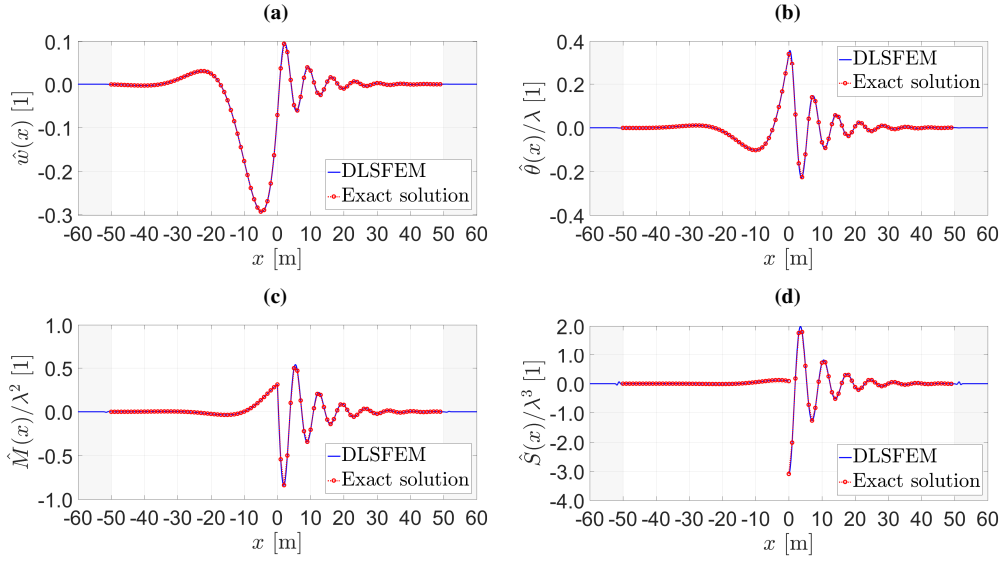

Figure 5.17: Comparison between DLSFEM-PML numerical results and analytical solution (g_P=0.5, ζ=0.5, v=1.3 $v_{cr,P}$, A=4×10^2). Normalized deflection $\hat{w}$ (a), rotation $\hat{\theta}$ (b), bending moment $\hat{M}$ (c), shear force $\hat{S}$ (d). For the reference mechanical parameters, see Table 5.2.

supercritical (v=1.3 $v_{cr,P}$) regime, with a mesh size of h=0.1 m. By observing the graphs in Figs. 5.19-5.20 the very good agreement between the DLSFEM

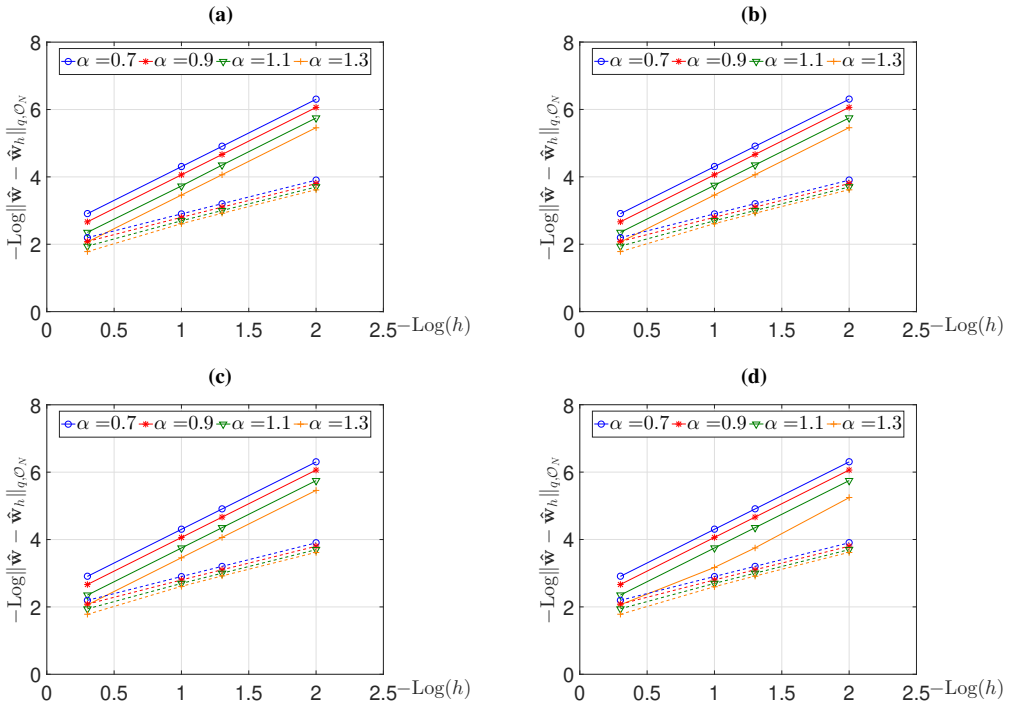

Figure 5.18: Convergence of DLSFEM-PML in L_2- (q=0, continuous line) and H^1-norms (q=1, dot-dashed line), at variable moving load velocity $v{=}\alpha\, v_{cr,P}$, for a damped system (ζ=0.5) with respect of amplitudes A ruling the real part of the projective transformation of the PML: $A{=}10^2$ (a); $A{=}2\times10^2$ (b); $A{=}4\times10^2$ (c); $A{=}10^3$ (d). Norms are evaluated on the computational domain of interest.

responses and the analytical ones may be gathered, again by using a few finite elements. In this case the response results strongly influenced by the presence or not of the PML.

The effect of the PML on the error in log-log plot against mesh size h is illustrated in Fig. 5.21. In the subcritical motion regime of velocities (evanescent waves) the error in the L_2-norm is again not influenced by the presence or not of the PML, and, in fact, the theoretical a priori L_2- and H_1-convergence rates in Eqs. (4.70)-(4.71) are always verified independently of the value of A, confirming previously discussed observations for the highly-damped case. At the supercritical motion regime an insufficient amount of real stretching in the PML (small amplitudes of functions $a(x)$) leads to inconsistent errors, as shown in Figs. 5.18a-5.18b), which means a non-appropriate modelization of the far-field conditions and thus the error results unrespectful of the a priori theoretical estimates. On the other hand, by introducing a more effective PML layer, that is by increasing the magnitude of A, the performance of the DLSFEM substantially improves until the expected convergence rate of the error in

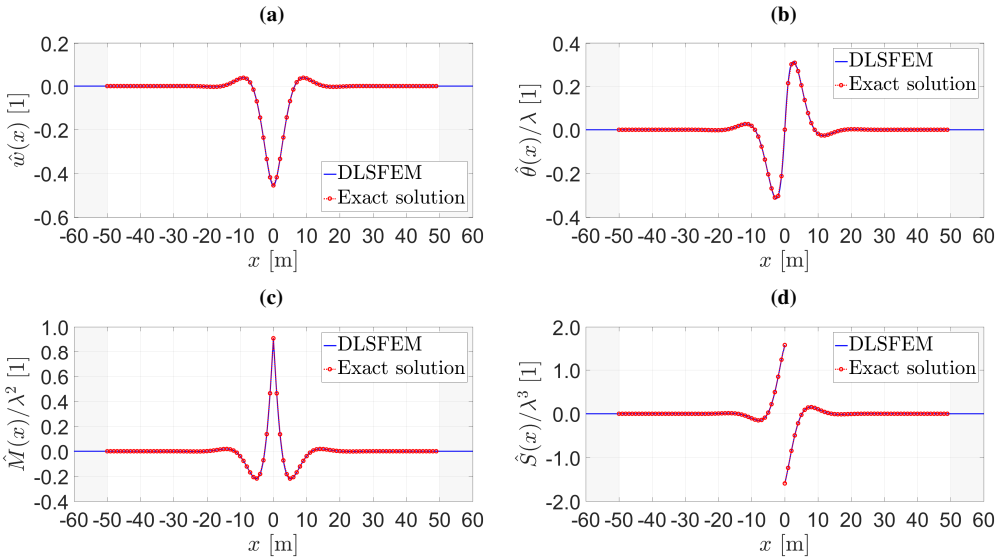

Figure 5.19: Comparison between DLSFEM-PML numerical results and analytical solution (g_P=0.5, ζ=0.001, v=0.7 $v_{cr,P}$, A=$\pm$ 4×10^2). Normalized deflection $\hat{w}$ (a), rotation $\hat{\theta}$ (b), bending moment $\hat{M}$ (c), shear force $\hat{S}$ (d). For the reference mechanical parameters, see Table 5.2.

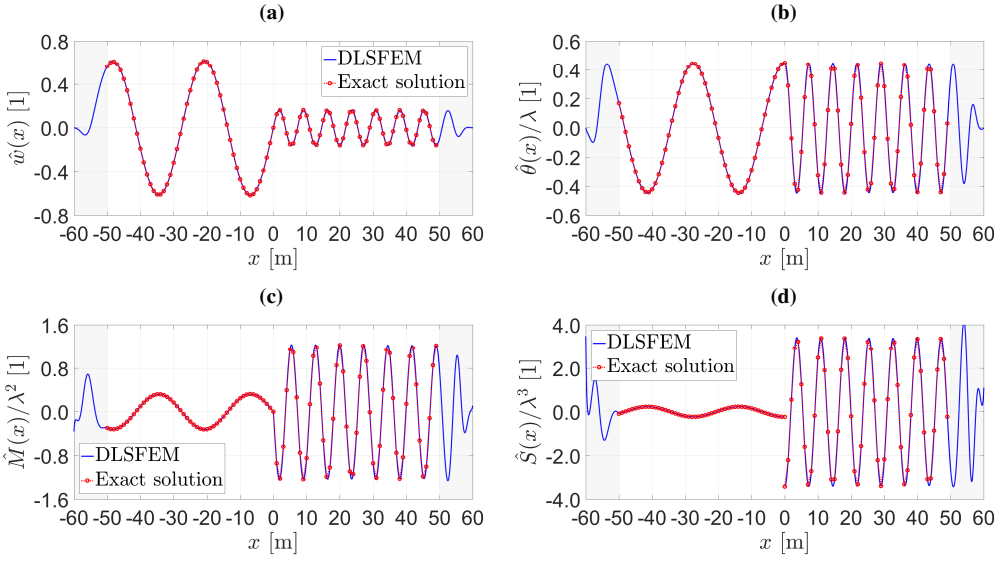

Figure 5.20: Comparison between DLSFEM-PML numerical results and analytical solution (g_P=0.5, ζ=0.001, v=1.3 $v_{cr,P}$, A=4 × 10^2). Normalized deflection $\hat{w}$ (a), rotation $\hat{\theta}$ (b), bending moment $\hat{M}$ (c), shear force $\hat{S}$ (d). For the reference mechanical parameters, see Table 5.2.

the L_2- and H^1-norms are progressively reached. Thus, as expected, either the higher the moving load velocity or the smaller the damping, the higher is the

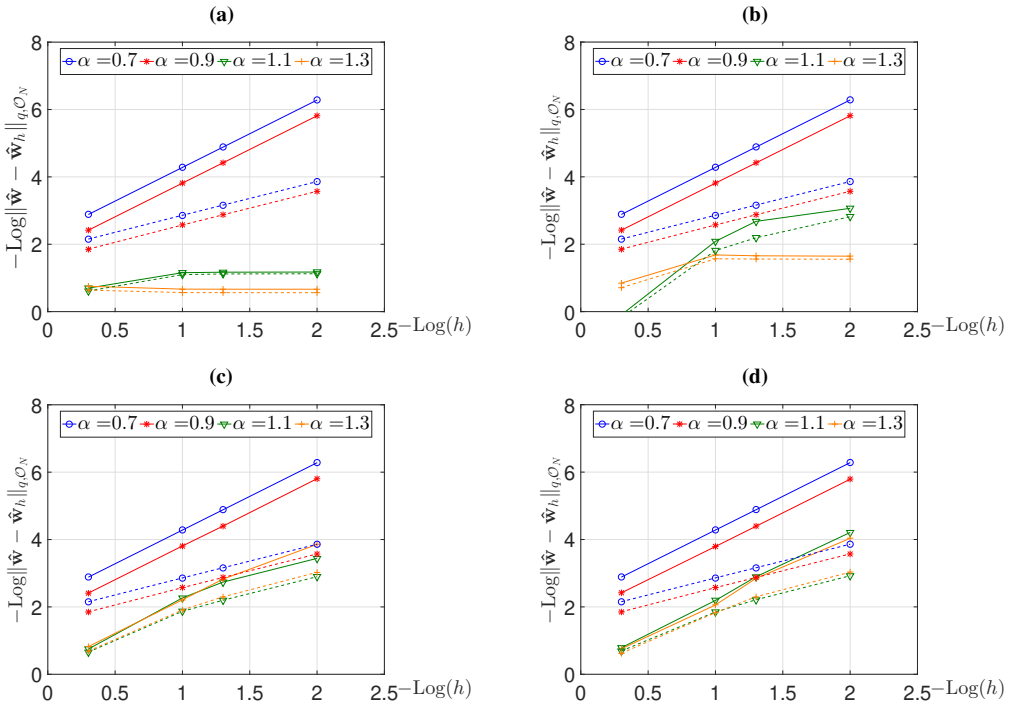

Figure 5.21: Convergence of DLSFEM-PML in L_2- (q=0, continuous line) and H^1-norms (q=1, dot-dashed line), at variable moving load velocity v=$\alpha\, v_{cr,P}$, for a nearly-damped system (ζ=0.001) with respect of amplitudes A ruling the real part of the projective transformation of the PML: A=10^2 (a); A=2×10^2 (b); A=4×10^2 (c); A=10^3 (d). Norms are evaluated on the computational domain of interest.

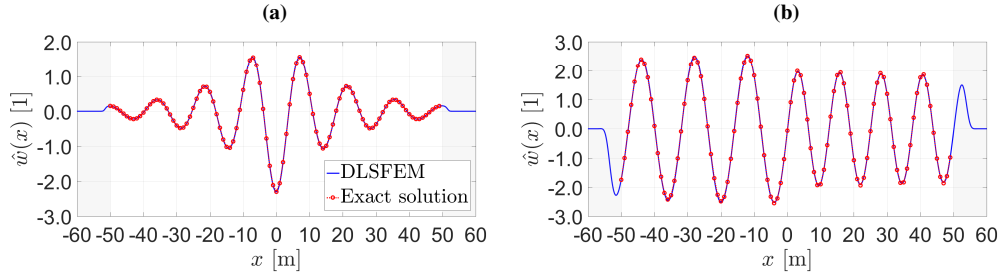

Figure 5.22: Comparison between DLSFEM-PML numerical results and analytical solution as approaching the critical velocity for a nearly undamped system (ζ=0.001, A=4×10^2). Normalized deflection: v=0.99 $v_{cr,P}$ (a) and v=1.01 $v_{cr,P}$ (b). For the reference mechanical parameters, see Table 5.2.

demanded capacity of the PML in absorbing the stationary propagating wave.

Numerical experiments have also been performed for an even more challenging configuration of the mechanical parameters, by considering the nearly undamped case (ζ=0.001), with two values of velocity, one just subcriti-

cal $v{=}0.99\, v_{cr,P}$ and one just supercritical $v{=}1.01\, v_{cr,P}$, thus very close to critical value $v_{cr,P}$. The numerical results in terms of normalized deflection are presented in Fig. 5.22, showing again a very good agreement with respect to the target solution, for the same mesh size. Thus, the range of velocity in which this method performs well is rather wide. In the same figures, the effect of the new PML may be truly appreciated at the extremes of the computational domain.

5.6 Closing chapter considerations

In the present chapter, the solution of the problem of the steady-state dynamic response of a homogeneous infinite Euler-Bernoulli elastic beam resting on a uniform Pasternak viscoelastic foundation and subjected to a constant transverse point load moving with a constant velocity along the beam has been investigated both analytically and numerically.

In the first part of the chapter, the Fourier transform technique has been applied to reduce the governing ordinary differential equation of motion of the beam into an algebraic equation and a universal fully parametric closed-form explicit analytical solution has been derived by inverting the Fourier transform, by means of the theory of complex analysis and the residue theorem. An a priori characterization on how the beam-foundation response changes according to the paths followed in the space of the system parameters, by varying the moving load velocity, the Pasternak shear modulus and the damping ratio, has been developed by a comprehensive classification of all solution behaviors, based on the parametric nature of the poles of the Fourier transform of the solution. In fact, depending on that, the wave form of the resulting response may present a wide variety of configurations.

Then, a rigorous derivation of the general solution has been obtained, leading to a universal parametric representation of the steady-state response, which depends on two non-dimensional physical parameters of the beam-Pasternak foundation system. The present derivation includes new solution appearances that may be obtained for given values of the physical parameters, such as for a high Pasternak modulus, outlining a unitary, comprehensive general formulation of the analyzed steady-state moving load problem.

The derived solution turns out to be fully consistent with available solutions reported in the literature, but, with respect to the literature contributions discussed in Section 5.1, the present newly-derived solution constitutes a unified analytical tool endowed of a general validity. Indeed, such an approach avoids the need of using distinct expressions of the analytical solution, like as it was proposed in previous research works, whose validity was limited only to some regions of the space of the characteristic parameters of the beam-Pasternak

foundation system. Moreover, the derived exact solution may be readily used to validate the reliability and accuracy of numerical methods (e.g. the developed DLSFEM modelization), which may be employed to obtain the response also for more complex problems, where an analytical treatment may not be possible.

The achieved analytical solution has been summarized in the self-contained chart reported in Fig. 5.4, which represents a main result of the present investigation and shall constitute an easily-accessible reference. The developed analytical investigation has drawn several interesting findings concerning the present formulation of the moving load problem. Furthermore, singular instances of the steady-state solution corresponding to a vanishing discriminant of the denominator of the associated Fourier representation, leading to the onset conditions of critical velocity and of critical damping have been consistently derived, analyzed, inspected and interpreted. The existence of two branches of the critical damping coefficient, pertaining to each one of the two bending waves (propagating backward and forward) characterizing the beam-Pasternak foundation response, has been revealed.

In the absence of damping, when the moving load approaches the critical velocity, the beam response becomes unbounded and a steady-state response cannot be attained, neither at the supercritical velocities. The critical velocity for a Pasternak elastic foundation in Eq. (5.51) is always greater than that for a Winkler elastic foundation in Eq. (5.13), and quickly raises at increasing Pasternak modulus. Similar response features have been deduced from the parametric analysis of the local normalized response characteristics at the moving load position, performed by considering variable velocity, Pasternak modulus and damping ratio.

Non-dimensional curves of deflection, cross-section rotation, bending moment and shear force versus non-dimensional spatial parameter have been presented, showing several important and characteristic features of the structural response. The normalized shapes and amplitudes of these curves are mostly controlled by non-dimensional parameter α in Eq. (5.10), whose magnitude in turn depends on the interrelation between the velocity of the moving load and the Pasternak modulus. Such a dependence, together with the effect of damping, as attached to non-dimensional parameter β in Eq. (5.11), has been widely discussed in this chapter. For positive values of parameter α, the presence of shear interaction in the foundation may be conceived as to be equivalent to having a simpler Winkler elastic foundation, but with a load moving at a lower velocity. As a general consideration, since the Pasternak model shall represent the ground behavior more accurately than the Winkler model, the developed solutions may supply a better guideline for possible ensuing contexts of parameter identification and for practical design purposes.

Finally, a complete parametric analysis on the effect of the moving load ve-

locity, the Pasternak modulus and the damping ratio on the beam-foundation response has been developed, for ranges of the parameters spanning a wide spectrum of the parametric space, thus including all possible physical instances. Consistently, extensive representations of the characteristic features of the steady-state response have been provided and discussed.

In the second part of the chapter, a new, effective fourth-order PML technique and a local Discontinuous Least-Squares Finite Element Method (DLSFEM) method have been formulated and implemented, as a robust and efficient joint computational tool for numerically simulating the same steady-state beam response. In order to handle the issue of spurious reflections and non-evanescence of the flexural waves arising from the geometric truncation of the original unbounded domain, a steady-state effective fourth-order PML technique has been innovative formulated and implemented.

The present derived and implemented DLSFEM-PML formulation has provided a unitary and robust numerical tool for numerically analyzing the steady-state moving load response in the whole space of variation of the characteristic mechanical parameters of the beam-foundation system, thus requiring neither special treatments nor user-tunable parameters associated to stabilization terms, which are prevalent in traditional schemes. Although the presence of only one moving load has been assumed in the analyzed problem, a more general formulation has been developed, by considering the possible treatment of multiple moving loads.

A stationary effective Perfectly-Matched Layer (PML) technique, derived, analyzed and discussed thoroughly in this chapter, has been successfully implemented within the DLSFEM formulation for the fourth-order beam problem, to accurately simulate far-field conditions of the original physical moving load exterior problem into an appropriate boundary value problem. The effectiveness of the PML technique and of the theoretical results attached to the DLSFEM formulation and of their practical validity have been proven through several numerical examples, in which the obtained numerical results have been compared with the previously derived analytical solution, showing highly accurate numerical outcomes for subcritical, quasi-critical and supercritical cases, both damped and undamped.

Numerical evidences have confirmed that the method is truly capable of accurately representing the prescribed jump discontinuity in the shear force at the loading points and of reproducing the predicted theoretical quasi-optimal convergence rates. At supercritical velocities, when the action of the PML becomes mandatory to provide the sought response, it is shown that the present DLSFEM-PML is robust, stable and convergent, even for a very slightly damped system, if a sufficient amount of projection imposed by the PML is selected. Even in this latter case, the rate of convergence of both H^1-norm and L_2-norm of the error is shown to be coherent with the theoretical a pri-

ori error estimates.

Chapter 6

Conclusions

6.1 Closing remarks

The present doctoral dissertation has presented the outcomes of an extensive research investigation carried out on the structural dynamic analysis of one-dimensional elements (strings, beams) on continuous elastic support, represented by a Winkler or Pasternak mechanical model, under the action of a transverse moving load, traveling at a constant high velocity. In particular, the aim was that to reveal the physical dynamic response characteristics of taut string/beam-foundation interacting systems, both in the linear and in the nonlinear regimes of response, through the formulation and implementation of analytical and/or numerical methodologies. These were specifically conceived to handle the mathematical issues inherent to the modelization of the mechanical problems under consideration, all originally developed and autonomously implemented within the body of the dissertation. A main background practical context of the analytical and numerical investigations exposed in the thesis is represented by the appropriate description of track vibrations induced by high-speed vehicles, e.g. trains, which looks crucial in contemporary transportation engineering.

Some global conclusive remarks on the whole investigation are briefly outlined in the following. Conclusions are presented by considering the two main parts treated in this work, i.e. the determination of the structural response of *finite* beam-foundation systems, in both static and dynamic contexts (fixed reference frame), and the analysis of the structural dynamic response of *infinite* systems, described within a moving reference frame (convected coordinate).

In *Chapter 2*, introducing the first part of the thesis, an historical review of the most common mechanical models used for representing a continuous elastic support, namely the Winkler and the Pasternak models, has been presented, both in the linear and nonlinear contexts, together with a brief state of the art on the application of such models in the context of elastostatics. After hav-

ing disclosed a substantial lack of knowledge in the literature of the analytical formulations relative to the case of a space-varying Winkler coefficient, two closed-form explicit analytical solutions regarding the static response of a finite Euler-Bernoulli elastic beam lying on a Winkler foundation, with stiffness coefficient varying according to a linear or a minus four power function, respectively, have been rigorously derived in full analytical closed form by the theory of Ordinary Differential Equations (as resumed in the charts of Figs. 2.15 and 2.4). The selected expressions for the support elastic stiffness coefficient result able to represent manifold space-variation trends, as well as to reproduce the limit cases of a constant stiffness modulus of the foundation, of the absence of a foundation and of the presence of an infinitely rigid support.

Fundamental mathematical derivations and manipulations have been summarized and presented. Then, complete parametric analyses on the beam-foundation system response as a function of the characteristic mechanical parameters of the system have been developed and their effects on the variations of the deflection and bending moment non-dimensional curves versus non-dimensional spatial parameter have been been widely discussed. Curves which can be used to compute the maximum static response have been displayed for both the considered problems. These curves may supply a guidance for the practical design of beams on a variable elastic Winkler support.

Also, the reference analytical model derived here may represent a powerful tool for the parametrization and interpretation of the structural response, and a reference analytical model appears undoubtedly more effective than a numerical one, especially for ensuing contexts of parameter identification or design purposes, also in terms of parametrization and interpretation of the achieved structural response. Moreover, the derived exact analytical solution may constitute a benchmark reference for validating reliability and accuracy of alternative numerical approaches, which may be useful to solve more complicated problems, where analytical treatments may become unfeasible, especially in explicit closed-form.

After the preliminary discussion on the constitutive behavior of the components of a beam-foundation system in Chapter 2, *Chapter 3* has regarded the dynamic transient response of a long finite, simply-supported beam, lying on linear and nonlinear elastic Winkler foundations, subjected to a concentrated load moving at a high constant velocity along the beam, with a harmonic-varying magnitude in time. At the beginning, in order to introduce the framework and motivations of the present analysis, a brief state of the art on the main contributions and researches that mostly have inspired the developments of the present work has been presented. Then, a FEM implementation coupled with a HHT-α integration algorithm has autonomously been implemented to numerically analyze the dynamic response of the beam-foundation system and to detect its critical velocities, leading to the largest displacements. In order

to validate the reliability of the present FEM implementation, the numerical outcomes of the linear foundation model, in terms of maximum displacements and critical velocities, have been compared with those reported in the dedicated literature (Chen et al., 2003 [55], Castro Jorge et al., 2015 [49, 50]), showing an excellent agreement.

The numerical outcomes have revealed that if the moving load magnitude is constant, only one critical velocity appears, while two critical velocities are instead observed for a harmonic moving load, for all types of underlying foundation. The two critical velocities tend to separate, one increasing, the other decreasing, as the moving load frequency increases. The higher critical velocity increases, starting from the value of the critical velocity obtained for a constant-magnitude load. On the contrary, the lower critical velocity decreases, until it reaches zero for a frequency of the load equal to the first natural frequency of the beam. The relationship between the critical velocities and the moving load frequency has been portrayed in appropriate multiple-branch numerical/analytical curves, at variable mechanical parameters, by fitting the values of the critical velocities computed at different load frequencies, through effective analytical interpolating proposals with calibrated coefficients. The employed models for the description of such curves appear very appropriate for the considered nonlinear beam-foundation systems. The derived formulas appear rather simple and possibly workable in practice; thus, they may supply a useful guideline for the design of railway tracks when the magnitude of the moving load is oscillating in time.

In more detail, regarding the bilinear support case, a progressive decrease of the stiffness for the upward motions increases the positive (upward) displacements of the beam; the increase of the displacements is particularly important for a nearly vanishing tension stiffness, for which upward displacements may become so large that the hypothesis of geometrical linearity may become no longer valid. The moving load critical velocities also decrease when the foundations stiffness ratio decreases. Further, convergence studies on the maximum beam deflection demonstrate the high accuracy of the retrieved results, for the adopted space discretization. In addition, an automated calculation has been implemented to evaluate the time step to be adapted for the numerical integration, for each simulation, in order to optimize the computational effort. Potential implications in terms of practical design scenarios may be deduced from the study on the bilinear foundation case, especially in possibly lowering down the ranges of admissible vehicle velocities, as for a structural requirement or for preventing potential passenger discomfort.

Concerning instead the cubic superlinear elastic Winkler foundation, several numerical simulations have been performed by varying moving load velocity, magnitude mean value and frequency. Three critical velocities have newly been detected for a harmonic moving load with a non-zero mean magnitude,

depending on both the frequency and the mean magnitude of the moving load. Also in this case, the highest and lowest critical velocities tend to separate, one increasing, the other decreasing, as the moving load frequency increases, while the intermediate critical velocity remains fixed with respect to the frequency.

The second part of the present thesis has pertained to the analysis of the steady-state response of uniform infinite one-dimensional structural elements lying on visco-elastic foundations, induced by the action of a constant transverse point load moving with a high constant velocity. By describing such responses in a moving reference frame attached to the position of the load, a steady-state response has been obtained, similarly to solving a static problem, posed on an unbounded domain. Two types of one-dimensional structural elements have been considered: a taut string and an elastic Euler-Bernoulli beam.

The aim was that of developing a unitary and robust numerical method, from which the steady-state moving load response could be obtained, in the whole space of variation of the characteristic mechanical parameters of the taut string/beam-foundation systems, thus requiring neither special treatments nor user-tunable parameters associated to stabilization terms, which are instead prevalent in traditional schemes. Towards such a scope, a local Discontinuous Least-Squares FEM (DLSFEM) formulation, namely a non-standard FEM approach, has been successfully derived and implemented, mainly due to its several theoretical and computational advantages in this field. Among these, it is worthwhile to mention the absence of stabilization terms and associated user-tunable parameters, which are prevalent in traditional schemes, the construction of always sparse, symmetric and positive-definite algebraic discrete systems and the possibility to employ a single piecewise polynomial, even discontinuous space, for approximating all the involved variables, circumventing well-known stability conditions arising in mixed methods, thus making programming much easier by using equal-order elements. Such advantageous numerical properties result useful when one is interested in the numerical solution of a problem within a complete range of values of the involved parameters.

In addition, in order to simulate a problem originally defined on an unbounded domain, effective dedicated steady-state PML techniques in moving coordinates have been implemented within the DLSFEM formulation, thus balancing the geometric truncation of the original unbounded domain and accurately simulating the far-field conditions of the original exterior problem into an appropriate boundary value problem.

In particular, *Chapter 4* has dealt with the description of the DLSFEM and its application to the infinite taut string moving load problem. The convergence of the method has rigorously been demonstrated (see Theorem 1 in Section 4.4) by an innovative arrangement in matrix form, valid for any linear ordinary differential problem of any order, with complex-valued coefficients (rewritten as a first-order system), with interface conditions, thus advancing and completing

previous literature derivations. On this basis, theoretical a priori error estimates have been consistently derived for the finite element approximation, asserting that the uniform rate of convergence of the present DLSFEM with equal-order finite elements is of order two in L_2-norm and of order one in H^1-norm. The validation of the derived theoretical results, together with the effectiveness of the PML as a valuable absorbing layer, have been proven through several numerical examples, for the moving load physical context of interest, in which the obtained numerical results have been compared with an available analytical solution from the literature.

In *Chapter 5*, the solution of the problem of the steady-state dynamic response of a homogeneous infinite Euler-Bernoulli elastic beam resting on a uniform Pasternak viscoelastic foundation and subjected to a constant transverse point load moving with a high constant velocity along the beam has been determined, both analytically and numerically.

First, a rigorous derivation of the general closed-form explicit analytical solution has been obtained, summarized in the self-contained chart reported in Fig. 5.4, leading to a universal parametric representation of the steady-state response, by means of a Fourier transform technique, the theory of complex analysis and the residue theorem. The present derivation includes new solution appearances that may be obtained for given values of the physical parameters, such as for a high Pasternak modulus, outlining a unitary, comprehensive general formulation of the analyzed steady-state moving load problem, thus constituting a unified analytical tool endowed of a general validity.

The developed analytical investigation has drawn several interesting findings concerning the present formulation of the moving load problem. Complete parametric analyses on the effect of the moving load velocity, the Pasternak modulus and the damping ratio on the beam-foundation response has been developed, for ranges of the parameters spanning a wide spectrum of the parametric space, thus including all possible physical instances. Consistently, extensive representations of the characteristic features of the steady-state response have been provided and discussed.

Furthermore, singular instances of the steady-state solution corresponding to a vanishing discriminant of the denominator of the associated Fourier representation, leading to the onset conditions of critical velocity and of critical damping have been consistently derived, analyzed, inspected and interpreted. The existence of two branches of the critical damping coefficient, pertaining to each one of the two bending waves (propagating behind and in front of the moving load position) characterizing the beam-Pasternak foundation response, has been revealed.

Finally, in the second part of Chapter 5, a new, effective fourth-order PML technique and a local Discontinuous Least-Squares Finite Element Method (DLSFEM) have been formulated and implemented, as a robust and effi-

cient joint computational tool for the numerical simulation of the same steady-state beam response. In order to handle the issue of spurious reflections and non-evanescence of the flexural waves arising from the geometric truncation of the original unbounded domain, a stationary effective Perfectly-Matched Layer (PML) technique has been derived for the fourth-order beam problem, to accurately simulate the far-field conditions of the original physical moving load exterior problem into an appropriate boundary value problem.

The effectiveness of the new PML technique and of the theoretical results attached to the present DLSFEM formulation and of their practical validity have been proven through several numerical examples, in which the obtained numerical results have been compared with the previously derived exact analytical solution, showing highly accurate numerical outcomes, for subcritical, quasi-critical and supercritical cases, both damped and undamped. Thus, the derived exact solution may also be readily used to validate the reliability and accuracy of numerical methods (e.g. the developed DLSFEM modelization), which may be employed to obtain the response also for more complex problems, where an analytical treatment may not be possible.

As a final conclusion, the results obtained and presented in this work are believed to satisfy the aims of the present thesis of providing consistent modelizations in the challenging structural dynamics vibration context of fast moving load problems. The analytical solutions and the numerical implementations appear as powerful theoretical and computational methodological tools, potentially amenable to feasible applications in practical situations. They allowed to reveal detailed information on the physical dynamic responses of the considered interacting beam-foundation structural systems, specifically regarding wave propagation characteristics, critical velocities and critical damping values and amount of structural response. Indeed, this information is believed to be crucial for design, optimization and identification processes, connected to the analyzed moving load problems.

6.2 Future developments

Specific future developments, as possible downstreams of the outcomes and open issues of the formulations and simulations developed in the thesis are finally outlined below in itemized form, for each of the considered mechanical problems:

- Regarding to the derivation of analytical solutions for the bending response of a finite uniform Euler-Bernoulli elastic beam resting on a Winkler elastic foundation with a spatially inhomogeneous stiffness coefficient, the analytical solutions explored in Chapter 2 could be enriched by other static problems involving further space trends, as, for instance,

parabolic, or by shifting them to a dynamical context. In the latter case, the determination of the modal properties and/or of the complete dynamic response of finite beam-foundation systems with varying $k(x)$ under several types of external actions (oscillating distributed load, moving loads, etc.) may be pursued.

- By referring to the action of moving vehicles on finite beams on elastic foundation, in order to obtain a more realistic dynamic response of the system, some further improvements of the modelization could be made to obtain an even more detailed dynamic response of the beam-foundation system. A moving oscillator interacting with the beam should be considered, instead as of a simple moving force. An accelerating/decelerating moving load may also be a subject of further dynamic analyses. The geometrical linear hypothesis on the kinematics of the beam could be relaxed and a more complex constitutive law of the support, which would be both a nonlinear function of the beam displacements and with a different behavior in compression and in tension, may be included. Further, more accurate models could even consider wave propagation phenomena in both beam and underlying substratum, by modelling the foundation as a continuum of a finite or infinite depth. Real applications usually require extensions to infinite lenghts; it is then necessary to eliminate the effect of the supports, by mitigating the perturbation induced by the reflection of the traveling waves. This could be achieved by implementing further appropriate artificial (absorbing) boundary techniques.
- With regard to the formulated and implemented DLSFEM-PML formulation, analogous approaches could be developed for other moving load problems, such as those pertaining to plates or to other structural elements, both in the linear and nonlinear contexts, which actually provided an underlying main motivation to pursue the present numerical formulation of linear problems, already endowed with a closed-from explicit analytical solutions as for a benchmark reference.

Appendix

Short historical profile of Emil Winkler [1835-1888]

Emil Winkler was with no doubts one of the most important German civil engineers of the XIX century. He is well known as forerunner in the study of influence lines, high curvature beams and strength of materials, as well as the inventor of the homonymus mechanical model of elastic soil (called in German *"Winklersche Bettung"*). He was contemporary of other European founding fathers of modern Structural Analysis, such as J.A. Charles Bresse [1822-1883], C.L. Navier [1785-1836], B.P.E. Clapeyron [1799-1867], G. Lamé [1795-1870]. Main events about Winkler's life have been described e.g. by Timoshenko (1953) [252], Knothe (2000) [167], (2004) [166] and Kurrer (2008) [169].

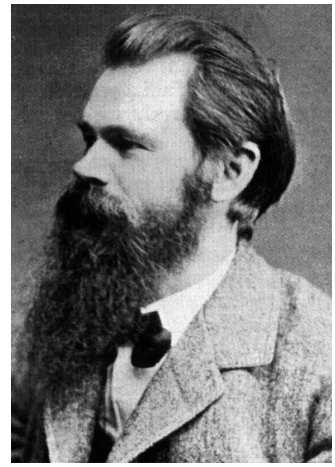

Figure A.1: Portrait of Emil Winkler taken in the period he lived in Prague (from Kurrer, 2008 [169]).

Emil Winkler (Fig. A.1) was born in 1835 in Falkenberg at Torgau (Saxony), the son of the forester Johann Leberecht Winkler. He attended elementary school in 1841 in Falkenberg and the Torgau Gymnasium from 1847. The same year, while Winkler was firstly visiting the high school in Torgau, his father committed suicide shooting himself in the mouth, as reported by the parish register. That must had been quite a traumatic event for him, since he was only twelve. Three years later he made the high school dropout decision and worked as apprentice bricklayer for sustaining his humble family. It is supposed that Johann Arndt Albert, his mathematics teacher, has pointed out to him the possibility of a second-chance education to obtain a certificate of professional education. Then, after he "graduated" as a bricklayer in Torgau, Winkler attended the "Baugewerkeschule", a kind of building trade school founded in Holzminden in 1831, in order to upgrade his skills for subsequent

studies. Later, in fact, Winkler studied cleverly calculus of structures for four years at the Dresden Polytechnic, where probably his mathematics professor Oscar Schlömilch helped in improving Winkler's mathematical skills, which were certainly inadequate after his brief high school attendance.

Since from his first publication[1] soon after graduating, Winkler's modeling capabilities were undeniable and remained a distinctive feature of all his works. He obtained his Doctor of Philosophy degree at the University of Leipzig in 1861, by presenting a dissertation on a topic of soil mechanics entitled "On the pressure inside of earth masses", a theory about retaining walls, with the physicist Wilhelm Gottlieb Hankel (father of mathematician Hermann Hankel) as advisor. The same year, two other important events occurred: Winkler was employed as a teacher of strength of materials at the Saxony Waterways Department of the Polytechnic of Dresden and got married to Clara Helene Crentz, the daughter of a Dresdner merchant. Later, in 1863, he became a lecturer in bridge engineering.

In 1865, just after his thirtieth birthday, Winkler was appointed as professor of bridge and railroad engineering at the Polytechnic Institute of Prague. He was a good teacher and during his lessons he crossed the quite whole field of civil engineering: bridge construction, tunnel construction, foundation problems, earth-moving, elasticity and strength of materials. In that period in Prague he wrote his famous book *"Die Lehre von der Elastizität und Festigkeit"* (Theory of Elasticity and Strength) [271], a general textbook on elastic theory and strength of materials for engineers published in 1867, in which a new method stood out, which allowed to analyze railway tracks on gravel (theory of the beam resting on an elastic foundation, as described here in Chapter 2).

Although nowadays engineers are rarely familiar with this book and other Winkler's writings, the name of Emil Winkler is still very much known by the international scientific community since the method he outlined is still used on gravel tracks after nearly 150 years and applied also to a number of other technical problems.

Winkler's successes in transforming classical mathematical elasticity theory into a practical methodology for the analysis of bridges and buildings were the reasons for his appointment at the Vienna Polytechnic in 1868, on a chair for the course of railway and bridge engineering. Finally, in 1877, Winkler was appointed for the planned construction of the Technical University of Berlin (Bau Akademie), where, besides his teaching and research activities, he served as chairman of the civil engineering department in 1880-81 and 1885-86, and was elected dean from 1881 to 1882. He devoted his increasingly dwindling forces to establishing the teaching of statics of structures. His teaching was,

[1] E. Winkler (1858), "Formänderung und Festigkeit gekrümmter Körper, insbesondere der Ringe" (Change of shape and strength of curved body, which helps users look at rings), *Civiling.*, 4, 232–246.

even by today's point of view, modern and didactic.

Emil Winkler was only 53 when, after a second stroke, died in August 1888 in his house in Berlin-Friedenau.

Bibliography

[1] Abu-Hilal M. Dynamic response of a double Euler-Bernoulli beam due to a moving constant load. *Journal of Sound and Vibration*, 297(3-5): 477–491, 2006.

[2] Achenbach J.D., Sun C.T. Moving load on a flexibly supported Timoshenko beam. *International Journal of Solids and Structures*, 1(4): 353–370, 1965.

[3] Adin M.A., Yankelevsky D.Z., Eisemberger M. Analysis of beams on a bi-moduli elastic foundation. *Computer Methods in Applied Mechanics and Engineering*, 49(3): 319–330, 1985.

[4] Amiri S.N., Onyango M. Simply supported beam response on elastic foundation carrying loads. *Journal of Engineering Science and Technology*, 5(1): 52–66, 2010.

[5] Andersen L., Nielsen S.R.K., Kirkegaard P.H. Finite element modelling of infinite Euler beams on kelvin foundations exposed to moving loads in convected co-ordinates. *Journal of Sound and Vibration*, 241(4): 587–604, 2001.

[6] Ansari M., Esmailzadeh E., Younesian D. Internal-external resonance of beams on non-linear viscoelastic foundation traversed by moving load. *Nonlinear Dynamics*, 61(1-2): 163–182, 2010.

[7] Ansari M., Esmailzadeh E., Younesian D. Frequency analysis of finite beams on nonlinear Kelvin-Voigt foundation under moving loads. *Journal of Sound and Vibration*, 330(7): 1455–1471, 2011.

[8] Arbabi F., Farzanian M.S. Propagation of waves in infinite beams: PML approach. In *Proceedings of the XI World Congress on Computational Mechanics (WCCM XI 2014), ISBN: 978-84-942844-7-2*, pages 1404–1415, 2014.

[9] Astley R.J. Infinite elements for wave problems: a review of current formulations and an assessment of accuracy. *International Journal for Numerical Methods in Engineering*, 49(7): 951–976, 2000.

[10] Avramidis I.E., Morfidis K. Bending of beams on three-parameter elastic foundation. *International Journal of Solids and Structures*, 43(2): 357–375, 2006.

[11] Aydogan M. Stiffness-matrix formulation of beams with shear effect on elastic foundation. *Journal of Structural Engineering, ASCE*, 121(9): 1265–1270, 1995.

[12] Ayoub A. A two-field mixed variational principle for partially connected composite beams. *Finite Elements in Analysis and Design*, 37(11): 929–959, 2001.

[13] Ayoub A. Mixed formulation of nonlinear beam on foundation elements. *Computers and Structures*, 81(7): 411–421, 2003.

[14] Babŭska I. The Finite Element Method with Lagrange multipliers. *Numerische Mathematik*, 20(3): 179–192, 1973.

[15] Bak J., Newman D.J. *Complex Analysis*. Springer, 2010.

[16] Barden L. Distribution of contact pressure under foundations. *Geotechnique*, 12(3): 181–198, 1962.

[17] Basu D., Kameswara Rao N.S.V. Analytical solutions for Euler-Bernoulli beam on visco-elastic foundation subjected to moving load. *International Journal for Numerical Analytical Methods in Geomechanics*, 37(8): 945–960, 2013.

[18] Basu U., Chopra A.K. Numerical evaluation of the damping-solvent extraction method in the frequency domain. *Earthquake Engineering and Structural Dynamics*, 31(6): 1231–1250, 2002.

[19] Basu U., Chopra A.K. Perfectly matched layers for time-harmonic elastodynamics of unbounded domains: theory and finite-element implementation. *Computer Methods in Applied Mechanics and Engineering*, 192(11-12): 1337–1375, 2003.

[20] Bathe K.J. *Finite Element Procedures, I Ed.* Prentice-Hall, 2006.

[21] Bayliss A., Gunzburger M., Turkel E. Boundary conditions for the numerical solution of elliptic equations in exterior regions. *Journal of Applied Mathematics (SIAM)*, 42(2): 430–451, 1982.

[22] Bayliss A., Turkel E. Radiation boundary conditions for wave-like equations. *Communications on Pure and Applied Mathematics*, 33: 707–725, 1980.

[23] Beaufait F.W. Numerical analysis of beams on elastic foundation. *Journal of the Mechanics Division, ASCE*, 103(EM1): 205–209, 1977.

[24] Beaufait F.W., Hoadley P.W. Analysis of elastic beams on nonlinear foundations. *Computer and Structures*, 12(5): 669–676, 1980.

[25] Belytschko T., Hughes T.J.R. *Computational Methods for Transient Analysis, Vol. 1 in Computational Methods in Mechanics*. North-Holland, 1983.

[26] Bensow R., Larson M.G. Discontinuous least-squares finite element method for the Div-Curl problem. *Numerische Mathematik*, 101(4): 601–617, 2005.

[27] Bensow R., Larson M.G. Discontinuous/continuous least-squares finite element methods for elliptic problems. *Mathematical Models and Methods in Applied Sciences*, 15(6): 825–842, 2005.

[28] Berenger J.P. A Perfectly Matched Layer for the absorption of electromagnetic waves. *Journal of Computational Physics*, 114(2): 185–200, 1994.

[29] Beskou N.D., Theodorakopoulos D.D. Dynamic effects of moving loads on road pavements: a review. *Soil Dynamics and Earthquake Engineering*, 31(4): 547–567, 2011.

[30] Bettess P. Infinite elements. *International Journal for Numerical Methods in Engineering*, 11(1): 53–64, 1977.

[31] Bettess P. Infinite elements for static problems. *Engineering Computations*, 1(1): 4–16, 1984.

[32] Bhattiprolu U., Bajaj A.K., Davies P. An efficient solution methodology to study the response of a beam on viscoelastic and nonlinear unilateral foundation: Static response. *International Journal of Solids and Structures*, 50(14-15): 2328–2339, 2013.

[33] Biermann J., von Estorff O., Petersen S., Wenterodt C. Higher order finite and infinite elements for the solution of Helmholtz problems. *Computer Methods in Applied Mechanics and Engineering*, 198(13-14): 1171–1188, 2009.

[34] Biot M.A. Bending of an infinite beam on an elastic foundation. *Journal of Applied Mechanics, ASME*, 59(203): 1–7, 1937.

[35] Bleistein N., Handelsman R.A. *Asymptotic Expansions of Integrals*. Dover Publications, 1986.

[36] Bochev P.B., Gunzburger M.D. Least-squares methods for the velocity-pressure-stress formulation of the Stokes equations. *Computer Methods in Applied Mechanics and Engineering*, 126(3-4): 267–287, 1995.

[37] Bochev P.B., Gunzburger M.D. Finite element methods of least-squares type. *SIAM Review*, 40(4): 789–837, 1998.

[38] Bochev P.B., Gunzburger M.D. Least-squares finite element methods. In *Proceedings of the International Congress of Mathematicians (ICM2006)*, volume 3, pages 1137–1162, 2006.

[39] Bochev P.B., Lai J., Olson L. A locally conservative, discontinuous least-squares finite element method for the Stokes equations. *International Journal for Numerical Methods in Fluids*, 68(6): 782–804, 2012.

[40] Bogacz R., Krzyỳski T., Popp K. On the generalization of Mathews problem of the vibrations of a beam on elastic foundation. *ZAMM - Journal of Applied Mathematics and Mechanics / Zeitschrift für Angewandte Mathematik und Mechanik*, 69(8): 243–252, 1989.

[41] Borák, P. Marcián L. Beams on elastic foundation using modified Betti's theorem. *International Journal of Mechanical Sciences*, 88: 17–24, 2014.

[42] Bowles J.E. *Analytical and Computer Methods in Foundation Engineering*. McGraw-Hill, 1974.

[43] Bramble J.H., Lazarov R.D., Pasciak J.E. Least-squares methods for linear elasticity based on a discrete minus one inner product. *Computer Methods in Applied Mechanics and Engineering*, 191(8–10): 727–744, 2001.

[44] Brenner S.C., Scott L.R. *The Mathematical Theory of Finite Element Methods*. Springer, 2008.

[45] Brezzi F. On the existence, uniqueness and approximation of saddle point problems arising from Lagrangian multipliers. *Analyse Numérique*, 8(R2): 129–151, 1974.

[46] Buschman R.G. *Integral Transformations, Operational Calculus, and Generalized Functions*. Springer, 1996.

[47] Buta P.G., Jones J.P. Response of cylindrical shells to moving loads. *Journal of Applied Mechanics, ASME*, 31(1): 105–111, 1964.

[48] Cao C.Y., Zhong Y. Dynamic response of a beam on a Pasternak foundation and under a moving load. *Journal of Chongqing University*, 7(4): 311–316, 2008.

[49] Castro Jorge P., Pinto da Costa A., Simões F.M.F. Finite element dynamic analysis of finite beams on a bilinear foundation under a moving load. *Journal of Sound and Vibration*, 346: 328–344, 2015.

[50] Castro Jorge P., Simões F.M.F., Pinto da Costa A. Dynamics of beams on non-uniform nonlinear foundations to moving loads. *Computer and Structures*, 148: 26–34, 2015.

[51] Chang S.Y. Performance of the HHT-α method for the solution of nonlinear systems. *International Journal of Structural Stability and Dynamics*, 8(2): 321–337, 2008.

[52] Chen C.N. Solution of beam on elastic foundation by DQEM. *Journal of Engineering Mechanics, ASCE*, 124(12): 1381–1384, 1998.

[53] Chen Y.H., Huang Y.H. Dynamic stiffness of infinite Timoshenko beam on viscoelastic foundation in moving co-ordinate. *International Journal for Numerical Methods in Engineering*, 48(1): 1–18, 2000.

[54] Chen Y.H., Huang Y.H. Dynamic characteristics of infinite and finite railways to moving loads. *Journal of Engineering Mechanics, ASCE*, 129(9): 987–995, 2003.

[55] Chen Y.H., Huang Y.H., Shih C.T. General dynamic-stiffness matrix of a Timoshenko beam for transverse vibrations. *Earthquake Engineering and Structural Dynamics*, 15(3): 391–402, 1987.

[56] Chen Y.H., Huang Y.H., Shih C.T. Response of an infinite Timoshenko beam on a viscoelastic foundation to a harmonic moving load. *Journal of Sound and Vibration*, 241(5): 809–824, 2001.

[57] Chen Y.H., Sheu J.T. Axially-loaded damped Timoshenko beam on viscoelastic foundation. *International Journal for Numerical Methods in Engineering*, 36(6): 1013–1027, 1993.

[58] Chonan S. Moving harmonic load on an elastically supported Timoshenko beam. *Zeitschrift für Angewandte Mathematik und Mechanik (ZAMM)*, 58(1): 9–15, 1978.

[59] Cifuentes A.O. Dynamic response of a beam excited by a moving mass. *Finite Elements in Analysis and Design*, 5(3): 237–246, 1989.

[60] Clastornik J., Eisenberger M., Yankelevsky D.Z., Adin M.A. Beams on variable Winkler foundation. *Journal of Applied Mechanics, ASME*, 53(4): 925–928, 1986.

[61] Coddington E.A., Levinson N. *Theory of Ordinary Differential Equations*. McGraw-Hill, New Delhi, 1955.

[62] Croft A. An application of convergence acceleration techniques to a class of two-point boundary value problems on a semi-infinite domain. *Numerical Algorithms*, 2: 307–320, 1992.

[63] Curnier A., He Q.C., Zysset P. Conewise linear elastic materials. *Journal of Elasticity*, 37(1): 1–38, 1995.

[64] De Hoog F.R., Weiss R. The numerical solution of boundary value problems with an essential singularity. *Journal of Numerical Analysis (SIAM)*, 16(4): 637–669, 1979.

[65] De Hoog F.R., Weiss R. An approximation theory for boundary value problems on infinite intervals. *Computing*, 24(2-3): 227–239, 1980.

[66] Dickson L.E. *Elementary Theory of Equations*. John Wiley and Sons, 1914.

[67] Dieterman H.A., Metrikine A.V. Steady-state displacements of a beam on an elastic half-space due to a uniformly moving constant load. *European Journal of Mechanics A/Solids*, 16(2): 295–306, 1997.

[68] Dimitrovová Z. A general procedure for the dynamic analysis of finite and infinite beams on piece-wise homogeneous foundation under moving loads. *Journal of Sound and Vibration*, 329(13): 2635–2653, 2010.

[69] Dimitrovová Z. Critical velocity of a uniformly moving load on a beam supported by a finite depth foundation. *Journal of Sound and Vibration*, 366: 325–342, 2016.

[70] Dimitrovová Z. Analysis of the critical velocity of a load moving on a beam supported by a finite depth foundation. *International Journal of Solids and Structures*, 122-123:128–147, 2017.

[71] Dimitrovová Z. New semi-analytical solution for a uniformly moving mass on a beam on a two-parameter visco-elastic foundation. *International Journal of Mechanical Sciences*, 127: 142–162, 2017.

[72] Dimitrovová Z., Rodrigues A.F.S. Critical velocity of a uniformly moving load. *Advances in Engineering Software*, 50(1): 44–56, 2012.

[73] Dimitrovová Z., Varandas J.N. Critical velocity of a load moving on a beam with a sudden change of foundation stiffness: Applications to highspeed trains. *Computers and Structures*, 87(19): 1224–1232, 2009.

[74] Ding H., Chen L.Q., Yang S.P. Convergence of Galerkin truncation for dynamic response of finite beams on nonlinear foundations under a moving load. *Journal of Sound and Vibration*, 331(10):2426–2442, 2012.

[75] Ding H., Shi K.L., Chen L.Q., Yang S.P. Adomian polynomials for nonlinear response of supported Timoshenko beams subjected to a moving harmonic load. *Acta Mechanica Solida Sinica*, 27(4):383–393, 2014.

[76] Dodge A. Influence functions for beams on elastic foundations. *Journal of the Structural Division, ASCE*, 90(ST4): 63–102, 1964.

[77] Duan H.Y., Gao S.Q., Jiang B.N., Tan R.C.E. Analysis of a least-squares finite element method for the thin plate problem. *Applied Numerical Mathematics*, 59(5): 976–987, 2009.

[78] Duffy D. The response of an infinite railroad track to a moving, vibrating mass. *Journal of Applied Mechanics, ASME*, 57(1): 66–73, 1990.

[79] Dyniewicz B. Space-time finite element approach to general description of a moving inertial load. *Finite Elements in Analysis and Design*, 62: 8–17, 2012.

[80] Eason E.D. A review of least squares methods for solving partial differential equations. *International Journal for Numerical Methods in Engineering*, 10(5): 1021–1046, 1976.

[81] Ebrahimi F., Barati M.R. A nonlocal higher-order refined magneto-electro-viscoelastic beam model for dynamic analysis of smart nanostructures. *International Journal of Engineering Science*, 107: 183–196, 2016.

[82] Eftekhari S.A. A differential quadrature procedure for linear and nonlinear steady state vibrations of infinite beams traversed by a moving point load. *Meccanica*, 51(10): 2417–2434, 2016.

[83] Eisenberger M., Clastornik J. Beams on variable two-parameters elastic foundation. *Journal of Engineering Mechanics*, 113(10): 1454–1466, 1987.

[84] Eisenberger M., Yankelevsky D.Z. Exact stiffness matrix for beams on elastic foundation. *Computer and Structures*, 21(6): 1355–1359, 1985.

[85] Engquist B., Majda A. Absorbing boundary conditions for the numerical simulation of waves. *Mathematics of Computation*, 31(139): 629–651, 1977.

[86] Engquist B., Majda A. Radiation boundary conditions for acoustic and elastic wave calculations. *Communications on Pure and Applied Mathematics*, 32: 313–357, 1979.

[87] Erdélyi A. *Higher Transcendetal Functions, Volume I.* McGraw-Hill, 1953.

[88] Erkal A., Laefer D.F., Tezcan S. Advantages of infinite elements over prespecified boundary conditions in unbounded problems. *Journal of Computing in Civil Engineering (ASCE)*, 29(6): 1–12, 2015.

[89] Ern A., Guermond J.L. *Theory and Practice of Finite Elements*. Springer, 2004.

[90] Evcan N., Hayir A. Dynamic response of a infinite beam on a Pasternak foundation and under a moving load. In *Proceedings of the VII International Structural Engineering and Construction Conference, ISBN: 978-981-07-5354-2*, pages 79–83, 2013.

[91] Fazio R. A novel approach to the numerical solution of boundary value problems on infinite intervals. *Journal of Numerical Analysis (SIAM)*, 33(4): 1473–1483, 1996.

[92] Filipich C.P., Rosales M.B. A further study about the behaviour of foundation piles and beams in a Winkler-Pasternak soil. *International Journal of Mechanical Sciences*, 44(1): 21–36, 2002.

[93] Filonenko-Borodich M.M. Some approximate theories of the elastic foundation (in russian). *Uchenyie Zapiski Moskovskogo Gosudarstvennogo Universiteta Mekhanica*, 46: 3–18, 1940.

[94] Fix G.J., Gunzburger M.D., Nicolaides R.A. On finite element methods of the least squares type. *Computers and Mathematics with Applications*, 5(2): 87–98, 1979.

[95] Franklin J.N., Scott R.F. Beam equation with variable foundation coefficient. *Journal of the Engineering Mechanics Division, ASCE*, 105(5): 811–827, 1979.

[96] Fraser D.C. Beams on elastic foundations. A computer-oriented solution for beams with free ends. *Civil Engineering Transactions*, 11(1): 25–30, 1969.

[97] Froio D., Moioli R., Rizzi E. Numerical dynamical analysis of beams on nonlinear elastic foundations under harmonic moving load. In *Proceedings of the VII European Congress on Computational Methods in Applied Sciences and Engineering (ECCOMAS2016), ISBN: 978-618-82844-0-1, 5–10 June, Crete Island, Greece*, volume 3, pages 4794–4809, doi: 10.7712/100016.2149.7515, 2016.

[98] Froio D., Rizzi E. Analytical solution for the elastic bending of beams lying on a variable Winkler support. *Acta Mechanica*, 227(4): 1157–1179, 2015.

[99] Froio D., Rizzi E. Analytical solution for the elastic bending of beams lying on a linearly variable Winkler support. *International Journal of Mechanical Sciences*, 128-129: 680–694, 2017.

[100] Froio D., Rizzi E., Simões F.M.F., Pinto da Costa A. Critical velocities of a beam on nonlinear elastic foundation under harmonic moving load. *Procedia Engineering*, 199: 2585–2590, *Special issue on the X International Conference on Structural Dynamics (EURODYN2017)*, 10–13 September, Rome, Italy, 2017.

[101] Froio D., Rizzi E., Simões F.M.F., Pinto da Costa A. Dynamics of beams on a bilinear elastic foundation under harmonic moving load. *Acta Mechanica*, 229(10): 4141–4165, 2017.

[102] Froio D., Rizzi E., Simões F.M.F., Pinto da Costa A. Universal analytical solution of the steady-state response of an infinite beam on a Pasternak elastic foundation under moving load. *International Journal of Solids and Structures*, 132-133: 245–263, 2018.

[103] Froio D., Rizzi E., Simões F.M.F., Pinto da Costa A. DLSFEM-PML formulation for the steady-state response of a taut string on elastic support under moving load. *Meccanica, doi: https://dx.doi.org/10.1007/s11012-019-01047-7*, 2019.

[104] Froio D., Rizzi E., Simões F.M.F., Pinto da Costa A. True PML for elastic-supported beam steady-state vibration under moving load by DLSFEM formulation. *Submitted for publication*, 2019.

[105] Frýba L. *Vibration of Solids and Structures under Moving Loads, III Ed.* Research Institute of Transport, 1972.

[106] Frydrýšek K. Beams on elastic foundation solved via probabilistic approach (SBRA Method). *In: Advances in Safety, Reliability and Risk Management, Bérenguer C., Grall A., Soares C.G. Eds.*, pages 1849–1854, 2012.

[107] Gavrilov S. Non-stationary problems in dynamics of a string on an elastic foundation subjected to a moving load. *Journal of Sound and Vibration*, 222(3): 345–361, 1999.

[108] Gazis D.C. Analysis of finite beams on elastic foundations. *Journal of the Structural Division, ASCE*, 84(ST4): 1–18, 1958.

[109] Gerritsma M.I., Proot M.M.J. Analysis of a discontinuous least squares spectral element method. *Journal of Scientific Computing*, 17(1): 297–306, 2002.

[110] Givoli D. *Numerical Methods for Problems in Infinite Domains*. Elsevier, 1992.

[111] Givoli D. A spatially exact non-reflecting boundary condition for time dependent problems. *Computer Methods in Applied Mechanics and Engineering*, 95: 97–113, 1992.

[112] Givoli D. High-order local non-reflecting boundary conditions: a review. *Wave Motion*, 39(4): 319–326, 2004.

[113] Givoli D., Keller J.B. A finite element method for large domains. *Computer Methods in Applied Mechanics and Engineering*, 76(1): 41–66, 1989.

[114] Givoli D., Keller J.B. Non-reflecting boundary conditions for elastic waves. *Wave Motion*, 12: 261–279, 1990.

[115] Givoli D., Neta B. High-order non-reflecting boundary scheme for time-dependent waves. *Journal of Computational Physics*, 186: 24–46, 2003.

[116] Graff K.F. *Wave Motion in Elastic Solids*. Dover Publications, 1975.

[117] Guo Y., Weitsman Y.J. Solution method for beams on nonuniform elastic foundations. *Journal of Engineering Mechanics, ASCE*, 128(5): 592–594, 2002.

[118] Hadi M.N.S., Bodhinayake B.C. Non-linear finite element analysis of flexible pavements. *Advances in Engineering Software*, 34(11–12): 657–662, 2003.

[119] Hagstrom T.M., Keller H.B. Asymptotic boundary conditions and numerical methods for nonlinear elliptic problems on unbounded domains. *Mathematics of Computation*, 48(178): 449–470, 1987.

[120] Hajiabadi M.R., Lotfi V. An effective approach for utilizing damping solvent extraction method in frequency domain. *Soil Dynamics and Earthquake Engineering*, 38:46–57, 2012.

[121] Han H., Wu X. The approximation of the exact boundary conditions at an artificial boundary for linear elastic equations and its application. *Mathematics of Computation*, 59(199): 21–37, 1992.

[122] Hayashi K. *Theory of the beam on an elastic foundation and its application to civil engineering, together with a table of circular and hyperbolic functions (in German)*. Springer-Verlag, Berlin, 1921.

[123] Hendry A.W. New method for the analysis of beams on elastic foundations. *Civil Engineering and Public Works Review*, 53(621): 297–299, 1958.

[124] Hertz H. On the equilibrium of floating elastic plates. *Wiedemann's Annalen*, 22: 449–455, 1884.

[125] Hetényi M. *Beams on Elastic Foundation*. The University of Michigan Press, 1946.

[126] Hetényi M. A general solution for the bending of beams on an elastic foundation of arbitrary continuity. *Journal of Applied Physics*, 21(1): 55–58, 1950.

[127] Hetényi M. Beams and plates on elastic foundations and related problems. *Applied Mechanics Reviews*, 19(2): 95–102, 1966.

[128] Higdon R.L. Radiation boundary conditions for dispersive waves. *Journal of Numerical Analysis (SIAM)*, 31(1): 64–100, 1994.

[129] Hilber H.M., Hughes T.J.R., Taylor R.L. Improved numerical dissipation for time integration algorithms in structural dynamics. *Earthquake Engineering and Structural Dynamics*, 3(10): 283–292, 1977.

[130] Horibe T. Boundary integral equation method analysis for beam-columns on elastic foundation. *Transactions of the Japan Society of Mechanical Engineers, Part A*, 62(601): 2067–2071, 1996.

[131] Hosur V., Bhavikatti S.S. Influence lines for bending moments in beams on elastic foundations. *Computer and Structures*, 58(6): 1225–1231, 1996.

[132] Ibdah H., Khuri S.A., Sayfy A. Two-point boundary-value problems over a semi-infinite domain: a coupled ABC and spline collocation approach. *International Journal for Computational Methods in Engineering Science and Mechanics*, 15(5): 448–456, 2014.

[133] Ince E.L. *Ordinary Differential Equations*. General Publishing Company, 1978.

[134] Iwiński T. *Theory of beams - The Application of the Laplace Transformation Method to Engineering Problems (edited and translated by E.P. Bernat)*. Pergamon Press, 1967.

[135] Iyengar K.T.S.R., Anantharamu S. Finite beam-columns on elastic foundations. *Journal of the Engineering Mechanics Division, ASCE*, 89(EM6): 139–160, 1963.

[136] Iyengar K.T.S.R., Anantharamu S. Finite beam-columns on elastic foundations. *Journal of the Structural Division, ASCE*, 91(ST3): 45–56, 1965.

[137] Jang T.S. A new semi-analytical approach to large deflections of Bernoulli-Euler-v. Kármán beams on a linear elastic foundation: Nonlinear analysis of infinite beams. *International Journal of Mechanical Sciences*, 66: 22–32, 2013.

[138] Jang T.S. A general method for analyzing moderately large deflections of a non-uniform beam: an infinite Bernoulli-Euler-v. Kármán beam on a nonlinear elastic foundation. *Acta Mechanica*, 225(7): 1967–1984, 2014.

[139] Jang T.S., Baek H.S., Paik J.K. A new method for the non-linear deflection analysis of an infinite beam resting on a non-linear elastic foundation. *International Journal of Non-Linear Mechanics*, 46(1): 339–346, 2011.

[140] Jang T.S., Sung H.G. A new semi-analytical method for the non-linear static analysis of an infinite beam on a non-linear elastic foundation: A general approach to a variable beam cross-section. *International Journal of Non-Linear Mechanics*, 47(4): 132–139, 2012.

[141] Jespersen D.C. A least squares decomposition method for solving elliptic equations. *Mathematics of Computation*, 31(140): 873–880, 1977.

[142] Jiang B.N. *The Least-Squares Finite Element Method*. Springer, 1998.

[143] Jiang B.N. On the least-squares method. *Computer Methods in Applied Mechanics and Engineering*, 152(1): 239–257, 1998.

[144] Jiang B.N. The least-squares finite element method in elasticity. Part I: Plane stress or strain with drilling degrees of freedom. *International Journal for Numerical Methods in Engineering*, 53(3): 621–636, 2002.

[145] Jiang B.N., Povinelli L.A. Optimal least-squares finite element method for elliptic problems. *Computer Methods in Applied Mechanics and Engineering*, 102(2): 199–212, 1993.

[146] Johnson W.H., Kouskoulas V. Beam on bilinear foundation. *Journal of Applied Mechanics, ASME*, 72(APM): 239–243, 1973.

[147] Jones G. *Analysis of Beams on Elastic Foundations Using Finite Difference Theory*. Thomas Telford Publishing, New York, 1997.

[148] Joodaky A., Joodaky I. A semi-analytical study on static behavior of thin skew plates on Winkler and Pasternak foundations. *International Journal of Mechanical Sciences*, 100: 322–327, 2015.

[149] Jou J., Yang S.-Y. Least-squares finite element approximations to the Timoshenko beam problem. *Applied Mathematics and Computation*, 115(1): 63–75, 2000.

[150] Kadalbajoo M.K., Raman K.S. Cubic spline solutions of boundary value problems over infinite intervals. *Journal of Computational and Applied Mathematics*, 15(3): 283–291, 1986.

[151] Kargarnovin M.H., Younesian D. Dynamics of Timoshenko beams on Pasternak foundation under moving load. *Mechanics Research Communications*, 31(6): 713–723, 2004.

[152] Kaschiev M.S., Mikhajlov K. A beam resting on a tensionless Winkler foundation. *Computer and Structures*, 55(2): 261–264, 1995.

[153] Kaynia A.M., Madshus C., Zackrisson P. Ground vibration from high speed trains: prediction and countermeasure. *Journal of Geotechnical and Geoenvironmental Engineering*, 126(6): 531–537, 2000.

[154] Keller J.B., Givoli D. Exact non-reflecting boundary conditions. *Journal of Computational Physics*, 82(1):172–192, 1989.

[155] Kenney J.T.Jr. Steady-state vibrations of beams on elastic foundations for moving load. *Journal of Applied Mechanics, ASME*, 21(4): 359–364, 1954.

[156] Kerr A.D. Elastic and viscoelastic foundation models. *Journal of Applied Mechanics, ASME*, 31(3): 491–498, 1964.

[157] Kerr A.D. A study of a new foundation model. *Acta Mechanica*, 1(2): 135–147, 1965.

[158] Kerr A.D. The continuously supported rail subjected to an axial force and a moving load. *International Journal of Mechanical Sciences*, 14(1): 71–78, 1972.

[159] Kerr A.D. Continuously supported beams and plates subjected to moving loads: a survey. *Solid Mechanics Archives*, 6(4): 401–449, 1981.

[160] Kerr A.D. On the determination of the rail support modulus k. *International Journal of Solids and Structures*, 37(32): 4335–4351, 2000.

[161] Khajeansari A., Baradaran G.H., Yvonnet J. An explicit solution for bending of nanowires lying on Winkler-Pasternak elastic substrate medium based on the Euler-Bernoulli beam theory. *International Journal of Engineering Science*, 52: 115–128, 2012.

[162] Kien N.D. Dynamic response of prestressed Timoshenko beams resting on two-parameter foundation to moving harmonic load. *Technische Mechanik*, 28(3-4): 237–258, 2008.

[163] Kien N.D., Ha L.T. Dynamic characteristics of elastically supported beam subjected to a compressive axial force and a moving load. *Vietnam Journal of Mechanics*, 33(2): 113–131, 2011.

[164] Kien N.D., Hai T.T. Dynamic analysis of prestressed Bernoulli beams resting on two-parameter foundation under moving harmonic load. *Vietnam Journal of Mechanics*, 28(3): 176–188, 2006.

[165] Klepikov A.N. Calculation of beams on an elastic foundation with a variable modulus of subgrade reaction. *Osnovaniya, Fundamenty i Mekhanika Gruntov (Soil Mechanics and Foundation Engineering)*, 2(3): 296–299, 1968.

[166] Knothe K. *Fiedlerbriefe und Bibliographie Emil Winklers*. Institut für Geschichte der Naturwissenschaften, 2004.

[167] Knothe K., Tausendfreund D. *Emil Oskar Winkler <1835–1888>. Begründer der Statik der Baukonstruktionen an der TH Berlin. Leben und Werk. In: 1799–1999. Von der Bauakademie zur Technischen Universität Berlin. Geschichte und Zukunft, K. Schwarz for the president of Berlin TU Eds.,*. Ernst and Sohn, 2000.

[168] Kumar C.P.S., Sujatha C., Shankar K. Vibration of simply supported beams under a single moving load: A detailed study of cancellation phenomenon. *International Journal of Mechanical Sciences*, 99: 40–47, 2015.

[169] Kurrer K.E., Ramm E. *The History of the Theory of Structures: From Arch Analysis to Computational Mechanics*. Ernst and Sohn Verlag für Architektur und technische Wissenschaften, 2008.

[170] Ladyzhenskaya O.A. *The Mathematical Theory of Viscous Incompressible Flows*. Gordon and Breach, 1969.

[171] Lancioni G. High-order absorbing boundary conditions and perfectly matched layers for cables and beams laid on elastic supports. In *Proceedings of the V European Congress on Computational Methods in Applied Sciences and Engineering (ECCOMAS2012), ISBN: 978-3-9503537-0-9*, pages 551–563, 2012.

[172] Lancioni G. Numerical comparison of high-order absorbing boundary conditions and perfectly matched layers for a dispersive one-dimensional medium. *Computer Methods in Applied Mechanics and Engineering*, 209-212: 74–86, 2012.

[173] Lee S.L., Wang T.M., Kao J.S. Continuous beam-columns on elastic foundation. *Journal of the Engineering Mechanics Division, ASCE*, 87(EM2): 55–70, 1961.

[174] Lentini M. Numerical solution of the beam equation with nonuniform foundation coefficient. *Journal of Applied Mechanics, ASME*, 46(4): 901–904, 1979.

[175] Lentini M., Keller H.B. Boundary value problems on semi-infinite intervals and their numerical solution. *Journal of Numerical Analysis, SIAM*, 17(4): 577–604, 1980.

[176] Levinton Z. Elastic foundations analyzed by the method of redundant reactions. *Journal of the Structural Division, ASCE*, 73(12): 1529–1541, 1949.

[177] Liang F., Li Y., Li L., Wang J. Analytical solution for laterally loaded long piles based on Fourier-Laplace integral. *Applied Mathematical Modelling*, 38(21–22): 5198–5216, 2014.

[178] Limkatanyu S., Damrongwiriyanupap N., Kwon M., Ponbunyanon P. Force-based derivation of exact stiffness matrix for beams on Winkler-Pasternak foundation. *Zeitschrift für Angewandte Mathematik und Mechanik (ZAMM)*, 95(2): 140–155, 2015.

[179] Limkatanyu S., Sae-Long W., Prachasaree W., Kwon M. Improved nonlinear displacement-based beam element on a two-parameter foundation. *European Journal of Environmental and Civil Engineering*, 19(6): 649–671, 2015.

[180] Lin R. Discontinuous discretization for least-squares formulation of singularly perturbed reaction-diffusion problems in one and two dimensions. *SIAM Journal on Numerical Analysis*, 47(1): 89–108, 2008.

[181] Lin R. Discontinuous Galerkin least-squares finite element methods for singularly perturbed reaction-diffusion problems with discontinuous coefficients and boundary singularities. *Numerische Mathematik*, 112(2): 295–318, 2009.

[182] Ma X., Butterworth J.W., Clifton G.C. Response of an infinite beam resting on a tensionless elastic foundation subjected to arbitrarily complex transverse loads. *Mechanics Research Communications*, 36(7): 818–825, 2009.

[183] Madhav M.R., Kameswara Rao N.S.V., Madhavan K. Laterally loaded pile in elasto-plastic soil. *Soil and Foundations*, 11(2): 1–15, 1971.

[184] Madsen S.S., Krenk S. Asymptotically matched layer (aml) for transient wave propagation in a moving frame of reference. *Computers and Geotechnics*, 82: 124–133, 2017.

[185] Madshus C., Kaynia A.M. High-speed railway lines on soft ground: dynamic behavior at critical train speed. *Journal of Sound and Vibration*, 231(3): 689–701, 2003.

[186] Mallik A.K., Chandra S., Singh A.B. Steady-state response of an elastically supported infinite beam to a moving load. *Journal of Sound and Vibration*, 291(3): 1148–1169, 2006.

[187] Malter H. Numerical solutions for beams on elastic foundations. *Journal of the Structural Division, ASCE*, 84(2): 1–20, 1958.

[188] Markowich P.A. A theory for the approximation of solutions of boundary value problems on infinite intervals. *Journal of Mathematical Analysis (SIAM)*, 13(3): 484–513, 1982.

[189] Mathews P.M. Vibrations of a beam on elastic foundation. *Zeitschrift für Angewandte Mathematik und Mechanik (ZAMM)*, 38(3–4): 105–115, 1958.

[190] Mathews P.M. Vibrations of a beam on elastic foundation II. *Zeitschrift für Angewandte Mathematik und Mechanik (ZAMM)*, 39(1–2): 13–19, 1959.

[191] Matzen R. An efficient finite element time-domain formulation for the elastic second-order wave equation: A non-split complex frequency shifted convolutional PML. *International Journal for Numerical Methods in Engineering*, 88(10): 951–973, 2011.

[192] Mazilu T. Instability of a train of oscillators moving along a beam on a viscoelastic foundation. *Journal of Sound and Vibration*, 332(19): 4597–4619, 2013.

[193] Metrikine A.V. Stationary waves in a nonlinear elastic system interacting with a moving load. *Acustical Physics*, 40(4): 573–576, 1994.

[194] Metrikine A.V., Dieterman H. Instability of vibrations of a mass moving uniformly along an axially compressed beam on a viscoelastic foundation. *Journal of Sound and Vibration*, 201(5): 567–576, 1997.

[195] Metrikine A.V., Verichev S.N. Instability of vibrations of a moving two-mass oscillator on a flexibly supported Timoshenko beam. *Archive of Applied Mechanics*, 71(9): 613–624, 2001.

[196] Miranda C., Nair K. Finite beams on elastic foundation. *Journal of the Structural Division, ASCE*, 92(ST2): 131–142, 1966.

[197] Miyahara F., Ergatoudis J.G. Matrix analysis of structure foundation interaction. *Journal of the Structural Division, ASCE*, 102(ST1): 251–265, 1976.

[198] Mofid M., Shadnam M. On the response of beams with internal hinges, under moving mass. *Advances in Engineering Software*, 31(5): 323–328, 2000.

[199] Mofid M., Tehranchi A., Ostadhossein A. On the viscoelastic beam subjected to moving mass. *Advances in Engineering Software*, 41(2): 240–247, 2010.

[200] Moioli R. *Numerical Analysis of Beams on Nonlinear Winkler Elastic Foundations under Moving Load*. M.Sc. Thesis in Mechanical Engineering, Advisor E. Rizzi, Co-Advisor D. Froio, 31 March 2016, 201 pages.

[201] Moleiro F., Mota Soares C.M., Mota Soares C.A., Reddy J.N. Mixed least-squares finite element models for static and free vibration analysis of laminated composite plates. *Computer Methods in Applied Mechanics and Engineering*, 198(21-26): 1848–1856, 2009.

[202] Monk P., Wang D.-Q. A least-squares method for the Helmholtz equation. *Computer Methods in Applied Mechanics and Engineering*, 175(1-2): 121–136, 1999.

[203] Morfidis K. Vibration of Timoshenko beams on three-parameter elastic foundation. *Computers and Structures*, 88(5-6): 294–308, 2010.

[204] Morvaridi M., Brun M. Perfectly matched layers for flexural waves: An exact analytical model. *International Journal of Solids and Structures*, 102-103: 1–9, 2016.

[205] Mullapudi R., Ayoub A. Nonlinear finite element modeling of beams on two-parameter foundations. *Computers and Geotechnics*, 37(3): 334–342, 2010.

[206] Murphy G.M. *Ordinary Differential Equations and their Solutions*. Van Nostrand, 1960.

[207] Museros P., Moliner E. Letter to the Editor: Comments on "Vibration of simply supported beams under a single moving load: A detailed study of cancellation phenomenon" by C.P. Sudheesh Kumar, C. Sujatha, K. Shankar [Int. J. Mech. Sci. 99 (2015) 40–47, doi:10.1016/j.ijmecsci.2015.05.001]. *International Journal of Mechanical Sciences*, 128–129: 709–713, 2017.

[208] Nguyen D.K., Nguyen Q.H., Tran T.T., Bui V.T. Vibration of bi-dimensional functionally graded Timoshenko beams excited by a moving load. *Acta Mechanica*, 228(1): 141–155, 2017.

[209] Nguyen V.H., Duhamel D. Finite element procedures for nonlinear structures in moving coordinates, Part I: Infinite bar under moving axial loads. *Computers and Structures*, 84(21): 1368–1380, 2006.

[210] Oden J.T., Demkowicz L.F. *Applied Functional Analysis, II Ed.* Chapman and Hall/CRC, 2010.

[211] Olsson M. On the fundamental moving load problem. *Journal of Sound and Vibration*, 145(2): 299–307, 1991.

[212] Ouyang H. Moving-load dynamic problems: A tutorial (with a brief overview). *Mechanical Systems and Signal Processing*, 25(6): 2039–2060, 2011.

[213] Pasternak P.L. *On a new method of analysis of an elastic foundation by means of two foundation constants (in Russian)*. Gosudarstvennoe Izdatelstvo Literaturi po Stroitelstvu i Arkhitekture, 1954.

[214] Pavlović M.N. and Tsikkos S. Beams on quasi-Winkler foundations. *Engineering Structures*, 4(2): 113–118, 1982.

[215] Penzien J. Discontinuity stresses in beams on elastic foundations. *Journal of the Structural Division, ASCE*, 86(ST4): 1083–1095, 1960.

[216] Pipes L.A. *Applied Mathematics for Engineers and Physicists*. Mc-Graw Hill, 1946.

[217] Pontaza J.P. Least-squares variational principles and the finite element method: theory, formulations, and models for solid and fluid mechanics. *Finite Elements in Analysis and Design*, 41(7-8): 703–728, 2005.

[218] Pontaza J.P., Reddy J.N. Mixed plate bending elements based on least-squares formulation. *International Journal for Numerical Methods in Engineering*, 60(5): 891–922, 2004.

[219] Pontaza J.P., Reddy J.N. Least-squares finite element formulation for shear-deformable shells. *Computer Methods in Applied Mechanics and Engineering*, 194(21-24): 2464–2493, 2005.

[220] Popov E.P. Successive approximations for beams on an elastic foundation. *Proceedings of the American Society of Civil Engineers, ASCE*, 76(5): 1–13, 1950.

[221] Prasad B. On the response of a Timoshenko beam under initial stress to a moving load. *International Journal of Engineering Science*, 19(5): 615–628, 1981.

[222] Randolph M.F. The response of flexible piles to lateral loading. *Géotechnique*, 31(2): 247–259, 1981.

[223] Ravi Kanth A.S.V., Reddy Y.N. A numerical method for solving two-point boundary value problems over infinite intervals. *Applied Mathematics and Computation*, 144(2-3): 483–494, 2003.

[224] Ray K.C. Influence lines for pressure distribution under a finite beam on elastic foundation. *Journal of the American Concrete Institute, ACI*, 30(6): 729–740, 1958.

[225] Razaqpur A.G., Shah K.R. Exact analysis of beams on two-parameter elastic foundations. *International Journal of Solids and Structures*, 27(4): 435–454, 1991.

[226] Rees E.L. Graphical discussion of the roots of a quartic equation. *The American Mathematical Monthly*, 29(2): 51–55, 1922.

[227] Reissner E. A note on deflection of plates on a viscoelastic foundation. *Journal of Applied Mechanics, ASME*, 25(1): 144–145, 1958.

[228] Rieker J.R., Lin Y.-H., Trethewey M.W. Discretization considerations in moving load finite element beam models. *Finite Elements in Analysis and Designs*, 21(3): 129–144, 1996.

[229] Rodrigues C., Simões F.M.F., Pinto da Costa A., Froio D., Rizzi E. Finite element dynamic analysis of beams on nonlinear elastic foundations under a moving oscillator. *European Journal of Mechanics - A/Solids*, Accepted for publication on 05 October 2017.

[230] Saito H., Terasawa T. Steady-state vibrations of a beam on a Pasternak foundation for moving loads. *Journal of Applied Mechanics (ASME)*, 47(4): 879–883, 1980.

[231] Salsa S. *Partial Differential Equations in Action, From Modelling to Theory*. Springer, 2008.

[232] Sapountzakis E.J., Kampitsis A.E. Nonlinear response of shear deformable beams on tensionless nonlinear viscoelastic foundation under moving loads. *Journal of Sound and Vibration*, 330(22): 5410–5426, 2011.

[233] Schulkes R.M.S.M., Sneyd A.D. Time-dependent response of floating ice to a steadily moving load. *Journal of Fluid Mechanics*, 186: 25–46, 1988.

[234] Schwedler J.W. Discussion on iron permanent way. In *Proceedings of the Institution of Civil Engineers*, volume 67, pages 95–118, 1882.

[235] Selvadurai A.P.S. *Elastic Analysis of Soil-Foundation Interaction*. Elsevier, 1979.

[236] Senalp A.D., Arikoglu A., Ozkol I., Dogan V.Z. Dynamic response of a finite length Euler-Bernoulli beam on linear and nonlinear viscoelastic foundations to a concentrated moving force. *Journal of Mechanical Science and Technology*, 24(10): 1957–1961, 2010.

[237] Sheehan J.P., Debnath L. On the dynamic response of an infinite Bernoulli-Euler beam. *Pure and Applied Geophysics*, 97(1): 100–110, 1971.

[238] Silveira R.A.M., Pereira W.L.A., Gonçalves P.B. Nonlinear analysis of structural elements under unilateral contact constraints by a Ritz type approach. *International Journal of Solids and Structures*, 45(9): 2629–2650, 2008.

[239] Simkins T.E. Wave Coupling and Resonance in Gun Tubes, Technical Report AECCB-TR-89008, 1–20, 1989.

[240] Singer I., Turkel E. A perfectly matched layer for the helmholtz equation in a semi-infinite strip. *Journal of Computational Physics*, 201(2): 439–465, 2004.

[241] Snitko A.N. Design of flexible supports embedded with variable subgrade coefficient. *Osnovaniya, Fundamenty i Mekhanika Gruntov (Soil Mechanics and Foundation Engineering)*, 5(3): 156–159, 1968.

[242] Soldatos K.P., Selvadurai A.P.S. Flexure of beams resting on hyperbolic elastic foundations. *International Journal of Solids and Structures*, 21(4): 373–388, 1985.

[243] Song C., Wolf J.P. Dynamic stiffness of unbounded medium based on damping-solvent extraction. *earthquake engineering and structural dynamics*, 23(2): 169–181, 1994.

[244] Squire V.A., Hosking R.J., Kerr A.D., Langhorne P.J. *Moving Loads on Ice Plates*. Kluwer Academic Publishers, 1996.

[245] Stadler W. The general solution of the classical problem of the response of an infinite plate with an elastic foundation and damping. *Journal of Elasticity*, 1(1): 37–49, 1971.

[246] Stadler W., Shreeves R.W. The transient and steady-state response of the infinite Bernoulli-Euler beam with damping and an elastic foundation. *The Quarterly Journal of Mechanics and Applied Mathematics*, 23(2): 197–208, 1970.

[247] Steele C.R. The finite beam with a moving load. *Journal of Applied Mechanics, ASME*, 34(1): 111–118, 1967.

[248] Szuladzinski G. Discrete models of beams on an elastic foundation. *Journal of the Engineering Mechanics Division, ASCE*, 101(EM6): 839–853, 1975.

[249] Terzaghi K. Evaluation of coefficients of subgrade reaction. *Geotechnique*, 5(4): 297–326, 1955.

[250] Thambiratnam D., Zhuge Y. Dynamic analysis of beams on an elastic foundation subjected to moving loads. *Journal of Sound and Vibration*, 198(2): 149–169, 1996.

[251] The MathWorks, Inc. *MatLab*, 2016. available online at http://www.mathworks.com/products/matlab.

[252] Timoshenko S.P. Method of analysis of statical and dynamical stresses in rail. In *Proceedings of the 2nd International Congress for Applied Mechanics*, volume 54, pages 1–12, 1927.

[253] Timoshenko S.P. *History of Strength of Materials*. Mc-Graw Hill, New York, 1953.

[254] Ting B.Y. Finite beams on elastic foundation with restraints. *Journal of the Structural Division, ASCE*, 108(ST3): 611–621, 1958.

[255] Tsai N.C., Westmann R.E. Beams on tensionless foundation. *Journal of the Engineering Mechanics Division, ASCE*, 93(EM5): 1–12, 1967.

[256] Tsiatas B.Y. Nonlinear analysis of non-uniform beams on nonlinear elastic foundation. *Acta Mechanica*, 209(1): 141–152, 2010.

[257] Tsynkov S.V. Numerical solution of problems on unbounded domains. a review. *Applied Numerical Mathematics*, 27(4): 465–532, 1998.

[258] Usmani R.A. A uniqueness theorem for a boundary value problem. *Proceedings of the American Mathematical Society*, 77(3): 329–335, 1979.

[259] Uzzal R.U.A., Bhat R.B., Ahmed W. Dynamic response of a beam subjected to moving load and moving mass supported by Pasternak foundation. *Shock and Vibration*, 19(2): 205–220, 2012.

[260] Vallabhan C.V.G., Das Y.C. Parametric study of beams on elastic foundations. *Journal of Engineering Mechanics, ASCE*, 114(12): 2072–2082, 1988.

[261] Vallabhan C.V.G., Das Y.C. Modified Vlasov model for beams on elastic foundations. *Journal of Geotechnical Engineering*, 117(6): 956–966, 1991.

[262] Vallabhan C.V.G., Das Y.C. A refined model for beams on elastic foundations. *International Journal of Solids and Structures*, 27(5): 629–637, 1991.

[263] van Dalen K.N., Metrikine A.V. Transition radiation of elastic waves at the interface of two elastic half-planes. *Journal of Sound and Vibration*, 310(3): 702–717, 2008.

[264] van Dalen K.N., Steenbergen M.J.M.M. Modeling of train-induced transitional wavefields. In *Proceedings of the III International Conference on Railway Technology: Research, Development and Maintenance (RAILWAYS2016)*, volume 110, pages 1–16, 2016.

[265] van Dalen K.N., Tsouvalas A., Metrikine A.V., Hoving J.S. Transition radiation excited by a surface load that moves over the interface of two elastic layers. *International Journal of Solids and Structures*, 73-74: 99–112, 2015.

[266] Vinberg E.B. *A Course in Algebra*. American Mathematical Society, 2003.

[267] Vlasov V.Z., Leontiev U.N. *Beams, Plates, and Shells on Elastic Foundations (translated from Russian)*. Israel Program for Scientific Translations, 1966.

[268] Wang Y.H., Tham L.G., Cheung Y.K. Beams and plates on elastic foundation: a review. *Progress in Structural Engineering and Materials*, 7(4): 174–182, 2005.

[269] Watanabe K. Response of an elastic plate on a Pasternak foundation to a moving load. *Bulletin of the Japan Society of Mechanical Engineers*, 24(191): 775–780, 1981.

[270] Weitsman Y. On foundations that react in compression only. *Journal of Applied Mechanics, ASME*, 37(4): 1019–1030, 1970.

[271] Winkler E. *Die Lehre von der Elastizität und Festigkeit*. mit Besonderer Rücksichtauf ihre Anwendung in der Technik, für Polytechnische Schulen, Bauakademien, Ingenieure, Maschinenbauer, Architekten, etc., Verlag H. Dominicus, 1867.

[272] Wolfert A.R.M., Dieterman H., Metrikine A.V. Stability of vibrations of two oscillators moving uniformly along a beam on a viscoelastic foundation. *Journal of Sound and Vibration*, 211(5): 829–842, 1998.

[273] Wolfert A.R.M., Dieterman H.A. Passing through the "elastic wave barrier" by a load moving along a waveguide. *Journal of Sound and Vibration*, 203(4): 597–606, 1997.

[274] Wolfram Research, Inc. *Mathematica, User Guide*. available online at http://www.wolfram.com.

[275] Wu Y., Gao Y. Analytical solutions for simply supported viscously damped double-beam system under moving harmonic loads. *Journal of Engineering Mechanics, ASCE*, 141(7): 04015004, 1–11, 2015.

[276] Yang S.Y. Analysis of a least squares finite element method for the circular arch problem. *Applied Mathematics and Computation*, 114(2-3): 263–278, 2000.

[277] Yankelevsky D.Z., Adin M.A., Eisenberger M. Beams on nonlinear Winkler foundation with gaps. *Computers and Geotechnics*, 6(1): 1–11, 1988.

[278] Yankelevsky D.Z., Eisenberger M., Adin M.A. Analysis of beams on nonlinear Winkler foundation. *Computer and Structures*, 31(2): 287–292, 1989.

[279] Yavari A., Nouri M., Mofid M. Discrete element analysis of dynamic response of Timoshenko beams under moving mass. *Advances in Engineering Software*, 33(3): 143–153, 2002.

[280] Yen D.H.Y., Tang S.C. On the non-linear response of an elastic string to a moving load. *International Journal of Non-Linear Mechanics*, 5(3): 465–474, 1970.

[281] Younesian D., Kargarnovin M.H. Response of the beams on random Pasternak foundations subjected to harmonic moving loads. *Journal of Mechanical Science and Technology*, 23(11): 3013–3023, 2009.

[282] Zhang Y., Murphy K.D. Response of a finite beam in contact with a tensionless foundation under symmetric and asymmetric loading. *International Journal of Solids and Structures*, 41(24-25): 6745–6758, 2004.

[283] Zhaohua F., Cook R.D. Beam elements on two-parameter elastic foundations. *Journal of Engineering Mechanics*, 109(6): 1390–1402, 1983.

[284] Zienkiewicz O.C., Emson C., Bettess P. A novel boundary infinite element. *International Journal for Numerical Methods in Engineering*, 19(3): 393–404, 1983.

[285] Zienkiewicz O.C., Owen D.R.J., Lee K.N. Least square-finite element for elasto-static problems. use of 'reduced' integration. *International Journal for Numerical Methods in Engineering*, 8(2): 341–358, 1974.

[286] Zimmermann H. *Die Berechnung des Eisenbahnoberbaues*. Wiley Ernst and Sohn, 1888.

List of Figures

List of Tables